

**Antibacterial Properties of Silver(I) and Gold(I) Complexes of
Imidazole- and 1,2,4-Triazole-based *N*-Heterocyclic Carbene
Ligands**

Joel Charles Mather

Bachelor of Science (BSc) La Trobe University 2018

A thesis submitted in total fulfilment of the requirement for the degree of
Master of Science by Research

School of Molecular Sciences

College of Science, Health and Engineering

La Trobe University

Victoria, Australia

April 2021

Abstract

During the past two decades, gold and silver complexes of *N*-heterocyclic carbene ligands have received much attention for their biological properties and are currently being investigated as potential treatments for malaria, cancer and neurodegenerative diseases. Numerous studies have also focussed on the use of these complexes as antibacterial agents and in the interest of broadening the current understanding of the structural activity relationships, a larger diversity of structural analogues is required. In this project a comparison of the antibacterial activities of gold(I) and silver(I) complexes of 1,2,4-triazole- and imidazole-based *N*-heterocyclic carbene ligands has been undertaken to investigate the potential biological differences arising from the third peripheral nitrogen of the 1,2,4-triazole moiety. The synthesis and antibacterial activity of novel gold(I) and silver(I) 1,2,4-triazole-based *N*-heterocyclic carbene complexes and their imidazole equivalents is reported, along with an investigation into their solution and gas phase stabilities using a combination of ¹H-NMR, HR-MS and theoretical calculations. The complexes have been fully characterised using ¹H-NMR, ¹³C-NMR, HR-MS, and in the cases of **2.17**, **2.24**, **2.25** and **2.36** by X-ray crystallography. The gold(I)- and silver(I)-NHC complexes that gave the best results in the antibacterial assays were further tested against multi-drug resistant bacterial strains and little difference in antibacterial activity was detected when compared to the non-resistant strains. The potential for antibacterial resistance to develop against these metal containing complexes was also investigated and significantly, no resistance was observed against the tested gold(I)- and silver(I)-NHC complexes, whilst a substantial increase in resistance was observed against the widely used broad-spectrum antibiotic ciprofloxacin in the same bacterial strains.

Statement of Authorship and Ethics

Except where reference is made in the text of the thesis, this thesis contains no material published elsewhere or extracted in whole or in part from a thesis accepted for the award of any other degree or diploma. No other person's work has been used without due acknowledgment in the main text of the thesis. This thesis has not been submitted for the award of any degree or diploma in any other tertiary institution.

All biological experiments within this thesis were carried out in collaboration with Jessica Wyllie of the Soares Da Costa laboratory in the Department of Biochemistry and Genetics, La Trobe University. The antimicrobial assays and resistance studies in Sections 3.2 – 3.4 were carried out by the author and Jessica Wyllie, and the photoluminescent studies within Section 2.5.1 were carried out by Laena D'Alton of the Hogan laboratory in the Department of Physics and Chemistry, La Trobe University.

Signature:

Date: 21-April-2021

Acknowledgments

I would like to thank my supervisor, Dr. Peter J. Barnard for his guidance, encouragement and access to laboratory equipment throughout the last two years. I would also like to thank my co-supervisor Dr. Tatiana Soares Da Costa for being very enthusiastic and motivating throughout this project. Thank you to the current Barnard group members Quoc Dat Duong, Tahmineh Hashemzadeh, Nutchareenat Wiratpruk, Pria Ramkissoo and Dr. Rebecca Karmis who have been accommodating, welcoming and helpful. A big thank-you to Jessica Wyllie for her assistance and collaboration with the microbiology side of this project, and thank you to Emily Mackie, Rachael Impey and the Soares Da Costa lab group for allowing me to use the microbiology cabinet. I would like to thank my fellow Masters student Michael Dewar-Oldis for the companionship. Thanks to Laena D'Alton for help with the photoluminescent studies, and Dr. Andrew Barrow for proofreading and pointing out the little mistakes in my synthetic schemes. Finally, I would like to say a special thank you to Dr. Zili Li for teaching me valuable synthetic chemistry skills that made this project possible.

This work was supported by an Australian Government Research Training Program Scholarship.

TABLE OF CONTENTS

Abstract.....	I
Statement of Authorship and Ethics	II
Acknowledgments	III
Table of Figures.....	VII
Table of Schemes.....	X
Table of Tables	XI
Abbreviations.....	XII
CHAPTER ONE	1
SILVER AND GOLD BASED ANTIBACTERIALS AS A RESPONSE TO THE INCREASING RATES OF ANTIBIOTIC RESISTANT BACTERIA.....	1
1.1 Introduction	1
1.2 Carbene Chemistry	3
1.3 <i>N</i> -Heterocyclic Carbenes	5
1.4 Antibacterial Silver <i>N</i> -Heterocyclic Carbene Complexes	6
1.4.1 Synthesis of Silver <i>N</i> -Heterocyclic Carbene Complexes.....	8
1.5 Antibacterial Gold(I) <i>N</i> -Heterocyclic Carbene Complexes.....	9
1.5.1 Synthesis of Gold <i>N</i> -Heterocyclic Carbene Complexes	10
1.6 Project Aim.....	11
CHAPTER TWO	13
SYNTHESIS AND CHARACTERISATION OF THE GOLD(I) AND SILVER(I) COMPLEXES OF IMIDAZOLE- AND 1,2,4-TRIAZOLE-BASED NHC LIGANDS.....	13
2.1 Synthesis of the Azolium Precursor Salts.....	13
2.2 Synthesis of the Silver(I) Imidazolylidene and 1,2,4-triazolylidene <i>N</i> -Heterocyclic Carbene Complexes	15
2.3 Synthesis of the Gold(I) Imidazolylidene and 1,2,4-triazolylidene <i>N</i> -Heterocyclic Carbene Complexes	16

2.4	Synthesis of the Bridged <i>Bis</i> -Imidazolium and 1,2,4-Triazolium Pro-Ligand Salts	
2.5	Synthesis of the Dinuclear Gold(I) Imidazolylidene and 1,2,4-Triazolylidene Complexes	20
2.5.1	Photoluminescent Studies	20
2.6	Summary.....	22
CHAPTER THREE		23
ANTIBACTERIAL AND ANTIBACTERIAL RESISTANCE STUDIES.....		23
3.1	Introduction	23
3.2	Antibacterial Assays	23
3.3	Assays Against Antibiotic Resistant Bacterial Strains	28
3.4	Antibacterial Resistance Studies	29
CHAPTER FOUR.....		31
AN INVESTIGATION INTO THE STABILITY OF THE SYNTHESISED ANTIBACTERIAL GOLD(I) AND SILVER(I) <i>N</i>-HETEROCYCLIC CARBENE COMPLEXES		31
4.1	Stability Studies Using ESI-HR-MS	31
4.2	Theoretical Stability Studies.....	34
4.3	Experimental Stability Studies Using WATERGATE ¹ H-NMR	37
4.4	Discussion of the Results.....	42
4.4.1	Antibacterial Silver(I)-NHC Complexes	42
4.4.2	Antibacterial Gold(I)-NHC Complexes	43
CHAPTER FIVE		45
CONCLUSION AND FUTURE WORK		45
CHAPTER SIX		47
EXPERIMENTAL.....		47
5.1	General Information and Methods.....	47
5.2	X-Ray Crystallography	47

5.3	UV-vis and Photoluminescence Studies.....	48
5.4	Antibacterial Activity	48
5.5	Resistance Studies	48
5.6	Bacterial Strains and Growth Conditions	49
5.7	Synthesis	49
REFERENCES		64

Table of Figures

Figure 1. Molecular orbital diagrams of singlet (1a) and triplet (1b) state carbenes.....	4
Figure 2. Possible electron configurations and relative energy levels for carbene carbon atoms.....	4
Figure 3. Examples of isolable carbenes stabilised by amino substituents.	5
Figure 4. Examples of commonly studied <i>N</i> -heterocyclic carbene ligand scaffolds.....	6
Figure 5. Silver(I) complexes of <i>N</i> -heterocyclic carbene ligands with antibacterial properties.	8
Figure 6. Antirheumatic gold metallodrug Auranofin TM containing a phosphine ligand, and <i>bis</i> -NHC gold complexes with antibacterial and anti-cancer properties.	10
Figure 7. The IUPAC numbering system for imidazole and 1,2,4-triazoles. This numbering system is frequently referred to within this text.	11
Figure 8. Proposed structures of silver(I) and gold(I) complexes of imidazolylidene and 1,2,4-triazolylidene complexes to be synthesised and tested for their antibacterial properties.	12
Figure 9. Representation of X-ray crystal structure of 4-methyl-1-phenyl-1 <i>H</i> -1,2,4-triazolium (2.5) with C5-N1 and C5-N4 bond distances of 1.33 Å.....	14
Figure 10. Representation of the molecular structure of the <i>bis</i> -1,2,4-triazolylidene silver(I) complex 2.17 (2.17a) and polymeric silver(I) iodide counterion for 2.17 (2.17b). Refer to Table S1 for crystallographic data. Hydrogen atoms have been omitted for clarity.	16
Figure 11. Representation of the molecular structure of the <i>bis</i> -imidazolylidene gold(I) complex 2.24 as an iodide salt. Hydrogen atoms have been omitted for clarity. Refer to Table S1 for crystallographic data.....	18
Figure 12. Representation of the single unit cell for the <i>bis</i> -1,2,4-triazolylidene gold(I) complex 2.25 as a tetraphenylborate salt. Hydrogen atoms have been omitted for clarity. Refer to Table S1 for crystallographic data.....	18

Figure 13. Unsupported, semi-supported and fully-supported types of Auophilic interactions.....	21
Figure 14. X-ray crystal structure of dinuclear gold(I) complex 2.35 with Au-Au distances of 3.57 Å. Hydrogen atoms have been excluded for clarity.	21
Figure 15. Room temperature electronic excitation and emission spectra for the ethylene linked dinuclear gold(I) complexes of bridged 1,2,4-triazolylidene ligands 2.35 and 2.36 excited at 273 nm for complex 2.35 and 269 nm for complex 2.36	22
Figure 16. Position of the R-groups on imidazolium and 1,2,4-triazolium salts referred to in Tables 1– 3. Note the differences in numbering systems between the imidazolium and 1,2,4-triazolium salts.	24
Figure 17. Normalised ESI-HR-MS plots at selected cone voltages for gold(I) complex of <i>bis</i> -1-phenyl-3-methyl-imidazolylidene ligands 2.23	32
Figure 18. Normalised ESI-HR-MS plots at selected cone voltages for gold(I) complex of <i>bis</i> -1-phenyl-4-methyl-1,2,4-triazolylidene ligands 2.25	32
Figure 19. Normalised ESI-HR-MS plots at selected cone voltages for gold(I) complex of <i>bis</i> -1,3-diethyl-imidazolylidene ligands 2.28	33
Figure 20. Normalised ESI-HR-MS plots at selected cone voltages for gold(I) complex of <i>bis</i> -1,4-diethyl-1,2,4-triazolylidene ligands 2.30	34
Figure 21. Optimised structures of the 1-phenyl-3-methyl substituted imidazolylidene and 1-phenyl-4-methyl substituted 1,2,4-triazolylidene gold(I) and silver(I) complexes 2.15 , 2.17 , 2.23 and 2.25	36
Figure 22. ¹ H-NMR spectra recorded at the indicated times for gold(I)-NHC complex 2.25 at 37 °C in 300 µL DMSO- <i>d</i> ₆ and 300 µL H ₂ O. No degradation was observed over a time period of 21 days.	38
Figure 23. ¹ H-NMR spectra recorded at the indicated times for silver(I)-NHC complex 2.15 at 37 °C in 300 µL DMSO- <i>d</i> ₆ and 300 µL H ₂ O. The precursor pro-ligand 2.3 is included for visual comparisons in the same solvent system.	39

Figure 24. ^1H -NMR spectra recorded at the indicated times for silver(I)-NHC complex 2.17 at 37 °C in 300 μL $\text{DMSO-}d_6$ and 300 μL H_2O	40
Figure 25. ^1H -NMR spectra recorded at the indicated times for the degradation of dimethyl substituted silver(I)-NHC complexes 2.19 of imidazolylidene ligands (left) and 2.21 of 1,2,4-triazolylidene ligands (right) at 37 °C in 300 μL $\text{DMSO-}d_6$ and 300 μL H_2O	41
Figure 26. ^1H -NMR spectra recorded at the indicated times for the degradation of silver(I)-NHC complex 2.20 at 37 °C in 300 μL $\text{DMSO-}d_6$ and 300 μL H_2O	41
Figure 27. Minimum inhibitory concentrations of vancomycin; a last resort treatment for Gram-positive infections and colistin; a last resort treatment for Gram-negative infections.	44

Table of Schemes

Scheme 1. Synthesis of silver(I)-NHC complexes by the in-situ deprotonation of azolium salts. R = alkyl, aryl, X = PF ₆ , I, Br, (a) AgCO ₂ CH ₃ , (b) Ag ₂ O, (c) Ag ₂ CO ₃	9
Scheme 2. Three different techniques used for the synthesis of gold-NHC complexes, (a) in situ deprotonation, (b) transmetallation, and (c) free carbene generation.	11
Scheme 3. Synthetic route for the imidazolium and 1,2,4-triazolium precursors 2.3 – 2.6	13
Scheme 4. Synthesis of the azolium salt pro-ligands and mono alkylated precursors.....	14
Scheme 5. Synthetic route of imidazolylidene and 1,2,4-triazolylidene silver(I) complexes (a) 1,2-dichloroethane, RT, 4 h, (b) CH ₃ OH/1,2-dichloroethane, RT, 4 h, (c) 1,2-dichloroethane, 60 °C, 24 h.	15
Scheme 6. Synthesis of the gold(I) complexes of <i>bis</i> -1,2,4-triazolylidene and <i>bis</i> -imidazolylidene ligands via reaction conditions (a) NaOAc, DMF, 110 °C, 4 h. (b) K ₂ CO ₃ , DMF, 110 °C, 24 h.	17
Scheme 7. Synthesis of the bridged <i>bis</i> -imidazolium or triazolium dibromide salts with ethylene linker groups. (a) dibromoethane, acetonitrile, reflux, 24 h, (b) dibromoethane, sealed, 110 °C, 4 h.	19
Scheme 8. Synthesis of dinuclear gold(I) complexes of bridged <i>bis</i> -NHC ligands.....	20
Scheme 9. Overall reaction mechanism for the decomposition of silver(I) and gold(I) complexes of NHC ligands.....	38

Table of Tables

Table 1. Minimum Inhibitory Concentration (MIC $\mu\text{g}\cdot\text{mL}^{-1}$) values of the imidazolium and 1,2,4-triazolium precursor pro-ligand salts, reported in $\mu\text{g}\cdot\text{mL}^{-1}$	24
Table 2. Minimum Inhibitory Concentration (MIC $\mu\text{g}\cdot\text{mL}^{-1}$) values of the silver(I) complexes.	25
Table 3. Minimum Inhibitory Concentration (MIC $\mu\text{g}\cdot\text{mL}^{-1}$) values of the gold(I) complexes.	27
Table 4. Minimum Inhibitory Concentration (MIC $\mu\text{g}\cdot\text{mL}^{-1}$) values of two of the best performing silver(I) and gold(I) antibacterial complexes against bacterial strains with higher levels of antibacterial resistance (except for <i>E. coli</i> K12 that is a sensitive strain).	29
Table 5. BDEs of the Metal-NHC bonds of gold(I) and silver(I) complexes of NHC ligands with methyl <i>N</i> -substituents.	35
Table 6. BDEs of the metal-NHC bonds of the gold(I) and silver(I) complexes of 1-phenyl-3-methyl imidazolylidene and 1-phenyl-4-methyl substituted 1,2,4-triazolylidene ligands.	37
Table 7. Bacterial strains sourced from the American Type Culture Collection.....	49

Abbreviations

BDE	Bond Dissociation Energy
CDCl ₃	Deuterated Chloroform
CH ₃ CN	Acetonitrile
CO-ADD	Community for Open Antimicrobial Drug Discovery
DFT	Density Functional Theory
DMF	<i>N,N</i> -Dimethyl Formamide
DMSO	Dimethyl Sulfoxide
D ₂ O	Deuterium Oxide
Et ₂ O	Diethyl Ether
Hz	Hertz
HOMO	Highest Occupied Molecular Orbital
Hour	h
<i>Im</i>	Imidazole
<i>J</i>	Coupling Constant
LUMO	Lowest Unoccupied Molecular Orbital
MeOH	Methanol
MIC	Minimum Inhibitory Concentration
MS	Mass Spectrometry
MW	Molecular Weight
NaOAc	Sodium Acetate
NHC	<i>N</i> -Heterocyclic Carbene
NMR	Nuclear Magnetic Resonance
Ph	Phenyl

ROS	Reactive Oxygen Species
SAR	Structural Activity Relationship
SOMO	Singularly Occupied Molecular Orbital
<i>t</i> -Bu	<i>Tert</i> -Butyl
THF	Tetrahydrofuran
THT	Tetrahydrothiophene
TPB	Tetraphenylborate
TrxR	Thioredoxin Reductase
<i>Trz</i>	Triazole
WHO	World Health Organisation

CHAPTER ONE

Silver and Gold Based Antibacterials as a Response to the Increasing Rates of Antibiotic Resistant Bacteria

1.1 Introduction

Antibacterials are considered to be one of the greatest discoveries of the 20th century.¹ In 1928, Alexander Fleming first reported that *Penicillium notatum* produced a bacteria-inhibiting substance now known as penicillin, which was studied in collaboration with Florey and Chain.² By 1945, penicillin was mass produced by pharmaceutical companies and Chain, Florey and Fleming shared a Nobel Prize for the discovery and its implications for the treatment of infectious diseases.³ The period following the development of penicillin was termed the ‘golden age’ of antibiotics and a significant portion of the antibacterial treatments discovered during this era are still in use today. This newfound ability to treat bacterial infections allowed for significant advances in modern medicine, but the golden age of antibiotics was unfortunately short-lived. The extensive overuse of these antibiotics has resulted in widespread microbial resistance to many existing treatments.⁴⁻⁷ In the present day, antibiotic resistant bacteria have become a significant health issue and there is an urgent need to develop new novel classes of antibacterial agents that are effective against multi-drug resistant pathogens.^{8,9}

A scarce number of antibacterials are currently in clinical trials and a significant portion of these are derivatives of current drugs, and thus are still prone to existing resistance mechanisms. A contributor to the low number of antibacterials under development is the predilection for specific physiochemical or functionality guidelines (*e.g.* Lipinski’s Rule of Five) by the pharmaceutical industry where many leading structures are based upon purely organic compounds.^{10,11} As a consequence, many potential antibacterial compounds are excluded from synthetic libraries, particularly those belonging to inorganic and organometallic areas of chemical research. Despite this apparent medicinal chemist bias, organisations such as the Community for Open Antimicrobial Drug Discovery (CO-ADD) have recently identified antibacterial activity in a substantial number of compounds that lie outside of typical “drug-like” conventions, many of which also display low levels of toxicity to mammalian cells.¹⁰⁻¹²

To encourage the research and development (R & D) of new antibacterial treatments, the World Health Organisation (WHO) has recently identified and categorised twelve of the highest priority bacterial pathogens with the highest levels of antibacterial resistance.¹³ A significant portion of the bacterial pathogens identified are Gram-negative and have become increasingly difficult to treat, largely due to the lipopolysaccharide outer layers that are difficult for antibacterial treatments to pass.¹⁴ *Acinetobacter baumannii* as well as members of the *Enterobacteriaceae* family have been classified as of critical importance, and vancomycin resistant *Enterococcus faecium* and methicillin-resistant and vancomycin resistant *Staphylococcus aureus* have been classified as high priority.

Recent screening by the CO-AAD found a substantial number of metal containing complexes that displayed antibacterial activity, whilst not displaying cytotoxicity against mammalian cells.¹⁵ A significant factor contributing to the appeal of metal containing antibacterials is the limited number of mechanisms by which microbes are able to develop resistance. Unlike antibacterials based on organic molecules, metals cannot be modified or deactivated and consequently, resistance mechanisms are mostly limited efflux/segregation,^{16,17} and reduction to less toxic oxidation states through enzymic detoxification.¹⁸ In addition, bacterial import systems are not discriminatory enough to allow only required metals and recent studies have indicated that cellular uptake is likely to play a key role in their antibacterial activity.¹⁹ The investigation of metal containing compounds for the purpose of antibacterial treatments provides an opportunity to address the low number of truly novel antibiotics in clinical development.^{10,11} A large number of groups are currently investigating metal complexes bearing *N*-heterocyclic carbene ligands (NHCs) due to their strong bonding properties that allow easy modification of the NHC scaffold.¹⁰

Silver(I) complexes of NHC ligands have received considerable attention due to the known antibacterial properties of silver and relatively low toxicity to human cells.²⁰ A range of silver(I)-NHC complexes have been found to have greater antibacterial activity compared to existing silver based medications, and more recently, the introduction of lipophilic substituents to the NHC ligands have been shown to improve antibacterial activity of the silver complexes.²¹⁻²⁴ Gold complexes of NHC ligands have also received attention for their antibacterial properties. As well as having high bond dissociation energies, the appeal of gold(I)-NHC complexes has been driven to a large extent by the high affinity of gold for thiols and selenols and numerous groups are currently investigating the use of gold NHCs

to target thiol/selenol containing biological molecules present in bacteria such as thioredoxin reductase (TrxR).^{25,26}

To facilitate the further development of metallodrugs of this type, a robust understanding of the structural activity relationships (SAR) is needed, that will benefit from studying a wider variety of molecules.²⁷⁻²⁹ The vast majority of studies investigating the antibacterial properties of gold(I) and silver(I) complexes of NHC ligands are based on imidazole and benzimidazole scaffolds, whereas very few studies have investigated ligands based on 1,2,4-triazole-based carbenes.^{30,31} Within this body of work the synthesis, characterisation and antibacterial activity of a variety of gold(I) and silver(I) complexes of imidazolylidene and 1,2,4-triazolylidene ligands is reported and discussed. This allows for a direct comparison between the biological activity of coordination complexes of imidazolylidene and 1,2,4-triazolylidene ligands to the same metal, as well as a comparison between the antibacterial activity of gold and silver metals with identical NHC scaffolds.

1.2 Carbene Chemistry

A carbene can be defined as a divalent carbon atom with a vacant $2p$ -orbital with two non-bonding electrons and only six electrons in its valence shell.³² The reactivity of carbenes is dictated by the ground state spin multiplicity and the molecular geometry. The lone pair can be arranged in a spin paired singlet state **1a** or a parallel spin triplet state **1b** as shown in Figure 1. Singlet state carbene ligands are chemically important as they can donate a lone pair of electrons, while retaining a vacant p -orbital, thus giving ambiphilic character. The stability of carbene centres is greatly affected by electronic interactions and partially influenced by steric effects.

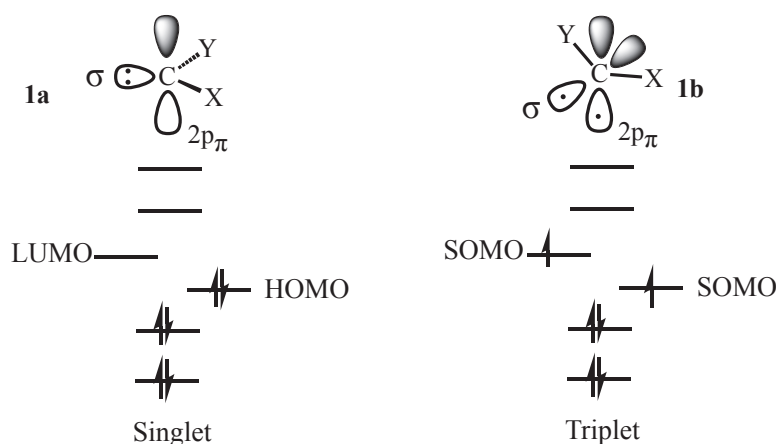


Figure 1. Molecular orbital diagrams of singlet (1a) and triplet (1b) state carbenes.

Singlet carbenes arise from two electrons occupying the σ -orbital at the sp^2 hybridised carbene carbon with antiparallel spin orientation (Figure 2, **2a**). Triplet ground states arise from the two nonbonding electrons at the sp^2 hybridised carbene occupying two P_π -orbitals with parallel spin orientation (Figure 2, **2b**). Carbenes with linear geometry arise from an sp -hybridised carbene carbon with two energetically degenerate p -orbitals (P_x, P_y) (Figure 2, **2c**), although this geometry is higher in energy and constitutes an extreme case. The greater stability of carbenes with bent geometries arises from the formation of a sp^2 -hybridised orbital that is lower in energy than the original p -orbital due to the partial s -character.³³

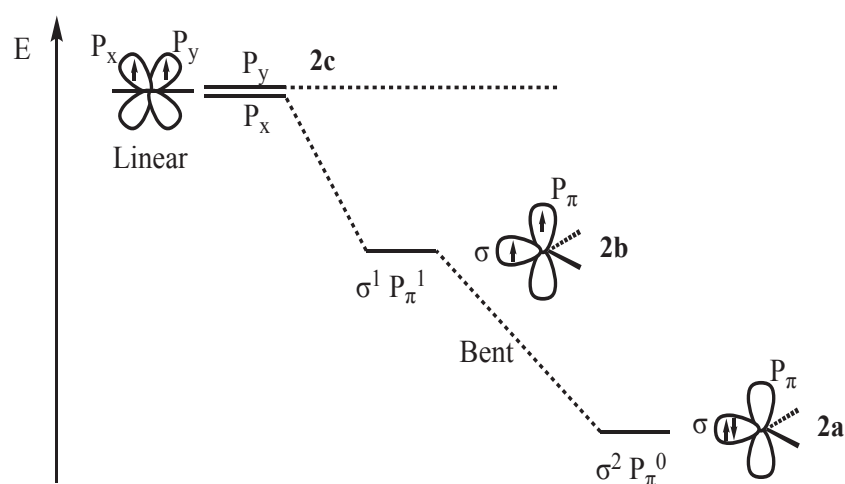


Figure 2. Possible electron configurations and relative energy levels for carbene carbon atoms.

1.3 N-Heterocyclic Carbenes

N-Heterocyclic carbenes are singlet carbenes substituted with two amino π -donor atoms, with bent geometry at the carbene carbon (Figure 3). The P_π orbital of the carbene carbon interacts with π -electron pairs from the amino substituents resulting in raised energy of the P_π orbital.³⁶ The σ -orbital at the carbene carbons relative energy is not affected by this interaction, and as a consequence the energy gap between the σ -orbital and the p_π orbital becomes larger, resulting in increased stabilisation of the singlet ground state and bent geometry. NHCs are also stabilised by the inductive σ -electron withdrawing nitrogens lowering the relative energy of the non-bonding σ -orbital. NHCs can be regarded as alternatives to phosphine ligands due to their ability to donate electron density to metal centers, however the sp^2 directional lone pair of an NHC allows stronger sigma bonds to be formed in comparison to the s-type lone pairs of phosphines.³⁴⁻³⁶

Formative studies by Hine and Doering in the 1950's concluded that carbenes would be too reactive to be isolated and would exist only as reactive intermediates.^{37,38} Wanzlick attempted to crystallise a saturated NHC in 1962, but was only able to isolate the dimeric form (Figure 3, **1.1**).³⁹ The first crystallised carbene was synthesised by Arduengo in 1991 who reported the isolation of 1,3-diadamantyl-imidazolylidene (**1.2**), a carbene that could be isolated and stored with the relatively high stability that was attributed to both steric and electronic factors.⁴⁰ Arduengo subsequently investigated the impact of varying steric and electronic effects by preparing NHCs with varying *N*-substituents (**1.3-1.5**).⁴¹ Isolation of the 1,3-dimethyl-imidazolylidene (**1.5**) showed that a carbene could be stabilised from electronic factors alone. The NHCs have since had major implications in organometallic chemistry,³⁴ transition metal catalysis,⁴² materials chemistry,⁴³ and biochemistry.⁵⁰

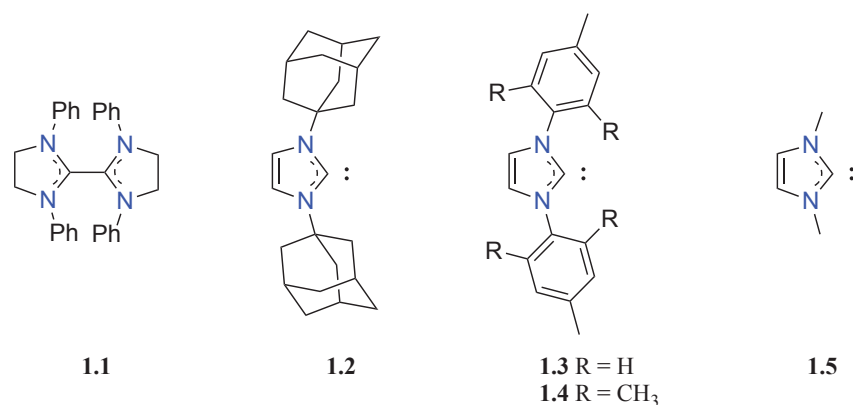


Figure 3. Examples of isolable carbenes stabilised by amino substituents.

N-heterocyclic carbenes are commonly prepared by deprotonation of the corresponding azolium salt and are named using the suffix -ylidene following the name of the corresponding heterocycle (Figure 4). The most studied *N*-heterocyclic carbenes are the imidazolylidenes however there are many structural variations that exist. Small changes to the NHC architectures cause a dramatic change in the electronic donor properties of the carbene moieties and impose geometric constraints on the *N*-substituents, influencing their steric impact. The *N*-substituents allow for a modulation of the steric pressure on both the carbene and the coordinated metal.⁴¹

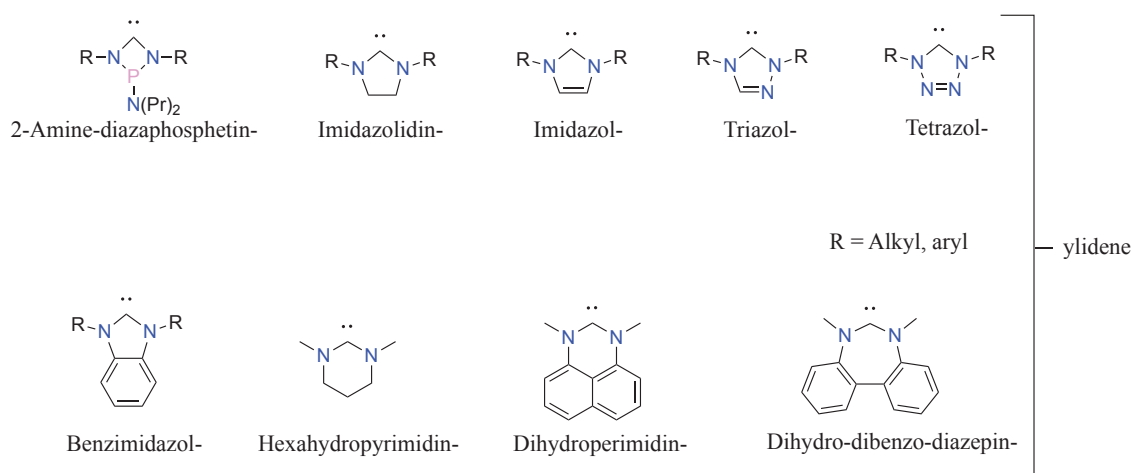


Figure 4. Examples of commonly studied *N*-heterocyclic carbene ligand scaffolds.

The stability of NHC complexes of transition metals can be rationalised by the σ -donor ability of the sp^2 -lone pair on the carbene carbon, however the contribution of π -back bonding from the metal to the carbene carbon is also significant. Theoretical calculations by Frenking and co-workers showed that π -back bonding can account for about 20% of the overall bond energy for imidazolylidenes and imidazolineylidenes coordinated to elements from group 11 of the periodic table.⁴⁴

1.4 Antibacterial Silver *N*-Heterocyclic Carbene Complexes

The use of silver as an antibacterial treatment is well documented throughout history.⁴⁵ Silver nitrate has been used to prevent infections in severe burns since as early as the 1840's and its use continued well into the 20th century for a variety of medical applications.⁴⁶ Although the use of silver nitrate was substantially decreased with the discovery and widespread use of antibiotics in the mid 20th century, the emergence of antibiotic resistant bacteria prompted a resurgence of interest in silver based medications

for their antibacterial activity. This led to the development of silver sulphadiazine that is still used as an antibacterial treatment in burn wards. There are a number of modern examples where silver is used for its antibacterial properties including endotracheal tubes,⁴⁷ catheters,⁴⁸ dressings,⁴⁹ and even water purification on the Russian sector of the International Space Station.⁵⁰

Significant advances have been made in recent years towards understanding the possible modes of action of silver ions, and it has been shown that silver(I) targets the enzyme glyceraldehyde-3-phosphate dehydrogenase in *Escherichia coli*, which plays a key role in the glycolysis pathway.^{51,52} Many reports have shown that the silver(I) ion is the bioactive species and a steady release of silver(I) ions is a key factor for the design of silver containing antibacterials.⁵³ Although silver ions have been shown to inhibit growth against a wide range of Gram-positive and Gram-negative bacteria, medications based on silver ions quickly lose their effectiveness due to the rapid loss of the silver(I) ions.⁵⁴ It is widely reported that a steady release of the silver(I) ions is required to improve the currently available silver based antibacterial treatments.^{53,54}

Silver complexes bearing NHC ligands have been extensively studied for their potential antibacterial activity, largely due to the ability of this class of ligand to bond strongly to metals resulting in stabilised complexes and prolongs the release of silver(I) ions.^{15,21,22,24,55-59} The pioneering work in this field was performed by Youngs and co-workers, who prepared a silver-NHC coordination polymer of imidazolylidene ligands (**1.6**, Figure 5) that had more potent antibacterial activity than silver nitrate.²¹ Shortly thereafter, a dinuclear silver(I) complex of *bis*-imidazolylidene cyclophane ligands (**1.7**) was synthesised and was found to have significantly enhanced antibacterial activity when encapsulated into a hydrophilic tectophilic polymer, as well as having a sustained release of the active silver species.²² This strengthened the argument for the release of the silver ion being responsible for the antibacterial effect, although more recently, the antibacterial activity of silver(I)-NHC complexes has also been attributed to non-covalent interactions between the complexes and biomolecules.^{60,61}

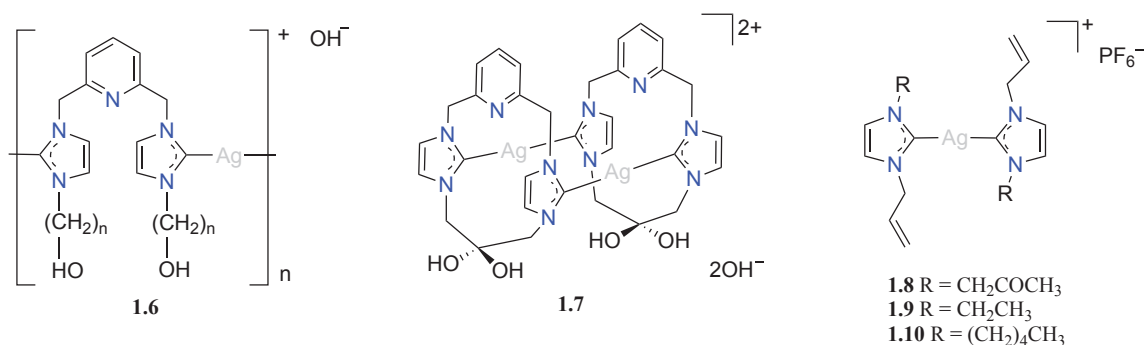
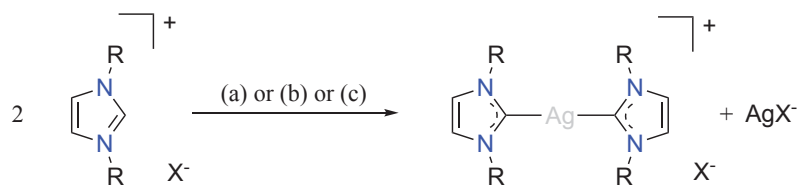


Figure 5. Silver(I) complexes of *N*-heterocyclic carbene ligands with antibacterial properties.

The lipophilicity of silver(I)-NHC complexes is also thought to play a significant role in the ability of these compounds to penetrate cellular membranes. This is attributed to improved antibacterial activity being associated with increased complex lipophilicity due to modification of the NHC wingtip substituents.²⁻⁴⁴ In 2014, Haque and co-workers synthesised a range of silver(I)-NHC complexes and evaluated their antibacterial and nuclease activity. Complex **1.10** (Figure 5) was found to be the most effective antibacterial, and also was the most efficient in promoting the cleavage of nucleic acids due to the lipophilic substituents on the nitrogen atoms.²⁴

1.4.1 Synthesis of Silver *N*-Heterocyclic Carbene Complexes

Silver complexes of NHC ligands are commonly synthesised by the *in-situ* deprotonation of azolium salts, while the use of free carbenes for the synthesis of silver complexes is not routinely used due to the reactive nature of most free carbenes.⁶² A number of methods have been devised to synthesise silver NHC complexes from basic silver salts, including the use of silver acetate by Bertrand and co-workers,⁶³ silver oxide by Lin and Wang⁶⁴ and silver carbonate as described by Danopoulos and co-workers (Scheme 1).⁶⁵ These procedures enable the simple synthesis of silver(I)-NHC complexes, and can also lead to the generation of other metal carbene complexes through transmetallation reactions with a large number of transition metals.⁶⁶



Scheme 1. Synthesis of silver(I)-NHC complexes by the in-situ deprotonation of azolium salts. R = alkyl, aryl, X = PF₆, I, Br, (a) AgCO₂CH₃, (b) Ag₂O, (c) Ag₂CO₃.

1.5 Antibacterial Gold(I) N-Heterocyclic Carbene Complexes

Although interest in the therapeutic properties of gold predates modern history, the first scientific reports of gold complexes with medicinal properties originated in the 19th century when Robert Koch demonstrated the antibacterial activity of potassium dicyanidoaurate(I) against *Mycobacterium tuberculosis*.⁶⁷ Gold has since been investigated for a number therapeutic applications, and gold metallodrugs such as Auranofin (Figure 6, **1.11**) which is used for the treatment of rheumatoid arthritis, became available during the 1970's. Many of the gold containing complexes developed around this time are substituted with phosphine or thiolate ligands that are more weakly coordinating in comparison to NHCs, and as a consequence gold(I)-NHC complexes have received considerable attention due to their higher bond dissociation energies.^{26,68} Gold(I)-NHC complexes have been investigated for a wide variety of biological applications during the past two decades, in particular for the development of potential anticancer agents.^{67,69-71}

Although the mechanism (or mode) of action of gold metallodrugs has not yet been fully elucidated, several targets have been identified, most notably cancer cell mitochondria and the selenoenzyme thioredoxin reductase (TrxR).⁷²⁻⁷⁵ It has been demonstrated that gold(I) complexes exert their biological effects through both ligand exchange reactions,⁷⁶ and also non-covalent interactions with DNA.^{77,78} Gold(I)-NHC complexes have also been shown to have antibacterial properties,²⁶ and recent work by Ott and co-workers has elucidated important SAR for compounds in this class (e.g. **1.12** – **1.15**, Figure 6).^{25,26}

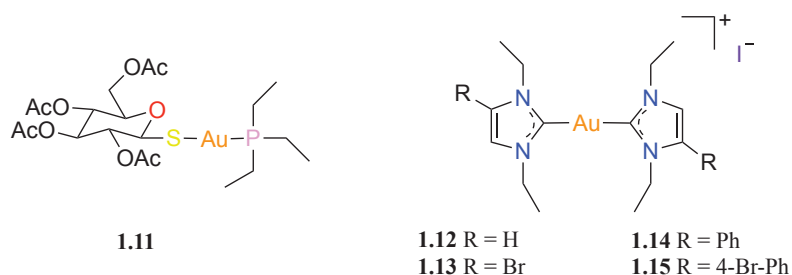
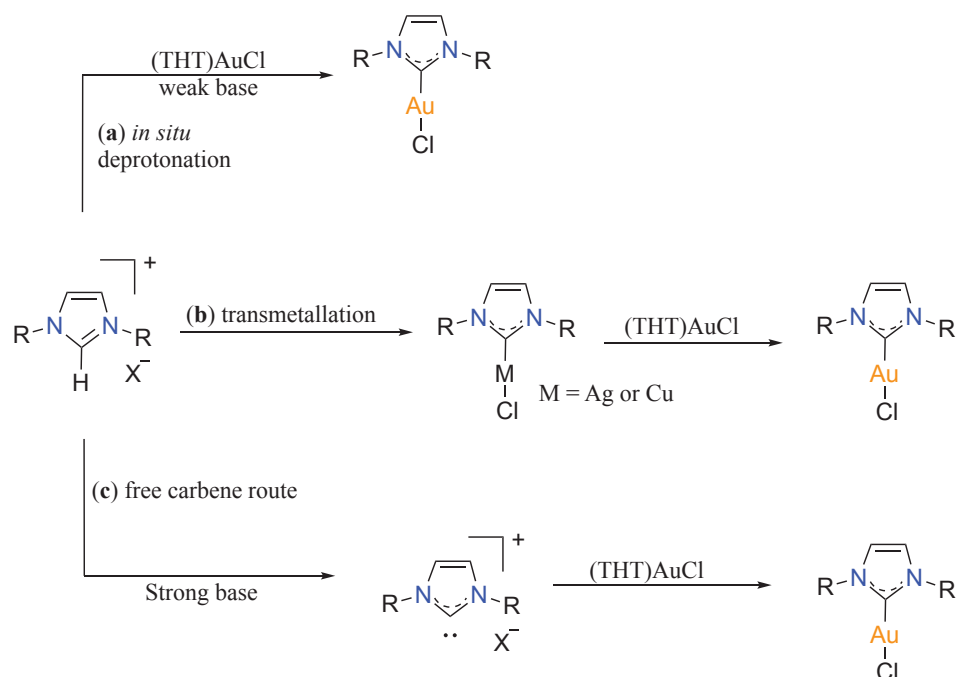


Figure 6. Antirheumatic gold metallodrug AuranofinTM containing a phosphine ligand, and *bis*-NHC gold complexes with antibacterial and anti-cancer properties.

Gold(I)-NHC complexes have been observed to damage peptidoglycan layers of Gram-positive bacteria, hence the more pronounced antibacterial activity observed against these pathogens.⁷⁹ Structural variations have been shown to have a substantial effect on the antibacterial activity of gold(I)-NHC complexes. For example, compound **1.12** (Figure 6, R = H) was found to have a minimum inhibitory concentration (MIC) of 57.2 $\mu\text{g}\cdot\text{mL}^{-1}$ against multi-drug resistant *S. aureus* (MRSA) RKI 11-02670, whereas **1.14** (R = Ph) yielded a MIC of 1.7 $\mu\text{g}\cdot\text{mL}^{-1}$ against the same bacterial strain.^{26,61} This study also showed that compound **1.14** had higher levels of cellular gold compared to **1.12**, indicating that cellular uptake plays an important role in the antibacterial activity of these complexes.²⁵

1.5.1 Synthesis of Gold *N*-Heterocyclic Carbene Complexes

Gold complexes are commonly prepared by the *in-situ* deprotonation of an azolium salt followed by subsequent reaction with gold containing precursors (Scheme 2, **a**). Tetrahydrothiophene gold chloride ((THT)AuCl) and dimethylsulfide gold chloride ((DMS)AuCl) are frequently used as convenient entry points to gold chemistry as the THT and DMS ligands are weakly coordinating and are readily substituted with stronger ligands.⁸⁰ Gold(I)-NHC complexes can also be prepared via ligand exchange reactions from Ag-NHC or Cu-NHC precursors that undergo concerted carbene transfer reactions favored by enthalpy due to the stronger gold(I)-NHC bond, and formation of insoluble silver halides (**b**).⁸¹ The generation of free carbenes for the formation of gold(I)-NHC complexes is less frequently used due to the requirement of strong bases such as lithium dimethyl silyl amide (LiHMDS), and stringent inert conditions (**c**). In contrast to the generation of free carbenes, transmetallation and *in-situ* deprotonation methods are thermodynamically driven based on the electronegativity of the metals, and thus can be performed in the presence of weaker bases.⁸¹



Scheme 2. Three different techniques used for the synthesis of gold-NHC complexes, (a) *in situ* deprotonation, (b) transmetalation, and (c) free carbene generation.

1.6 Project Aim

This project aims to synthesise and characterise a range of silver(I) and gold(I) complexes of imidazolylidene and 1,2,4-triazolylidene ligands, and evaluate their antibacterial activity. This allows the antibacterial activity of complexes of imidazolylidene and 1,2,4-triazolylidene-based NHC ligands coordinated to the same metal to be directly compared, as well as a comparison between gold and silver metals coordinated to these ligand.



Figure 7. The IUPAC numbering system for imidazole and 1,2,4-triazoles. This numbering system is frequently referred to within this text.

N-heterocyclic carbenes derived from 1,2,4-triazoles differ from the more commonly studied imidazolyidenes due to the third nitrogen of the heterocyclic ring (Figure 7).³⁰ The extra nitrogen causes dissymmetry to the heterocycle and reduces the ligand sigma donor properties in metal complexes, whilst increasing the π -accepting character of the ligand

when coordinated to a metal. The degree of π -bonding interaction originating from the metal has been shown to increase with formal d electron count, making π -accepting character of ligands coordinated to d^{10} metal complexes an important consideration.⁸²⁻⁸⁸ The additional nitrogen not only influences the nature of the NHC bond, but also provides an additional hydrogen bonding site that has the potential to interact with biological targets in physiological environments.⁸⁹ Finally, the increased acidity of the 1,2,4-triazolium precarbenic C5 proton allows for milder reaction conditions to be employed in the formation of metal-NHC complexes.⁹⁰

A variety of structural analogues of both mononuclear and dinuclear complexes of imidazolyliidene and 1,2,4-triazolyliidene ligands are to be investigated, as depicted in Figure 8. The potential for antibacterial resistance to these metal-NHC complexes is also to be investigated, along with an exploration into a possible relationship between stability of the complexes and antibacterial activity.

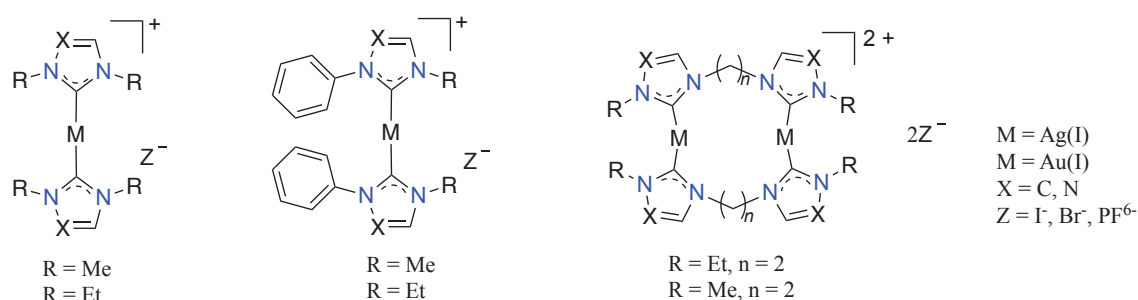


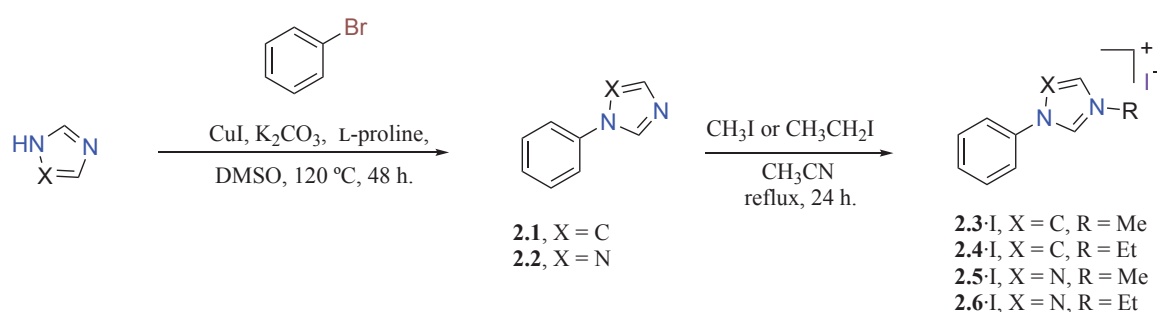
Figure 8. Proposed structures of silver(I) and gold(I) complexes of imidazolyliidene and 1,2,4-triazolyliidene complexes to be synthesised and tested for their antibacterial properties.

CHAPTER TWO

Synthesis and Characterisation of the Gold(I) and Silver(I) Complexes of Imidazole- and 1,2,4-Triazole-Based NHC Ligands

2.1 Synthesis of the Azolium Precursor Salts

The phenyl substituted precursor 1,2,4-triazolium and imidazolium salts were synthesised using a two-step procedure. The synthesis was initiated with an Ullmann-type coupling of 1,2,4-triazole or imidazole and bromobenzene to produce the corresponding 1-phenylazoles **2.1** and **2.2** (Scheme 3). Ullmann-type coupling reactions require elevated temperatures and often result in moderate yields.⁹¹ Despite these disadvantages this method of coupling for the synthesis of these phenyl-azoles results in the formation of a single product, thereby avoiding the potentially difficult separation of isomeric mixtures.⁹²



Scheme 3. Synthetic route for the imidazolium and 1,2,4-triazolium precursors **2.3** – **2.6**.

The phenyl substituted azolium salts **2.3** – **2.6** were synthesised by heating **2.1** or **2.2** with iodomethane or iodoethane to reflux in acetonitrile for 24 h. ¹H-NMR analysis for 1,2,4-triazolium pro-ligands **2.5** and **2.6** in (CDCl₃) showed the pre-carbenic C5-protons to be highly downfield shifted to 11.57 ppm and 11.84 ppm respectively, while the C2-protons of the imidazolium analogue **2.3** and **2.4** resonated at 10.15 ppm and 10.29 ppm respectively. The proton on the C3 carbon of the triazolium pro-ligands (situated between two nitrogen substituents) resonated at 9.17 ppm for **2.5** and 9.13 ppm for **2.6** compared with the C4-H imidazolium proton at (CDCl₃) 7.79 ppm for **2.3** and 7.84 ppm for **2.4**. These pro-ligands were used as NHC precursors for metal complex synthesis. The molecular structure of **2.5** was further confirmed by single-crystal X-ray diffraction analysis (Figure 9). The C5 – N1 and C5 – N4 bond distances were found to be 1.325 and 1.333 Å respectively, which is in agreement with literature values for 1,2,4-triazolium salts.³¹

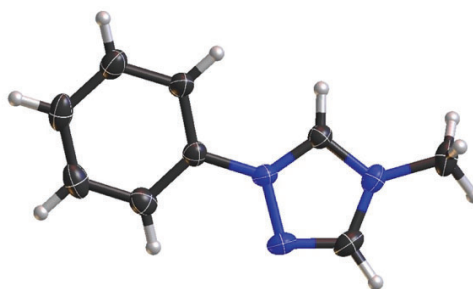
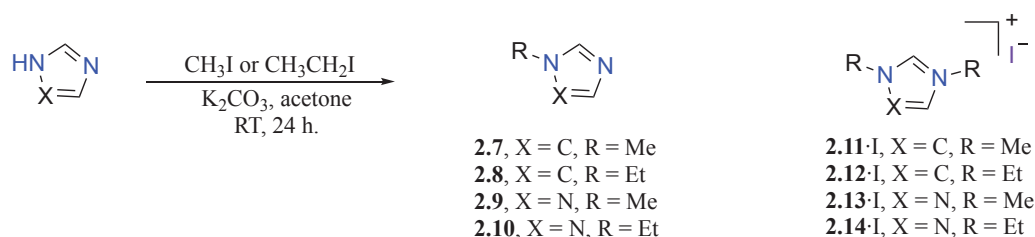


Figure 9. Representation of X-ray crystal structure of 4-methyl-1-phenyl-1*H*-1,2,4-triazolium (**2.5**) with C5-N1 and C5-N4 bond distances of 1.33 Å.



Scheme 4. Synthesis of the azolium salt pro-ligands and mono alkylated precursors.

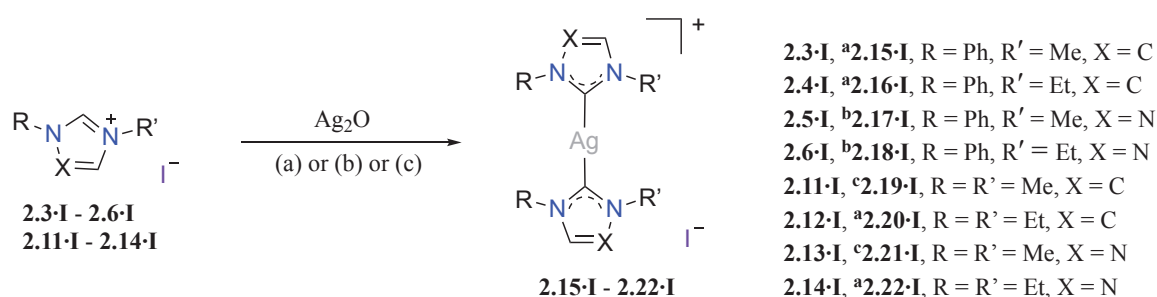
Separately, dialkyl substituted 1,2,4-triazolium and imidazolium salts (**2.11** – **2.14**, Scheme 4) were prepared by a single step using iodomethane or iodoethane in the presence of a mild base. Although several methods have been devised to achieve regioselective alkylation of *N*-heterocycles,⁹³ mono- and dialkylated azolium species can be easily separated due to the lower solubility of the 1,2,4-triazolium and imidazolium salts in organic solvents. On this basis the mono-alkylated species **2.7** – **2.10** were separated for the synthesis of *bis*-azolium pro-ligands in future steps.

Analysis of the ¹H-NMR spectra showed the hydrogen atoms on the alkyl chain linked to the nitrogens in the N1 and N3 positions of the imidazolium salts **2.11** and **2.12** are equivalent due to symmetry, whereas dissymmetry caused by the third peripheral nitrogen of the triazolium salts **2.13** and **2.14** results in separate sets of 1H signals for each of the alkyl groups. The signal corresponding to the ethyl CH₂-CH₃ group for **2.12** resonates at 4.20 ppm (DMSO-*d*⁶), whereas the signal of ethyl CH₂-CH₃ protons of the 1,2,4-triazole analogue **2.14** was observed at 4.28 ppm (N1 substituent) while the N4 CH₂-CH₃ resonance was found at 4.39 ppm. The ¹H-NMR spectra also showed the C3 proton of the triazolium salts to be significantly more downfield shifted than the C4/C5 protons of the imidazolium equivalent **2.12**. The C3-H proton of **2.14** resonated at 9.24 ppm, whereas the imidazole analogue **2.12** showed the C4/C5 protons at 7.82 ppm. The ¹³C-NMR spectrum showed the

carbon atoms adjacent to the N4 nitrogen of the triazolium units to be downfield shifted compared to the carbons adjacent to the N1 nitrogen. This finding is expected due to the positive charge on the N4 nitrogen.

2.2 Synthesis of the Silver(I) Imidazolylidene and 1,2,4-triazolylidene *N*-Heterocyclic Carbene Complexes

The silver(I) complexes **2.15** – **2.22** were prepared by treatment of the azolium salt NHC ligand precursors with silver(I) oxide in 1,2-dichloroethane at room temperature, with the exception of compounds **2.19** and **2.21** that required the addition of methanol as a co-solvent due to the low solubility of the dimethyl substituted pro-ligand salts **2.11** and **2.13** (Scheme 5). The imidazolylidene silver(I) complexes were prepared following the same procedure, however required longer reaction times and elevated temperatures. The successful formation of the complexes was confirmed by the disappearance of the pro-carbenic proton of the corresponding azolium salt in the ¹H-NMR spectrum along with the analysis of the ¹³C-NMR, and in the case of **2.17**, X-ray crystallography.



Scheme 5. Synthetic route of imidazolylidene and 1,2,4-triazolylidene silver(I) complexes (a) 1,2-dichloroethane, RT, 4 h, (b) CH₃OH/1,2-dichloroethane, RT, 4 h, (c) 1,2-dichloroethane, 60 °C, 24 h.

Single crystals of complex **2.17** were grown by slow evaporation of a solution of this compound in acetonitrile (Figure 10). The complex (Figure 10a) crystallises along an anionic silver iodide polymer (Figure 10b) in the monoclinic P2₁/n space group with two nearly identical silver(I) complexes in the single unit cell. Each silver(I) complex has C5-N1 bond lengths of (1.343 and 1.349 Å) and C5-N4 (1.352 and 1.353 Å) that are identical for each coordinating ligand to the same metal centre and are slightly longer than that of the corresponding triazolium salt **2.5** as shown in Figure 9. The phenyl rings are twisted with dihedral angles of approximately 119.8° with respect to the planar 1,2,4-triazolylidene

core and are in the same plane with respect to one another, contrasting to the 1,2,4-triazolium precursor where the phenyl ring is nearly co-planar with respect to the 1,2,4-triazolylidene heterocycle.

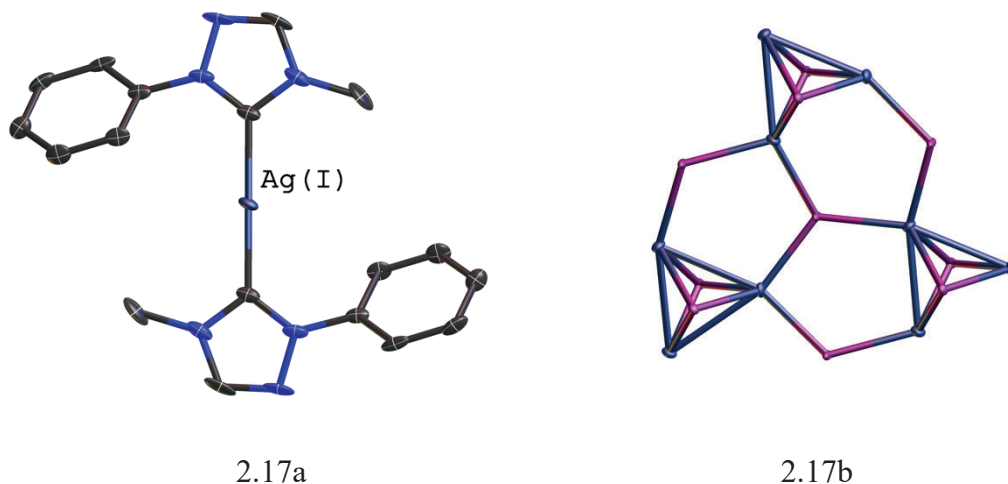
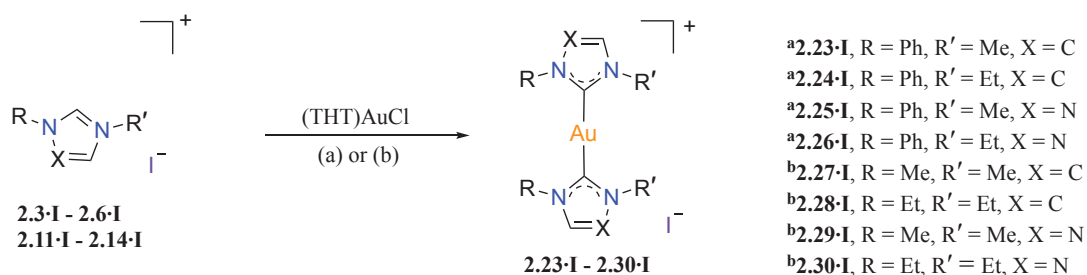


Figure 10. Representation of the molecular structure of the *bis*-1,2,4-triazolylidene silver(I) complex **2.17** (2.17a) and polymeric silver(I) iodide counterion for **2.17** (2.17b). Refer to Table S1 for crystallographic data. Hydrogen atoms have been omitted for clarity.

2.3 Synthesis of the Gold(I) Imidazolylidene and 1,2,4-triazolylidene *N*-Heterocyclic Carbene Complexes

The mononuclear gold(I) complexes **2.23** – **2.30** (Scheme 6) were prepared by reacting (THT)AuCl with two equivalents of the appropriate imidazolylidene or 1,2,4-triazolylidene by the *in-situ* deprotonation of the azolium salt precursor using a weak base in DMF at 110 °C. The phenyl substituted gold(I) complexes **2.23** – **2.26** were synthesised using sodium acetate as the base and were isolated from the reaction mixture by the addition of diethyl ether yielding the compounds as white solids that were purified further via recrystallisation with methanol. The synthesis of the *bis-N*-alkyl gold(I) complexes **2.27** – **2.30** using sodium acetate was also investigated, however only starting materials were recovered from the reaction mixtures. Complexes **2.27** – **2.30** were instead synthesised using carbonate as the base (K_2CO_3) and required longer reaction times (24 h). Although this synthetic strategy frequently produced both *bis*- and *mono*- NHC gold(I) complexes in the reaction mixture, the undesired *mono*- NHC gold(I) site product could be easily removed using fractional recrystallisation from a solvent mixture of dimethylformamide and diethyl ether to obtain the desired *bis*-NHC gold(I) complexes as iodide salts.



Scheme 6. Synthesis of the gold(I) complexes of *bis*-1,2,4-triazolyli-dene and *bis*-imidazolyli-dene ligands via reaction conditions (a) NaOAc, DMF, 110 °C, 4 h. (b) K₂CO₃, DMF, 110 °C, 24 h.

Single crystals of complex **2.24** (Figure 11) were grown in a solution of the titled complex in methanol, which was layered with diethyl ether. The X-ray crystal structure of **2.24** showed that the phenyl rings are found to have dihedral angles of 119.8(3)° and 118.8(3)° in respect to the 1,2,4-triazolyli-dene heterocycles with dihedral angles 10.7(4)° to each other. The complex adopted a slightly distorted two-linear coordinated geometry with the C5-Au-C5 angle of 174.67(13)° indicating a potential weak bonding interaction between the gold(I) and the iodide counter ion which is located 3.542 Å from the gold(I) centre (Figure 11). Single crystals of complex **2.25** were obtained by switching the anionic iodide counterion to a tetraphenylborate anion (Ph₄B⁻) as shown in Figure 12. Gold(I) complex **2.25** of 1-phenyl-4-methyl substituted *bis*-1,2,4-triazolyli-dene ligands crystallises in the triclinic crystal system in the centrosymmetric *P*-1 space group as two different polymorphs. One of the complex ions (2.25a) shows that the phenyl ring adopts a twisted noncoplanar arrangement with dihedral angles 29.2(6)° and 53.4(7)° with respect to the 1,2,4-triazolyli-dene heterocycle. The second polymorphic complex (2.25b) displays almost coplanar phenyl rings with dihedral angles of 41.6(6)° and 49.7(6)° with respect to the nearly coplanar 1,2,4-triazolyli-dene heterocycles that have dihedral angles 11.2(5)° to each other.

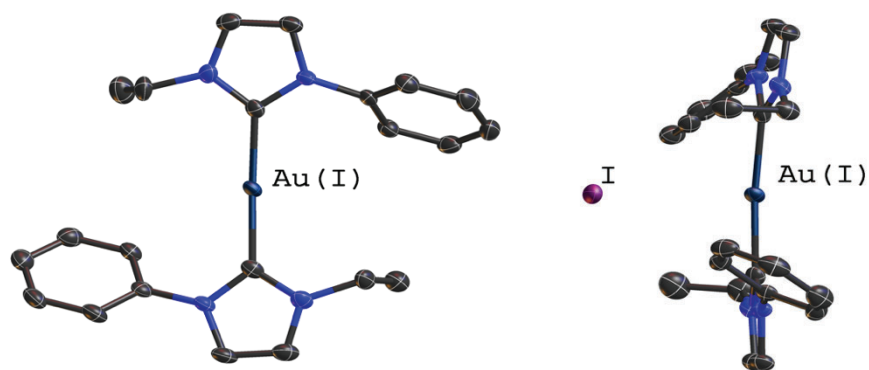


Figure 11. Representation of the molecular structure of the *bis*-imidazolylidene gold(I) complex **2.24** as an iodide salt. Hydrogen atoms have been omitted for clarity. Refer to Table S1 for crystallographic data.

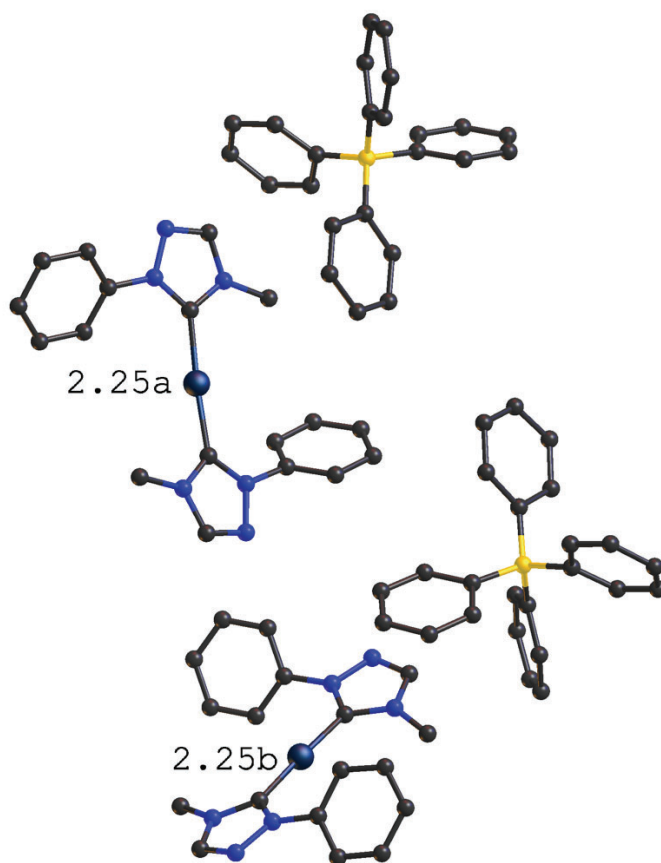
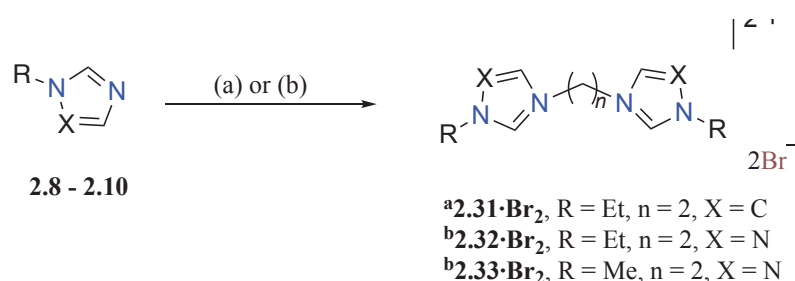


Figure 12. Representation of the single unit cell for the *bis*-1,2,4-triazolylidene gold(I) complex **2.25** as a tetraphenylborate salt. Hydrogen atoms have been omitted for clarity. Refer to Table S1 for crystallographic data.

2.4 Synthesis of the Bridged *Bis*-Imidazolium and 1,2,4-Triazolium Pro-Ligand Salts

One bridging bidentate pro-ligand with imidazolium rings and two bridging bidentate pro-ligands with 1,2,4-triazolium rings connected by ethylene bridges were synthesised from the mono-alkylated compounds **2.8** – **2.10** described previously. The ethylene linked *bis*-imidazolium salt **2.31** was prepared by reacting the *N*-ethyl imidazole **2.8** with dibromoethane in acetonitrile, whereas the ethylene linked *bis*-1,2,4-triazolium salts **2.32** and **2.33** were prepared by reacting the *N*-alkyl triazoles (**2.9** and **2.10**) with neat dibromoethane (Scheme 7). The reaction progress could be monitored by the formation of white precipitate, as both the dibromoethane and *N*-alkyl triazoles are liquids.⁹⁴

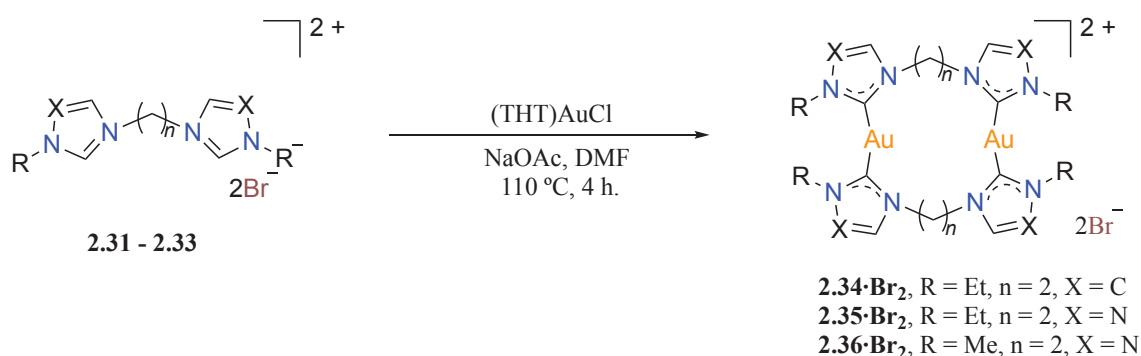


Scheme 7. Synthesis of the bridged *bis*-imidazolium or triazolium dibromide salts with ethylene linker groups. (a) dibromoethane, acetonitrile, reflux, 24 h, (b) dibromoethane, sealed, 110 °C, 4 h.

The bridged bidentate azolium pro-ligand salts were characterised by ¹H-NMR and ¹³C-NMR spectroscopy in DMSO-*d*₆. As observed by ¹H-NMR spectroscopy, the C2 proton of the ethylene linked *bis*-imidazolium salt **2.31** resonated as a singlet signal at 9.32 ppm, in a similar range to methylene linked *bis*-imidazolium pro-ligand salts previously reported by our group.⁹⁵ The C5-proton signals of the ethylene linked *bis*-triazolium salts were found more downfield compared to the imidazolium analogue at 10.21 and 10.23 ppm for **2.32** and **2.33** respectively.

2.5 Synthesis of the Dinuclear Gold(I) Imidazolylidene and 1,2,4-Triazolylidene Complexes

Three dinuclear gold(I) complexes **2.34** – **2.36** were synthesised from the bridged bidentate pro-ligands **2.31** – **2.33** (Scheme 8) and (THT)AuCl in the presence of sodium acetate as a mild base. The structures of the dinuclear gold(I) complexes were confirmed by ^1H -NMR and ^{13}C -NMR spectroscopy, while complex **2.35** was identified by ^1H -NMR, ^{13}C -NMR and X-ray crystallography.



Scheme 8. Synthesis of dinuclear gold(I) complexes of bridged *bis*-NHC ligands

2.5.1 Photoluminescent Studies

Gold(I) complexes with short attractive Auophilic interactions between the gold(I) centres within the sum of the van der Waals radii have received considerable interest for their frequent association with luminescence in the solid and solution state.⁹⁶ Mononuclear ‘unsupported’ gold(I) complexes (Figure 13) typically have linear two coordinate gold(I) centres and exist as monomeric species in solution with little or no luminescence originating from the metal centre. Short Au-Au contact can be retained in solution through ‘supported’ molecular framework in dinuclear gold(I) complexes, and solution phase luminescence that originates from the metal centres has been observed in a variety of complexes.⁹⁷ The supported structural framework and potential for this to coincide with luminescence in solution prompted us to investigate the electronic absorption and emission properties of the dinuclear gold(I) complexes synthesised in Section 2.5.

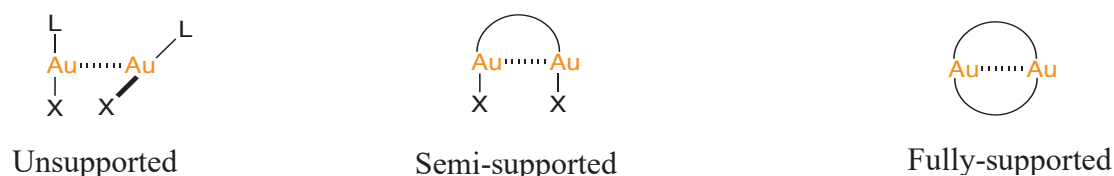


Figure 13. Unsupported, semi-supported and fully-supported types of Auophilic interactions.

A crystal structure was obtained for the ethylene bridged *bis*-triazolylidene dibromide complex **2.35** and this is depicted in Figure 14. The structure shows a twisted conformation with bromide anions that are interacting with the gold(I) metal centres at 3.75 Å and 3.52 Å. The Au-Au distance of 3.57 Å is within the sum of the van der Waals radii of 3.6 Å and can be considered an Auophilic interaction.

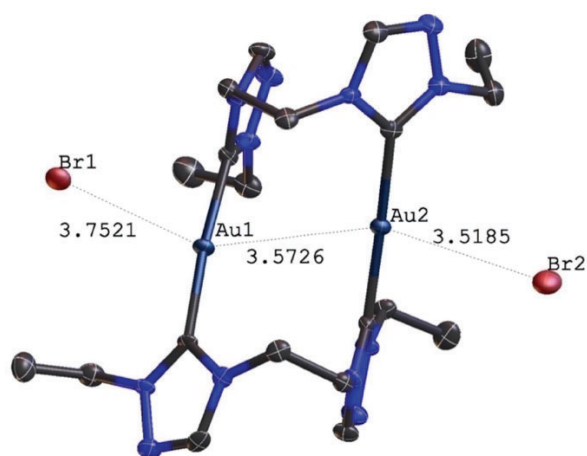


Figure 14. X-ray crystal structure of dinuclear gold(I) complex **2.35** with Au-Au distances of 3.57 Å. Hydrogen atoms have been excluded for clarity.

The excitation and steady-state emission spectra of the dinuclear gold(I) complexes of 1,2,4-triazolylidene ligands **2.35** and **2.36** was collected using a Nanolog spectrofluorometer, and these spectra are shown in Figure 15. The experiments were carried out by Laena D'Alton of the Hogan laboratory in the Department of Physics and Chemistry, La Trobe University. Complex **2.35** as seen in the crystal structure (Figure 14) was observed to have the strongest emission at 356 nm, in agreement with the previously reported solution phase luminescent properties of dinuclear gold(I) complexes with Au-Au distances less than 3.6 Å.⁹⁷ Complex **2.36** was also found to be luminescent at 364 nm with an additional weak emission peak at 430 nm, while the *bis*-triazolium salt **2.32** was found

to be non-emissive, confirming the luminescence properties of **2.35** and **2.36** are likely to originate from the short metal-metal interaction.

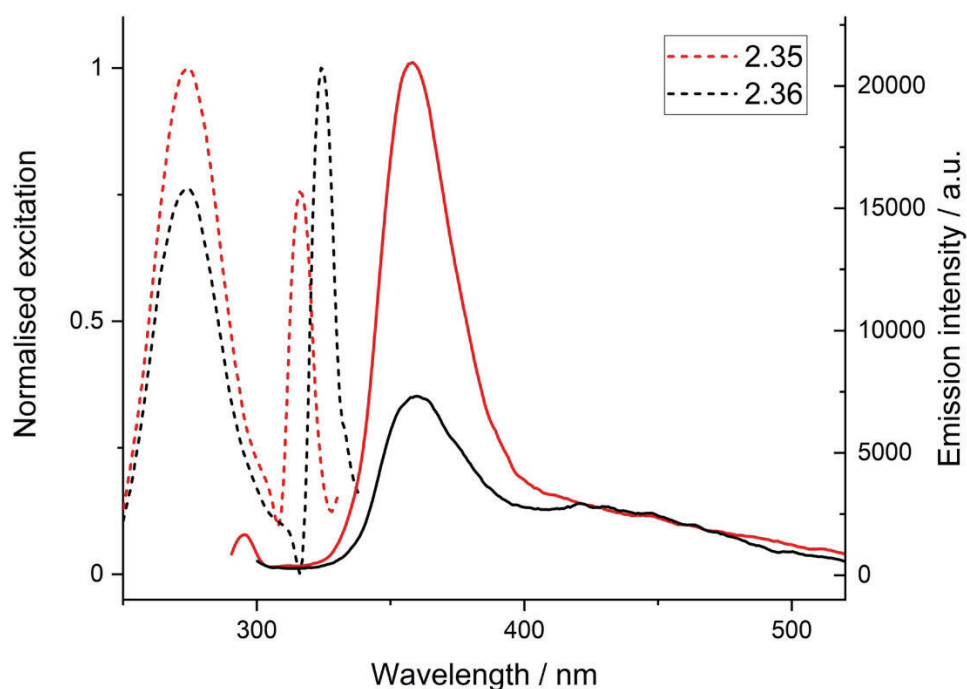


Figure 15. Room temperature electronic excitation and emission spectra for the ethylene linked dinuclear gold(I) complexes of bridged 1,2,4-triazolylidene ligands **2.35** and **2.36** excited at 273 nm for complex **2.35** and 269 nm for complex **2.36**.

2.6 Summary

A series of imidazolylidene and 1,2,4-triazolylidene NHC pro-ligands and their gold(I) and silver(I) complexes have been synthesised and characterised by ^1H -NMR and ^{13}C -NMR spectroscopy, and for **2.5**, **2.17**, **2.24**, **2.25**, and **2.35** single crystal X-ray diffraction. The successful formation of the complexes was determined by the absence of the most downfield shifted pro-carbenic proton in the ^1H -NMR spectra, as well as a downfield shift of the C2 carbon for the complexes of imidazolylidene ligands and C5 carbon for 1,2,4-triazolylidene ligands in the ^{13}C -NMR spectra. The crystal structure of complex **2.35** showed a gold-gold interaction within the sum of the van der Waals radii, and luminescence was observed upon excitation.

CHAPTER THREE

Antibacterial and Antibacterial Resistance Studies

3.1 Introduction

As a low estimate there are 700,000 deaths associated with antibacterial resistance annually that is predicted to reach 10 million by 2050.⁹⁸ This rise in antibiotic resistant bacteria has prompted a worldwide effort to develop new antibacterial treatments that are effective against pathogens resistant to current classes of antibiotics.^{99,100} The use of metal-based antibacterial compounds was largely discontinued with the appearance of the first antibiotics, however recent years have seen a renewed interest,^{10,11} and metals stabilised with *N*-heterocyclic carbenes have received considerable attention.^{21,66,10,54}

Using the gold(I) and silver(I) complexes synthesised in **Chapter 2**, antibacterial studies were performed in collaboration with the Soares Da Costa laboratory in the Department of Biochemistry and Genetics, La Trobe University. Broth microdilutions methods defined by the Clinical Laboratory Standards unit were employed to determine the Minimum Inhibitory Concentrations (MICs) of the gold(I) and silver(I) complexes of imidazolylidene and 1,2,4-triazolylidene ligands. The complexes were initially tested against two medically important Gram-positive bacteria, namely *Enterococcus faecium* 2127 and *Staphylococcus aureus* 9144. *Enterococcus faecium* 2127 is a strain resistant to copper, erythromycin, and tetracycline, but is sensitive to teicoplanin.¹⁰¹ *S. aureus* 9144 is a sensitive strain.¹⁰² Two medically significant Gram-negative bacterial strains were also tested, namely *Escherichia coli* 2340 and *Acinetobacter baumannii* 17978. *E. coli* 2340 is a strain resistant to carbapenems,¹⁰³ and *A. baumannii* 17978 is a sensitive strain.¹⁰⁴

3.2 Antibacterial Assays

The results from the antibacterial studies are summarised in Tables 1 – 3. For clarity, the silver(I) and gold(I) complex structures are included in the tables, and an abbreviation of the R-groups and corresponding heterocycle is included in the results table for the precursor pro-ligand salts. The abbreviations and positions of the R-groups on the azolium heterocycles are shown in Figure 16. Very little or no antibacterial activity was observed in the imidazolium and 1,2,4-triazolium pro-ligand precursor salts as shown in

Table 1, confirming that antibacterial activity observed for the metal complexes originates from the complex rather than the pro-ligands.

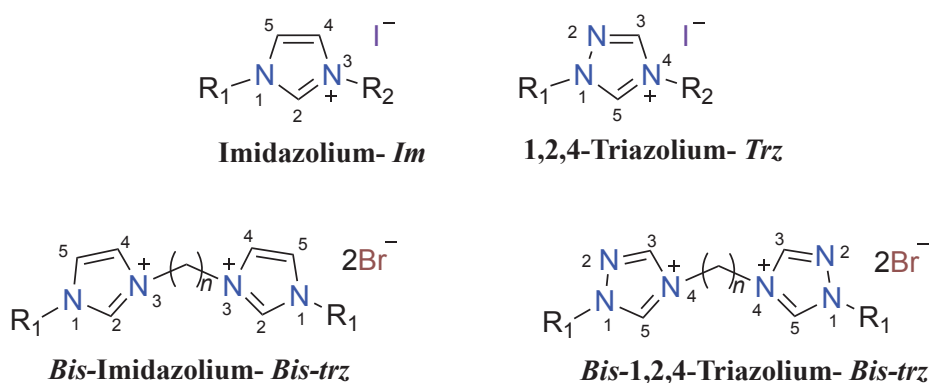


Figure 16. Position of the R-groups on imidazolium and 1,2,4-triazolium salts referred to in Tables 1– 3. Note the differences in numbering systems between the imidazolium and 1,2,4-triazolium salts.

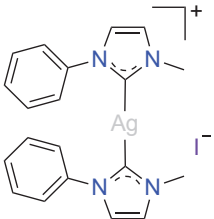
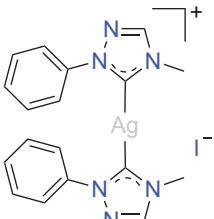
Table 1. Minimum Inhibitory Concentration (MIC $\mu\text{g}\cdot\text{mL}^{-1}$) values of the imidazolium and 1,2,4-triazolium precursor pro-ligand salts.

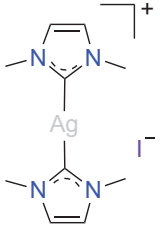
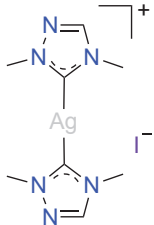
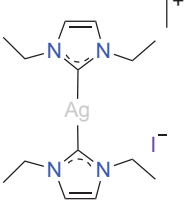
Compound	Gram-positive		Gram-negative	
	<i>E. faecium</i> ^a	<i>S. aureus</i> ^b	<i>A. baumannii</i> ^c	<i>E. coli</i> ^d
2.3_{Im} , (R ₁ = Ph, R ₂ = Me)	>128	>128	>128	>128
2.4_{Im} , (R ₁ = Ph, R ₂ = Et)	>128	>128	>128	>128
2.5_{trz} , (R ₁ = Ph, R ₂ = Me)	>128	>128	128	>128
2.6_{trz} , (R ₁ = Ph, R ₂ = Et)	>128	>128	>128	>128
2.11_{Im} , (R ₁ = R ₂ = Me)	>128	>128	>128	>128
2.12_{Im} , (R ₁ = R ₂ = Et)	>128	>128	>128	>128
2.13_{trz} , (R ₁ = R ₂ = Me)	>128	>128	>128	>128
2.14_{trz} , (R ₁ = R ₂ = Et)	>128	>128	>128	>128
2.31_{Bis-im} , (R ₁ = Et, n = 2)	>128	>128	>128	>128
2.32_{Bis-trz} , (R ₁ = Et, n = 2)	>128	>128	>128	>128

^a*E. faecium* ATCC® BAA-2127, ^b*S. aureus* ATCC® 9144™, ^c*A. baumannii* ATCC® 17978™, and ^d*E. coli* ATCC® BAA-2340™

The Minimum Inhibitory Concentrations (MICs) of the silver(I) complexes of imidazolylidene and 1,2,4-triazolylidene ligands are tabulated in Table 2. The silver(I) complexes **2.15** of 1-phenyl-3-methyl substituted imidazolylidene ligands and **2.17** of 1-phenyl-4-methyl substituted 1,2,4-triazolylidene ligands were found to have significantly different antibacterial activity, where **2.15** showed MICs against *E. faecium* ($64 \mu\text{g}\cdot\text{mL}^{-1}$) and *A. baumannii* ($16 - 32 \mu\text{g}\cdot\text{mL}^{-1}$), while **2.17** was found to have MICs $>128 \mu\text{g}\cdot\text{mL}^{-1}$ against all bacterial strains tested. Differences in antibacterial activity between the silver(I) complexes of dimethyl imidazolylidene and 1,2,4-triazolylidene ligands was also observed, where **2.19** of imidazolylidene ligands was found to have MICs against *E. faecium* ($>128 \mu\text{g}\cdot\text{mL}^{-1}$) and *A. baumannii* ($8 \mu\text{g}\cdot\text{mL}^{-1}$) whereas **2.21** of 1,2,4-triazolylidene ligands displayed MICs against *E. faecium* ($32 - 64 \mu\text{g}\cdot\text{mL}^{-1}$) and *A. baumannii* ($2 \mu\text{g}\cdot\text{mL}^{-1}$). The diethyl substituted silver(I) complex of imidazolylidene ligands **2.20** was found to have antibacterial activity against *A. baumannii* of ($2 \mu\text{g}\cdot\text{mL}^{-1}$), but results could not be obtained for the analogous diethyl substituted silver(I) complex of 1,2,4-triazolylidene ligands **2.22** which could not be tested due to poor solubility in aqueous solution. The phenyl-ethyl substituted silver(I)-NHC complexes **2.16** and **2.18** were also not tested due to poor solubility, highlighting the importance for future antibacterials of this type to be designed with aqueous solubility in mind.

Table 2. Minimum Inhibitory Concentration (MIC $\mu\text{g}\cdot\text{mL}^{-1}$) values of the silver(I) complexes.

Complex	Structure	Gram-positive		Gram-negative	
		<i>E. faecium</i> ^a	<i>S. aureus</i> ^b	<i>A. baumannii</i> ^c	<i>E. coli</i> ^d
2.15_{im}		64	>128	16 – 32	128
2.17_{trz}		>128	>128	>128	>128

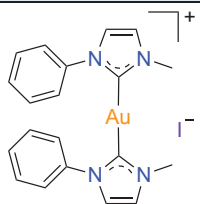
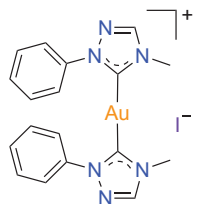
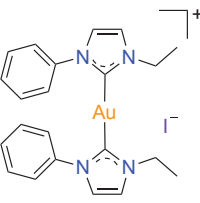
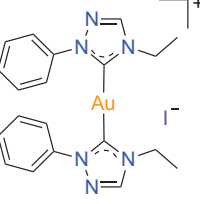
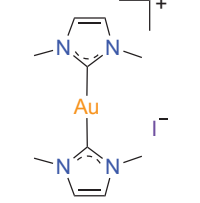
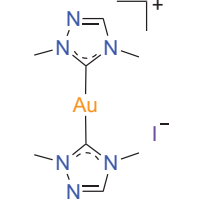
2.19_{im}		>128	>128	8	16
2.21_{trz}		32 – 64	>128	2	16
2.20_{im}		>128	>128	2 – 4	>128

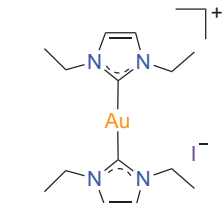
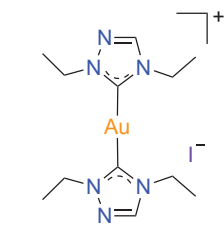
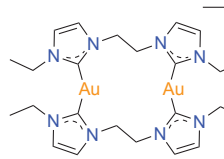
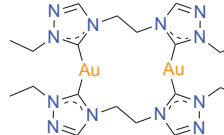
^a*E. faecium* ATCC® BAA-2127™, ^b*S. aureus* ATCC® 9144™, ^c*A. baumannii* ATCC® 17978™, and ^d*E. coli* ATCC® BAA-2340™.

The antibacterial activity of the gold(I) complexes of imidazolylidene and 1,2,4-triazolylidene ligands is shown in Table 3. In agreement with recent literature, the mononuclear gold(I)-NHC complexes (**2.23** – **2.30**) were found to have greater antibacterial activity against Gram-positive strains in comparison to the silver(I)-NHC complexes which displayed greater activity against Gram-negative bacteria.^{26,61} The dinuclear gold(I)-NHC complexes **2.34** and **2.35** displayed very little or no antibacterial activity against all strains tested, in agreement with recently published work by our group on similar imidazolylidene based dinuclear gold(I)-NHC complexes.⁹⁵ The 1-phenyl substituted gold(I)-NHC complexes **2.23** – **2.26** inhibited growth of the Gram-positives *E. faecium* and *S. aureus* at low microgram concentrations, and interestingly, the 1-phenyl-4-methyl substituted gold(I) complexes **2.25** and **2.26** of 1,2,4-triazolylidene ligands were found to have the best antibacterial activity against both Gram-positives and Gram-negative bacterial strains of the compounds tested. The gold(I)-NHC complexes of dimethyl or diethyl *N*-substituents (**2.27** – **2.30**) were found to have substantially lower antibacterial activity against all bacterial strains tested in comparison to the 1-phenyl substituted gold(I)-NHC complexes **2.23** – **2.26**. The greater antibacterial activity for phenyl-substituted compounds has been previously observed in a recent study by Ott and co-workers who showed that compound

1.12 (Figure 6, R = H) displayed a MIC of 57.2 $\mu\text{g}\cdot\text{mL}^{-1}$ for multidrug resistant *S. aureus* (MRSA) RKI 11-02670 and 45.2 $\mu\text{g}\cdot\text{mL}^{-1}$ against MRSA DSM 11822, whereas compound **1.14** (R = Ph) yielded MICs of 1.7 $\mu\text{g}\cdot\text{mL}^{-1}$ and 1.3 $\mu\text{g}\cdot\text{mL}^{-1}$ for these strains, respectively.^{26,61}

Table 3. Minimum Inhibitory Concentration (MIC $\mu\text{g}\cdot\text{mL}^{-1}$) values of the gold(I) complexes.

Complex	Structure	Gram-positive		Gram-negative	
		<i>E. faecium</i> ^a	<i>S. aureus</i> ^b	<i>A. baumannii</i> ^c	<i>E. coli</i> ^d
2.23_{im}		64	4 – 8	128	>128
2.25_{trz}		4 – 8	2	32	64
2.24_{im}		32	2	64 – 128	>128
2.26_{trz}		8	2	64	64
2.27_{im}		64 – 128	>128	>128	>128
2.29_{trz}		64 – 128	32	128	64 – 128

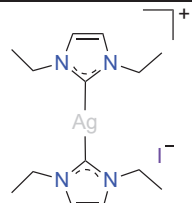
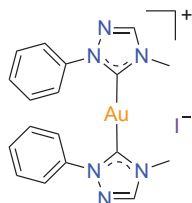
2.28_{im}		32 – 64	32	>128	>128
2.30_{trz}		128 – 64	64	>128	>128
2.34_{im}		>128	>128	>128	>128
2.35_{trz}		>128	>128	128	>128

^a*E. faecium* ATCC® BAA-2127™, ^b*S. aureus* ATCC® 9144™, ^c*A. baumannii* ATCC® 17978™, and ^d*E. coli* ATCC® BAA-2340™.

3.3 Assays Against Antibiotic Resistant Bacterial Strains

Two of the most active silver(I) and gold(I) complexes of imidazolylidene and 1,2,4-triazolylidene ligands were selected and further antibacterial assays were conducted to determine the MICs against bacterial strains with higher levels of antibiotic resistance. The strains were selected using the WHO list of priority pathogens with increasingly high levels of resistance to antibacterial treatments. Two Gram-positive bacterial strains were selected, namely *Enterococcus faecium* ATCC 700221 that is vancomycin resistant and *Staphylococcus aureus* BAA-1720 that is a methicillin resistant, vancomycin sensitive strain.^{105,106} Two Gram-negative bacterial strains were also selected namely *A. baumannii* BAA-1710 resistant to a wide range of antibiotics along with *E. coli* K12 which is a sensitive strain, (the ATCC BAA-2340 strain initially used is carbapenem resistant).^{107,108} As shown in Table 4, the silver(I) complex **2.20** of imidazolylidene ligands and gold(I) complex **2.25** of 1,2,4-triazolylidene ligands were found to have similar antibacterial activity in comparison to the results shown in Table 3, confirming that these metal-based antibacterial complexes are effective against multi-drug resistant bacterial pathogens.

Table 4. Minimum Inhibitory Concentration (MIC $\mu\text{g}\cdot\text{mL}^{-1}$) values of two of the best performing silver(I) and gold(I) antibacterial complexes against bacterial strains with higher levels of antibacterial resistance (except for *E. coli* K12 that is a sensitive strain).

Complex	Structure	Gram-positive		Gram-negative	
		<i>E. faecium</i> ^a	<i>S. aureus</i> ^b	<i>A. baumannii</i> ^c	<i>E. coli</i> ^d
2.20_{im}		64 – 128	>128	2	64 – 128
2.25_{trz}		4 – 8	4	32	16 – 32

^a*E. faecium* ATCC® 700221™, ^b*S. aureus* BAA-1720™, ^c*A. baumannii* BAA-1710™, and ^d*E. coli* K12™

3.4 Antibacterial Resistance Studies

Encouraged by the antibacterial activity of the gold(I) and silver(I)-NHC complexes **2.25** and **2.20** against drug resistant bacterial pathogens shown in Table 4, an investigation into the propensity for sensitive bacteria to develop resistance was performed. Two bacterial strains were used, namely *A. baumannii* 17978 and *E. faecium* 2127 that were continuously exposed to **2.20** and **2.25** using the extended gradient MIC method.¹⁰⁹ Starting at $0.25 \times$ the MIC of each antibacterial NHC-complex (Table 2 – Table 3), the concentration was incrementally increased up to $4 \times$ the MIC over a period of two weeks. A 1% (v/v) DMSO negative treatment control along with a positive treatment control using ciprofloxacin was also performed concurrently. After the two-week period, the MIC values of **2.20**, **2.25** and ciprofloxacin were determined using two biological replicates that were compared to the values for the DMSO-treatment controls to determine the fold-change in MIC values.

No change in the MIC of the silver(I)-NHC complex **2.20** against *A. baumannii* 17978 was observed after the two-week period of exposure, indicating that *A. baumannii* 17978 did not develop resistance to **2.20**, while an 8 – 16-fold increase in MIC was observed against

the broad-spectrum antibacterial ciprofloxacin. Similarly, *E. faecium* 2127 did not develop resistance to the gold(I)-NHC complex **2.25** over the two-week period whereas a 16-fold increase in MIC was observed against ciprofloxacin. The results from the antibacterial resistance study are in agreement with previous literature stating that the possible mechanisms of resistance to metals are limited,¹⁶⁻¹⁸ however to the best of our knowledge this is the first time a lack of bacterial resistance to metal complexes of this type has been demonstrated.

CHAPTER FOUR

An Investigation into the Stability of the Synthesised Antibacterial Gold(I) and Silver(I) *N*-Heterocyclic Carbene Complexes

4.1 Stability Studies Using ESI-HR-MS

The ability to control the degree of ion excitation by changing the potential between the capillary and the skimmer in the ESI source has been previously used to examine the fragmentation of metalloorganic and supramolecular noncovalent complexes.¹¹⁰⁻¹¹³ Kinetic energy and consequentially collision energy can be influenced significantly by the fragmentor, or cone voltage (CV) by changing the ion velocity of the initially sprayed charged particles.¹¹³ To examine differences in gas-phase stability of the gold(I) and silver(I) complexes of imidazolyliidene and 1,2,4-triazolyliidene ligands, a systemic investigation of variations in the ESI CV was performed using an Agilent 6530 series Accurate-Mass Q-TOF LC/MS in the positive ion mode. The CV effect on fragmentation was examined by varying the CV from 0 V to 370 V in 5 V intervals and 1 V intervals to identify points of substantial changes in fragmentation. In this study, the silver(I)-NHC complexes showed only their corresponding pro-ligands in the HR-MS (even at very low voltages) and the parent complexes could not be analysed using this method. The effect of CV variation on the gold(I)-NHC complexes can be seen for **2.23** in Figure 17 and **2.25** in Figure 18.

Gold(I) complex **2.23** (m/z 513.1539) of imidazolyliidene ligands with the form $[\text{Au}(\text{NHC})_2]^+$ begins fragmenting into the mono-ligand complex of the form $[\text{Au}(\text{NHC})]^+$ (m/z 355.0768) at a CV of 281 V and the relative abundance of this species increased substantially by 284 V. As the CV increases from 284 – 354 V the relative abundance of the intact complex decreases and then disappears at 354 – 355 V. The gold(I) complex **2.25** of 1,2,4-triazolyliidene ligands (m/z 515.1258) begins fragmenting into the mono-ligand complex (m/z 356.0607) at lower CV of 260 V, and the ion corresponding to the intact complex was no longer observed as the CV was increased to 285 – 286 V. An ion corresponding to Au^+ (m/z 196.9666) could be observed for both **2.23** and **2.25** at high cone voltages (> 355 V) (Refer to S74 SI for stacked HR-MS-chromatograms).

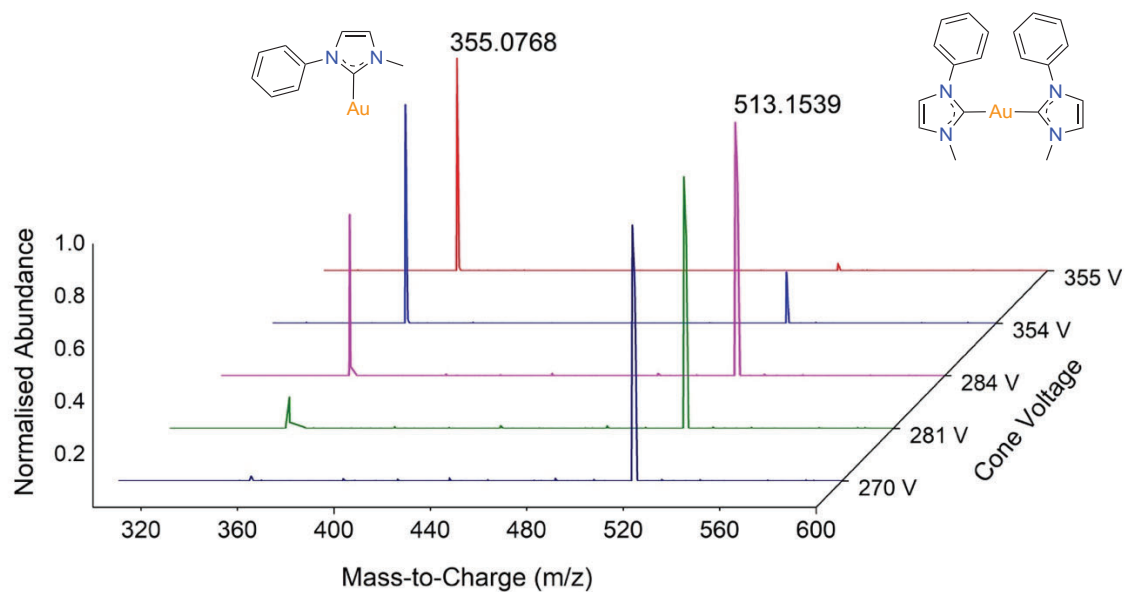


Figure 17. Normalised ESI-HR-MS plots at selected cone voltages for gold(I) complex of *bis*-1-phenyl-3-methyl-imidazolyli-dene ligands **2.23**.

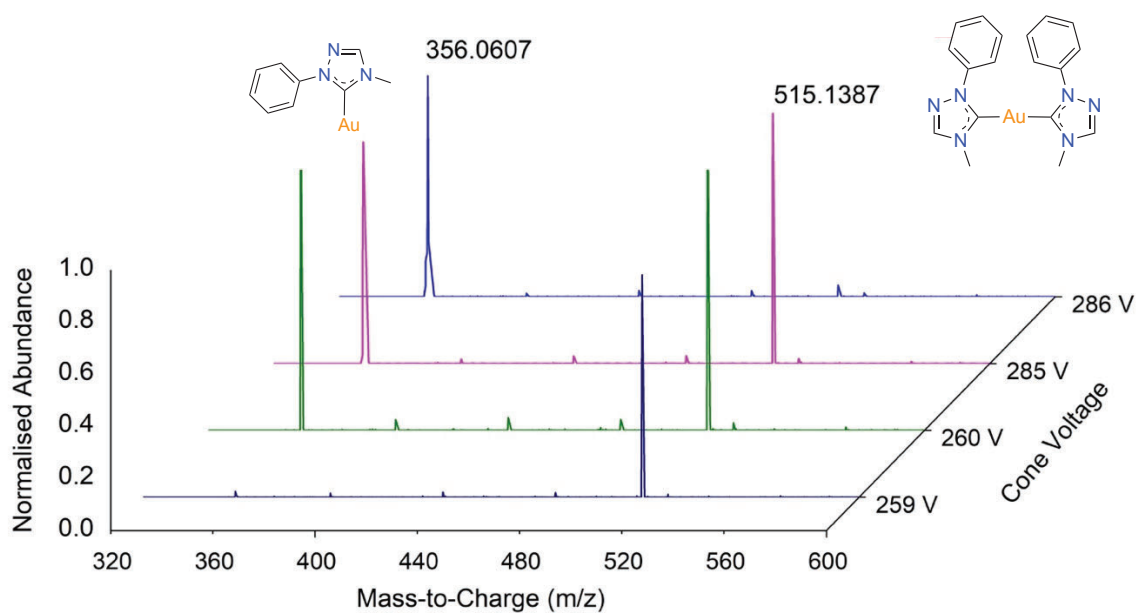


Figure 18. Normalised ESI-HR-MS plots at selected cone voltages for gold(I) complex of *bis*-1-phenyl-4-methyl-1,2,4-triazolyli-dene ligands **2.25**.

The observation that gold(I) complex **2.23** fragmented at higher cone voltages than the analogous gold(I) complex **2.25** inspired further investigation into gold(I) complexes of imidazolyli-dene and 1,2,4-triazolyli-dene ligands with different *N*-substituents. The gold(I) complexes **2.28** and **2.30** of diethyl substituted imidazolyli-dene and 1,2,4-triazolyli-dene

ligands were investigated using the same experimental technique of incrementally increasing the CV as shown in Figure 19 and Figure 20. Both of the diethyl substituted gold(I)-NHC complexes fragmented into mono-ligand complexes at lower CVs (227 V for **2.28** and 210 V for **2.30**) in comparison to the 1-phenyl substituted complexes **2.23** and **2.25**. Complexes **2.28** and **2.30** displayed behaviour consistent with the phenyl-methyl substituted gold(I) complexes **2.23** and **2.25**, in that fragmentation of the intact complexes occurred at higher voltages for the imidazolylidene complexes in comparison to the 1,2,4-triazolylidene complexes. The diethyl substituted gold(I)-NHC complexes also fragmented yielding Au^+ at high CV values (along with a number of unidentified ions) (Figure 19 and Figure 20).

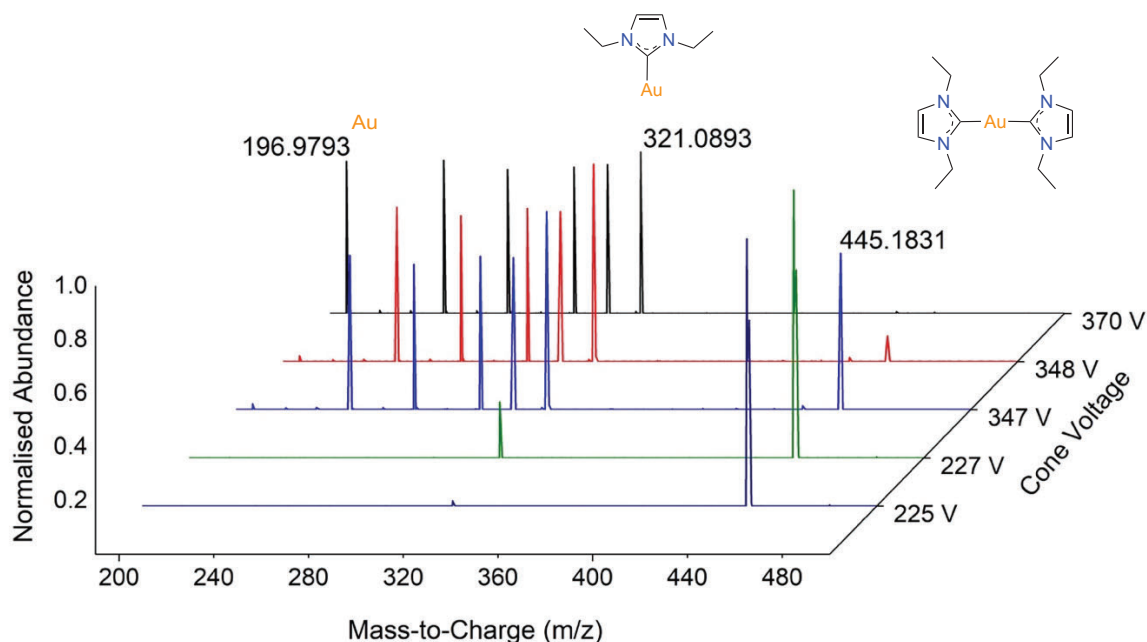


Figure 19. Normalised ESI-HR-MS plots at selected cone voltages for gold(I) complex of *bis*-1,3-diethyl-imidazolylidene ligands **2.28**.

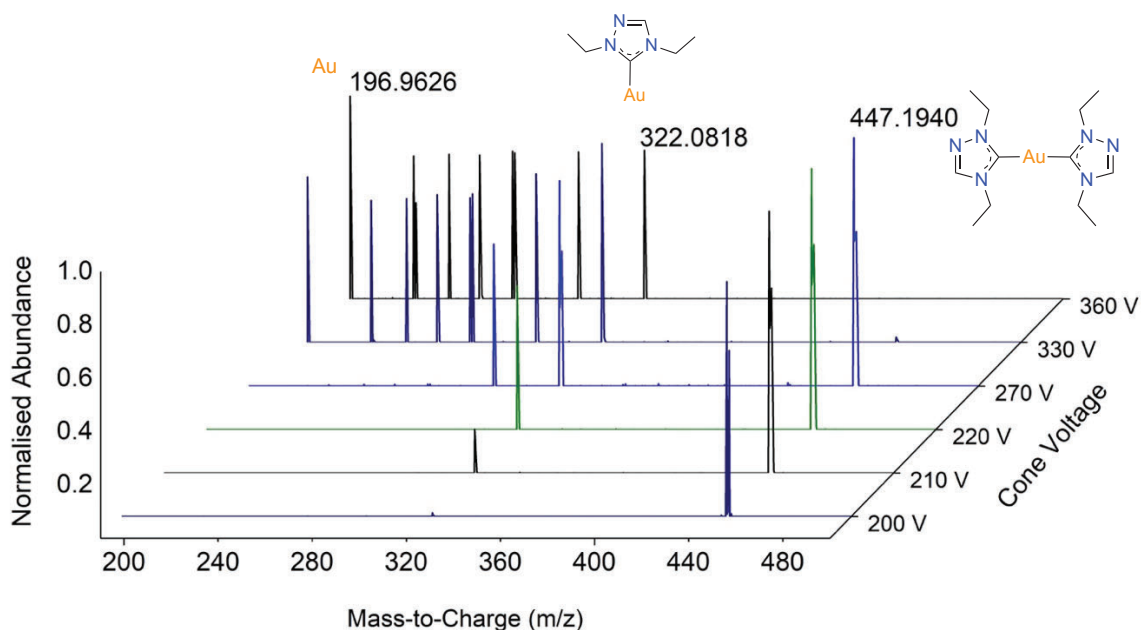


Figure 20. Normalised ESI-HR-MS plots at selected cone voltages for gold(I) complex of *bis*-1,4-diethyl-1,2,4-triazolylidene ligands **2.30**.

Based on the trends in fragmentation, it can be postulated that the carbene-gold bond dissociation energy (BDE) for the gold(I) complexes of imidazolylidene ligands may be higher than that of the gold(I) complexes of 1,2,4-triazolylidene ligands. The *N*-substituents on the imidazolylidene and 1,2,4-triazolylidene ligands may also influence the BDE, as both of the diethyl substituted gold(I) complexes fragmented into the mono-ligand complexes at lower voltages than the phenyl-methyl substituted complexes. These experimental results indicating potential differences in stability of the gold(I)-NHC complexes prompted a further investigation into the stability of the metal-NHC bonds using theoretical calculations.

4.2 Theoretical Stability Studies

Density functional theory (DFT) calculations were utilised to investigate the bond dissociation energies (BDE) of the carbene-metal bonds for the gold(I) and silver(I) complexes of imidazolylidene and 1,2,4-triazolylidene *N*-heterocyclic carbene ligands. In an initial experiment, methyl groups were used for computational efficiency. The geometries were optimised at the M06-L/def2svp level of theory, followed by single point energy calculations on the optimised structures at the M06-L/def2tzvpp level of theory. To obtain results in agreement with previously reported bond dissociation energies (BDEs) for metal complexes of this type, the inclusion of solvent effects was found to be vital and was

introduced via the polarizable continuum model (PCM). To further ensure accuracy of the theoretical techniques, the BDE of a previously reported gold(I) complex of *bis*-benzimidazolylidene ligands was calculated and found to be in a very similar range to the previously reported values.¹¹⁴ The geometry optimisation calculations confirmed the expected linear coordinated geometry, and each azolium heterocycle was found to be in the same plane to each other. The BDEs of the NHC-metal bonds are tabulated in Table 5.

The calculated BDE values were found to be in agreement with the well known property of silver-NHC complexes having lower BDEs than corresponding gold-NHC complexes.¹¹⁴ The BDE of the complexes with 1,2,4-triazolylidene ligands were found to be lower in energy than the complexes of imidazolylidene ligands (16.37 kJ/mol less for gold(I)-1,2,4-triazolylidene complex **2.29** and 11.29 kJ/mol less for the silver(I) 1,2,4-triazolylidene complex **2.21**).

Table 5. BDEs of the Metal-NHC bonds of gold(I) and silver(I) complexes of NHC ligands with methyl *N*-substituents.

Complex	BDE (kJ·mol ⁻¹)
2.19 (Ag-NHC _{2im})	111.43
2.21 (Ag-NHC _{2trz})	100.14
2.27 (Au-NHC _{2im})	231.04
2.29 (Au-NHC _{2trz})	214.67
Au-NHC _{2benz-im}	224.78
*Au-NHC _{2benz-im}	225.39

*Previous literature value *bis*-benzimidazole gold(I) complex of imidazolium ligands.¹¹⁴

The BDE of the gold(I) and silver(I)-NHC complexes was further investigated using complexes that displayed a greater variation in antibacterial activity between the complexes of imidazolylidene and 1,2,4-triazolylidene ligands. Antibacterial activity was observed for silver(I) complex **2.15** of 1-phenyl-4-methyl substituted imidazolylidene ligands with MICs against *E. faecium* (64 µg·mL⁻¹) and *A. baumannii* (16 – 32 µg·mL⁻¹), while its silver(I) 1,2,4-triazolylidene analogue **2.17** displayed MICs of >128 µg·mL⁻¹ against all strains tested. The gold(I)-NHC complexes with phenyl-methyl *N*-substituents (**2.23** and **2.25**) were also investigated as the gold(I) complex **2.25** displayed notably greater antibacterial activity against *E. faecium* (4 – 8 µg·mL⁻¹ for **2.25** and 64 µg·mL⁻¹ for **2.23**)

and also displayed greater antibacterial activity against all strains tested compared to its imidazolylidene analogue **2.23** (refer to Table 3, Section 3.2, **Chapter 3** for MICs).

The geometries were optimised starting from crystal structures of the silver(I) complex **2.17** and the gold(I) complex **2.25** (Section 2.3, **Chapter 2**) as shown in Figure 21. Geometries of the gold(I) and silver(I) complexes **2.15** and **2.23** were optimised by changing the nitrogen atom in the 2' position of the 1,2,4-triazolylidene ligand to a carbon atom, and single point energy calculations were carried out on all of the optimised structures.

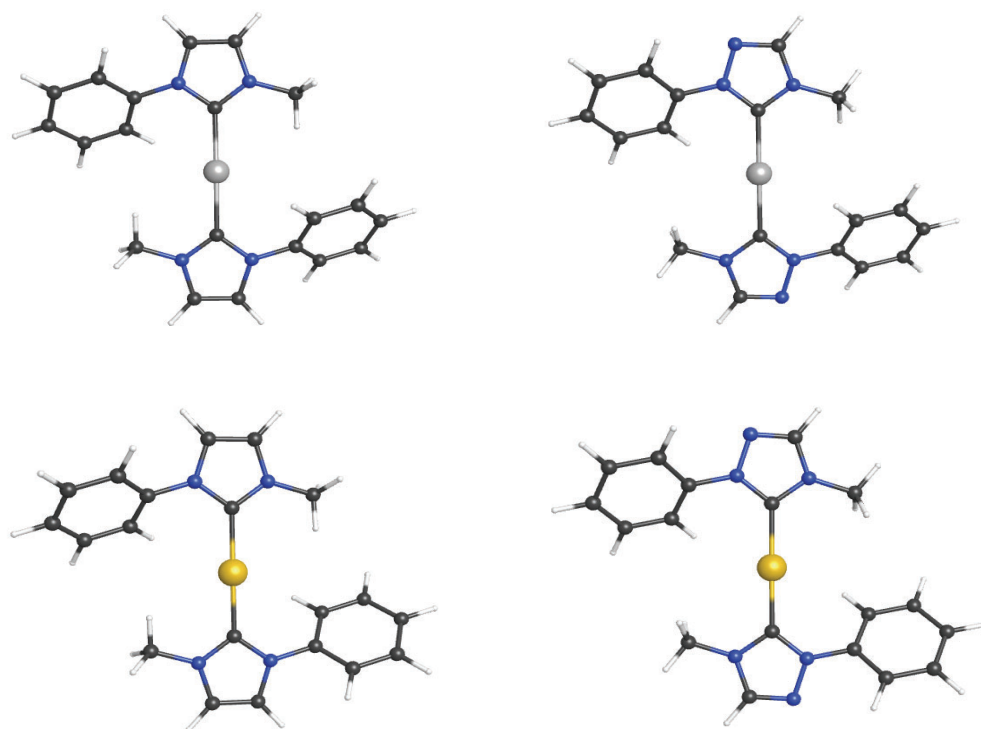


Figure 21. Optimised structures of the 1-phenyl-3-methyl substituted imidazolylidene and 1-phenyl-4-methyl substituted 1,2,4-triazolylidene gold(I) and silver(I) complexes **2.15**, **2.17**, **2.23** and **2.25**.

The 1-phenyl-3-methyl substituted imidazolylidene and 1-phenyl-4-methyl substituted 1,2,4-triazolylidene complexes were found to have lower BDEs in comparison to the dimethyl substituted complexes as shown in **Table 6**. In agreement with the results obtained for the NHC complexes with methyl-*N*-substituents, silver(I) and gold(I) complexes **2.15** and **2.23** displayed higher BDEs in comparison to their 1-phenyl substituted 1,2,4-triazolylidene analogues **2.17** and **2.25**. The experimental and theoretical results investigating the stability of the gold(I) and silver(I)-NHC complexes prompted a further investigation into the aqueous stability of these complexes.

Table 6. BDEs of the metal-NHC bonds of the gold(I) and silver(I) complexes of 1-phenyl-3-methyl imidazolylidene and 1-phenyl-4-methyl substituted 1,2,4-triazolylidene ligands.

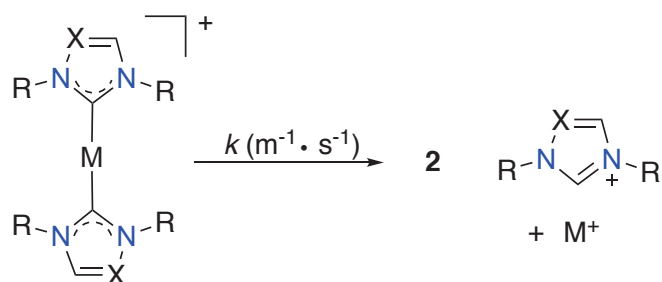
Complex	BDE (kJ·mol ⁻¹)
2.15 (Ag-NHC _{2im})	107.81
2.17 (Ag-NHC _{2trz})	91.41
2.23 (Au-NHC _{2im})	223.69
2.25 (Au-NHC _{2trz})	204.70

4.3 Experimental Stability Studies Using WATERGATE ¹H-NMR

Many medicinal compounds undergo chemical changes in aqueous physiological conditions, and the decomposition rate of silver(I) and gold(I) metallodrugs frequently coincide with biological activity as previously discussed. The steady release of the silver(I) ion in aqueous physiological conditions is widely reported to be responsible for the antibacterial activity of silver(I)-NHC complexes, although antibacterial activity for intact silver(I)-NHCs has also been reported.¹¹⁵ The decomposition rate of antibacterial silver(I)-NHC complexes is therefore of significant importance for the design of antibacterial silver(I)-NHC complexes. The aqueous stability of gold(I)-NHC complexes is also significant, largely due to the tendency of gold(I) complexes of NHC ligands to undergo ligand exchange reactions with cysteine and selenocysteine amino acids under physiological conditions.⁷⁶

To assess the stability of the gold(I) and silver(I) complexes of *N*-heterocyclic carbene ligands in aqueous environments, WATERGATE ¹H-NMR spectroscopy studies were performed. Decomposition of the complexes (Scheme 9) was observed by monitoring time dependent changes in the ¹H-NMR resonances of the H4/H5 protons for imidazolylidene and H3 protons for 1,2,4-triazolylidene-based complexes. As shown in Figure 22, no degradation was observed in the ¹H-NMR WATERGATE spectra of complex **2.25** over a time period of 21 days. Degradation was not observed for the analogous gold(I)-complex

2.23 of 1-phenyl-3-methyl imidazolylidene ligands over the same time period in agreement with the theoretically calculated high BDEs of **2.23** and **2.25** shown in Table 6.



Scheme 9. Overall reaction mechanism for the decomposition of silver(I) and gold(I) complexes of NHC ligands.

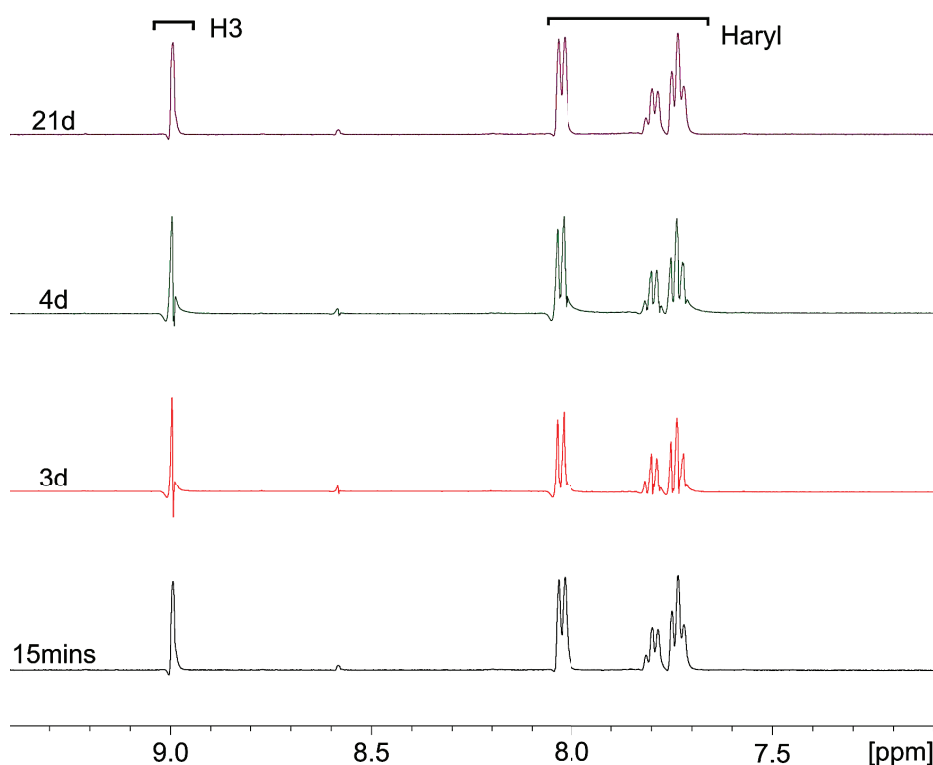


Figure 22. ^1H -NMR spectra recorded at the indicated times for gold(I)-NHC complex **2.25** at 37 °C in 300 μL $\text{DMSO-}d_6$ and 300 μL H_2O . No degradation was observed over a time period of 21 days.

The ^1H -NMR WATERGATE spectra of silver(I) complex **2.15** showed a small amount of degradation immediately upon contact with water and then continuously degraded into the ligand over a period of 25 days as shown in Figure 23. In contrast, the silver(I) complex **2.17** of 1-phenyl-4-methyl substituted 1,2,4-triazolylidene ligands (Figure 24) appeared to

degrade entirely into its precursor pro-ligand almost immediately. The signal corresponding to the pro-carbenic peak of **2.15** did not re-appear upon degradation from **2.15** into its corresponding pro-ligand **2.3**, while the pro-carbenic peak of **2.17** slowly appeared and became sharper over a period of five days.

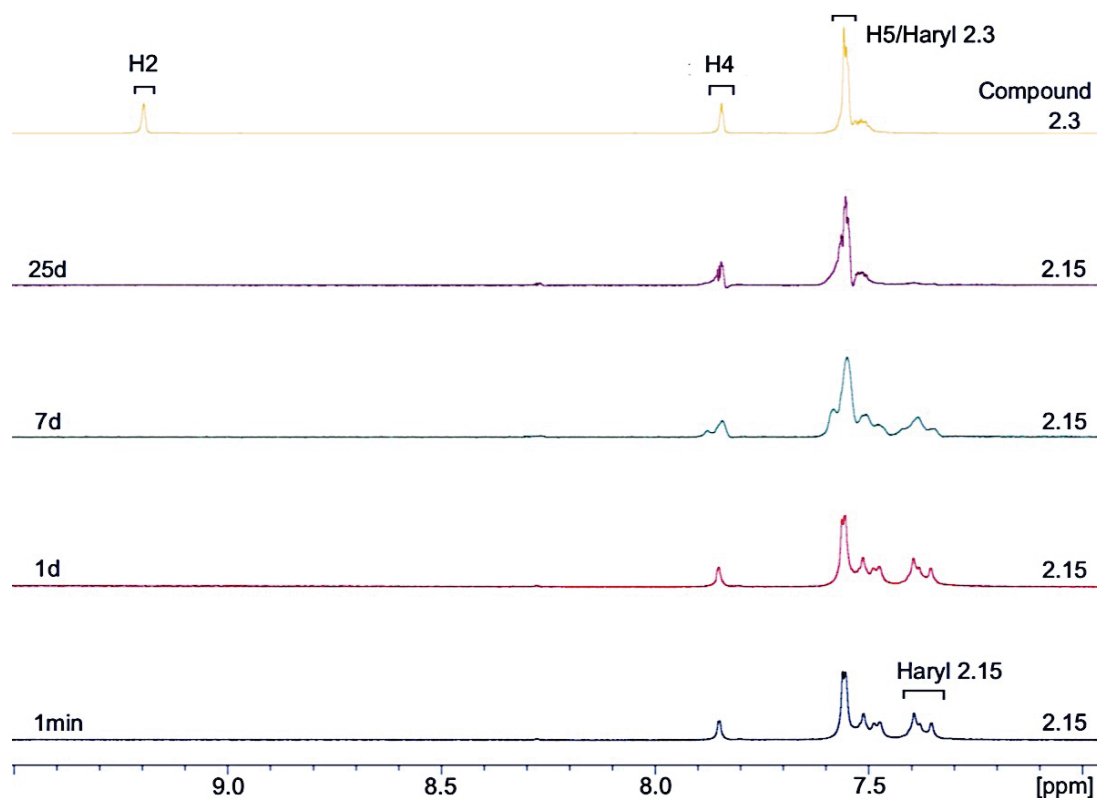


Figure 23. ^1H -NMR spectra recorded at the indicated times for silver(I)-NHC complex **2.15** at 37 °C in 300 μL $\text{DMSO-}d_6$ and 300 μL H_2O . The precursor pro-ligand **2.3** is included for visual comparisons in the same solvent system.

Interestingly the silver(I) complex **2.17** of 1,2,4-triazolylidene ligands displayed antibacterial activity $>128 \mu\text{g}\cdot\text{mL}^{-1}$ against all bacterial strains tested, whereas the equivalent silver(I) complex **2.15** of imidazolylidene ligands displayed MICs against *E. faecium* ($64 \mu\text{g}\cdot\text{mL}^{-1}$) and *A. baumannii* ($16 - 32 \mu\text{g}\cdot\text{mL}^{-1}$). The differences in antibacterial activity between silver(I) complexes **2.15** and **2.17** may be attributed to differences in the stability of these complexes as observed in the WATERGATE ^1H -NMR (Figure 23, Figure 24) and the theoretically calculated BDEs (Table 6).

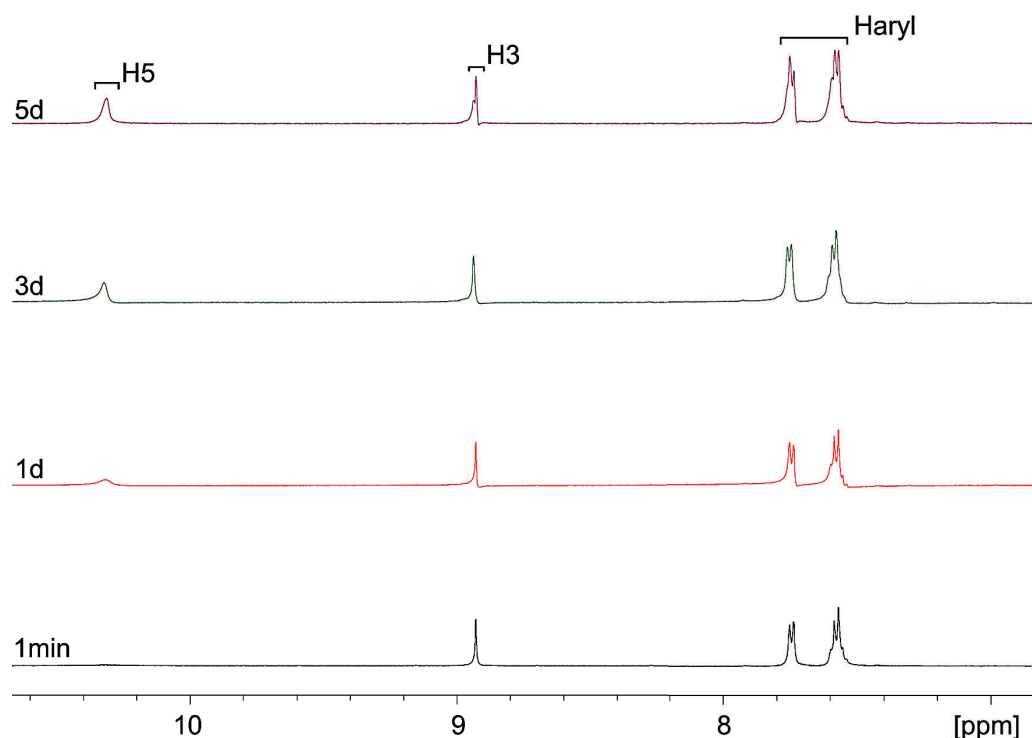


Figure 24. ^1H -NMR spectra recorded at the indicated times for silver(I)-NHC complex **2.17** at 37 °C in 300 μL $\text{DMSO-}d_6$ and 300 μL H_2O .

WATERGATE ^1H -NMR was also performed on the dimethyl substituted silver(I)-NHC complexes, where notable differences in antibacterial activity were observed between the complexes of imidazolylidene and 1,2,4-triazolylidene ligands. The dimethyl complex of 1,2,4-triazolylidene ligands **2.19** showed MIC values of $2\ \mu\text{g}\cdot\text{mL}^{-1}$ against *A. baumannii* and $32 - 64\ \mu\text{g}\cdot\text{mL}^{-1}$ against *E. faecium*, while the dimethyl imidazolylidene complex **2.21** showed MIC values of $8\ \mu\text{g}\cdot\text{mL}^{-1}$ and $>128\ \mu\text{g}\cdot\text{mL}^{-1}$ against *A. baumannii* and *E. faecium* respectively. The silver(I) complex of dimethyl substituted imidazolylidene ligands **2.19** quickly degraded into 65% precursor pro-ligand upon addition of water, and then slowly degraded to 80% precursor pro-ligand over a period of 24 days. Monitoring the degradation of silver(I) complex of dimethyl substituted 1,2,4-triazolylidene ligands **2.21** was somewhat challenging due to the broad nature of the H3 proton signal, however integration of the H3 signal indicated that **2.21** had broken down into approximately 27% precursor pro-ligand **2.13** after a period of 23 days as shown in Figure 25. The slower degradation of **2.21** in comparison to **2.19** may be related to the greater antibacterial activity observed for **2.21**, in agreement with previous literature stating a slow release of silver(I) ions is responsible for the antibacterial activity of silver(I) based medications.^{53,54}

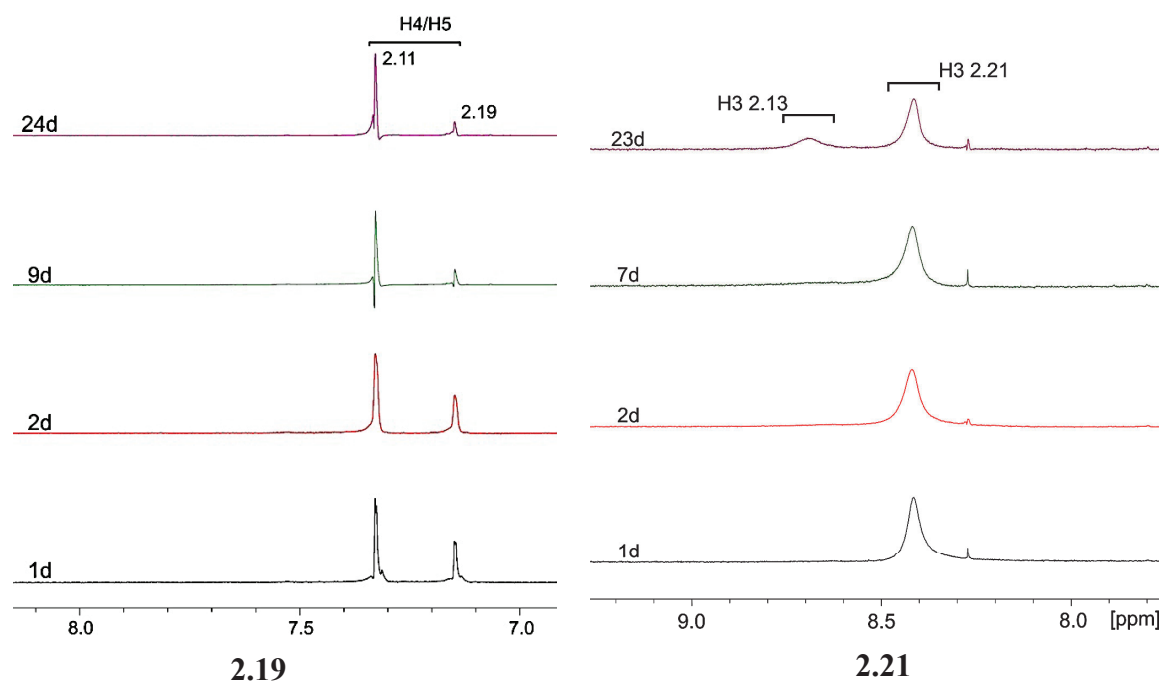


Figure 25. ^1H -NMR spectra recorded at the indicated times for the degradation of dimethyl substituted silver(I)-NHC complexes **2.19** of imidazolylidene ligands (left) and **2.21** of 1,2,4-triazolylidene ligands (right) at 37 °C in 300 μL $\text{DMSO-}d_6$ and 300 μL H_2O .

The ^1H -NMR WATERGATE spectra of silver complex **2.20** shown in Figure 26 revealed immediate and steady degradation in aqueous solution and contrasting to the 1-phenyl-methyl and dimethyl substituted silver(I)-NHC complexes, the precarbenic proton of the precursor pro-ligand was observed immediately.

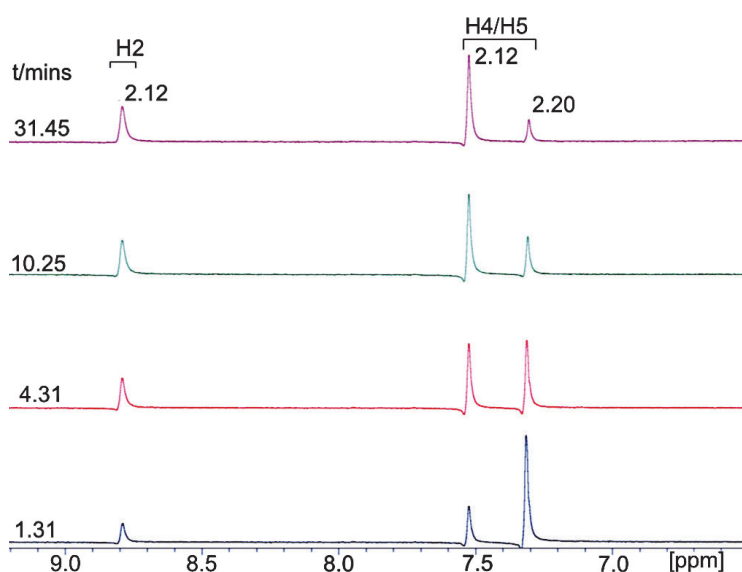


Figure 26. ^1H -NMR spectra recorded at the indicated times for the degradation of silver(I)-NHC complex **2.20** at 37 °C in 300 μL $\text{DMSO-}d_6$ and 300 μL H_2O .

4.4 Discussion of the Results

4.4.1 Antibacterial Silver(I)-NHC Complexes

The silver(I)-NHC complexes were found to have stronger Gram-negative directed antibacterial activity in comparison to the gold(I)-NHC complexes in agreement with previous literature.^{26,61} Two of the silver(I)-NHC complexes **2.20** and **2.21** were found to have MICs of 2 – 4 $\mu\text{g}\cdot\text{mL}^{-1}$ and 2 $\mu\text{g}\cdot\text{mL}^{-1}$ against *A. baumannii* ATCC 17978TM respectively, which are similar in magnitude to colistin (Figure 27), which is considered to be a last resort treatment for Gram-negative bacterial infections. The silver(I)-NHC complex **2.20** was also evaluated against bacterial strains with higher levels of drug-resistance and was found to have similar antibacterial activity indicating that the silver(I)-NHC complexes are also effective against multi-drug resistant bacterial pathogens. In addition to the significant antibacterial activity observed for some of the silver(I)-NHC complexes, the strain *A. baumannii* 17978 did not develop antibacterial resistance against the silver(I)-NHC complex **2.20** after a period of two weeks, while substantial resistance (8 – 16-fold increase in MIC) developed against the broad-spectrum antibacterial ciprofloxacin. The antibacterial activity, and lack of antibacterial resistance observed against these silver(I)-NHC complexes is significant, as carbapenems including colistin resistant *A. baumannii* is listed as a critical priority in the WHO priority pathogens list.¹¹⁶

The silver(I)-NHC complexes that displayed antibacterial activity were found to undergo steady degradation in the ¹H-NMR WATERGATE experiments in agreement with previous literature stating that a steady release of silver(I) ions is responsible for the antibacterial activity of complexes of this type.^{15,21,22,24,55-59} The silver(I) complex **2.17** was found to degrade immediately in the ¹H-NMR WATERGATE experiments, whereas its silver(I) imidazolylidene analogue **2.15** was found to undergo steady degradation over a prolonged period of time. The theoretical calculations shown in Table 6, Section 4.3 support these findings, indicating that the bond dissociation energy of **2.15** of imidazolylidene ligands is higher than that of **2.17** of 1,2,4-triazolylidene ligands. The steady degradation of silver(I) complex **2.15** of imidazolylidene ligands may be associated with its greater antibacterial activity in comparison to silver(I) complex **2.17** of 1,2,4-triazolylidene ligands.

4.4.2 Antibacterial Gold(I)-NHC Complexes

The gold(I)-NHC complexes displayed increased Gram-positive directed antibacterial activity, in agreement with previous literature.^{26,61} In addition to the experimentally determined high levels of aqueous stability in the WATERGATE ¹H-NMR experiments (Section 4.3), the gold(I)-NHC complexes were found to have high theoretically calculated bond dissociation energies (Section 4.2) in comparison to the silver(I)-NHC complexes. The theoretical calculations revealed that the gold(I) complexes of imidazolylidene ligands had higher BDEs than the gold(I) complexes 1,2,4-triazolylidene ligands. The electrospray mass spectrometric cone voltage (CV) variation experiments (Section 4.1) showed that gold(I) complexes of imidazolylidene ligands fragment at higher CV values compared to their gold(I) 1,2,4-triazolylidene counterparts, indicating higher BDEs for the gold(I) complexes of imidazolylidene ligands.

The phenyl substituted gold(I) complexes **2.23** – **2.26** of imidazolylidene and 1,2,4-triazolylidene ligands displayed substantially greater antibacterial activity in comparison to the gold(I) complexes **2.27** – **2.30** of dimethyl and diethyl substituted NHC ligands (Section 3.2, Table 3). Phenyl substituted gold(I) complexes of imidazolylidene ligands have previously been shown to have greater antibacterial activity against Gram-positive bacterial strains in comparison to gold(I) complexes containing only alkyl-substituents, in agreement with the results shown in Section 3.2, Table 3.^{25,26,61} This study also showed higher levels of cellular gold for the phenyl-substituted gold(I)-NHC complexes, indicating that the greater antibacterial activity observed for the phenyl-substituted gold(I)-NHC complexes **2.23** – **2.26** in comparison to the di-alkyl substituted gold(I)-NHC complexes **2.27** – **2.30** may be as a result of increased cellular uptake.²⁵

Interestingly, the phenyl-substituted gold(I) complexes of 1,2,4-triazolylidene ligands **2.25** and **2.26** were found to have greater antibacterial activity in comparison to the phenyl-substituted gold(I) complexes of imidazolylidene ligands **2.23** and **2.24**, as shown in Section 3.2, Table 3. Based on the results from the theoretical calculations and trends in fragmentation in the HR-MS stability experiments, it can be postulated that the greater antibacterial activity of **2.25** and **2.26** may arise from the lower BDE of the NHC-Au bond of the 1,2,4-triazolylidenes in comparison to the gold(I) complexes of imidazolylidene ligands **2.23** and **2.24** (Section 4.1).

The MIC values for the best performing gold(I)-NHC complexes **2.23** – **2.26** against *S. aureus* were found to be similar in magnitude to vancomycin (Figure 27) which is considered to be a last resort medication for the treatment of multidrug resistant *S. aureus* (MRSA).¹¹⁷⁻¹¹⁹ The best overall performing gold(I)-NHC complex **2.25** was evaluated against bacterial strains with higher levels of drug-resistance, and similar to the silver(I)-NHC complex **2.20** returned similar MIC values to more sensitive bacterial strains (Section 3.3, Table 4). The resistance studies carried out in Section 3.4 showed that *E. faecium* 2127 did not develop antibacterial resistance to **2.25** after a period of two weeks, whereas a 16-fold increase in bacterial resistance developed against ciprofloxacin.

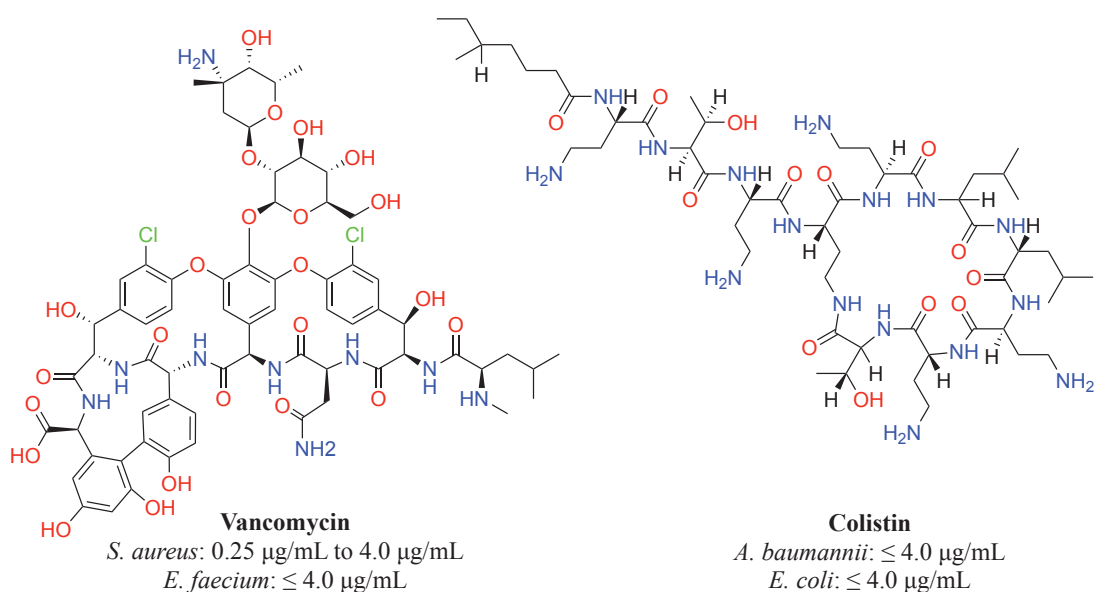


Figure 27. Minimum inhibitory concentrations of vancomycin; a last resort treatment for Gram-positive infections and colistin; a last resort treatment for Gram-negative infections.

CHAPTER FIVE

Conclusion and Future Work

Sixteen gold(I) and silver(I) complexes of imidazolylidene and 1,2,4-triazolylidene ligands have been synthesised characterised by ^1H -NMR, ^{13}C -NMR, and for **2.5**, **2.17**, **2.24**, **2.25**, and **2.35** single crystal X-ray diffraction. Three dinuclear gold(I) complexes of imidazolylidene and 1,2,4-triazolylene ligands that differ in the terminal wingtip substituents were synthesised and characterised, and the dinuclear gold(I)-NHC complexes **2.35** and **2.36** were found to be luminescent upon excitation.

The gold(I) and silver(I) complexes of imidazolylidene and 1,2,4-triazolylidene ligands were investigated for their antibacterial activity against four medically relevant Gram-positive and Gram-negative bacteria. The gold(I)-NHC complexes were found to have stronger Gram-positive directed antibacterial activity, and the silver(I)-NHC complexes were found to have stronger Gram-negative directed antibacterial activity in agreement with previous literature.^{26,61} Two of the silver(I)-NHC complexes **2.20** and **2.21** were found to have antibacterial activity within the range of colistin that is considered a last resort treatment for the treatment of Gram-negative bacterial infections. The greatest performing gold(I)-NHC complexes with 1-Phenyl *N*-substituents **2.23** – **2.26** were found to have antibacterial activity against *S. aureus* within a similar range to vancomycin which is considered to be a last resort medication for the treatment of multidrug resistant *S. aureus* (MRSA).¹¹⁷⁻¹¹⁹

Two of the best performing silver(I) and gold(I)-NHC complexes **2.20** and **2.25** were found to have similar antibacterial activity against bacteria with higher levels of antibacterial resistance. No increase in antibacterial resistance was noted for *A. baumannii* 17978 against the silver(I)-NHC complex **2.20**, while an 8 – 16-fold increase was observed for *A. baumannii* 17978 against ciprofloxacin. Similarly, no increase in antibacterial resistance was observed for *E. faecium* 2127 against the gold(I)-NHC complex **2.25**, while a 16-fold increase was observed for *A. baumannii* 17978 against ciprofloxacin. The results from the antibacterial resistance study are in agreement with previous literature stating that the possible mechanisms of resistance to metals is limited,¹⁶⁻¹⁸ however to the best of our knowledge this is the first time a lack of bacterial resistance to metal complexes of this type has been demonstrated.

The results of stability for the silver(I)-NHC complexes were found to be in agreement with the previous literature stating that steady release of the silver(I) ions is responsible for the antibacterial activity of complexes of this type.^{15,21,22,24,55-59} The 1-phenyl substituted gold(I)-NHC complexes **2.23** – **2.26** were found to have greater antibacterial activity in comparison to the alkyl *N*-substituted gold(I)-NHC complexes, and the gold(I) complexes **2.25** and **2.26** of 1,2,4-triazolylidene ligands were found to have greater antibacterial activity in comparison to their imidazolylidene analogues **2.23** and **2.24**. Based on the theoretically calculated BDEs and CV variation experimental data, the greater antibacterial activity of **2.25** and **2.26** may arise from the lower BDE of the carbene-Au bond of the 1,2,4-triazolylidenes in comparison to the gold(I) complexes of imidazolylidene ligands **2.23** and **2.24**.

In future work, bacterial cellular uptake studies should be performed as cellular uptake has been found to play a key role in the antibacterial activity of similar *N*-heterocyclic carbene complexes.²⁵ Silver(I) and gold(I) complexes of *N*-heterocyclic carbene ligands should be designed with good aqueous solubility, as silver(I)-NHC complexes **2.16**, **2.18** and **2.29** had poor aqueous solubility and could not be evaluated for their antibacterial activity in this study. A more robust understanding of the structural activity relationships is needed to further facilitate the development of metallodrugs of this type, along with detailed understandings of the mechanisms of action that are currently not well understood.^{25,26}

The strong Gram-positive directed antibacterial activity of the gold(I)-NHC complexes, and Gram-negative directed antibacterial activity of silver(I)-NHCs, along with the demonstrated limited ability of bacteria to develop resistance to these metal containing complexes emphasises the potential of this class of metallodrug to combat the increasing rates of antibiotic resistant bacteria.

CHAPTER SIX

Experimental

5.1 General Information and Methods

All reagents were purchased from Sigma-Aldrich, Alfa Aesar or Chem Supply and were of analytical grade or higher and were used without further purification unless otherwise stated. 400 and 500 MHz NMR spectrometers were employed to record ^1H and ^{13}C -NMR spectra. Chemical shifts (δ) are displayed in parts per million (ppm) referenced to residual solvent signals CDCl_3 ($\delta_{\text{H}} = 7.26$ and $\delta_{\text{C}} = 77.16$ ppm) and $\text{DMSO-}d_6$ ($\delta_{\text{H}} = 2.50$ and $\delta_{\text{C}} = 39.52$ ppm). ^1H -NMR spectroscopic data are reported in the order of multiplicity, which is characterized as s (singlet), d (doublet), t (triplet), q (quartet), m (multiplet) and br (broad), coupling constant (J) in hertz (Hz) and number of protons.

5.2 X-Ray Crystallography

The X-ray diffraction studies were carried out by Dr. Peter Barnard. Single crystals of the 1,2,4-triazolium salt **2.5** were grown by evaporative diffusion of acetonitrile and ether. Single crystals of the silver(I) complex **2.17** were grown by slow evaporation of acetonitrile solution of the complex. Single crystals of gold(I) complexes **2.24** and **2.25** were grown in a solution of methanol which was layered with diethyl ether, and single crystals of the dinuclear gold(I) complex **2.35** were grown by evaporative diffusion from a mixture of methanol and ether. Crystallographic data for all structures determined are given in **Table S1**. For all samples, crystals were removed from crystallisation vials and immediately coated in Paratone oil on a glass slide. A suitable crystal was mounted in Paratone oil on a Miller loop and rapidly cooled to 150 K with a stream of nitrogen using an Oxford low-temperature device. The crystals were kept at 292 K during data collection. Diffraction data was measured using a Rigaku Oxford Diffraction Supernova diffractometer mounted with a Mo $\text{K}\alpha$ ($\lambda = 0.71073$ Å) and Cu $\text{K}\alpha$ radiation ($\lambda = 1.54184$). Data were reduced and corrected for absorption using the CrysAlis Pro program. The SHELXL20132 program was used to solve the structures with direct methods, with refinement by the full-matrix least-squares refinement techniques on F^2 . The non-hydrogen atoms were refined anisotropically, and hydrogen atoms were placed geometrically and refined using the riding model. Coordinates and anisotropic thermal parameters of all non-hydrogen atoms were refined. All

calculations were carried out using the program Olex2-1.3. All images were generated using the program Olex2-1.3.¹²⁰

5.3 UV-vis and Photoluminescence Studies

Stock Solutions were prepared at 1-10 mM concentrations in DMSO (anhydrous, Sigma- Aldrich). 10 μ M sample solutions were prepared for analysis in acetonitrile (ACN) (HPLC grade, Honeywell) which was distilled over CaH₂ (95%, Sigma Aldrich) under N₂. Steady-state emission spectra were collected by Laena D'Alton using the Nanolog spectrofluorometer (HORIBA Jobin Yvon IBH), with a 450 W xenon-arc lamp as the excitation source (1200 g/mm grating blazed at 330 nm excitation monochromators). A 100 g/mm grating (blazed at a 450 nm) emission monochromator was used with slit sizes of 2-5 nm. Emission spectra were collected with a liquid nitrogen-cooled Symphony II (Model SII-1LS-256-06) CCD, then corrected for source intensity, gratings, and detector response. Samples were excited at 269-273 nm, and the excitation spectra obtained at the emission maximum (301-404 nm).

5.4 Antibacterial Activity

The minimum inhibitory concentrations (MICs) were determined using a broth microdilution assay according to guidelines defined by the Clinical Laboratory Standards Institute.^{121,122} The assay was conducted using tryptic soy broth in 96-well flat bottom microtiter plates and a bacterial inoculum of 1×10^5 colony forming units per mL. After 20 h of static incubation at 37 °C, growth was assessed by measuring the absorbance at 600 nm and the MIC defined as the lowest concentration of the compound where no bacterial growth was observed. Experiments were repeated with 3 biological replicates.

5.5 Resistance Studies

To determine the propensity for sensitive bacteria to develop resistance, *E. faecium* (ATCC® BAA-2127™) and *A. baumannii* (ATCC® 17978™) were continuously exposed to compounds **2.25** and **2.20**, respectively, using the extended gradient MIC method from $0.25 \times \text{MIC}$ up to $4 \times \text{MIC}$.¹²³ A 1% (v/v) DMSO negative treatment control and a positive treatment control using ciprofloxacin were performed concurrently. After 48 h of incubation with the compounds at $4 \times \text{MIC}$, aliquots of the cultures were streaked onto drug-free TSA plates. The MIC values were then determined using the broth microdilution

method as described above and compared to the values for the DMSO-treatment controls to determine the fold-change in MIC values. Experiments were carried out with 2 biological replicates.

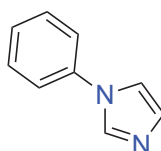
5.6 Bacterial Strains and Growth Conditions

The bacterial strains utilised in this study were sourced from the American Type Culture Collection (ATCC®) and are summarised in Table 7. All bacterial strains were cultured in tryptic soy broth (TSB) or on tryptic soy agar (TSA) plates at 37 °C.

Table 7. Bacterial strains sourced from the American Type Culture Collection.

ATCC No.	Species
17978	<i>Acinetobacter baumannii</i>
BAA-1710	<i>Acinetobacter baumannii</i>
BAA-2127	<i>Enterococcus faecium</i>
700221	<i>Enterococcus faecium</i>
K-12	<i>Escherichia coli</i>
BAA-2340	<i>Escherichia coli</i>
9144	<i>Staphylococcus aureus</i>
BAA-1720	<i>Staphylococcus aureus</i>

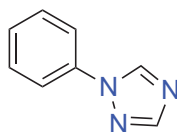
5.7 Synthesis



2.1

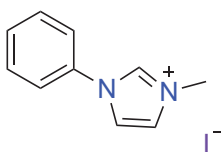
2.1. To a solution of imidazole (3.00 g, 44.06 mmol) and bromobenzene (5.07 mL, 48 mmol) in degassed DMSO (30 mL), potassium carbonate (12.00 g, 88.12 mmol), copper iodide (0.84 g, 4.41 mmol) and proline (0.50 g, 4.41 mmol) were added under nitrogen atmosphere and this mixture was stirred at 120 °C for 48 h. The resultant mixture was then cooled to RT and diluted with water followed by extraction with ethyl acetate (3 × 50 mL). The combined organic layers were washed with brine (30 mL) followed by drying over anhydrous MgSO₄. The crude product was purified via column chromatography to obtain a yellow liquid. Yield: 2.93 g, 46%. ¹H-NMR (500.14 MHz, CDCl₃) δ 7.79 (s, 1H, C2-*H_{im}*), 7.43 – 7.40 (m, 2H, *H_{aryl}*), 7.32 – 7.29 (m, 3H, *H_{aryl}*), 7.22 (s, 1H, C5-*H_{im}*), 7.15 (s, 1H, C4-*H_{im}*) ¹³C-NMR (125.77 MHz, CDCl₃) δ 136.3 (C_q), 134.5 (C2_{*im*}), 129.4 (C4_{*im*}),

128.8 (*C_{aryl}*), 126.4 (*C_{aryl}*), 120.4 (*C_{aryl}*), 117.2 (*C5_{im}*) HRESI-MS: $[\text{C}_9\text{H}_8\text{N}_2]^+$ $m/z = 145.0705$ calcd. = 144.0687.



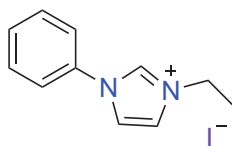
2.2

2.2. This compound was prepared using the same method for **2.1** from 1,2,4-triazole (1.00 g, 43.50 mmol) bromobenzene (5.0 mL, 47.80 mmol) potassium carbonate (12.00 g, 86.88 mmol) copper iodide (0.83 g, 4.34 mmol), and proline (0.50 g, 4.34 mmol). Volatiles were removed under reduced pressure producing a yellow crystalline solid. Yield: 3.48 g, 55%. ¹H-NMR (400.13 MHz, DMSO-*d*₆) δ 9.31 (s, 1H, C5-*H_{trz}*), 8.25 (s, 1H, C3-*H_{trz}*), 7.88 – 7.86 (m, 2H, *H_{aryl}*), 7.59 – 7.55 (m, 2H, *H_{aryl}*), 7.44 – 7.40 (m, 1H, *H_{aryl}*). ¹³C-NMR (125.77 MHz, DMSO-*d*₆) δ 152.9 (C5-*trz*), 142.8 (C3-*trz*) 137.2 (*C_q*), 130.2 (*C_{aryl}*), 128.3 (*C_{aryl}*), 119.9 (*C_{aryl}*). HRESI-MS: $[\text{C}_8\text{H}_7\text{N}_3]^+$ $m/z = 146.0704$ calcd. = 146.0604.



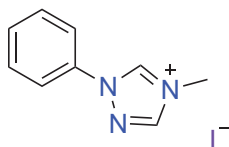
2.3

2.3. To a solution of 1-phenyl-1*H*-imidazole (**2.1**) (0.20 g, 1.38 mmol) in acetonitrile was added iodomethane (0.12 mL, 1.94 mmol). The resulting mixture was heated under reflux for 24 h and then cooled to RT and volatiles were removed under reduced pressure producing a yellow oil. The crude product was recrystallised with acetonitrile and ether producing a crystalline white powder. Yield: 0.26 g, 65%. ¹H-NMR (400.13 MHz, CDCl₃) δ 10.15 (s, 1H, C2-*H_{im}*), 7.79 (s, 1H, C4-*H_{im}*), 7.75 (s, 1H, C5-*H_{im}*), 7.71 – 7.69 (m, 2H, *H_{aryl}*), 7.50 – 7.42 (m, 3H, *H_{aryl}*), 4.17 (s, 3H, *CH₃*). ¹³C-NMR (125.77 MHz, DMSO-*d*₆) δ 136.4 (C2-*im*), (135.2 *C_q*) 130.7 (*C_{aryl}*) 130.2 (*C_{aryl}*), 124.9 (*C_{im}*), 122.3 (*C_{aryl}*), 121.5 (*C_{im}*) 36.7 (*CH₃*) HRESI-MS: $[\text{C}_{10}\text{H}_{11}\text{N}_2]^+$ $m/z = 159.0926$ calcd. = 159.1917.



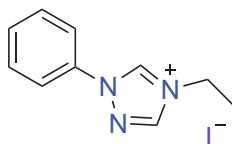
2.4

2.4. This compound was prepared using the same method as **2.3** from **2.1** (0.60 g, 4.16 mmol), and iodomethane (0.40 mL, 5.00 mmol) yielding a light brown powder. Yield: 0.95 g, 76%. $^1\text{H-NMR}$ (400.13 MHz, CDCl_3) δ 10.29 (s, 1H, C2- H_{im}), 7.84 (s 1H, C4- H_{im}), 7.77 (s, 1H, C5- H_{im}), 7.71-7.69 (m, H_{aryl}), 7.44-7.37 (m, H_{aryl}) 4.52 (q, $J = 8.0$ Hz, 2H, CH_2CH_3), 1.55 (t, $J = 8.0$ Hz, 3H, CH_2CH_3). $^{13}\text{C-NMR}$ (125.77 MHz, $\text{DMSO-}d_6$) δ 135.6 (C2 $_{im}$), 135.3 (C $_q$), 130.6 (C $_{aryl}$), 130.2 (C $_{aryl}$), 123.5 (C $_{im}$), 122.4 (C $_{aryl}$), 121.6 (C $_{im}$). 45.3 (CH_2CH_3), 15.3 (CH_2CH_3). HRESI-MS: $[\text{C}_{11}\text{H}_{13}\text{N}_2]^+$ $m/z = 173.1089$ calcd. = 173.1073.



2.5

2.5 was prepared using the same method as **2.3** from **2.2** (0.60 g, 4.13 mmol) and iodomethane (0.36 mL, 5.79 mmol) yielding a white powder. Yield: 0.95 g, 80%. $^1\text{H-NMR}$ (400.13 MHz, CDCl_3) δ 11.57 (s, 1H, C5- H_{trz}), 9.17 (s, 1H, C3- H_{trz}), 7.96 – 7.92 (m, 2H, H_{aryl}), 7.55 – 7.47 (m, 3H H_{aryl}), 4.33 (s, 3H, CH_3). $^{13}\text{C-NMR}$ (125.77 MHz, CDCl_3) δ 145.2 (C5 $_{trz}$), 140.8 (C3 $_{trz}$), 134.7 (C $_q$), 130.9 (C $_{aryl}$), 130.3 (C $_{aryl}$), 120.8 (C $_{aryl}$), 36.1 (CH_3). HRESI-MS: $[\text{C}_9\text{H}_{10}\text{N}_3]^+$ $m/z = 160.0868$, calcd. = 160.0869.



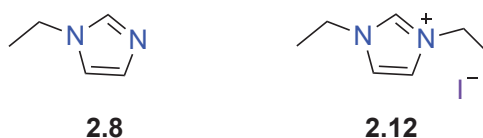
2.6

2.6 was prepared using the same methods as **2.3** from **2.2** (0.60 g, 4.13 mmol) and iodoethane (0.47 mL, 5.79 mmol) to give **2.6** as a crystalline white powder. Yield: 1.05 g, 84%. $^1\text{H-NMR}$ (400.13 MHz, CDCl_3) δ 11.84 (s, 1H, C5- H_{trz}), 9.13 (s, 1H, C3- H_{trz}), 8.06 – 8.02 (m, 2H, H_{aryl}), 7.58 – 7.50 (m, 3H, H_{aryl}), 4.78 (q, $J = 7.4$ Hz, 2H, CH_2CH_3), 1.74 (t, $J = 7.4$ Hz, 3H, CH_2CH_3). $^{13}\text{C-NMR}$ (125.77 MHz, CDCl_3) δ 143.9 (C5 $_{trz}$), 140.2 (C3 $_{trz}$),

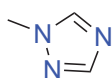
134.8 (C_q), 131.0 (C_{aryl}), 130.3 (C_{aryl}), 120.7 (C_{aryl}), 45.0 (CH_2CH_3), 15.7 (CH_2CH_3).
 HRESI-MS: $[C_{10}H_{12}N_3]^+$ m/z = 174.1024 calcd. = 174.1026.



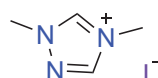
2.7 and **2.11**. A mixture of imidazole (2.00 g, 29.37 mmol), iodomethane (3.65 mL, 58.74 mmol) and potassium carbonate (4.06 g, 29.37 mmol) in acetone (30 mL) was stirred at RT for 24 h. The reaction mixture was filtered and volatiles were removed under reduced pressure producing an off-white powder. The crude product was redissolved in acetone (10 mL) followed by addition of ethyl acetate (15 mL) to obtain a white powder **2.11** that was collected and washed with ethyl acetate. The solvent of the filtrate was removed under reduced pressure yielding mono-alkylated product **2.7** as a yellow oil. **2.7**: Yield: 0.86 g, 36%. 1H -NMR (400.13 MHz, DMSO- d_6) δ 7.58 (s, 1H, C2- H_{im}), 7.10 (s, 1H, C5- H_{im}), 6.92 (s, 1H, C4- H_{im}) 3.64 (s, 3H, N3- CH_3). ^{13}C -NMR (125.77 MHz, DMSO- d_6) δ 138.3 (C2 $_{im}$), 128.9 (C5 $_{im}$), 120.9 (C4 $_{im}$) 33.1 (CH_3). **2.11**: (Yield: 1.84 g, 27%). 1H -NMR (400.13 MHz, DMSO- d_6) δ 9.06 (s, 1H, C2- H_{im}), 7.69 (m, 2H, H_{im}), 3.85 (s, 6H, N1- CH_3 , N3- CH_3). ^{13}C -NMR (100.62 MHz, DMSO- d_6) δ 137.5 (C2 $_{im}$), 123.9 (C4 $_{im}$, C5 $_{im}$), 36.2 (CH_3). HRESI-MS: $[C_5H_9N_2]^+$ m/z = 97.0760 calcd. = 97.0741.



2.8 and **2.12**. These compounds were prepared using the same methods as **2.7** and **2.11** from imidazole (2 g, 29.37 mmol), iodoethane (4.72 mL, 58.74 mmol), and potassium carbonate (4.06 g, 29.37 mmol), yielding **2.8** as a yellow oil, and **2.12** as a white crystalline powder. **2.8**: Yield: 0.59 g, 21%. 1H -NMR (400.13 MHz, DMSO- d_6) δ 7.64 (s, 1H, C2- H_{im}), 7.17 (s, C4- H_{im}), 6.90 (s, C5- H_{im}), 3.97 (q, J = 7.3, 4H, CH_2CH_3), 1.32 (t, J = 7.3, 3H, CH_2CH_3). ^{13}C -NMR (125.77 MHz, DMSO- d_6) δ 137.2 (C2 $_{im}$) 128.7 (C5 $_{im}$), 119.3 (C4 $_{im}$) 41.4 (CH_2CH_3) 16.71 (CH_2CH_3). **2.12**: Yield: 1.42 g, 19%. 1H -NMR (400.13 MHz, DMSO- d_6) δ 9.25 (s, 1H, C2- H_{im}), 7.82 (s, 2H H_{im}), 4.20 (q, J = 7.3, 4H, CH_2CH_3), 1.45 – 1.40 (m, 6H, CH_2CH_3). ^{13}C -NMR (125.77 MHz, DMSO- d_6) δ 135.9 (C2 $_{im}$) 122.5 (C4 $_{im}$, C5 $_{im}$) 44.7 (CH_2CH_3) 15.5 (CH_2CH_3). HRESI-MS: $[C_7H_{13}N_2]^+$ m/z = 125.1206 calcd. = 125.1073.

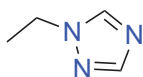


2.9

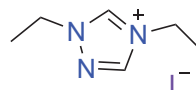


2.13

2.9 and **2.13**. These compounds were prepared using the same methods as **2.7** and **2.11** from 1,2,4-triazole (2 g, 28.96 mmol) methyl iodide (3.61 mL, 57.92 mmol), and potassium carbonate (4 g, 28.98 mmol) yielding **2.9** as a yellow oil, and **2.13** as a white crystalline powder. **2.9**: Yield: 0.87 g, 40%. $^1\text{H-NMR}$ (400.13 MHz, $\text{DMSO-}d_6$) δ 8.45 (s, 1H, $\text{C5-}H_{\text{trz}}$), 7.94 (s, 1H, $\text{C3-}H_{\text{trz}}$), 3.87 (s, 3H, N1-CH_3). $^{13}\text{C-NMR}$ (125.77 MHz, $\text{DMSO-}d_6$) δ 151.8 (C5_{trz}), 144.9 (C3_{trz}), 36.1 (N1-CH_3). **2.13**: Yield: 1.7 g, 26%. $^1\text{H-NMR}$ (400.13 MHz, $\text{DMSO-}d_6$) δ 9.99 (s, 1H, $\text{C5-}H_{\text{trz}}$), 9.12 (s, 1H, $\text{C3-}H_{\text{trz}}$), 4.07 (s, 3H, N4-CH_3), 3.90 (s, 3H, N1-CH_3). $^{13}\text{C-NMR}$ (125.77 MHz, $\text{DMSO-}d_6$) δ 145.8 (C5_{trz}), 143.8 (C3_{trz}), 39.1 (N4-CH_3), 34.5 (N1-CH_3). HRESI-MS: $[\text{C}_4\text{H}_8\text{N}_3]^+$ m/z = 98.0712 calcd. = 98.0713.

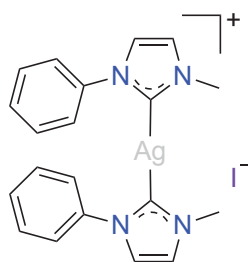


2.10



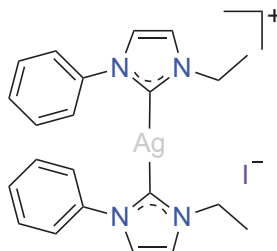
2.14

2.10 and **2.14**. These compounds were prepared using the same methods as **2.7** and **2.11** from 1,2,4-triazole (2 g, 29.00 mmol) iodoethane (4.66 mL, 57.91 mmol), and potassium carbonate (7.38 g, 29.00 mmol) yielding **2.10** as a yellow oil, and **2.14** as a white crystalline powder. **2.10**: Yield: 2.15 g, 76%. $^1\text{H-NMR}$ (400.13 MHz, $\text{DMSO-}d_6$) δ 8.50 (s, 1H, $\text{C5-}H_{\text{trz}}$), 7.94 (s, 1H, $\text{C3-}H_{\text{trz}}$), 4.20 (q, J = 7.3 Hz, 2H, $\text{N1-CH}_2\text{CH}_3$), 1.36 (t, J = 7.3 Hz, 3H, $\text{N1-CH}_2\text{CH}_3$). $^{13}\text{C-NMR}$ (125.77 MHz, $\text{DMSO-}d_6$) δ 151.6 (C5_{trz}), 143.7 (C3_{trz}), 44.3 ($\text{N1-CH}_2\text{CH}_3$), 15.4 ($\text{N1-CH}_2\text{CH}_3$). **2.14**: Yield: 1.61g, 22%. $^1\text{H-NMR}$ (400.13 MHz, $\text{DMSO-}d_6$) δ 10.16 (s, 1H, $\text{C5-}H_{\text{trz}}$), 9.24 (s, 1H, $\text{C3-}H_{\text{trz}}$), 4.39 (q, J = 7.3 Hz, 2H, $\text{N4-CH}_2\text{CH}_3$), 4.28 (q, J = 7.3 Hz, 2H, $\text{N1-CH}_2\text{CH}_3$), 1.47 (t, J = 7.3 Hz, 6H, CH_2CH_3). $^{13}\text{C-NMR}$ (125.77 MHz, $\text{DMSO-}d_6$) δ 144.8 (C5_{trz}), 142.4 (C3_{trz}), 47.6 ($\text{N4-CH}_2\text{CH}_3$), 43.5 ($\text{N1-CH}_2\text{CH}_3$), 14.9 ($\text{N4-CH}_2\text{CH}_3$), 14.1 ($\text{N1-CH}_2\text{CH}_3$). HRESI-MS: $[\text{C}_6\text{H}_{12}\text{N}_3]^+$ m/z = 126.1023 calcd. = 126.1026.



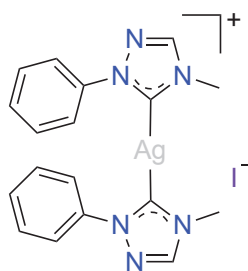
2.15

2.15. To a solution of **2.3** (100 mg, 0.35 mmol) in 1,2-dichloroethane (10 mL), Ag₂O (39 mg, 0.17 mmol) was added and this mixture was stirred at 60 °C for 24 hrs. The resultant mixture was then filtered through a plug of Celite and the volatiles were removed under reduced pressure to give an off-white crude product. The crude product was recrystallised from a mixture of dimethylformamide and ether as a white crystalline solid. Yield: 43 mg, 45%. ¹H-NMR (400.13 MHz, DMSO-*d*₆) δ 7.87 (d, *J* = 1.8 Hz, 2H, C4-*H*_{im}), 7.69 (d, *J* = 1.8 Hz, 2H, C5-*H*_{im}), 7.69 – 7.67 (m, 4H, *H*_{aryl}), 7.55 – 7.48 (m, 6H, *H*_{aryl}), 3.88 (s, 6H, CH₃). ¹³C-NMR (100.62 MHz, DMSO-*d*₆) δ 179.6 (C2_{im}), 140.2 (C_q), 130.2 (C_{aryl}), 129.1 (C_{aryl}), 124.5 (C4_{im}), 124.3 (C_{aryl}), 122.7 (C5_{im}), 39.0 (CH₃).



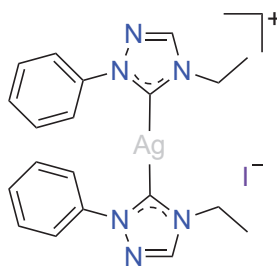
2.16

2.16. This compound was prepared using the same methods as **2.15** from **2.4** (100 mg, 0.33 mmol) and Ag₂O (38 mg, 0.16 mmol) in 1,2-dichloroethane (10 mL) to give **2.16** as a white powder. Yield: 53 mg, 55%. ¹H-NMR (400.13 MHz, DMSO-*d*₆) δ 7.87 (d, *J* = 1.8 Hz, 4H, C4-*H*_{im}), 7.77 (d, *J* = 1.8 Hz, 4H, C5-*H*_{im}), 7.72 – 7.69 (m, 4H, *H*_{aryl}), 7.56 – 7.0 (m, 6H, *H*_{aryl}), 4.17 (q, *J* = 7.3 Hz, 4H, CH₂CH₃), 1.38 (t, *J* = 7.2 Hz, 6H, CH₂CH₃). ¹³C-NMR (100.62 MHz, DMSO-*d*₆) δ 140.3 (C_q), 130.1 (C_{aryl}), 129.1 (C_{aryl}), 124.3 (C_{aryl}), 123.0 (C4_{im}), 122.8 (C5_{im}), 47.0 (CH₂CH₃), 17.3 (CH₂CH₃).



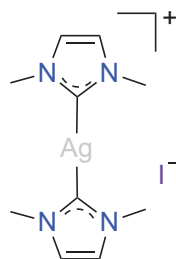
2.17

2.17. This compound was prepared using the same methods as **2.15** from **2.5** (100 mg, 0.34 mmol), and Ag₂O (40 mg, 0.17 mmol) in 1,2-dichloroethane (10 mL) that was stirred at room temperature for 4 h to give **2.17** as a white crystalline powder. Yield: 45 mg, 48%. ¹H-NMR (400.13 MHz, DMSO-*d*₆) δ 9.05 (s, 2H, C3-*H*_{trz}), 7.94 – 7.91 (m, 4H, *H*_{aryl}), 7.55 – 7.51 (m, 6H *H*_{aryl}), 3.98 (s, 6H, CH₃). ¹³C-NMR (125.77 MHz, DMSO-*d*₆) 184.0 (C5_{trz}), 146.0 (C3_{trz}), 139.8 (C_q), 130.1 (C_{aryl}), 129.5 (C_{aryl}), 123.1 (C_{aryl}), δ 36.2 (CH₃).



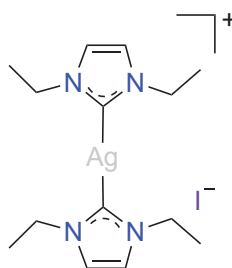
2.18

2.18. This compound was prepared using the same methods as **2.15** from **2.6** (100 mg, 0.33 mmol), and Ag₂O (39 mg, 0.16 mmol) in 1,2-dichloroethane (10 mL) that was stirred at room temperature for 4 h to give **2.18** as a white crystalline solid. Yield: 56 mg, 58%. ¹H-NMR (400.13 MHz, DMSO-*d*₆) δ 9.16 (s, 2H, (C3-*H*_{trz}), 7.93 (dd, *J* = 7.8, *J* = 1.7 Hz, 4H, *H*_{aryl}), 7.57 – 7.55 (m, 6H, *H*_{aryl}), 4.36 (q, *J* = 7.2 Hz, 4H, CH₂CH₃), 1.48 (t, *J* = 7.3 Hz, 6H, CH₂CH₃). ¹³C-NMR (125.77 MHz, DMSO-*d*₆) δ 182.0 (C5_{trz}), 145.1 (C3_{trz}), 139.8 (C_q), 130.1 (C_{aryl}), 129.6 (C_{aryl}), 123.3 (C_{aryl}), 44.7 (CH₂CH₃), 16.9 (CH₂CH₃).



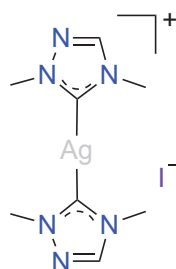
2.19

2.19. This compound was prepared using the same methods as **2.15** from **2.11** (100 mg, 0.45 mmol), and Ag₂O (52 mg, 0.23 mmol) in 1,2-dichloroethane to give **2.19** as a light brown crystalline powder. Yield: 63 mg, 65%. ¹H-NMR (400.13 MHz, DMSO-*d*₆) δ 7.43 (s, 4H, C4, C5-H_{im}), 3.82 (s, 12H, CH₃). ¹³C-NMR (100.62 MHz, DMSO-*d*₆) δ 181.3 (C2_{im}), 123.4 (C4_{im}, C5_{im}), 38.4 (CH₃).



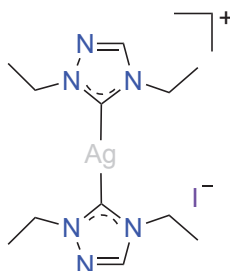
2.20

2.20. This compound was prepared using the same methods as **2.15** from **2.12** (100 mg, 0.40 mmol), and Ag₂O (46 mg, 0.20 mmol), in 1,2-dichloroethane to give **2.20** as a white crystalline powder. Yield: 34 mg, 35%. ¹H-NMR (400.13 MHz, DMSO-*d*₆) δ 7.51 (s, 4H, C4, C5-H_{im}), 4.17 (q, *J* = 7.0 Hz, 8H, CH₂CH₃), 1.40 (t, 7.1 Hz, 12H, CH₂CH₃). ¹³C-NMR (100.62 MHz, DMSO-*d*₆) δ 179.2 (C2_{im}), 121.8 (C4_{im}, C5_{im}), 46.5 (CH₂CH₃), 17.5 (CH₂CH₃).



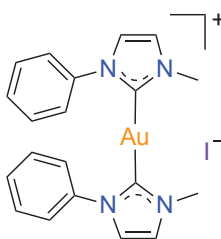
2.21

2.21. This compound was prepared using the same methods as **2.15** from **2.13** (100 mg, 0.45 mmol), and Ag₂O (51 mg, 0.22 mmol) in 1,2-dichloroethane (10 mL) and methanol (5 mL) that was stirred at room temperature for 24 h to give **2.21** as a white powder. Yield: 56 mg, 58%. ¹H-NMR (400.13 MHz, DMSO-*d*₆) δ 8.76 (s, 2H, C3-*H*_{trz}), 4.03 (s, 6H, N4-CH₃), 3.86 (s, 6H, N1-CH₃). ¹³C-NMR (100.62 MHz, DMSO-*d*₆) δ 184.0 (C5_{trz}), 144.8 (C3_{trz}), 40.7 (N4-CH₃) 35.8 (N1-CH₃).



2.22

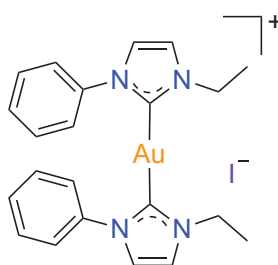
2.22. This compound was prepared using the same methods as **2.15** from **2.14** (100 mg, 0.40 mmol), and Ag₂O (45 mg, 0.20 mmol) in 1,2-dichloroethane (10 mL) that was stirred at room temperature for 4 h to give **2.22** as a white crystalline solid. Yield: 42 mg, 43%. ¹H-NMR (400.13 MHz, DMSO-*d*₆) δ 8.85 (s, 2H, C3-*H*_{trz}), 4.39 (q, *J* = 7.3 Hz, 4H, N4-CH₂CH₃), 4.27 (q, *J* = 7.3 Hz, 4H, N1-CH₂CH₃), 1.42 (t, *J* = 7.2, 12H, CH₂CH₃). ¹³C-NMR (125.77 MHz, DMSO-*d*₆) δ 182.1 (C5_{trz}), 143.9 (C3_{trz}), 48.4 (CH₂CH₃), 43.9 (CH₂CH₃), 17.0 (CH₂CH₃), 17.0 (CH₂CH₃).



2.23

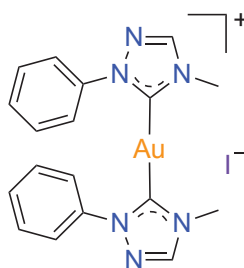
2.23. A mixture of **2.3** (100 mg, 0.34 mmol) and (THT)AuCl (62 mg, 0.19 mmol) in DMF (5 mL) was stirred at 110 °C for 0.5 h. To this mixture, sodium acetate (57 mg, 0.70 mmol) was then added and further stirring at 110 °C for 4 h. The resultant mixture was filtered through a plug of Celite while hot followed by addition of diethyl ether (30 mL) to the filtrate to obtain the crude product as white precipitate. The crude product was recrystallised from hot methanol and dried under high vacuum as a white powder. Yield:

46 mg, 42%. $^1\text{H-NMR}$ (400.13 MHz, $\text{DMSO-}d_6$) δ 7.88 (d, $J = 1.9$ Hz, 4H, H_{im}), 7.73 (d, $J = 1.9$ Hz, 4H, H_{im}), 7.69 – 7.67 (m, 4H, H_{aryl}), 7.53 – 7.51 (m, 6H, H_{aryl}), 3.85 (s, 6H, CH_3). $^{13}\text{C-NMR}$ (100.62 MHz, $\text{DMSO-}d_6$) δ 182.0 (C_{2im}), 139.2 (C_q), 130.0 (C_{aryl}), 129.4 (C_{aryl}), 125.1 (C_{aryl}), 124.7 (C_{4im}), 123.2 (C_{5im}), 38.2 (CH_3). HRESI-MS: $[\text{C}_{20}\text{H}_{20}\text{Au}_1\text{N}_4]^+$ $m/z = 513.1730$ calcd. = 513.1353.



2.24

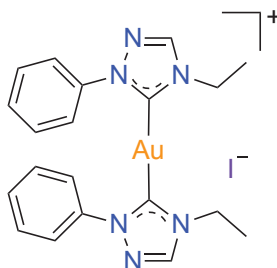
2.24. This compound was prepared using the same method for **2.23** from **2.4** (100 mg, 0.33 mmol), (THT)AuCl (58 mg, 0.18 mmol) and sodium acetate (54 mg, 0.66 mmol), producing **2.24** as a white crystalline powder that was stored under a nitrogen atmosphere. Yield: 34 mg, 41%. $^1\text{H-NMR}$ (400.13 MHz, $\text{DMSO-}d_6$) δ 7.88 (d, $J = 1.9$ Hz, 2H, H_{im}), 7.81 (d, $J = 1.9$ Hz, 2H, H_{im}), 7.71 – 7.69 (m, 4H, H_{aryl}), 7.55 – 7.73 (m, 6H, H_{aryl}), 4.17 (q, $J = 7.2$ Hz, 4H, CH_2CH_3), 1.36 (t, $J = 7.2$ Hz, 6H, CH_2CH_3). $^{13}\text{C-NMR}$ (100.62 MHz, $\text{DMSO-}d_6$) δ 181.3 (C_{2im}), 139.4 (C_q), 130.0 (C_{aryl}), 129.4 (C_{aryl}), 125.2 (C_{aryl}), 123.4 (C_{4im}), 123.1 (C_{5im}), 46.4 (CH_2CH_3), 17.1 (CH_2CH_3). HRESI-MS: $[\text{C}_4\text{H}_8\text{Au}_1\text{N}_3]^+$ $m/z = 541.1668$ calcd. = 541.1666.



2.25

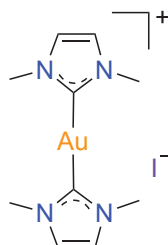
2.25. This compound was prepared using the same method for **2.23** from **2.5** (45 mg, 0.16 mmol), (THT)AuCl (27 mg, 0.08 mmol) and sodium acetate (26 mg, 0.31 mmol), producing **2.25** as a white crystalline powder. Yield: 37 mg, 72%. $^1\text{H-NMR}$ (400.13 MHz, $\text{DMSO-}d_6$) δ 9.18 (s, 2H, $\text{C}3\text{-H}_{trz}$), 7.92 – 7.89 (m, 4H, H_{aryl}), 7.58 – 7.56 (m, 6H, H_{aryl}),

3.96 (s, 6H, CH_3). ^{13}C -NMR (125.77 MHz, DMSO- d_6) δ 184.0 ($C5_{trz}$), 146.5 ($C3_{trz}$), 138.8 (C_q), 130.2 (C_{aryl}), 130.1 (C_{aryl}), 124.1 (C_{aryl}), 36.1 (CH_3). HRESI-MS: $[C_{18}H_{18}Au_1N_6^+]$ m/z = 515.1625 calcd. = 515.1258.



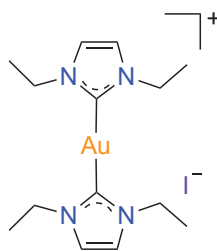
2.26

2.26. This compound was prepared using the same method for **2.23** from **2.6** (45 mg, 0.15 mmol), (THT)AuCl (26 mg, 0.08 mmol) and sodium acetate (24 mg, 0.30 mmol) to obtain a white crystalline solid. Yield: 32 mg, 63%. 1H -NMR (400.13 MHz, DMSO- d_6) δ 9.26 (s, 2H $C3-H_{trz}$), 7.92 (d, J = 6.6 Hz, 4H, H_{aryl}), 7.60 – 7.55 (m, 6H, H_{aryl}), 4.33 (q, J = 7.3 Hz, 4H, CH_2CH_3), 1.48 (t, J = 7.3 Hz, 6H, CH_2CH_3). ^{13}C -NMR (125.77 MHz, DMSO- d_6) δ 183.4 ($C5_{trz}$), 145.5 ($C3_{trz}$), 139.0 (C_q), 130.2 (C_{aryl}), 130.1 (C_{aryl}), 124.3, (C_{aryl}), 44.7 (CH_2CH_3), 16.7 (CH_2CH_3). HRESI-MS: $[C_{20}H_{22}Au_1N_6^+]$ m/z = 543.1572 calcd. = 543.1571.



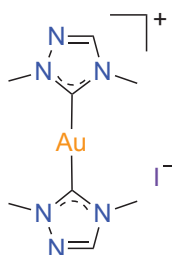
2.27

2.27. This compound was prepared using the same method for **2.23** from **2.11** (100 mg, 0.45 mmol), (THT)AuCl (74 mg, 0.23 mmol) and sodium carbonate (95 mg, 0.90 mmol) to obtain a white solid that was further purified via fractional recrystallisation from dimethylformamide and diethyl ether. Yield: 21 mg, 18%. 1H -NMR (400.13 MHz, DMSO- d_6) δ 7.50 (s, 4H, $C4$, $C5-H_{im}$), 3.86 (s, 12H, CH_3). ^{13}C -NMR (100.62 MHz, DMSO- d_6) δ 183.8 ($C2_{im}$), 123.7 ($C4_{im}$, $C5_{im}$), 37.8 (CH_3). HRESI-MS: $[C_{10}H_{16}Au_1N_4^+]$ m/z = 389.1828 calcd. = 389.1040.



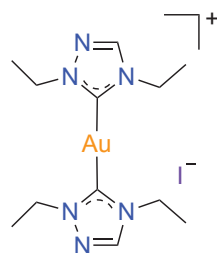
2.28

2.28. This compound was prepared using the same methods as **2.27** from **2.12** (100 mg, 0.40 mmol), (THT)AuCl (70 mg, 0.22 mmol), and sodium carbonate (84 mg, 0.80 mmol) producing a white powder. Yield: 30 mg, 26%. $^1\text{H-NMR}$ (400.13 MHz, $\text{DMSO-}d_6$) δ 7.58 (s, 4H, C4, C5- H_{im}), 4.23 (q, $J = 7.3$, 8H, CH_2CH_3), 1.45 (t, $J = 7.3$, 12H, CH_2CH_3). $^{13}\text{C-NMR}$ (100.62 MHz, $\text{DMSO-}d_6$) δ 182.2 (C2 $_{im}$), 122.2 (C4 $_{im}$, C5 $_{im}$), 46.1 (CH_2CH_3), 17.3 (CH_2CH_3). HRESI-MS: $[\text{C}_{14}\text{H}_{24}\text{Au}_1\text{N}_4]^+$ $m/z = 445.2086$ calcd. = 445.1666.



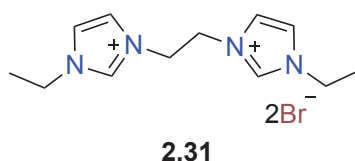
2.29

2.29. This compound was prepared using the same methods as **2.27** from **2.13** (100 mg, 0.45 mmol), (THT)AuCl (72 mg, 0.23 mmol) and sodium carbonate (84 mg, 0.80 mmol), producing a white powder. Yield: 42 mg, 36%. $^1\text{H-NMR}$ (400.13 MHz, $\text{DMSO-}d_6$) δ 8.90 (s, 2H, C3 $_{trz}$), 4.08 (s, 6H, N4- CH_3), 3.90 (s, 6H, N1- CH_3). $^{13}\text{C-NMR}$ (100.62 MHz, $\text{DMSO-}d_6$) δ 185.2 (C5 $_{trz}$), 145.6 (C3 $_{trz}$), 40.0 (CH_3), 35.4 (CH_3). HRESI-MS: $[\text{C}_8\text{H}_{14}\text{Au}_1\text{N}_6]^+$ $m/z = 393.2104$ calcd. = 391.0945.

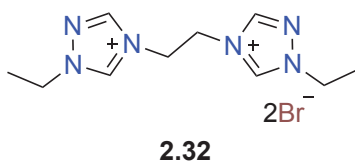


2.30

2.30. This compound was prepared using the same methods as **227** from **2.14** (100 mg, 0.40 mmol), (THT)AuCl (70 mg, 0.22 mmol), and sodium carbonate (84 mg, 0.80 mmol) producing an off-white greasy powder. Yield: 23 mg, 20%. ¹H-NMR (400.13 MHz, DMSO-*d*₆) δ 9.01 (s, 2H, C3_{trz}), 4.45 (q, *J* = 7.3 Hz, 4H, CH₂CH₃), 4.31 (q, *J* = 7.3 Hz, 4H, CH₂CH₃), 1.51 (t, *J* = 7.0 Hz, 6H, CH₂CH₃), 1.48 (t, *J* = 7.0 Hz, 6H, CH₂CH₃). ¹³C-NMR (100.62 MHz, DMSO-*d*₆) δ 183.7 (C5_{trz}), 144.6 (C3_{trz}), 48.5 (N4-CH₂CH₃), 44.1 (N1-CH₂CH₃), 16.8 (N4-CH₂CH₃), 16.0 (N1-CH₂CH₃). HRESI-MS: [C₁₂H₂₂AuN₆²⁺] *m/z* = 447.1973 calcd. = 447.1571.

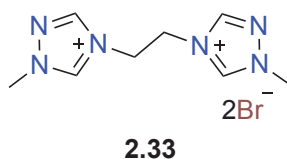


2.31. A mixture of 1-ethyl-imidazole (200 mg, 2.08 mmol) and dibromoethane (0.18 mL, 4.81 mmol) in acetonitrile (10 mL) was heated at reflux for 24 h. The off-white precipitate was collected followed by washing with acetonitrile and dried under vacuum to obtain the pure product as a white solid. Yield: 264 mg, 67%. ¹H-NMR (400.13 MHz, DMSO-*d*₆) δ 9.32 (s, 2H, C2-H_{im}), 7.86 (s, 4H, C4-H_{im}), 7.71 (s, 4H, C5-H_{im}), 4.75 (s, 4H, CH₂CH₂), 4.21 (q, *J* = 7.3 Hz, 4H, N1-CH₂CH₃), 1.41 (t, *J* = 7.3 Hz, N3-CH₂CH₃). ¹³C-NMR (100.62 MHz, DMSO-*d*₆) δ 136.9 (C2_{im}), 123.0 (C4_{im}), 122.9 (C5_{im}), 48.9 (C_{ethylene}), 44.9 (CH₂CH₃), 15.4 (CH₂CH₃). HRESI-MS: [C₁₂H₂₀N₄²⁺] *m/z* = 110.0702 calcd. = 110.0839.

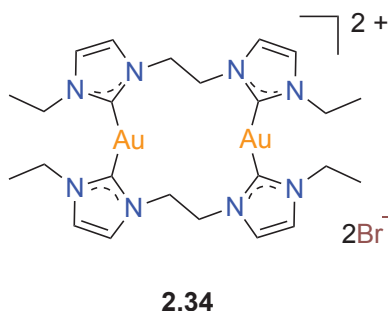


2.32. In a sealed tube, a mixture of 1-ethyl-1,2,4-triazole **2.10** (500 mg, 5.15 mmol) and dibromoethane (0.89 mL, 10.30 mmol) was stirred at 120 °C for 4 h. The resultant solid was collected followed by washing with acetonitrile (10 mL) to obtain the pure product as a white solid. Yield: 226 mg, 23%. ¹H-NMR (400.13 MHz, DMSO-*d*₆) δ 10.21 (s, 2H, C5-H_{trz}), 9.19 (s, 2H, C3-H_{trz}), 4.85 (s, 4H, N4-CH₂CH₂), 4.43 (q, *J* = 7.2 Hz, 4H, N1-CH₂CH₃), 1.57 – 1.42 (m, 6H, N1-CH₂CH₃). ¹³C-NMR (125.77 MHz, DMSO-*d*₆) δ 145.1 (C5_{trz}),

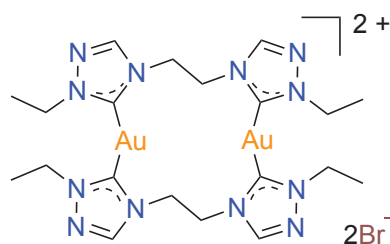
143.0 ($C3_{trz}$), 47.8 ($C_{ethylene}$). 47.0 (CH_2CH_3), 14.0 (CH_2CH_3). HRESI-MS: $[C_{10}H_{18}N_6]^{2+}$
 $m/z = 111.0746$ calcd. = 111.0791.



2.33. This compound was prepared using the same methods as **2.32** from **2.9** (400 mg, 4.81 mmol), and dibromoethane (0.42 mL, 4.82 mmol), producing a white powder. Yield: 203 mg, 24%. 1H -NMR (400.13 MHz, DMSO- d_6) δ 10.13 (s, 5H $C5-H_{trz}$), 9.17 (s, 2H $C3-H_{trz}$), 4.85 (s, 4H, $N4-CH_2CH_2$), 4.10 (s, 6H, CH_3). ^{13}C -NMR (125.77 MHz, DMSO- d_6) δ 145.1 ($C5_{trz}$), 143.8 ($C3_{trz}$), 47.1 ($C_{ethylene}$) 19.0 ($C-CH_3$). HRESI-MS: $[C_8H_{14}N_6]^{2+}$ $m/z = 97.0756$ calcd. = 97.0635.

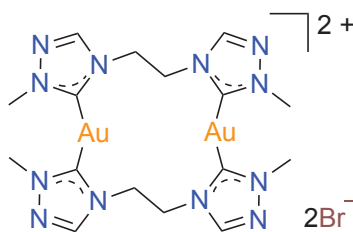


2.34. This compound was prepared using the same methods as **2.23** from **2.31** (100 mg, 0.26 mmol), (THT)AuCl (93 mg, 0.29 mmol), and sodium acetate (49 mg, 0.52 mmol) producing compound **2.34** as a white crystalline powder. Yield: 40 mg, 31%. 1H -NMR (400.13 MHz, DMSO- d_6) δ 7.55 (d, $J = 1.4$ Hz, 4H, $C4-H_{im}$), 7.47 (s, 4H, $C5-H_{im}$), 4.85 (s, 8H, CH_2CH_2), 4.14 (q, $J = 7.2$ Hz, 8H, CH_2CH_3), 1.33 (t, $J = 7.2$ Hz, 12H, CH_2CH_3). ^{13}C -NMR (125.77 MHz, DMSO- d_6) δ 182.4 ($C2_{im}$), 123.1 ($C4_{im}$), 122.1 ($C5_{im}$), 50.3 ($C_{ethylene}$), 46.3 (CH_2CH_3), 17.4 (CH_2CH_3). HRESI-MS: $[C_{24}H_{36}Au_2N_8]^{2+}$ $m/z = 415.1170$ calcd. = 415.1197.



2.35

2.35. This compound was prepared using the same methods as **2.23** from **2.32** (96 mg, 0.25 mmol), (THT)AuCl (87 mg, 0.28 mmol), sodium acetate (41 mg, 0.50 mmol), producing compound **2.35** as a white crystalline powder. Yield: 31 mg, 25%. ^1H -NMR (400.13 MHz, DMSO- d_6) δ 8.97 (s, 4H, C3- H_{trz}), 4.98 (s, 8H, CH_2CH_2), 4.39 (q, $J = 7.2$ Hz, 8H, N4- CH_2CH_3), 1.39 (t, $J = 7.2$ Hz, 12H, CH_2CH_3). ^{13}C -NMR (100.62 MHz, DMSO- d_6) δ 183.1 (C5 $_{\text{trz}}$), 145.2 (C3 $_{\text{trz}}$), 48.8 (C $_{\text{ethylene}}$) 47.9 (CH_2CH_3), 16.0 (CH_2CH_3) HRESI-MS: $[\text{C}_{20}\text{H}_{32}\text{Au}_2\text{N}_{12}]^{2+}$ $m/z = 417.1098$ calcd. = 417.1102.



2.36

2.36. This compound was prepared using the same methods as **2.23** from **2.33** (50 mg, 0.14 mmol), (THT)AuCl (50 mg, 0.16 mmol), sodium acetate (46 mg, 0.57 mmol), producing compound **2.36** as a white crystalline powder. Yield: 25 mg, 38%. ^1H -NMR (400.13 MHz, DMSO- d_6) δ 8.92 (s, 4H, C3- H_{trz}), 4.92 (s, 8H, CH_2CH_2), 4.05 (s, 12H, CH_3). ^{13}C -NMR (125.77 MHz, DMSO- d_6) δ 183.8 (C5 $_{\text{trz}}$), 145.1 (C3 $_{\text{trz}}$), 48.0 (C $_{\text{ethylene}}$) 19.8 (CH_3). HRESI-MS: $[\text{C}_{16}\text{H}_{24}\text{Au}_2\text{N}_{12}]^{2+}$ $m/z = 389.0792$ calcd. = 389.0789.

REFERENCES

1. M. Dryden, *J. Antimicrob. Chemother.*, 2009, **64**, 1121-1121.
2. A. Fleming, *Br. J. Exp. Pathol.*, 1929, **10**, 226-236.
3. R. Aminov, *Front. Microbiol.*, 2010, **1**.
4. N. D. Friedman, E. Temkin and Y. Carmeli, *Clin. Microbiol. Infect*, 2016, **22**, 416-422.
5. B. Ribeiro da Cunha, L. P. Fonseca and C. R. C. Calado, *Antibiotics (Basel)*, 2019, **8**, 45.
6. K. Lewis, *Nat. Rev. Drug. Discov.*, 2013, **12**, 371-387.
7. H. C. Neu, *Science*, 1992, **257**, 1064.
8. I. Nicolas, V. Bordeau, A. Bondon, M. Baudy-Floc'h and B. Felden, *PLOS Biol.*, 2019, **17**, e3000337.
9. S. B. Zaman, M. A. Hussain, R. Nye, V. Mehta, K. T. Mamun and N. Hossain, *Cureus*, 2017, **9**, e1403.
10. N. A. Johnson, M. R. Southerland and W. J. Youngs, *Molecules*, 2017, **22**, 20.
11. J.-Y. Maillard and P. Hartemann, *Crit. Rev. Microbiol.*, 2013, **39**, 373-383.
12. M. R. Desselle, R. Neale, K. A. Hansford, J. Zuegg, A. G. Elliott, M. A. Cooper and M. A. Blaskovich, *Future. sci. OA.*, 2017, **3**, FSO171.
13. S. Shrivastava, P. Shrivastava and J. Ramasamy, *J. Med. Soc.*, 2018, **32**, 76-77.
14. Z. Breijyeh, B. Jubeh and R. Karaman, *Molecules (Basel, Switzerland)*, 2020, **25**, 1340.
15. A. Frei, J. Zuegg, A. G. Elliott, M. Baker, S. Braese, C. Brown, F. Chen, C. G. Dowson, G. Dujardin, N. Jung, A. P. King, A. M. Mansour, M. Massi, J. Moat, H. A. Mohamed, A. K. Renfrew, P. J. Rutledge, P. J. Sadler, M. H. Todd, C. E. Willans, J. J. Wilson, M. A. Cooper and M. A. T. Blaskovich, *Chem. Sci.*, 2020, **11**, 2627-2639.
16. P. Chandrangsu, C. Rensing and J. D. Helmann, *Nat Rev Microbiol.*, 2017, **15**, 338-350.
17. S. Silver, *FEMS Microbiol. Rev.*, 2003, **27**, 341-353.
18. D. H. Nies, *Appl. Microbiol. Biotechnol.*, 1999, **51**, 730-750.

19. M. Claudel, J. V. Schwarte and K. M. Fromm, *Chemistry*, 2020, **2**, 849-899.
20. P. L. Drake and K. J. Hazelwood, *Ann. Occup. Hyg.*, 2005, **49**, 575-585.
21. A. Melaiye, R. S. Simons, A. Milsted, F. Pingitore, C. Wesdemiotis, C. A. Tessier and W. J. Youngs, *J. Med. Chem.*, 2004, **47**, 973-977.
22. A. Melaiye, Z. Sun, K. Hindi, A. Milsted, D. Ely, D. H. Reneker, C. A. Tessier and W. J. Youngs, *J. Am. Chem. Soc.*, 2005, **127**, 2285-2291.
23. R. A. Haque, S. Budagumpi, S. Y. Choo, M. K. Choong, B. E. Lokesh and K. Sudesh, *Appl. Organomet. Chem.*, 2012, **26**, 689-700.
24. R. A. Haque, P. O. Asekunowo, M. R. Razali and F. Mohamad, *Heteroat. Chem.*, 2014, **25**, 194-204.
25. C. Schmidt, L. Albrecht, S. Balasupramaniam, R. Misgeld, B. Karge, M. Brönstrup, A. Prokop, K. Baumann, S. Reichl and I. Ott, *Metallomics*, 2019, **11**, 533-545.
26. C. Schmidt, B. Karge, R. Misgeld, A. Prokop, M. Brönstrup and I. Ott, *MedChemComm.*, 2017, **8**, 1681-1689.
27. T. V. Serebryanskaya, A. A. Zolotarev and I. Ott, *MedChemComm.*, 2015, **6**, 1186-1189.
28. J. F. Arambula, R. McCall, K. J. Sidoran, D. Magda, N. A. Mitchell, C. W. Bielawski, V. M. Lynch, J. L. Sessler and K. Arumugam, *Chem. Sci.*, 2016, **7**, 1245-1256.
29. J. Fernández-Gallardo, B. T. Elie, M. Sanaú and M. Contel, *Chem. Commun.*, 2016, **52**, 3155-3158.
30. L. Zhang and Y.-F. Han, *Dalton Trans.*, 2018, **47**, 4267-4272.
31. G. Achar, S. C. R, S. A. Patil, J. G. Małecki and S. Budagumpi, *New. J. Chem.*, 2019, **43**, 1216-1229.
32. D. Bourissou, O. Guerret, F. P. Gabbaï and G. Bertrand, *Chem. Rev.*, 2000, **100**, 39-92.
33. F. E. Hahn and M. C. Jahnke, *Angew. Chem. Int. Ed.*, 2008, **47**, 3122-3172.
34. H. V. Huynh, in *The Organometallic Chemistry of N-heterocyclic Carbenes*, 2017, DOI: <https://doi.org/10.1002/9781118698785.ch6>, ch. 6, Group 11 Metal-NHC Complexes, pp. 171-219.
35. C. Köcher and W. A. Herrmann, *J. Organomet. Chem.*, 1997, **532**, 261-265.
36. J. Hine, *J. Am. Chem. Soc.*, 1950, **72**, 2438-2445.

37. W. von E. Doering, R. G. Buttery, R. G. Laughlin and N. Chaudhuri, *J. Am. Chem. Soc.*, 1956, **78**, 3224-3224.
38. H. W. Wanzlick, *Angew. Chem. Int. Ed.*, 1962, **1**, 75-80.
39. D. Dixon and A. Arduengo, *J. Phys. Chem.*, 1991, **95**, 4180-4182.
40. A. J. Arduengo, H. V. R. Dias, R. L. Harlow and M. Kline, *J. Am. Chem. Soc.*, 1992, **114**, 5530-5534.
41. P. de Frémont, N. Marion and S. P. Nolan, *Coord. Chem. Rev.*, 2009, **253**, 862-892.
42. E. Peris, *Chem. Rev.*, 2018, **118**, 9988-10031.
43. C. A. Smith, M. R. Narouz, P. A. Lummis, I. Singh, A. Nazemi, C.-H. Li and C. M. Crudden, *Chem. Rev.*, 2019, **119**, 4986-5056.
44. D. Nemcsok, K. Wichmann and G. Frenking, *Organometallics*, 2004, **23**, 3640-3646.
45. A. D. Russell and W. B. Hugo, in *Prog. Med. Chem.*, eds. G. P. Ellis and D. K. Luscombe, Elsevier, 1994, vol. 31, pp. 351-370.
46. H. J. Klasen, *Burns*, 2000, **26**, 117-130.
47. G. Tokmaji, H. Vermeulen, M. C. A. Müller, P. H. S. Kwakman, M. J. Schultz and S. A. J. Zaat, *Cochrane Database Syst. Rev.*, 2015, DOI: 10.1002/14651858.CD009201.pub2, CD009201.
48. S. Saint, J. G. Elmore, S. D. Sullivan, S. S. Emerson and T. D. Koepsell, *Am. J. Med.*, 1998, **105**, 236-241.
49. Z. Aziz, S. F. Abu and N. J. Chong, *Burns*, 2012, **38**, 307-318.
50. M. Petala, V. Tsiridis, E. Darakas and M. Kostoglou, *Water*, 2020, **12**, 258.
51. H. Wang, M. Wang, X. Yang, X. Xu, Q. Hao, A. Yan, M. Hu, R. Lobinski, H. Li and H. Sun, *Chem. Sci.*, 2019, **10**, 7193-7199.
52. H. Wang, A. Yan, Z. Liu, X. Yang, Z. Xu, Y. Wang, R. Wang, M. Koohi-Moghadam, L. Hu, W. Xia, H. Tang, Y. Wang, H. Li and H. Sun, *PLOS Biol.*, 2019, **17**, e3000292.
53. R. M. Joyce-Wohrmann and H. Munstedt, *Infection*, 1999, **27**, 46-48.
54. K. M. Hindi, M. J. Panzner, C. A. Tessier, C. L. Cannon and W. J. Youngs, *Chem. rev.*, 2009, **109**, 3859-3884.
55. S. Patil, K. Dietrich, A. Deally, B. Gleeson, H. Müller-Bunz, F. Paradisi and M. Tacke, *Helv. Chim. Acta.*, 2010, **93**, 2347-2364.

56. S. Patil, A. Deally, B. Gleeson, H. Müller-Bunz, F. Paradisi and M. Tacke, *Metallomics*, 2011, **3**, 74-88.
57. X. Liang, S. Luan, Z. Yin, M. He, C. He, L. Yin, Y. Zou, Z. Yuan, L. Li, X. Song, C. Lv and W. Zhang, *Eur. J. Med. Chem.*, 2018, **157**, 62-80.
58. M. A. Sierra, L. Casarrubios and M. C. de la Torre, *Chem. Eur. J.*, 2019, **25**, 7232-7242.
59. N. A. Johnson, M. R. Southerland and W. J. Youngs, *Molecules*, 2017, **22**, 1263.
60. R. Sakamoto, S. Morozumi, Y. Yanagawa, M. Toyama, A. Takayama, N. C. Kasuga and K. Nomiya, *J. Inorg. Biochem.*, 2016, **163**, 110-117.
61. K. Nomiya, S. Morozumi, Y. Yanagawa, M. Hasegawa, K. Kurose, K. Taguchi, R. Sakamoto, K. Mihara and N. C. Kasuga, *Inorg. Chem.*, 2018, **57**, 11322-11332.
62. A. J. Arduengo, H. V. R. Dias, J. C. Calabrese and F. Davidson, *Organometallics*, 1993, **12**, 3405-3409.
63. O. Guerret, S. Solé, H. Gornitzka, M. Teichert, G. Trinquier and G. Bertrand, *J. Am. Chem. Soc.*, 1997, **119**, 6668-6669.
64. H. M. J. Wang and I. J. B. Lin, *Organometallics*, 1998, **17**, 972-975.
65. A. A. D. Tulloch, A. A. Danopoulos, S. Winston, S. Kleinhenz and G. Eastham, *Dalton Trans.*, 2000, DOI: 10.1039/B007504N, 4499-4506.
66. J. C. Garrison and W. J. Youngs, *Chem. Rev.*, 2005, **105**, 3978-4008.
67. I. Ott, in *Inorganic and Organometallic Transition Metal Complexes with Biological Molecules and Living Cells*, ed. K. K.-W. Lo, Academic Press, 2017, DOI: <https://doi.org/10.1016/B978-0-12-803814-7.00005-8>, pp. 147-179.
68. D. Marchione, L. Belpassi, G. Bistoni, A. Macchioni, F. Tarantelli and D. Zuccaccia, *Organometallics*, 2014, **33**, 4200-4208.
69. I. Ott, *Coord. Chem. Rev.*, 2009, **253**, 1670-1681.
70. B. Bertrand and A. Casini, *Dalton Trans.*, 2014, **43**, 4209-4219.
71. T. Zou, C. T. Lum, C.-N. Lok, J.-J. Zhang and C.-M. Che, *Chem. Soc. Rev.*, 2015, **44**, 8786-8801.
72. A. Bindoli, M. P. Rigobello, G. Scutari, C. Gabbiani, A. Casini and L. Messori, *Coord. Chem. Rev.*, 2009, **253**, 1692-1707.
73. W. Liu, K. Bensdorf, M. Proetto, U. Abram, A. Hagenbach and R. Gust, *J. Med. Chem.*, 2011, **54**, 8605-8615.

74. M. V. Baker, P. J. Barnard, S. J. Berners-Price, S. K. Brayshaw, J. L. Hickey, B. W. Skelton and A. H. White, *Dalton Trans.*, 2006, 3708-3715.
75. P. J. Barnard, M. V. Baker, S. J. Berners-Price and D. A. Day, *J. Inorg. Biochem.*, 2004, **98**, 1642-1647.
76. J. L. Hickey, R. A. Ruhayel, P. J. Barnard, M. V. Baker, S. J. Berners-Price and A. Filipovska, *J. Am. Chem. Soc.*, 2008, **130**, 12570-12571.
77. G. Gasser and N. Metzler-Nolte, *Curr. Opin. Chem. Biol.*, 2012, **16**, 84-91.
78. C. Huerta-Aguilar, J. M. Talamantes Gómez, P. Thangarasu, I. Camacho-Arroyo, A. González-Arenas, J. Narayanan and R. Srivastava, *Appl. Organomet. Chem.*, 2013, **27**, 578-587.
79. G. Roymahapatra, S. M. Mandal, W. F. Porto, T. Samanta, S. Giri, J. Dinda, O. L. Franco and P. K. Chattaraj, *Curr. Med. Chem.*, 2012, **19**, 4184-4193.
80. H. G. Raubenheimer and S. Cronje, *Chem. Soc. Rev.*, 2008, **37**, 1998-2011.
81. A. Collado, A. Gómez-Suárez, A. R. Martin, A. M. Z. Slawin and S. P. Nolan, *Chem. Commun.*, 2013, **49**, 5541-5543.
82. H. V. Huynh, *Chem. Rev.*, 2018, **118**, 9457-9492.
83. D. J. Nelson and S. P. Nolan, *Chem. Soc. Rev.*, 2013, **42**, 6723-6753.
84. T. Dröge and F. Glorius, *Angew. Chem. Int. Ed.*, 2010, **49**, 6940-6952.
85. H. Jacobsen, A. Correa, C. Costabile and L. Cavallo, *J. Organomet. Chem.*, 2006, **691**, 4350-4358.
86. X. Hu, I. Castro-Rodriguez, K. Olsen and K. Meyer, *Organometallics*, 2004, **23**, 755-764.
87. X. Hu, Y. Tang, P. Gantzel and K. Meyer, *Organometallics*, 2003, **22**, 612-614.
88. D. Munz, *Organometallics*, 2018, **37**, 275-289.
89. A. P. Railliet, D. A. Safin, K. Robeyns and Y. Garcia, *CrystEngComm.*, 2012, **14**, 4812-4818.
90. M. Andersson Trojer, A. Movahedi, H. Blanck and M. Nydén, *J. Chem.*, 2013, **2013**, 1-23.
91. H. Lin and D. Sun, *Org. Prep. Proced. Int.*, 2013, **45**, 341 – 394.
92. H. Qian, Z. Wang, W. Yue and D. Zhu, *J. Am. Chem. Soc.*, 2007, **129**, 10664-10665.
93. A. Tam, I. S. Armstrong and T. E. La Cruz, *Org. Lett.*, 2013, **15**, 3586-3589.

94. J. Zhao, L. Yang, L. Zhang, J. Guo, Y. Shi, G. Pang and C. Cao, *J. Chem. Res.*, 2011, **35**, 686-688.
95. Z. Li, E. R. R. Mackie, P. Ramkissoon, J. C. Mather, N. Wiratpruk, T. P. Soares da Costa and P. J. Barnard, *Dalton Trans.*, 2020, **49**, 12820-12834.
96. H. Schmidbaur and A. Schier, *Chem. Soc. Rev.*, 2012, **41**, 370-412.
97. V. W.-W. Yam and E. C.-C. Cheng, *Chem. Soc. Rev.*, 2008, **37**, 1806-1813.
98. R. Sugden, R. Kelly and S. Davies, *Nat. Microbiol.*, 2016, **1**, 16187.
99. U. Theuretzbacher, K. Outtersson, A. Engel and A. Karlén, *Nat. Rev. Microbiol.*, 2020, **18**, 275-285.
100. S. H. Podolsky, *Palgrave. Commun.*, 2018, **4**, 124.
101. H. Wang, M. Lee, Z. Peng, B. Blázquez, E. Lastochkin, M. Kumarasiri, R. Bouley, M. Chang and S. Mobashery, *J. Med. Chem.*, 2015, **58**, 4194-4203.
102. M. Carrera, K. Böhme, J. M. Gallardo, J. Barros-Velázquez, B. Cañas and P. Calo-Mata, *Front. Microbiol.*, 2017, **8**, 2458-2458.
103. Z. Zong, S. Fenn, C. Connor, Y. Feng and A. McNally, *J. Antimicrob. Chemother.*, 2018, **73**, 2340-2346.
104. M. D. Adams, K. Goglin, N. Molyneaux, K. M. Hujer, H. Lavender, J. J. Jamison, I. J. MacDonald, K. M. Martin, T. Russo, A. A. Campagnari, A. M. Hujer, R. A. Bonomo and S. R. Gill, *J. Bacteriol.*, 2008, **190**, 8053-8064.
105. J. C. Rees, C. L. Pierce, D. M. Schieltz and J. R. Barr, *Anal. Chem.*, 2015, **87**, 6769-6777.
106. P. T. McKenney, L. Ling, G. Wang, S. Mane and E. G. Pamer, *Genome. announ.*, 2016, **4**, e00386-00316.
107. M. Ghosh, Y.-M. Lin, P. A. Miller, U. Möllmann, W. C. Boggess and M. J. Miller, *Infect. Dis.*, 2018, **4**, 1529-1535.
108. A. J. Clark and A. D. Margulies, *Proc. Natl. Acad. Sci. U. S. A.*, 1965, **53**, 451.
109. M. E. Wand, L. J. Bock, L. C. Bonney and J. M. Sutton, *Antimicrob. Agents. Chemother.*, 2017, **61**, e01162-01116.
110. P. J. Dyson, A. K. Hearley, B. F. G. Johnson, J. S. McIndoe and P. R. R. Langridge-Smith, *Dalton Trans.*, 2000, **0**, 2521-2525.
111. P. J. Dyson, A. K. Hearley, B. F. G. Johnson, J. S. McIndoe, P. R. R. Langridge-Smith and C. Whyte, *Rapid Commun. Mass Spectrom.*, 2001, **15**, 895-897.

112. P. J. Dyson, J. S. McIndoe and D. Zhao, *Chem. Commun.*, 2003, DOI: 10.1039/B211669C, 508-509.
113. V. A. Pashynska, M. V. Kosevich, H. V. d. Heuvel and M. Claeys, *Rapid Commun. Mass Spectrom.*, 2006, **20**, 755-763.
114. R. Rubbiani, S. Can, I. Kitanovic, H. Alborzinia, M. Stefanopoulou, M. Kokoschka, S. Mönchgesang, W. S. Sheldrick, S. Wölfl and I. Ott, *J. Med. Chem.*, 2011, **54**, 8646-8657.
115. K. M. Hindi, T. J. Siciliano, S. Durmus, M. J. Panzner, D. A. Medvetz, D. V. Reddy, L. A. Hogue, C. E. Hovis, J. K. Hilliard, R. J. Mallet, C. A. Tessier, C. L. Cannon and W. J. Youngs, *J. Med. Chem.*, 2008, **51**, 1577-1583.
116. M. J. Satlin, *J. Clin. Microbiol.*, 2019, **57**, e01608-01618.
117. S. Rincon, D. Panesso, L. Diaz, L. P. Carvajal, J. Reyes, J. M. Munita and C. A. Arias, *Biomedica.*, 2014, **34**, 191-208.
118. I. G. Boneca and G. Chiosis, *Expert Opin. Ther. Targets.*, 2003, **7**, 311-328.
119. N. P. S. f. A. S. Testing, *NCCLS. Performance Standards for Antimicrobial Susceptibility Testing*, 2020, **30**, NCCLS publication no. M100.
120. O. V. Dolomanov, L. J. Bourhis, R. J. Gildea, J. A. K. Howard and H. Puschmann, *J. Appl. Crystallogr.*, 2009, **42**, 339-341.
121. W. National Committee for Clinical Laboratory Standards (2003) Methods for Dilution Antimicrobial Susceptibility Tests for Bacteria that Grow Aerobically: M7-A6. Approved Standard. National Committee for Clinical Laboratory Standards, 2003.
122. W. National Committee for Clinical Laboratory Standards (2004) Standards for Antimicrobial Susceptibility Testing: M100-S14. National Committee for Clinical Laboratory Standards, PA., 2004.
123. M. E. Wand, L. J. Bock, L. C. Bonney and J. M. Sutton, *Antimicrob. Agents Chemother.*, 2017, **61**, 1162-1116.

APPENDIX

NMR Spectra

Figure S1. ^1H -NMR spectrum of compound **2.1**

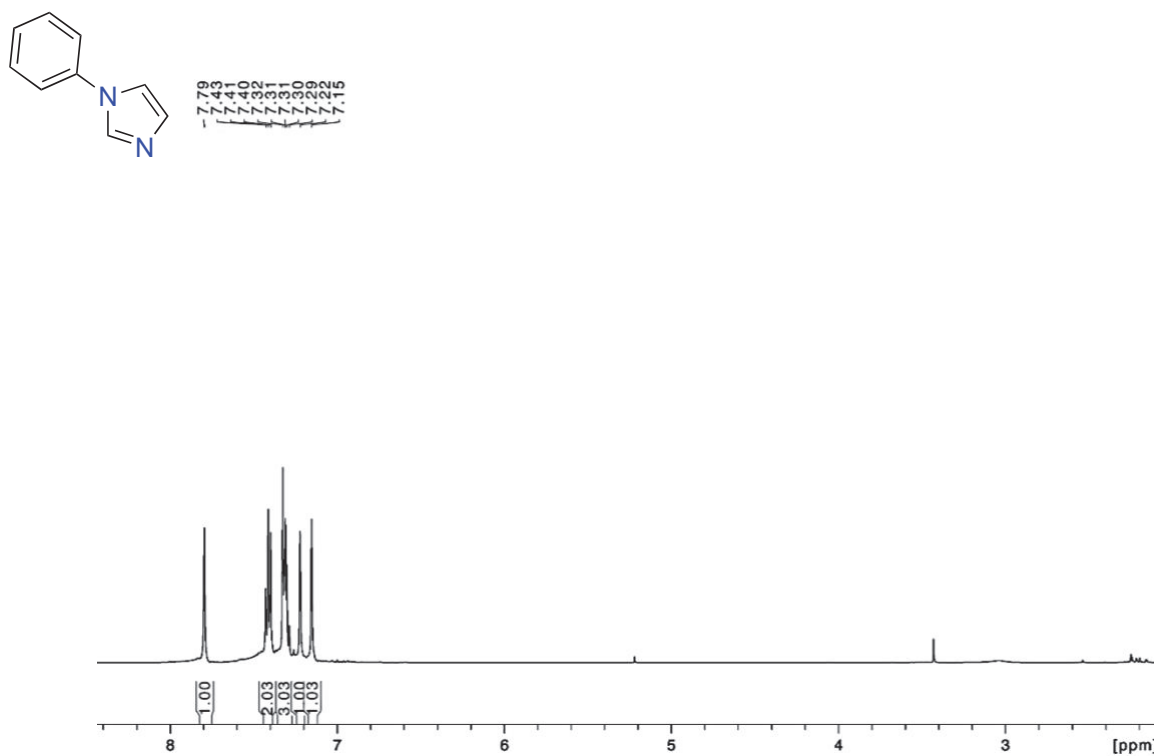


Figure S2. ^{13}C -NMR spectrum of compound **2.1**

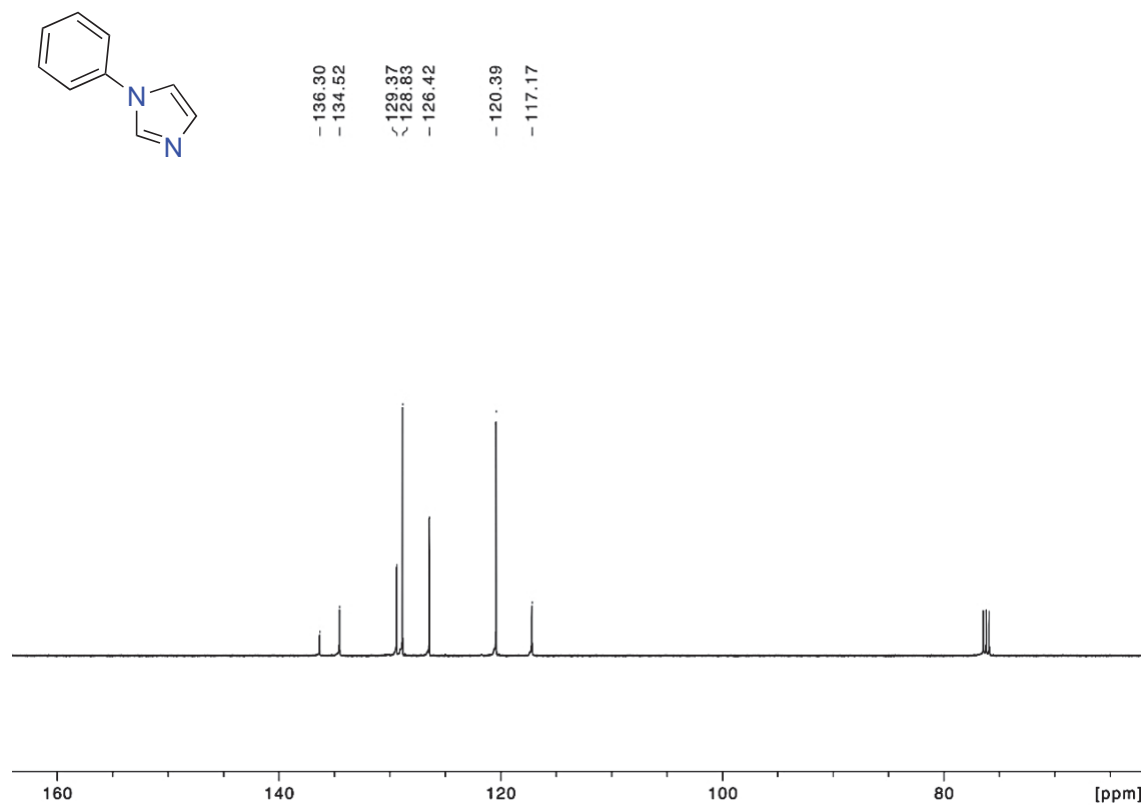


Figure S3. ^1H -NMR spectrum of compound **2.2**

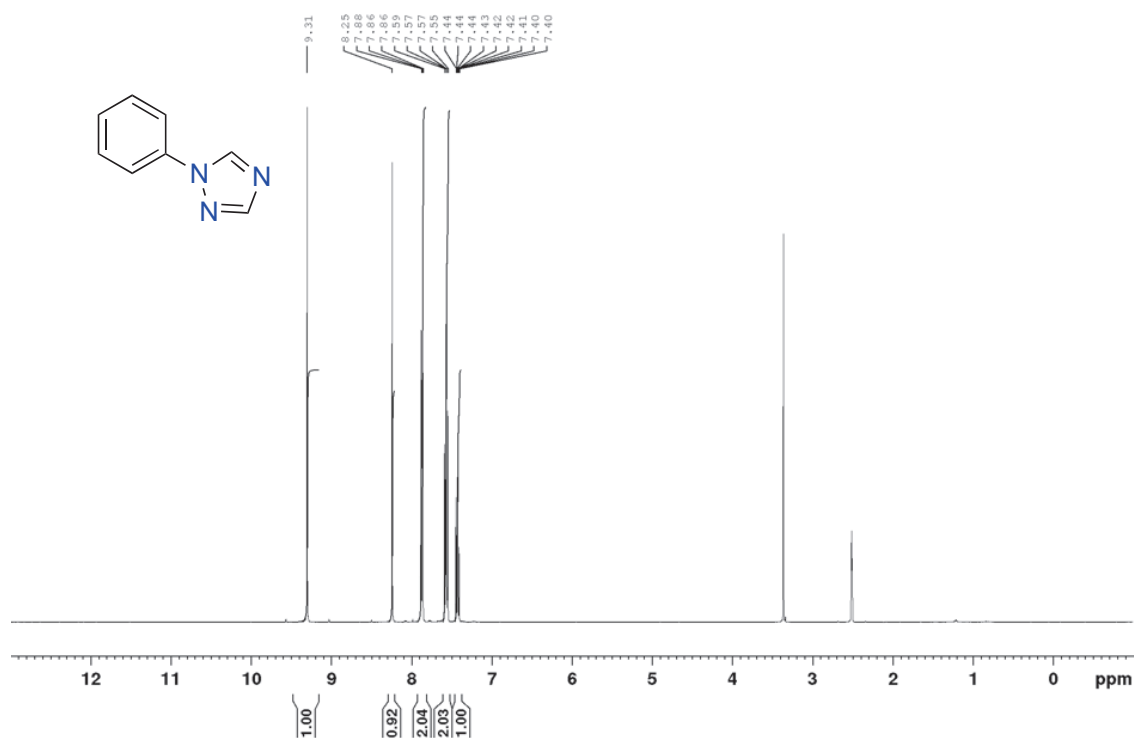


Figure S4. ^{13}C -NMR spectrum of compound **2.2**

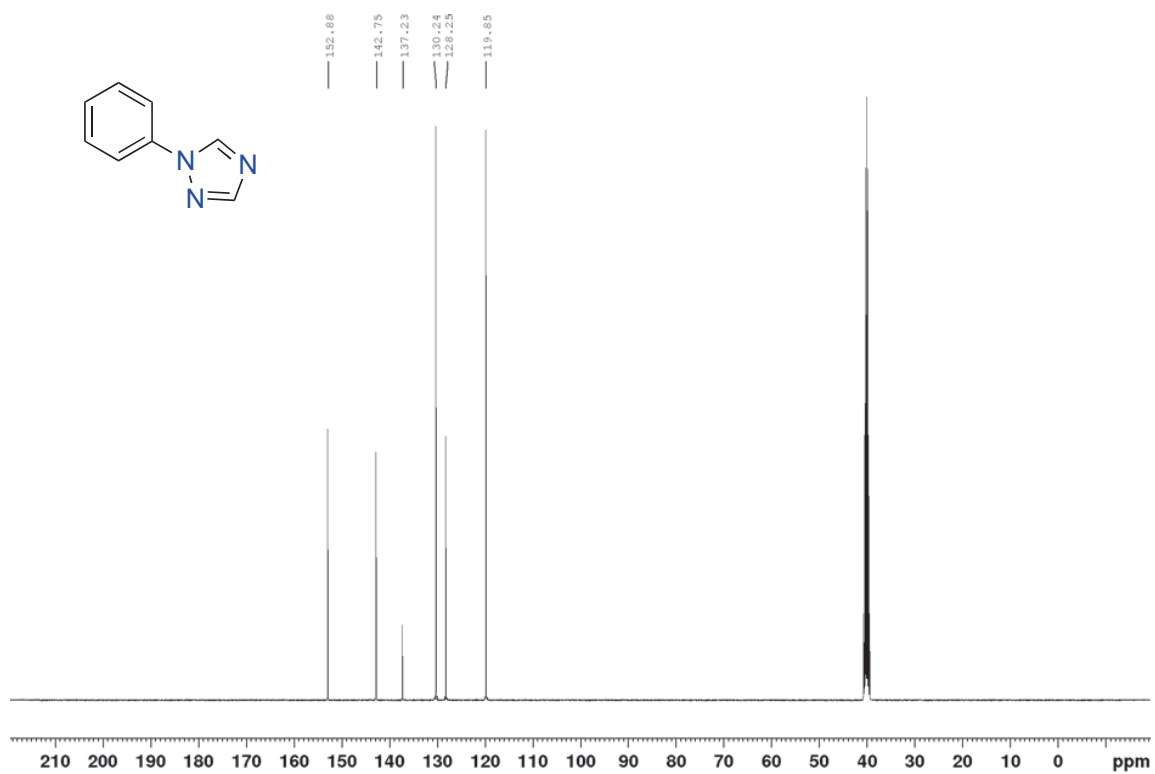


Figure S5. ^1H -NMR spectrum of compound **2.3**

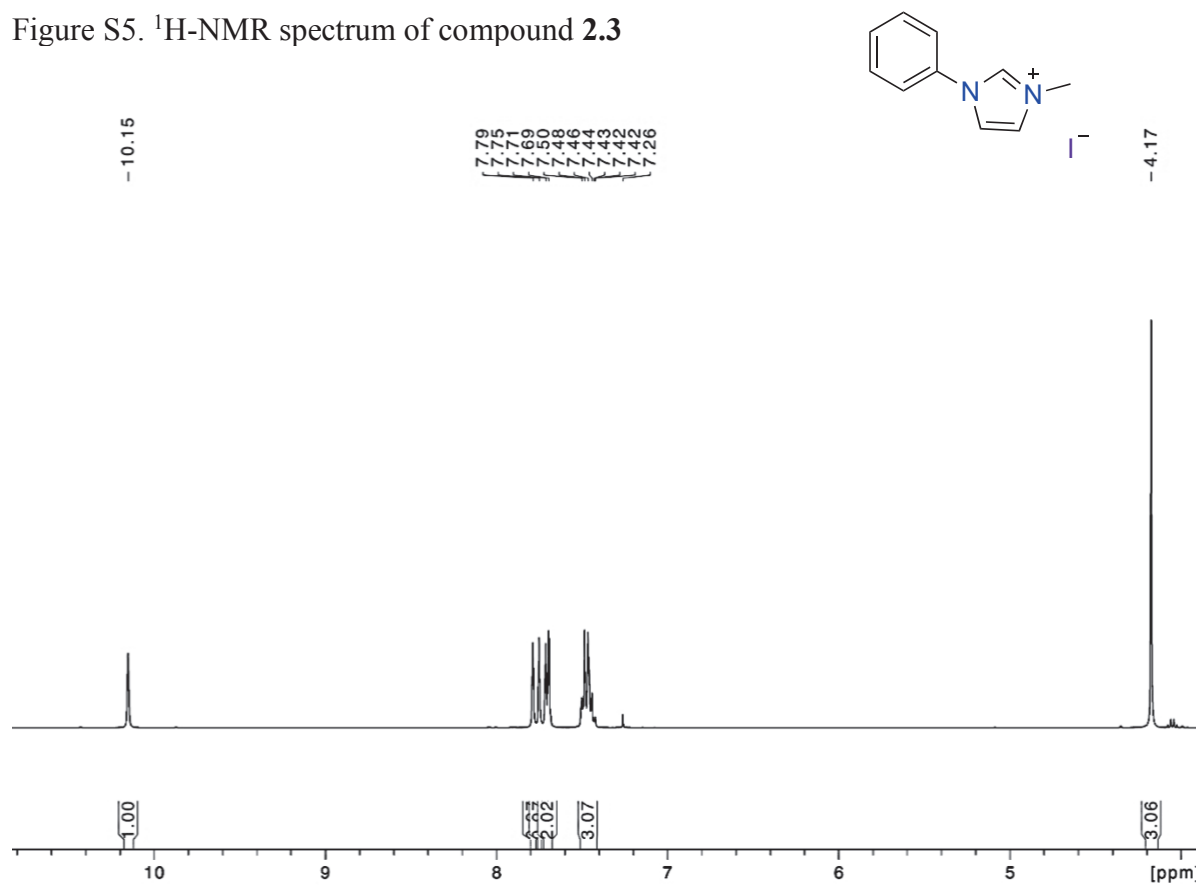


Figure S6. ^{13}C -NMR spectrum of compound **2.3**

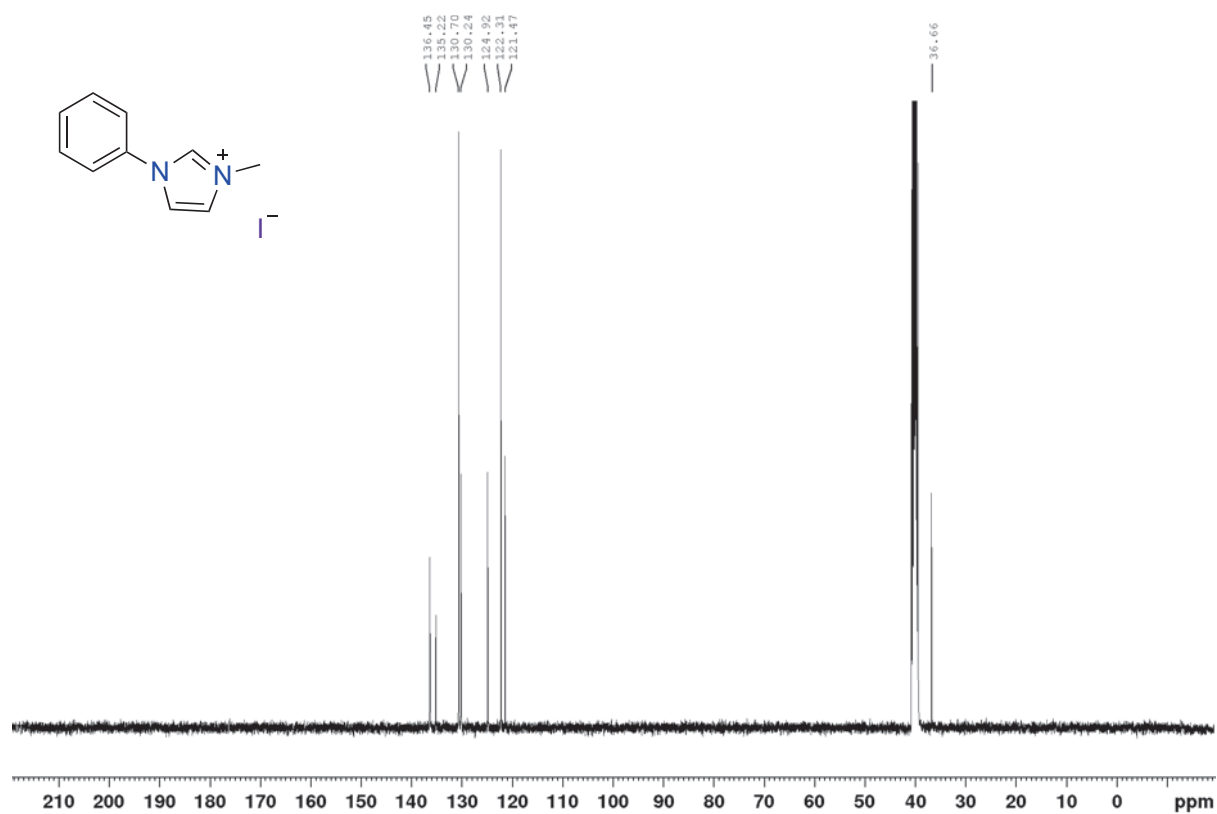


Figure S7. ^1H -NMR spectrum of compound **2.4**

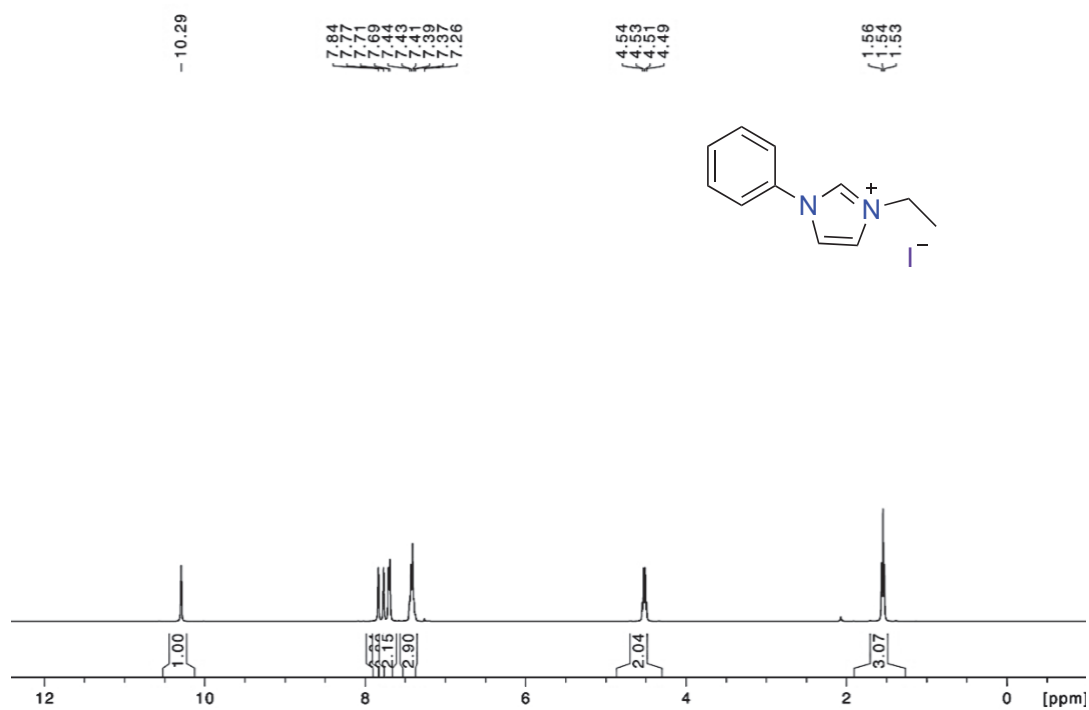


Figure S8. ^{13}C -NMR spectrum of compound **2.4**

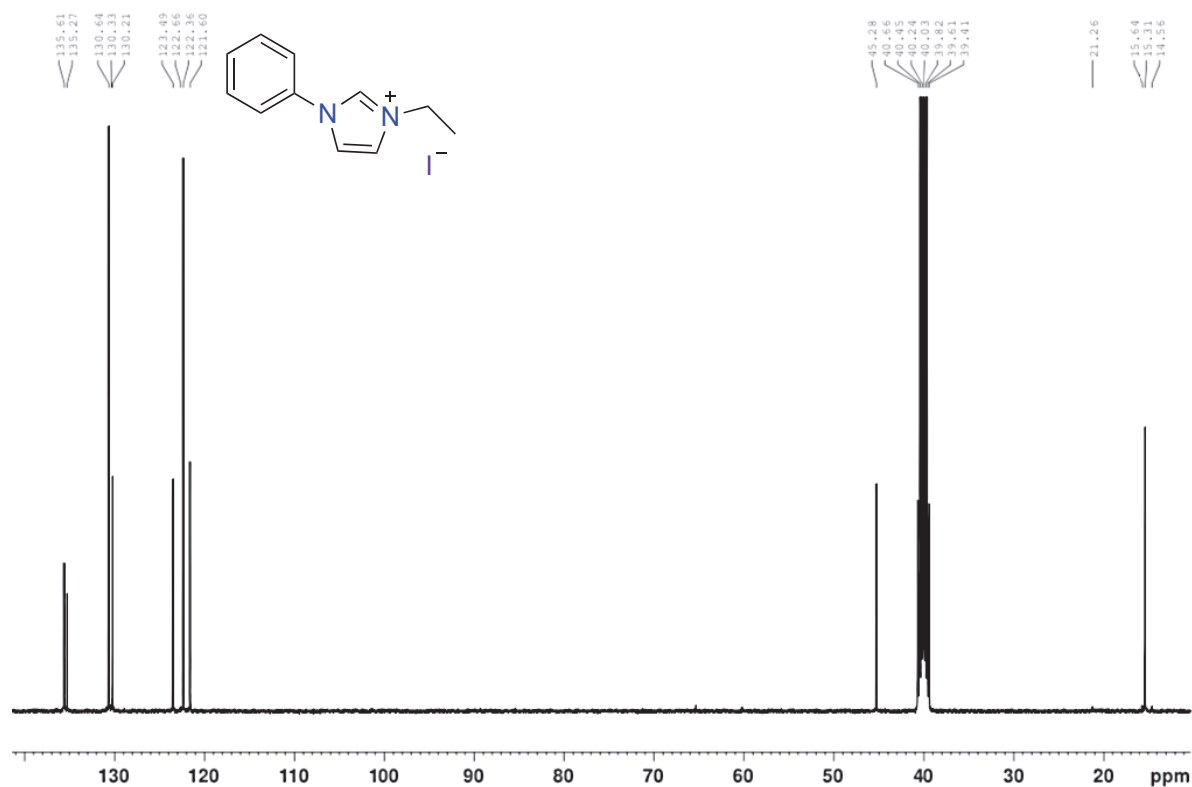


Figure S9. ^1H -NMR spectrum of compound **2.5**

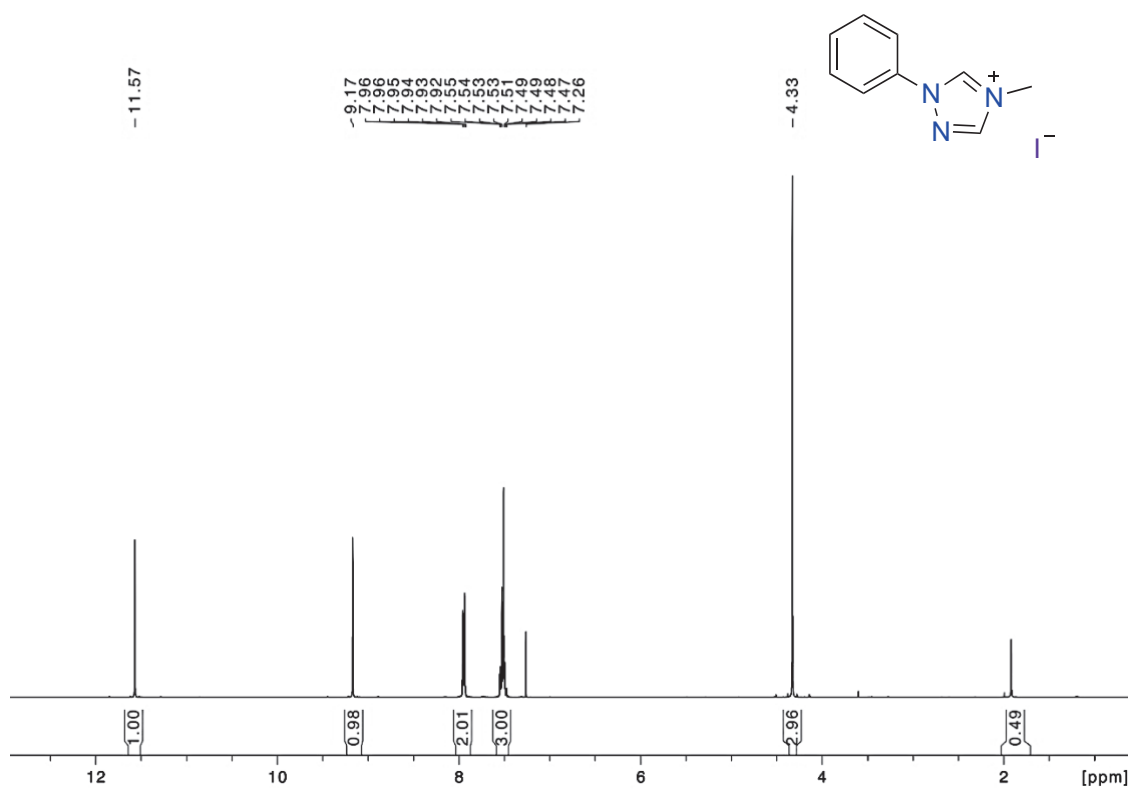


Figure S10. ^{13}C -NMR spectrum of compound **2.5**

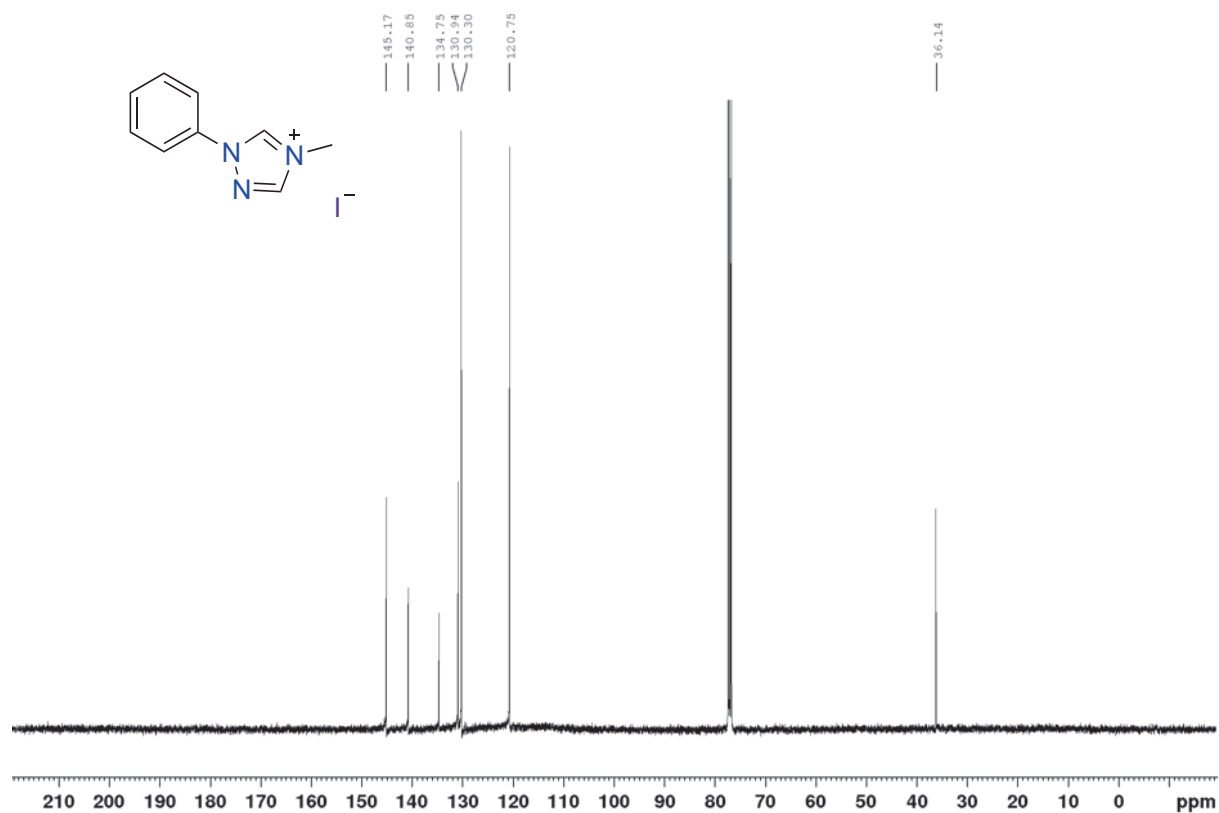


Figure S11. ^1H -NMR spectrum of compound **2.6**

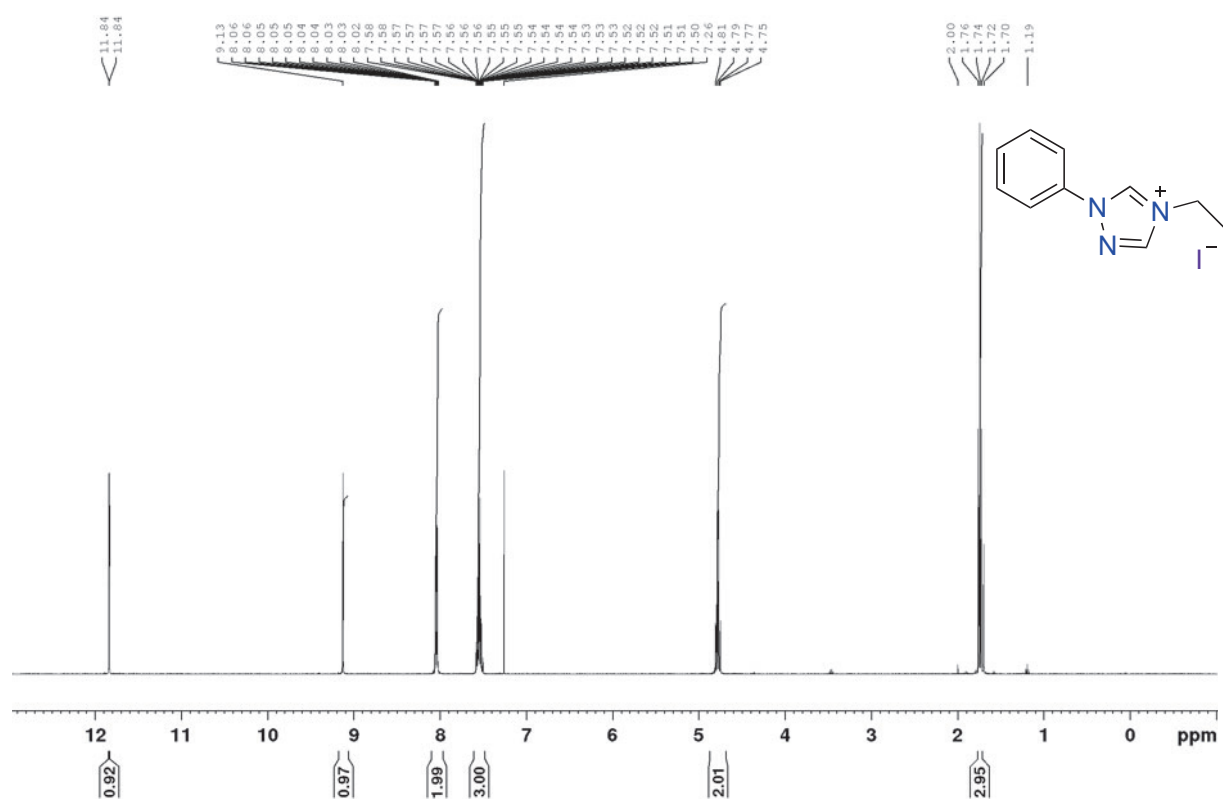


Figure S12. ^{13}C -NMR spectrum of compound **2.6**

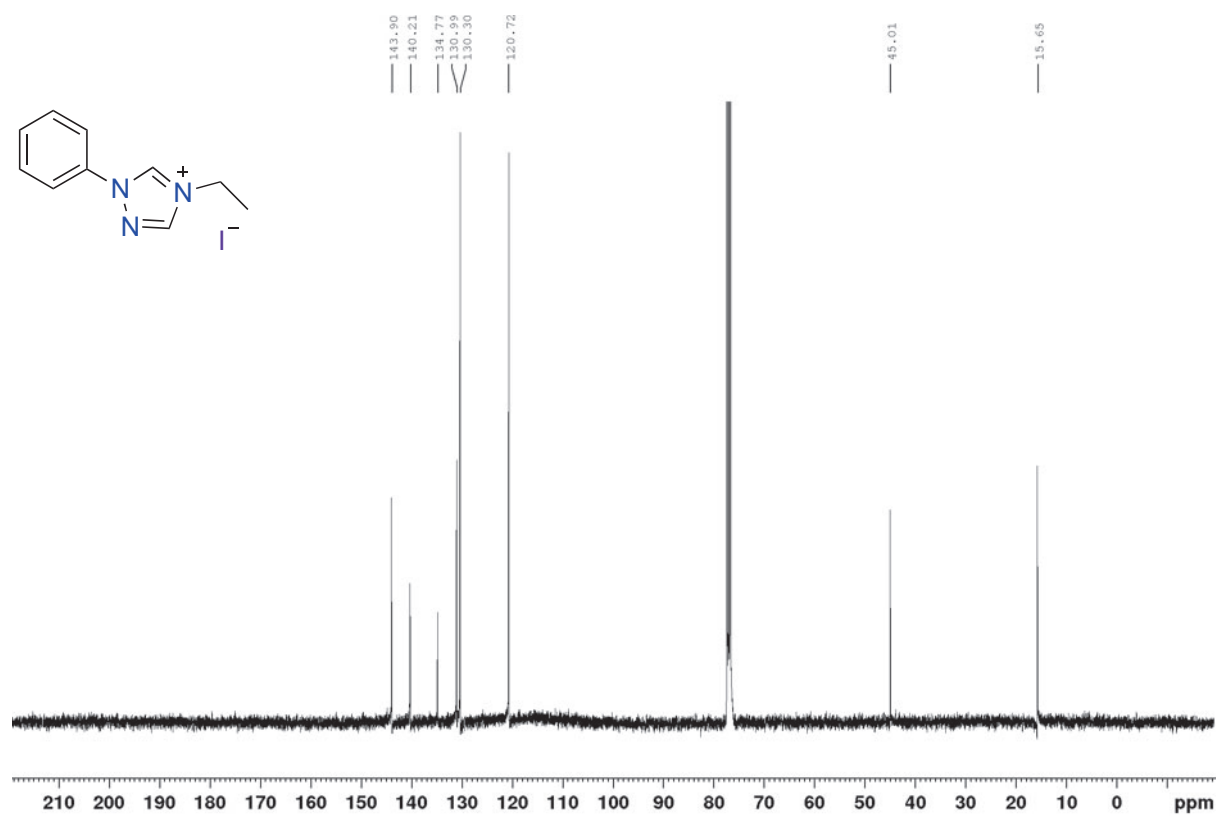


Figure S13. ^1H -NMR spectrum of compound **2.7**

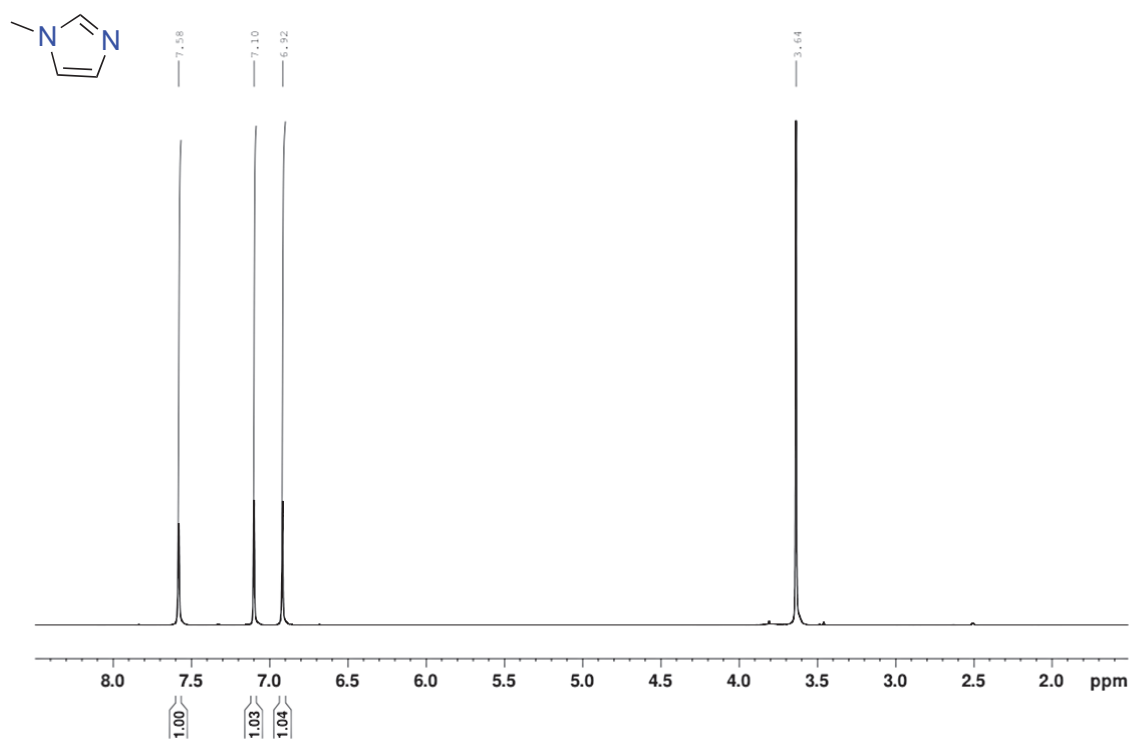


Figure S14. ^{13}C -NMR spectrum of compound **2.7**

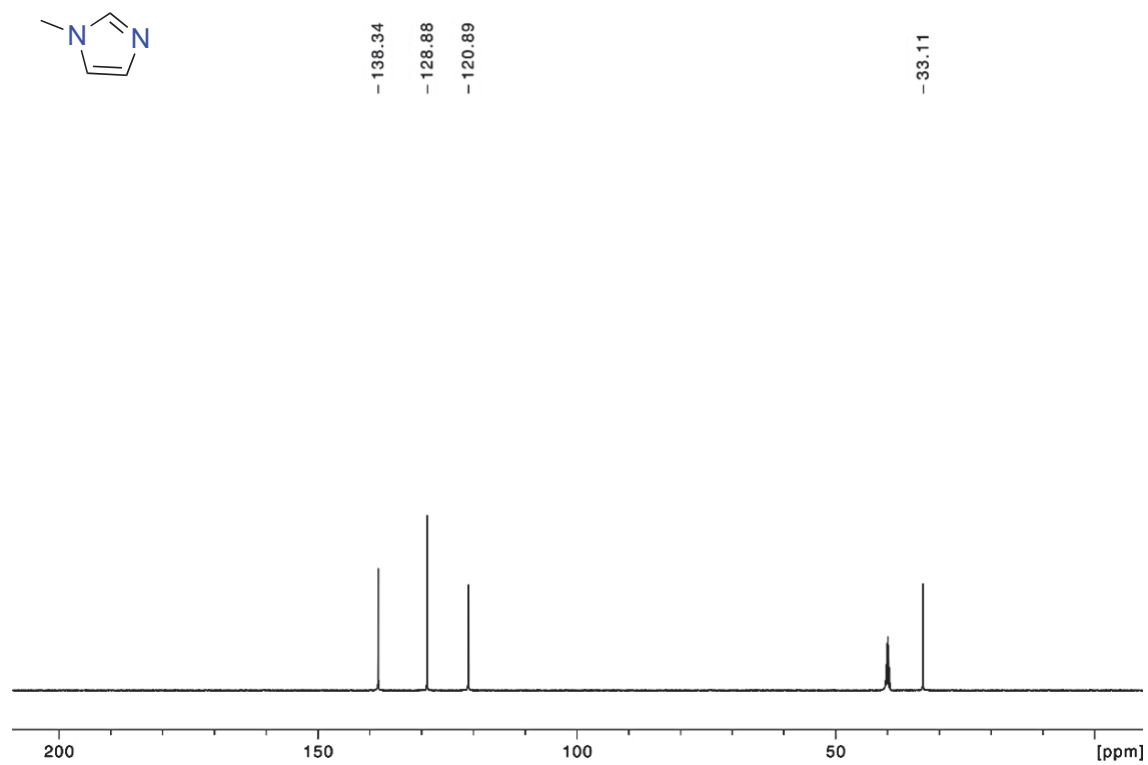


Figure S15. ^1H -NMR spectrum of compound **2.8**

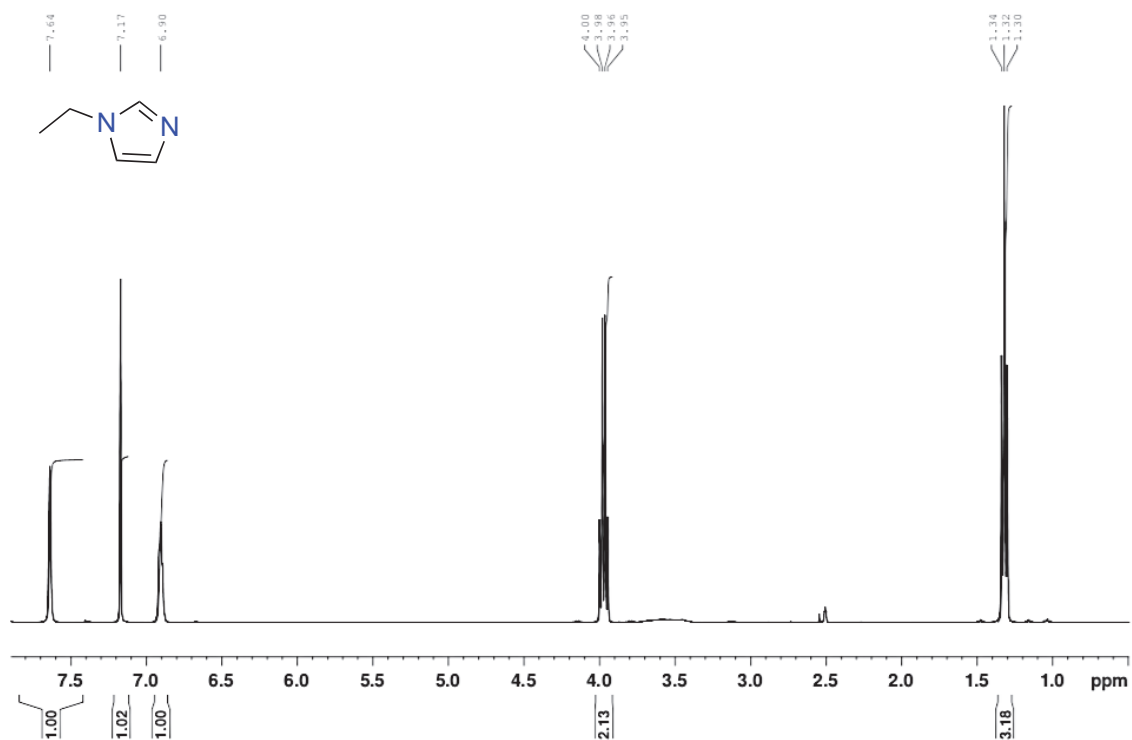


Figure S16. ^{13}C -NMR spectrum of compound **2.8**

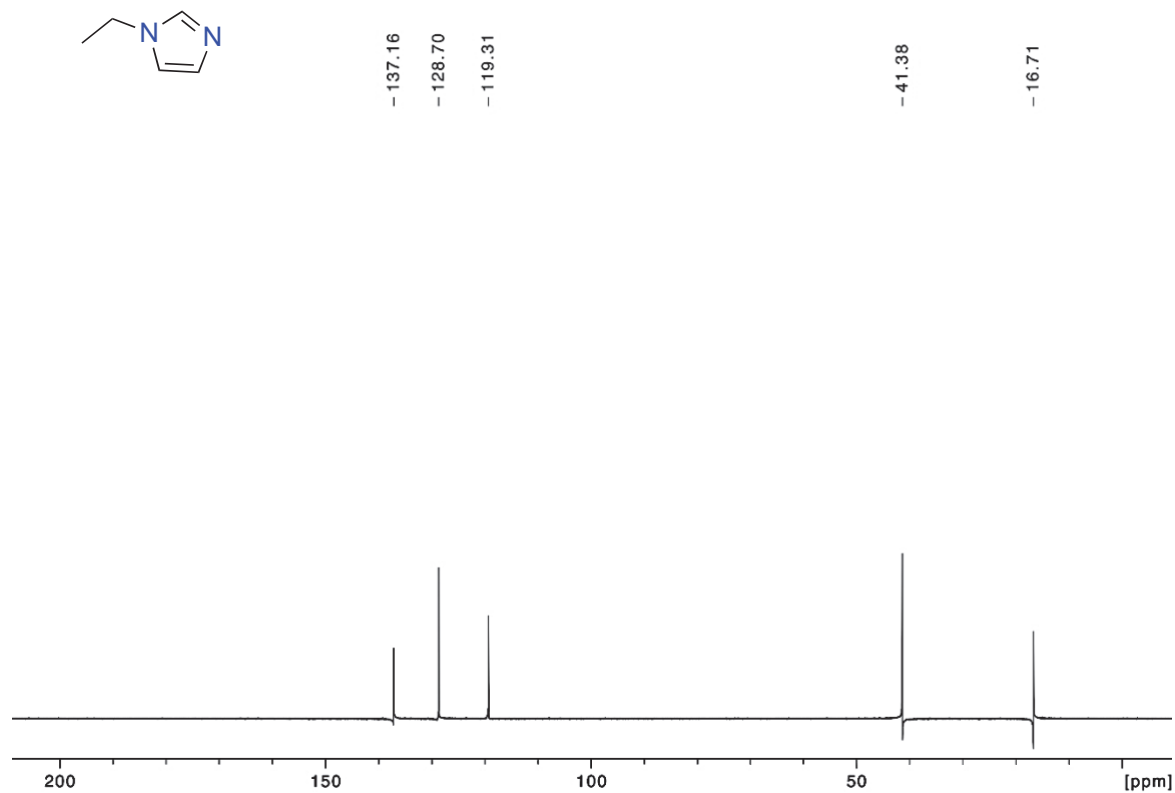


Figure S17. ^1H -NMR spectrum of compound **2.9**

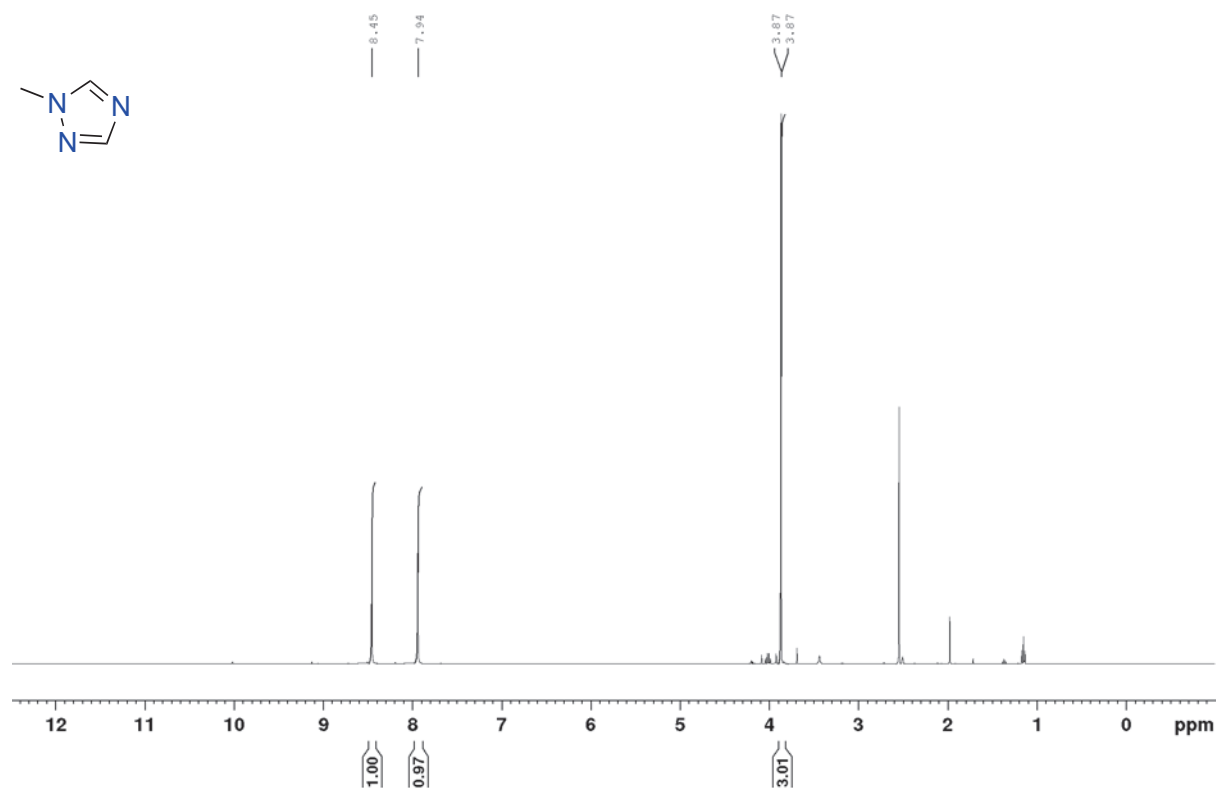


Figure S18. ^{13}C -NMR spectrum of compound **2.9**

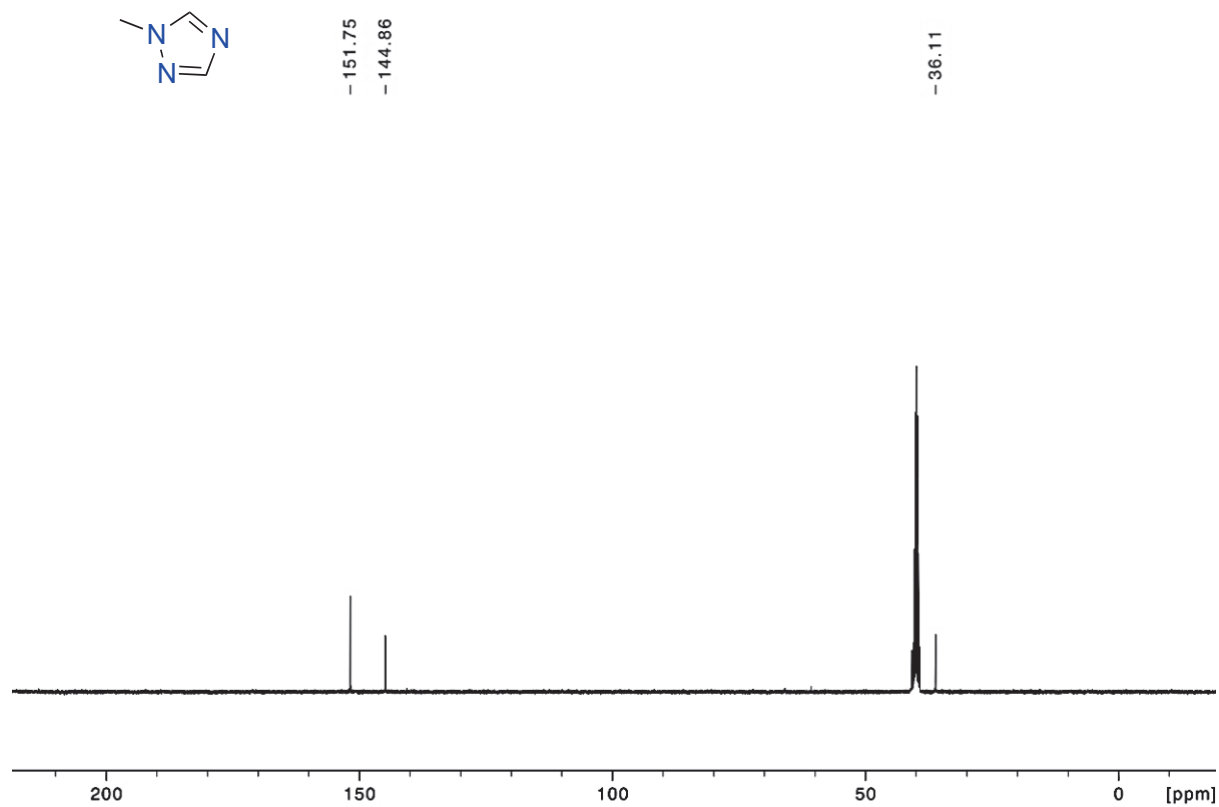


Figure S19. ^1H -NMR spectrum of compound **2.10**

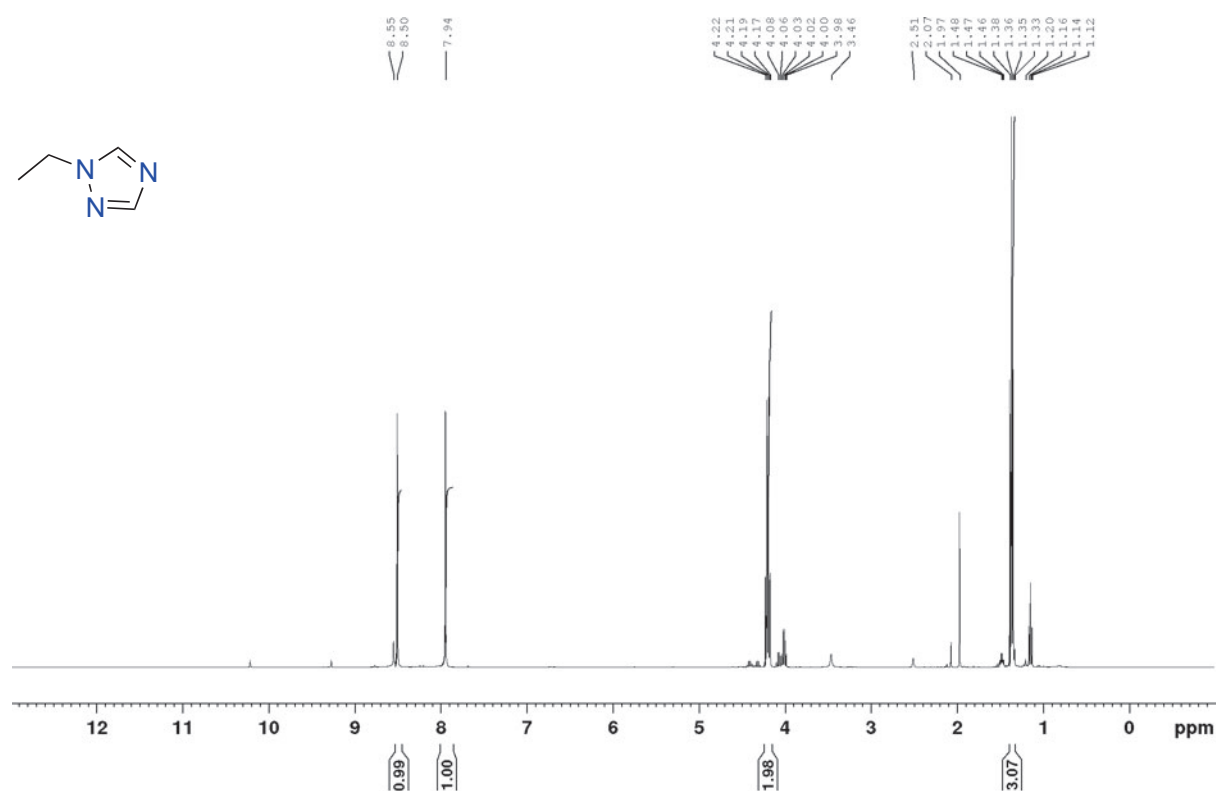


Figure S20. ^{13}C -NMR spectrum of compound **2.10**

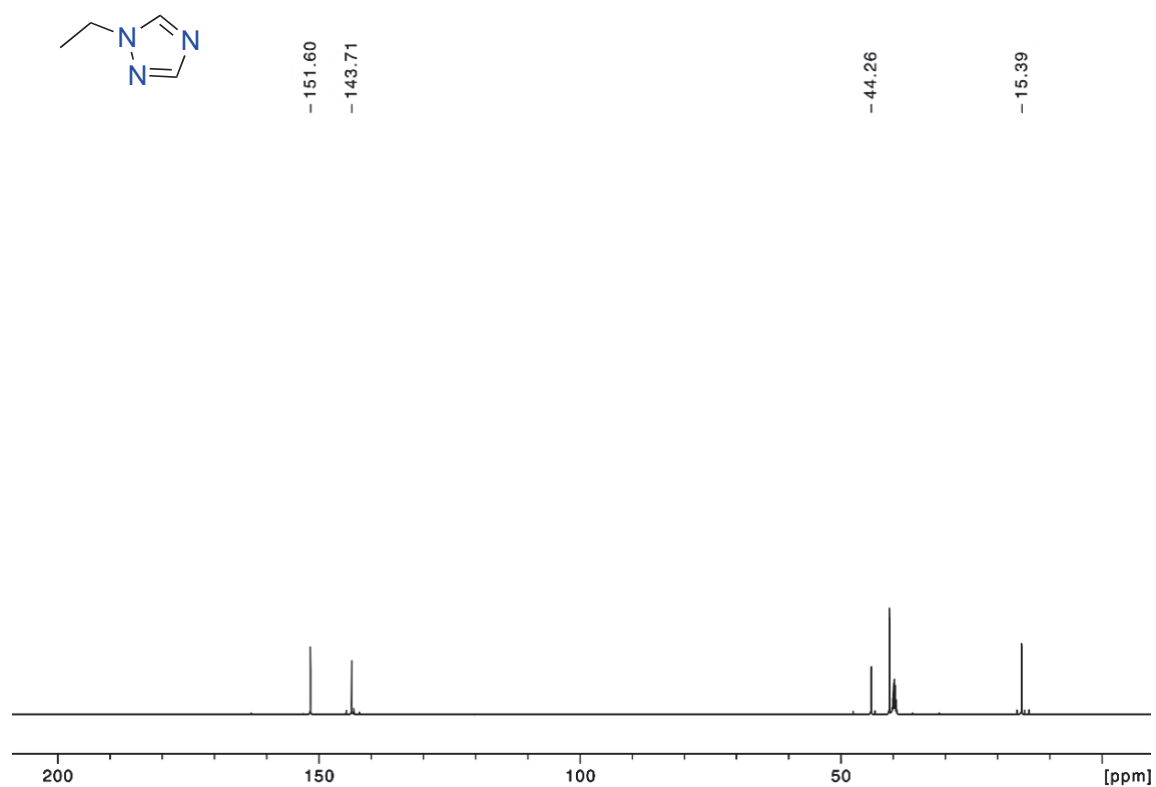


Figure S21. ^1H -NMR spectrum of compound **2.11**

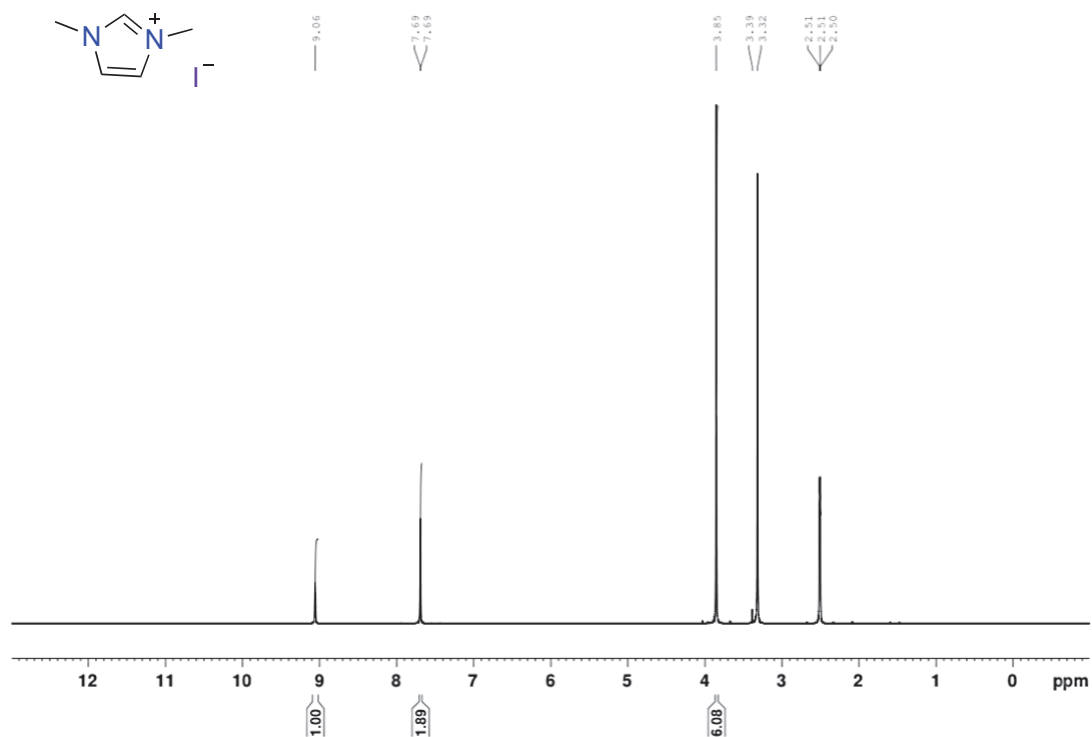


Figure S22. ^{13}C -NMR spectrum of compound **2.11**

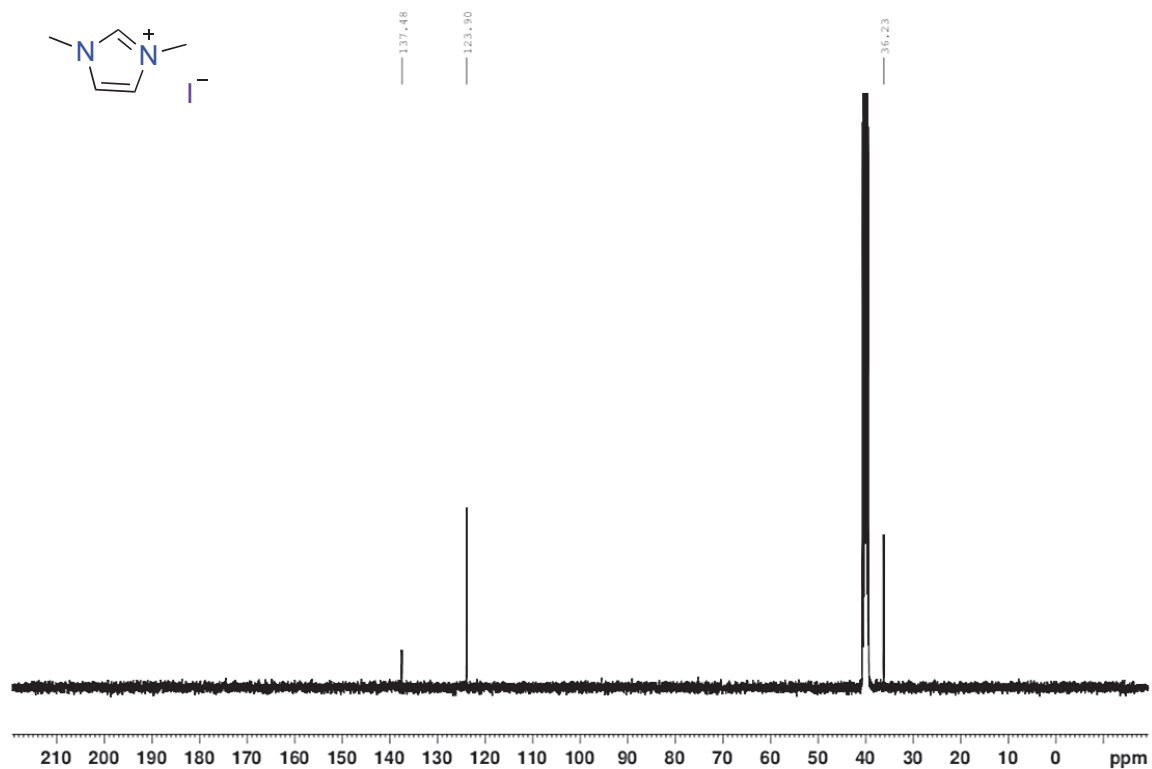


Figure S23. ^1H -NMR spectrum of compound **2.12**

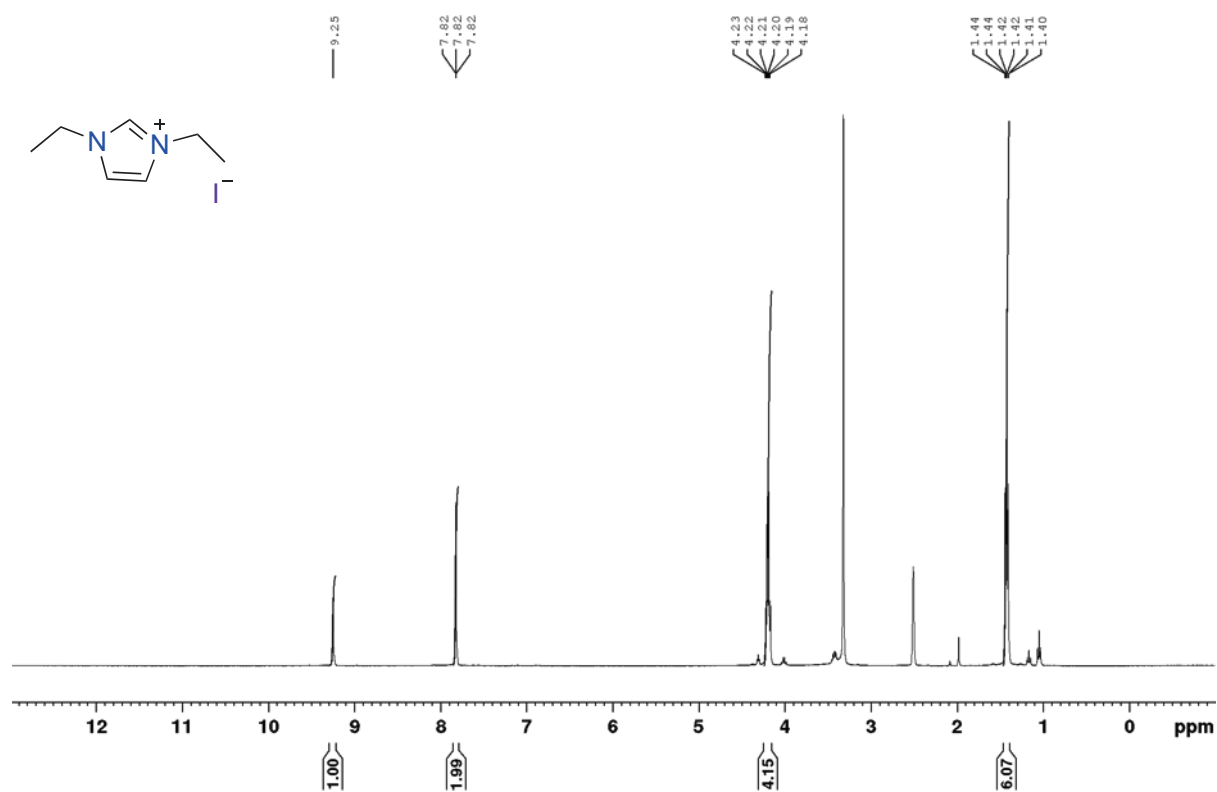


Figure S24. ^{13}C -NMR spectrum of compound **2.12**

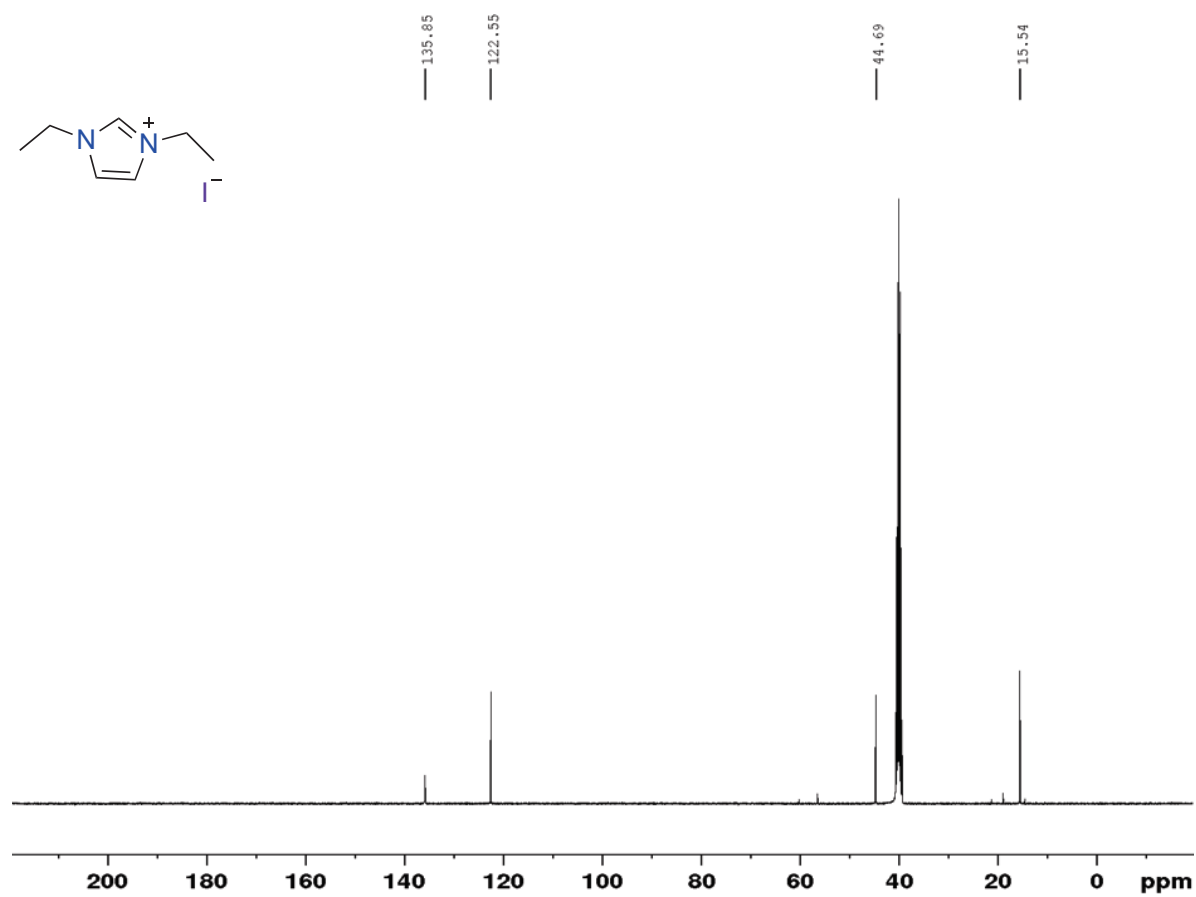


Figure S25. ^1H -NMR spectrum of compound **2.13**

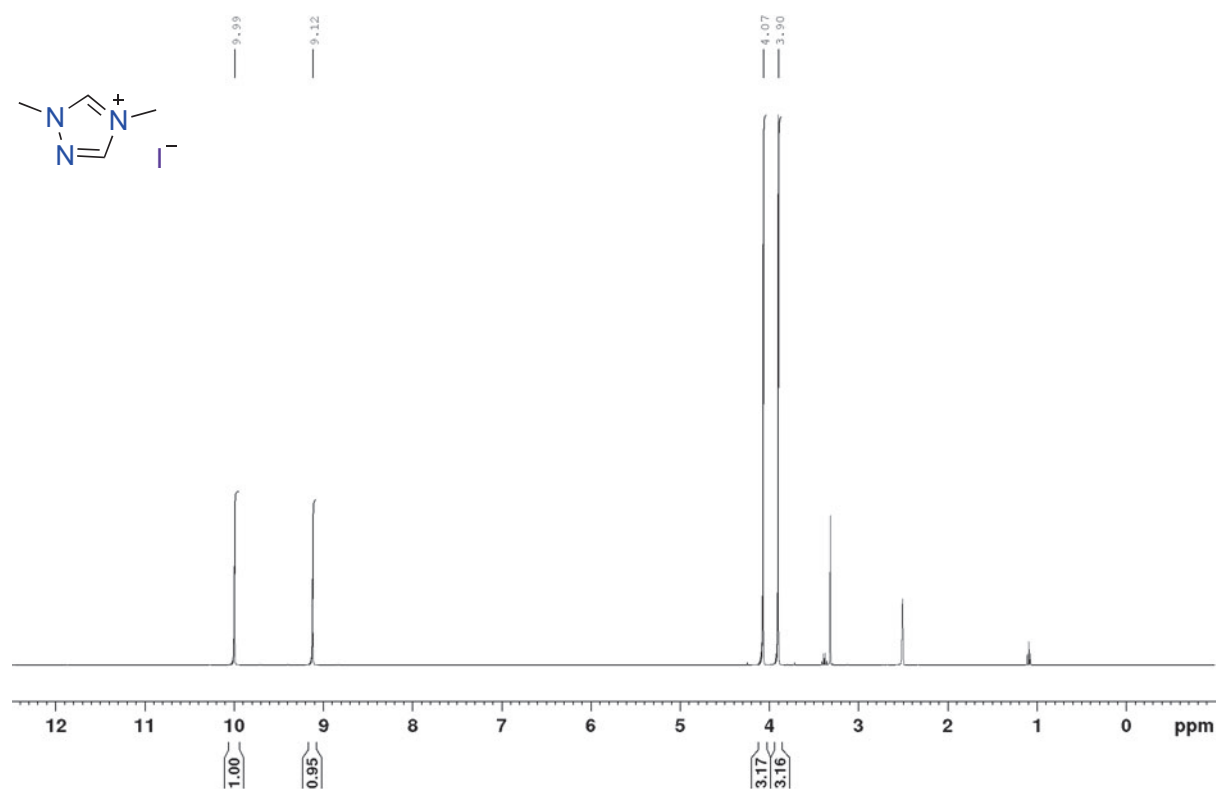


Figure S26. ^{13}C -NMR spectrum of compound **2.13**

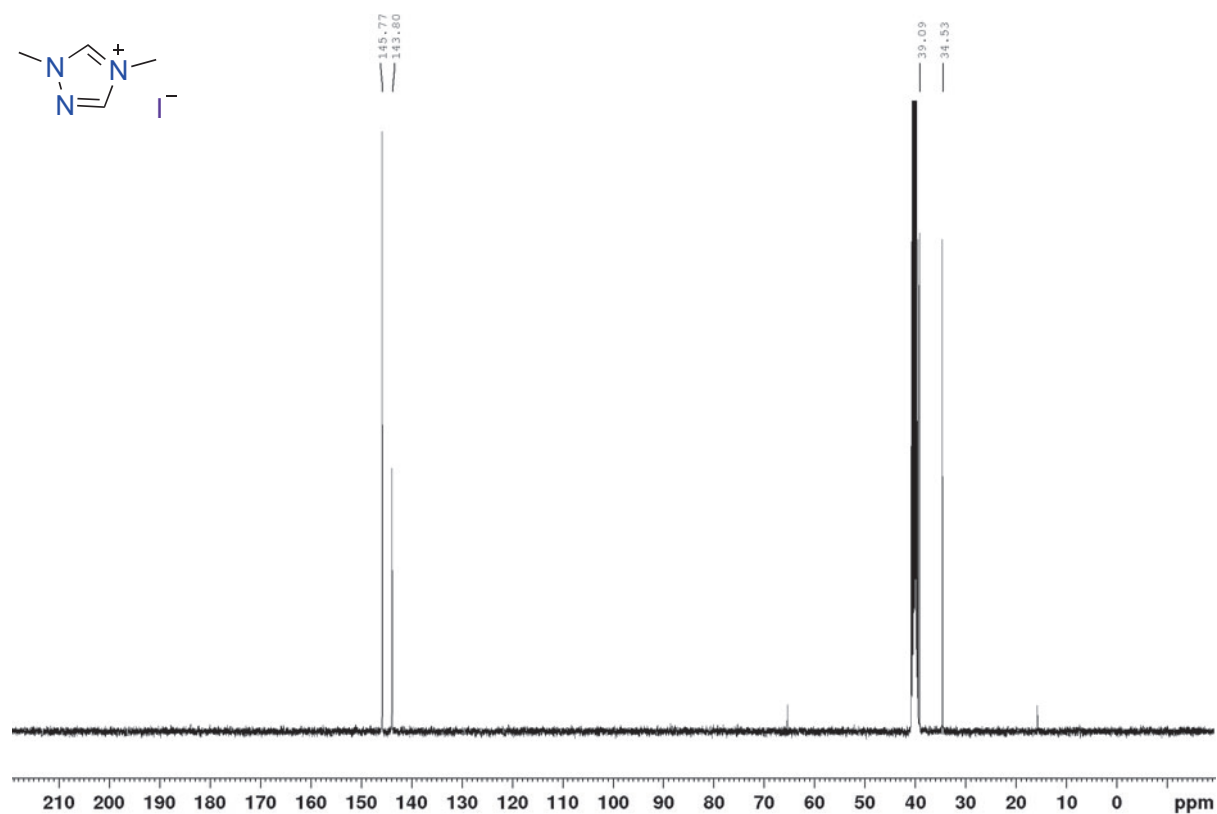


Figure S27. ^1H -NMR spectrum of compound **2.14**

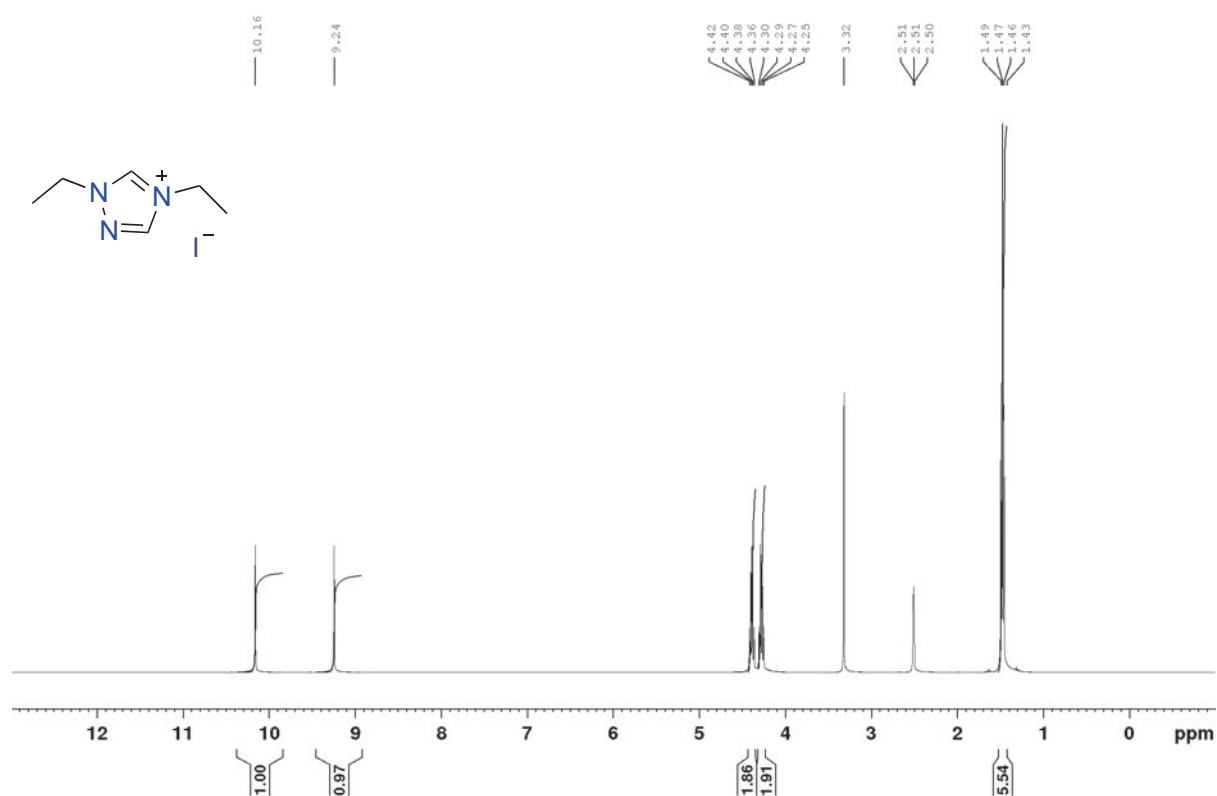


Figure S28. ^{13}C -NMR spectrum of compound **2.14**

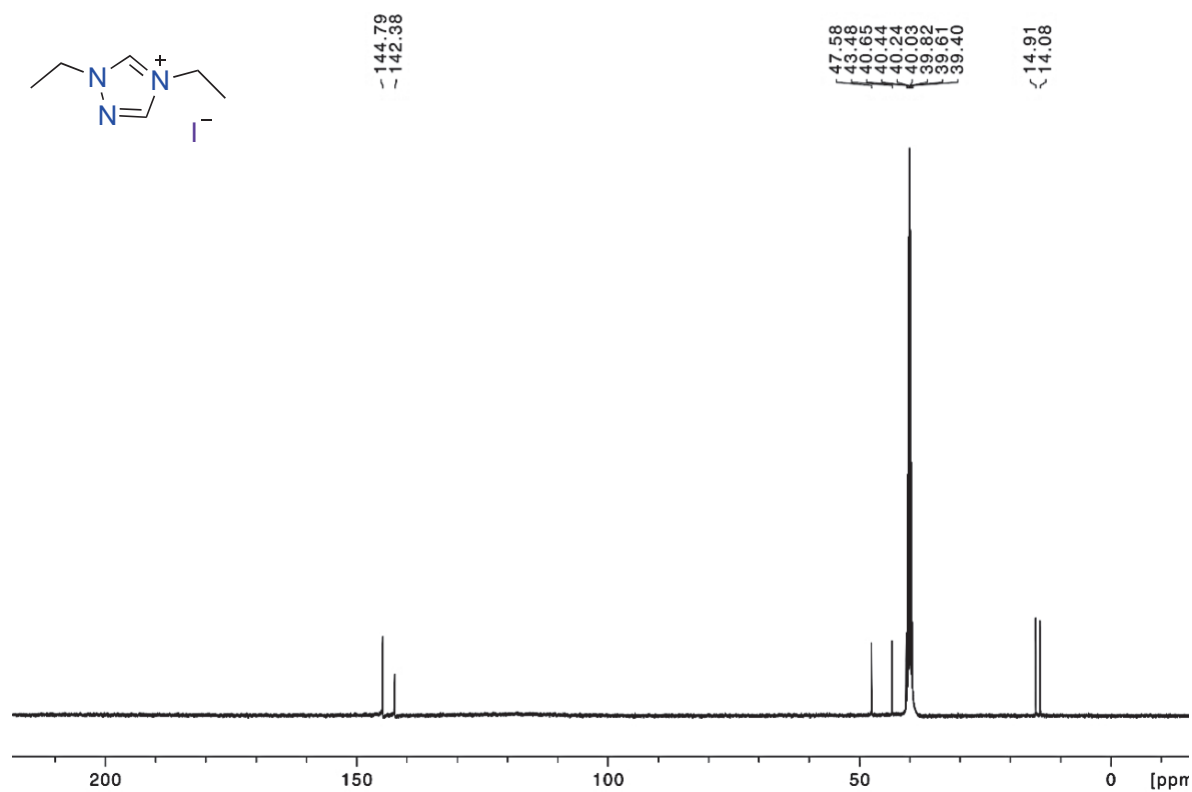


Figure S29. ^1H -NMR spectrum of compound **2.15**

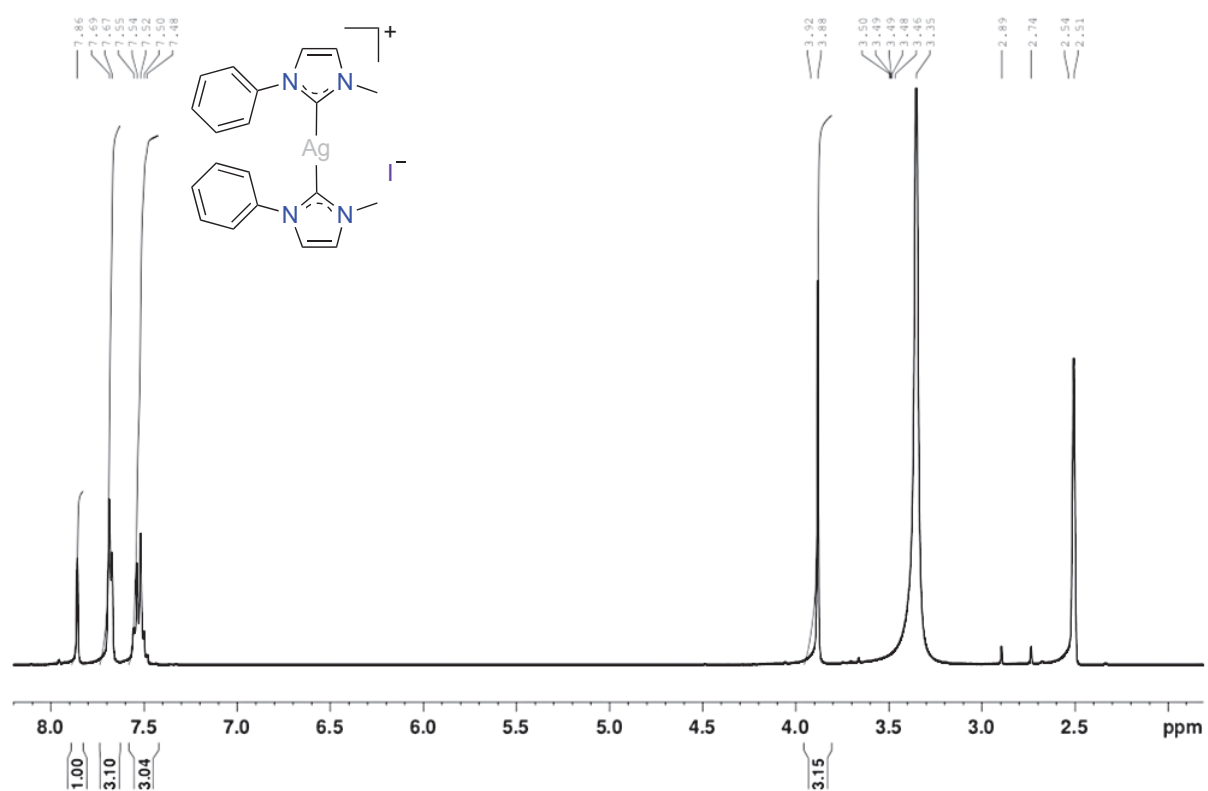


Figure S30. ^{13}C -NMR spectrum of compound **2.15**

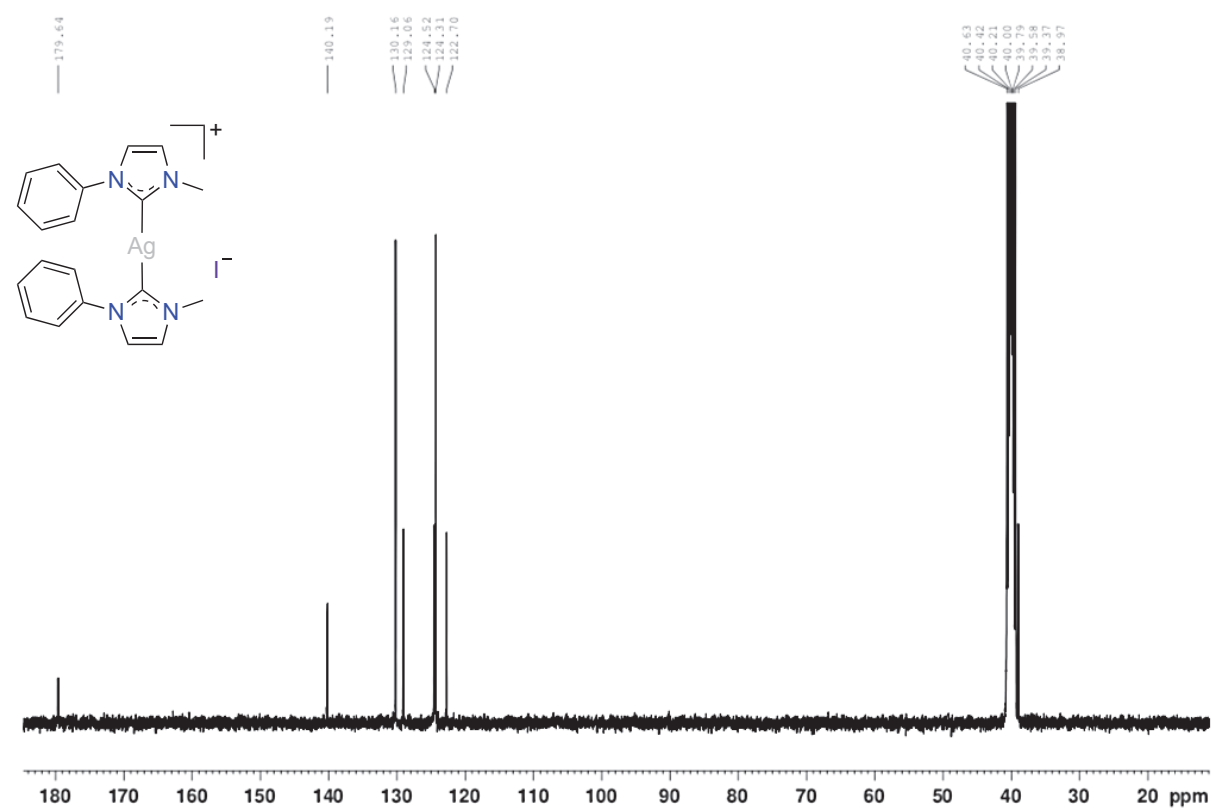


Figure S31. ^1H -NMR spectrum of compound **2.16**

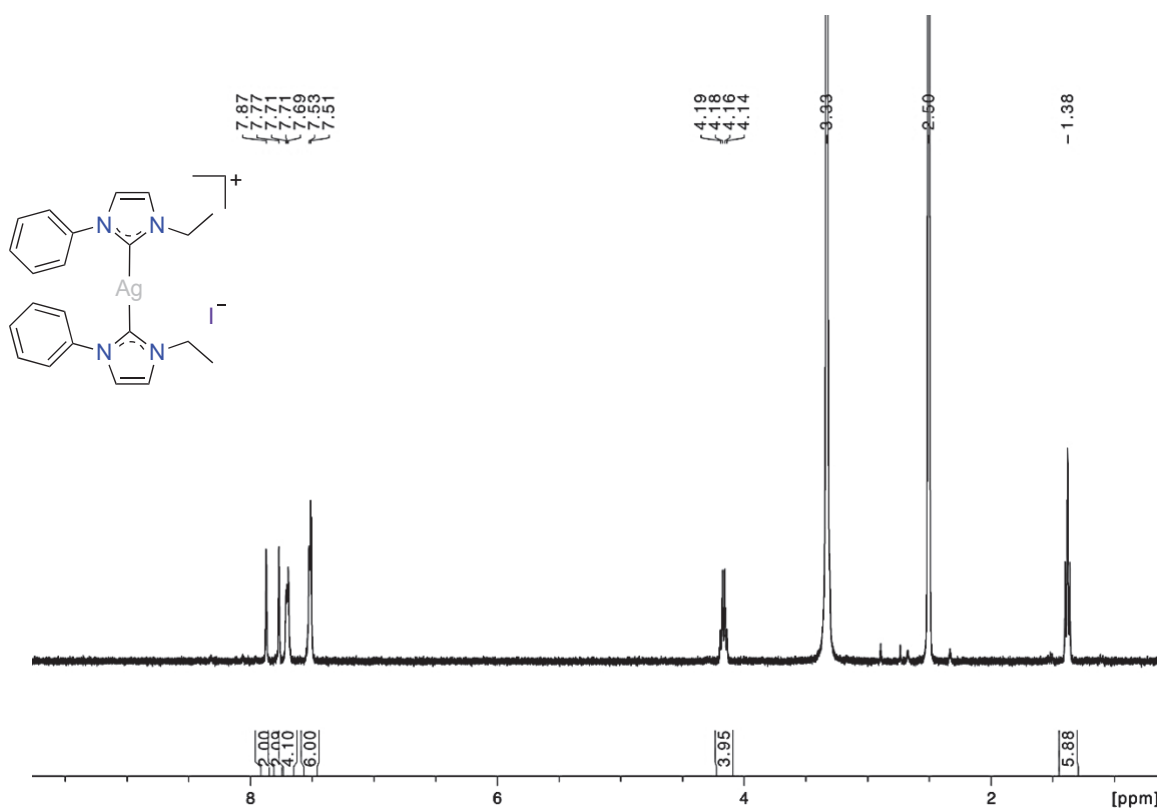


Figure S32. ^{13}C -NMR spectrum of compound **2.16**

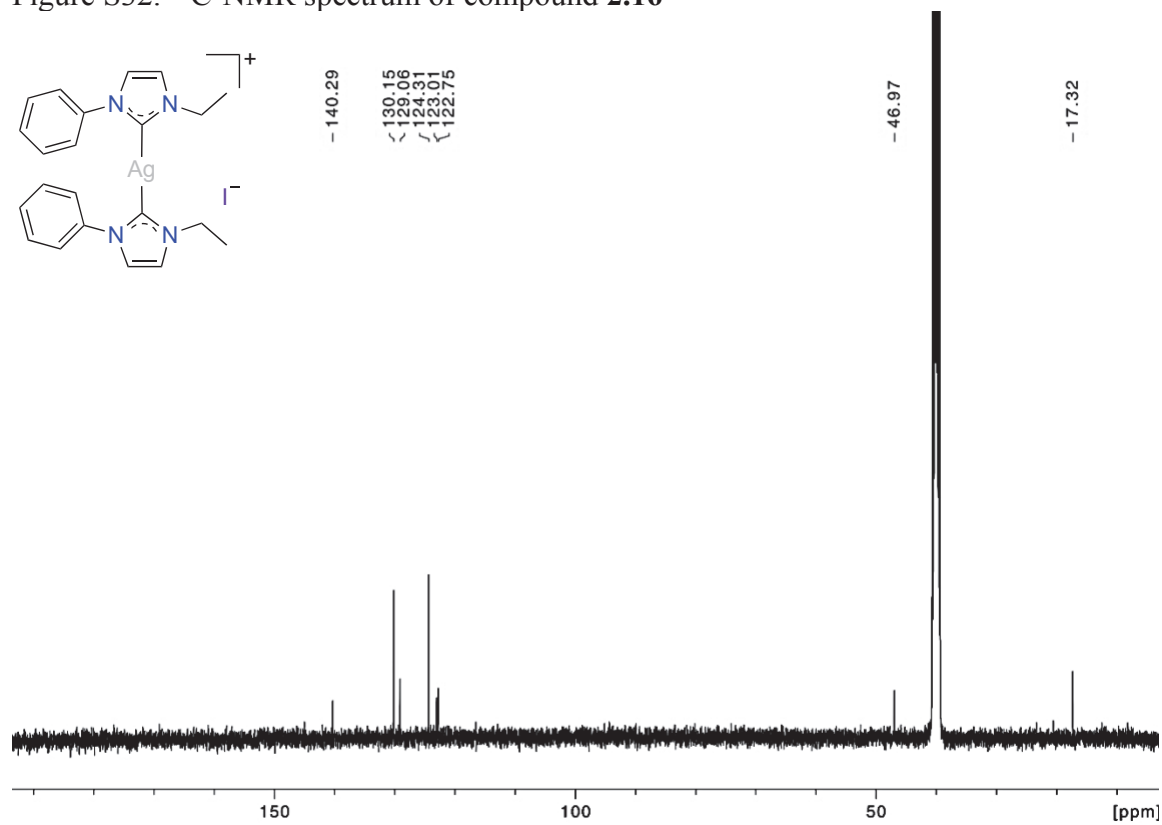


Figure S33. ^1H -NMR spectrum of compound **2.17**

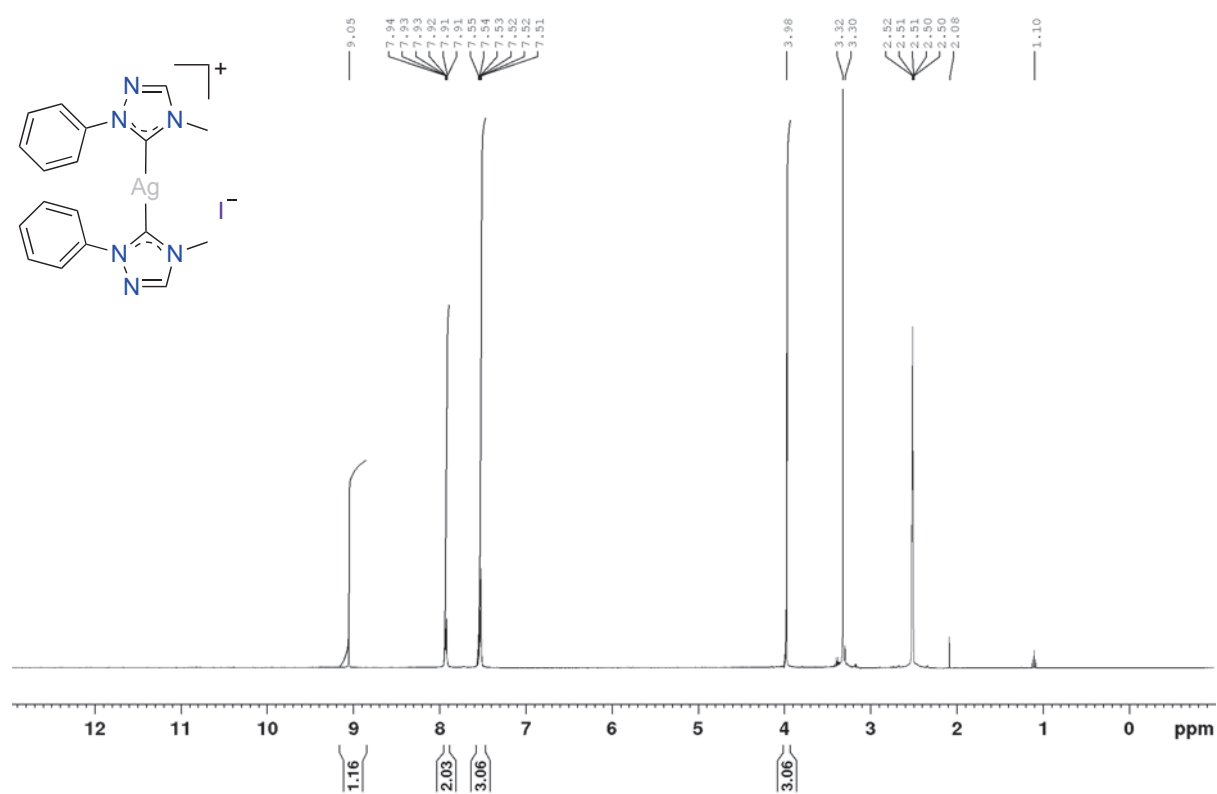


Figure S34. ^{13}C -NMR spectrum of compound **2.17**

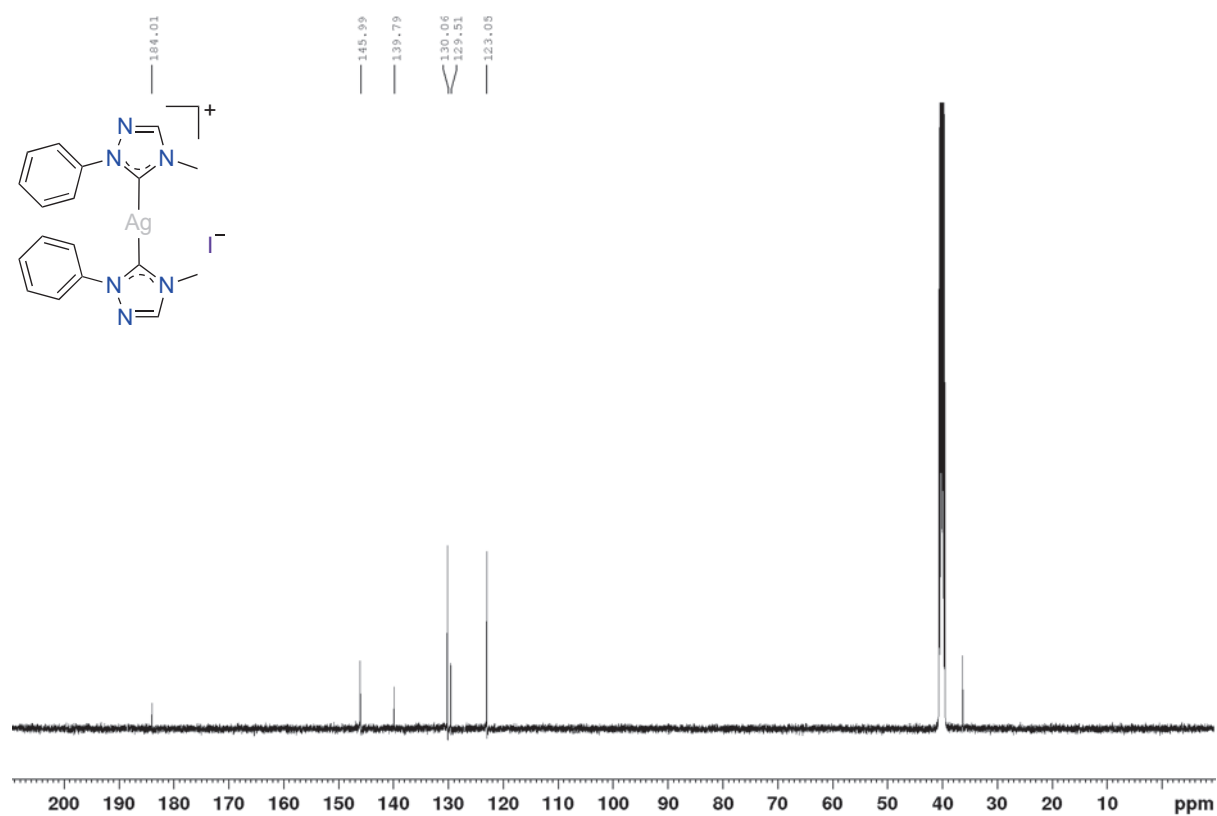


Figure S35. ^1H -NMR spectrum of compound **2.18**

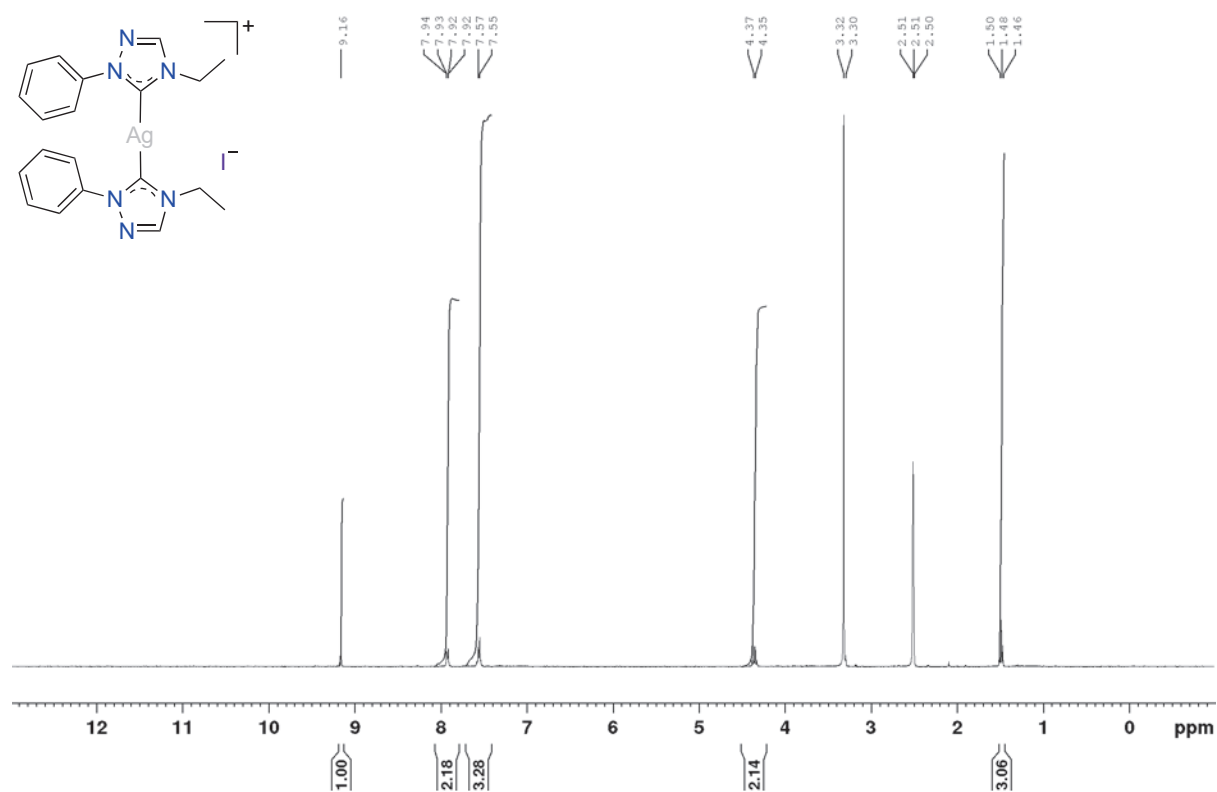


Figure S36. ^{13}C -NMR spectrum of compound **2.18**

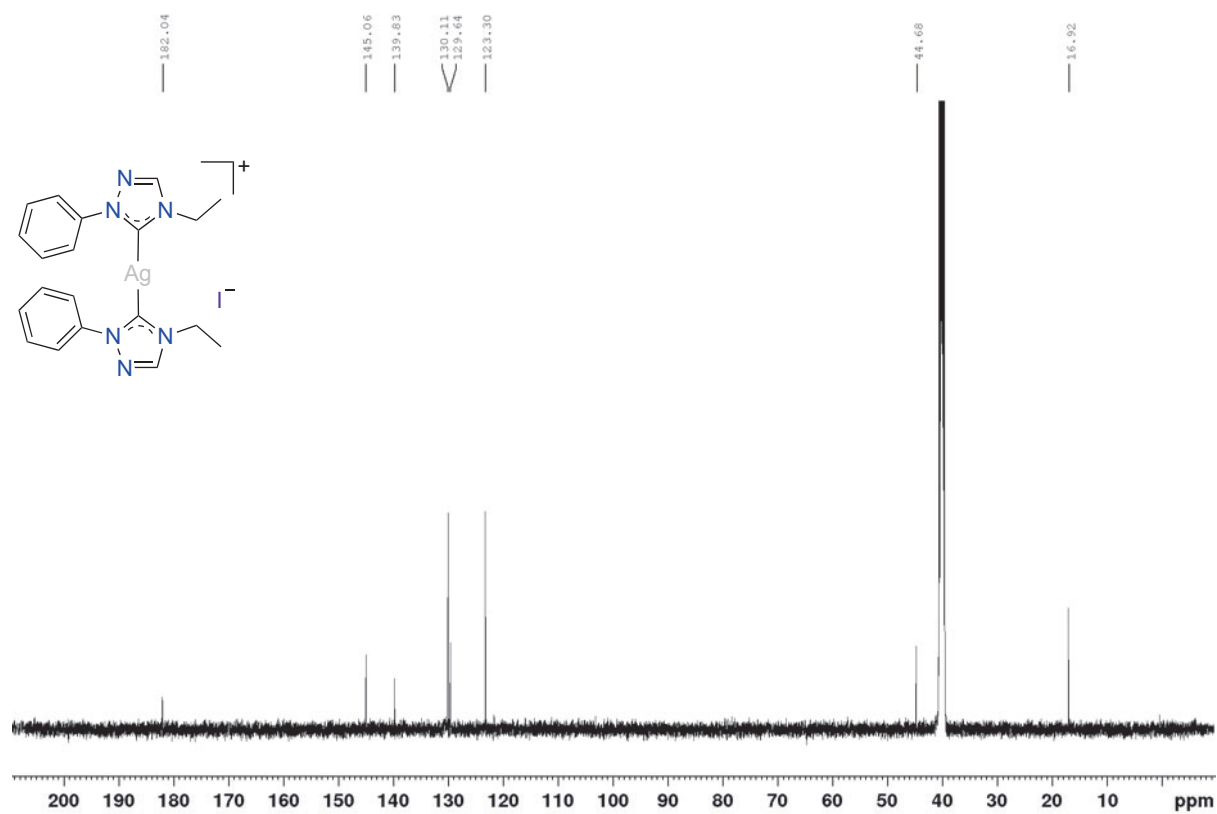


Figure S37. ^1H -NMR spectrum of compound **2.19**

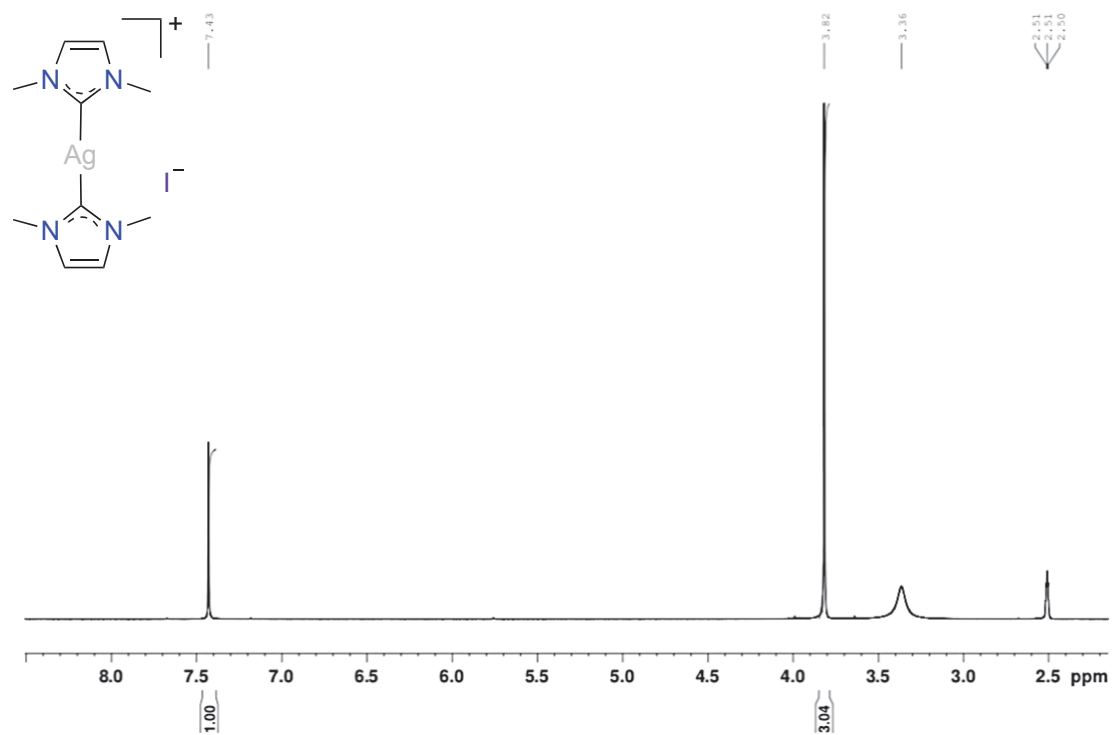


Figure S38. ^{13}C -NMR spectrum of compound **2.19**

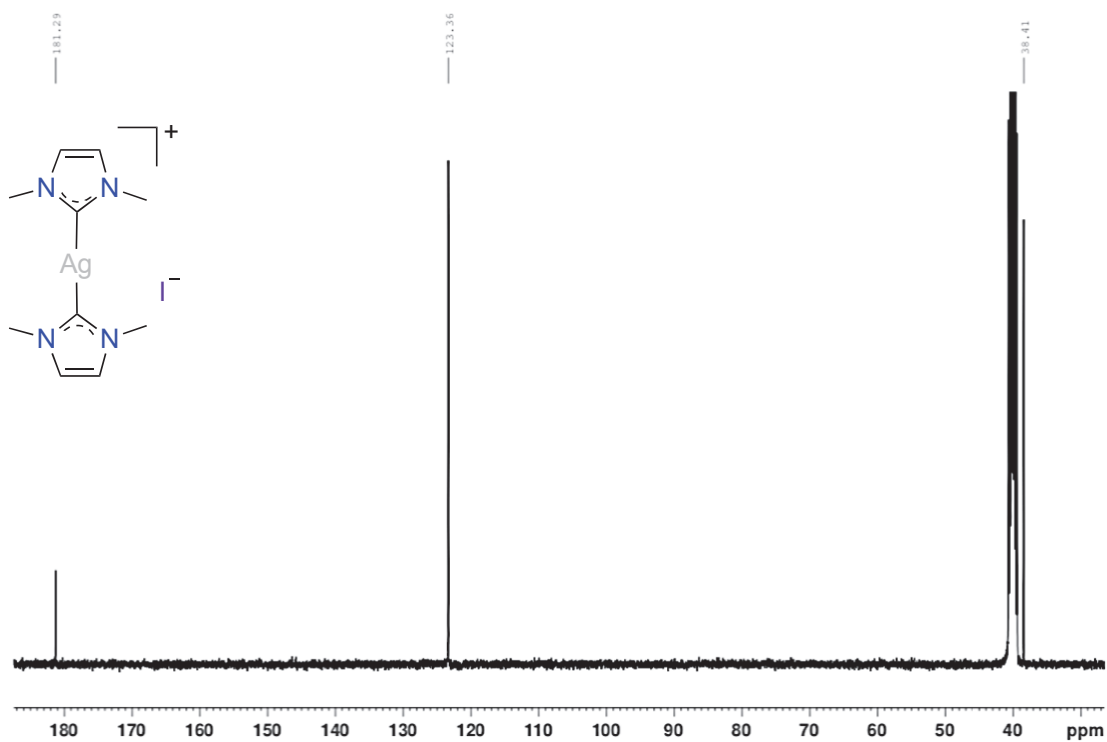


Figure S39. ^1H -NMR spectrum of compound **2.20**

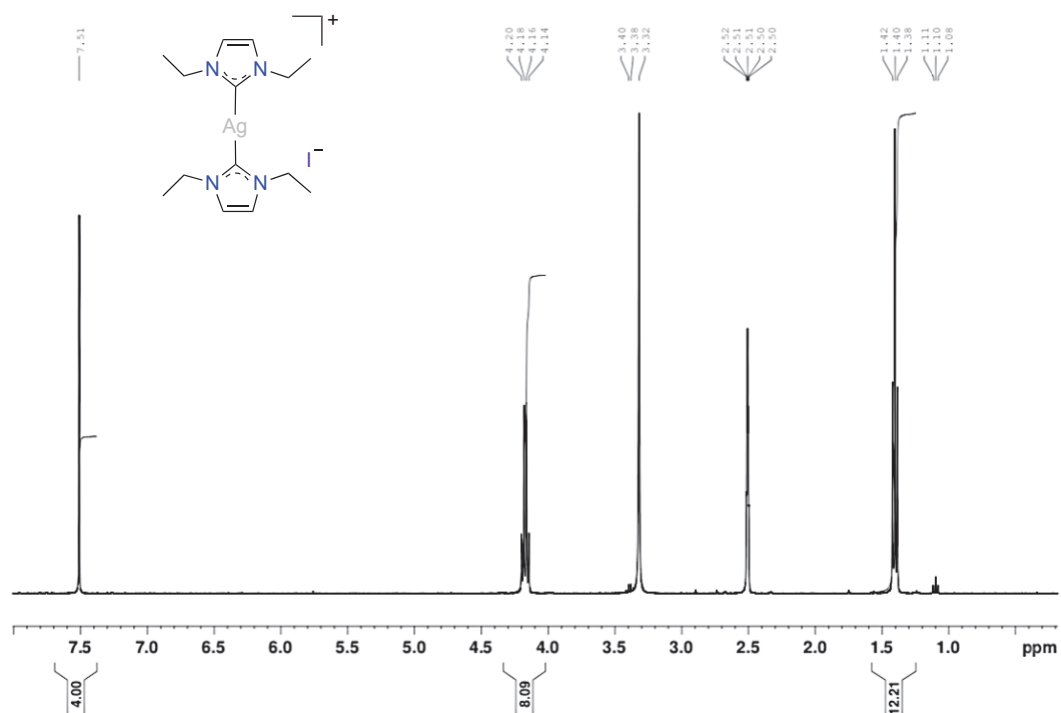


Figure S40. ^{13}C -NMR spectrum of compound **2.20**

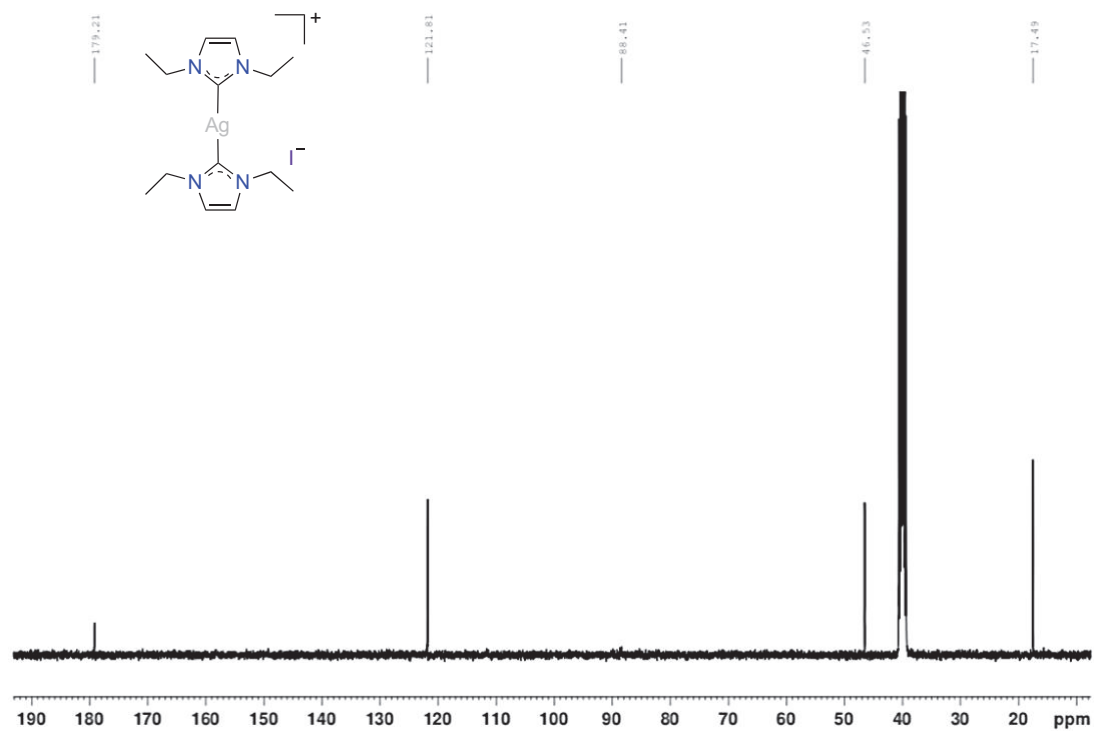


Figure S41. ^1H -NMR spectrum of compound **2.21**

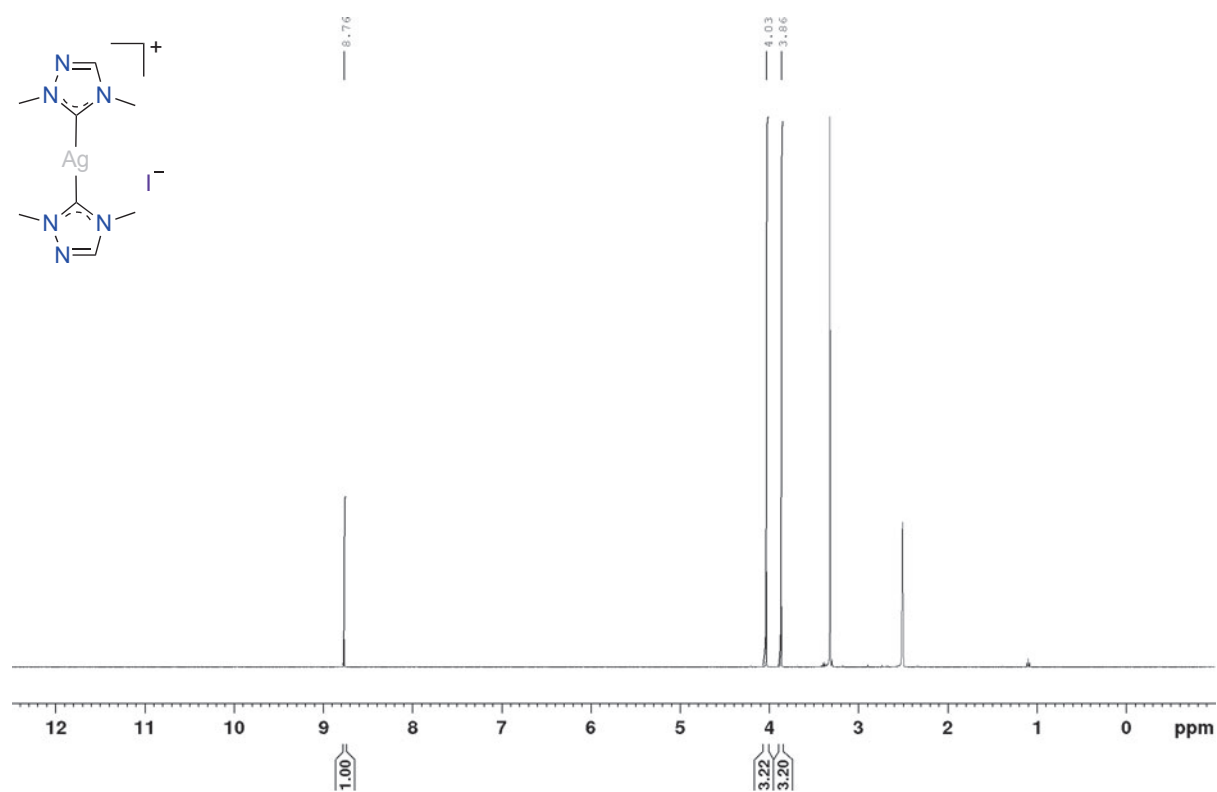


Figure S42. ^{13}C -NMR spectrum of compound **2.21**

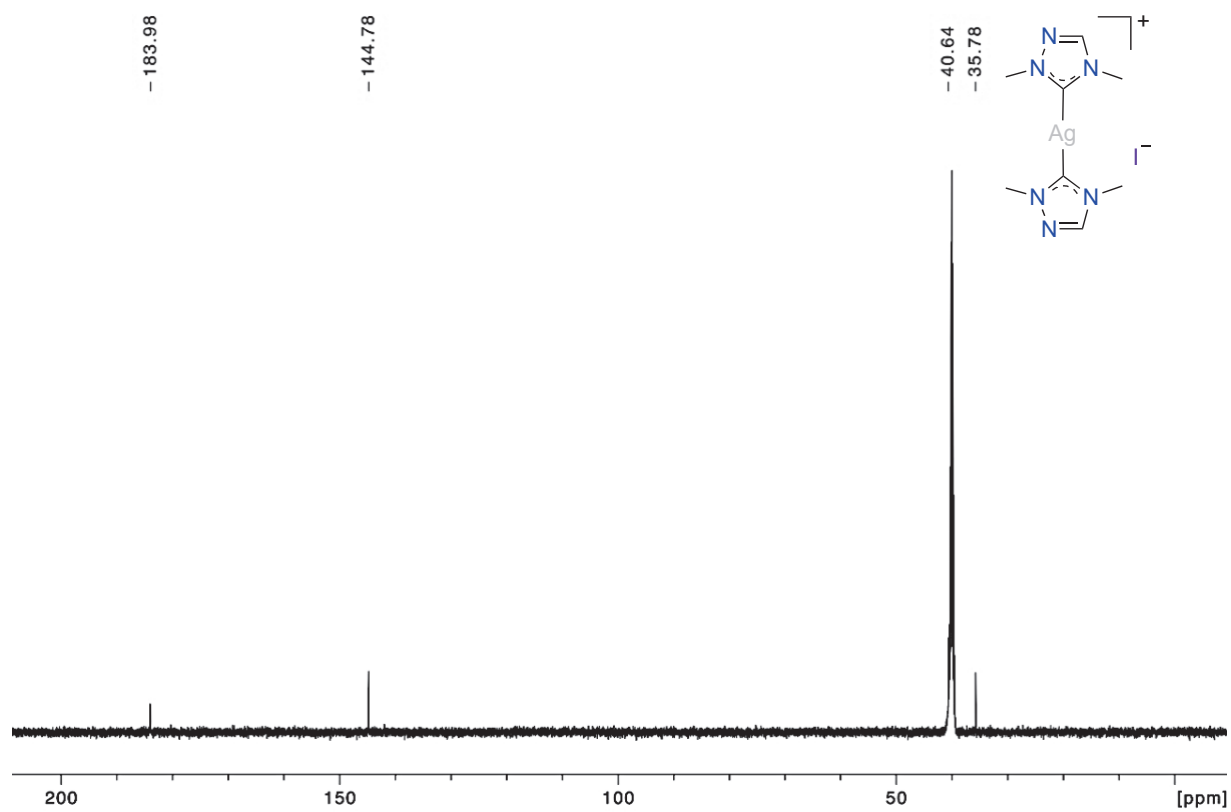


Figure S43. ^1H -NMR spectrum of compound **2.22**

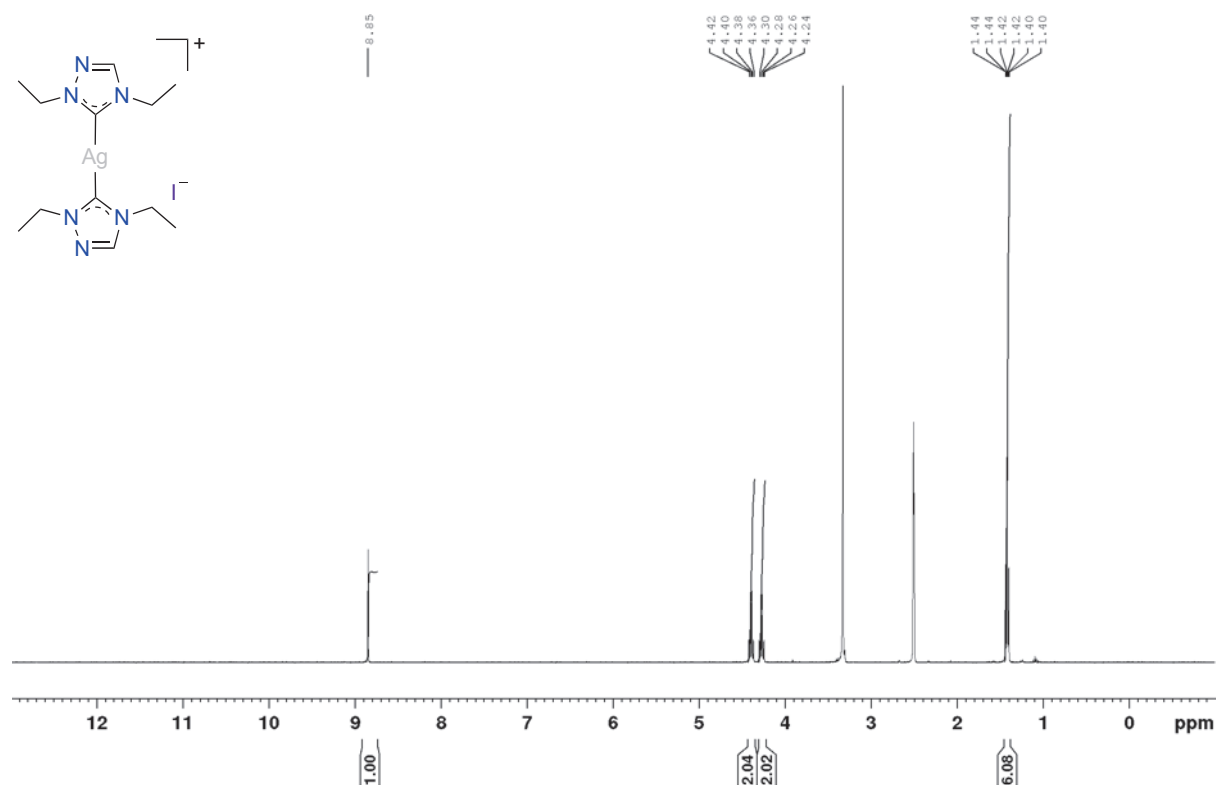


Figure S44. ^{13}C -NMR spectrum of compound **2.22**

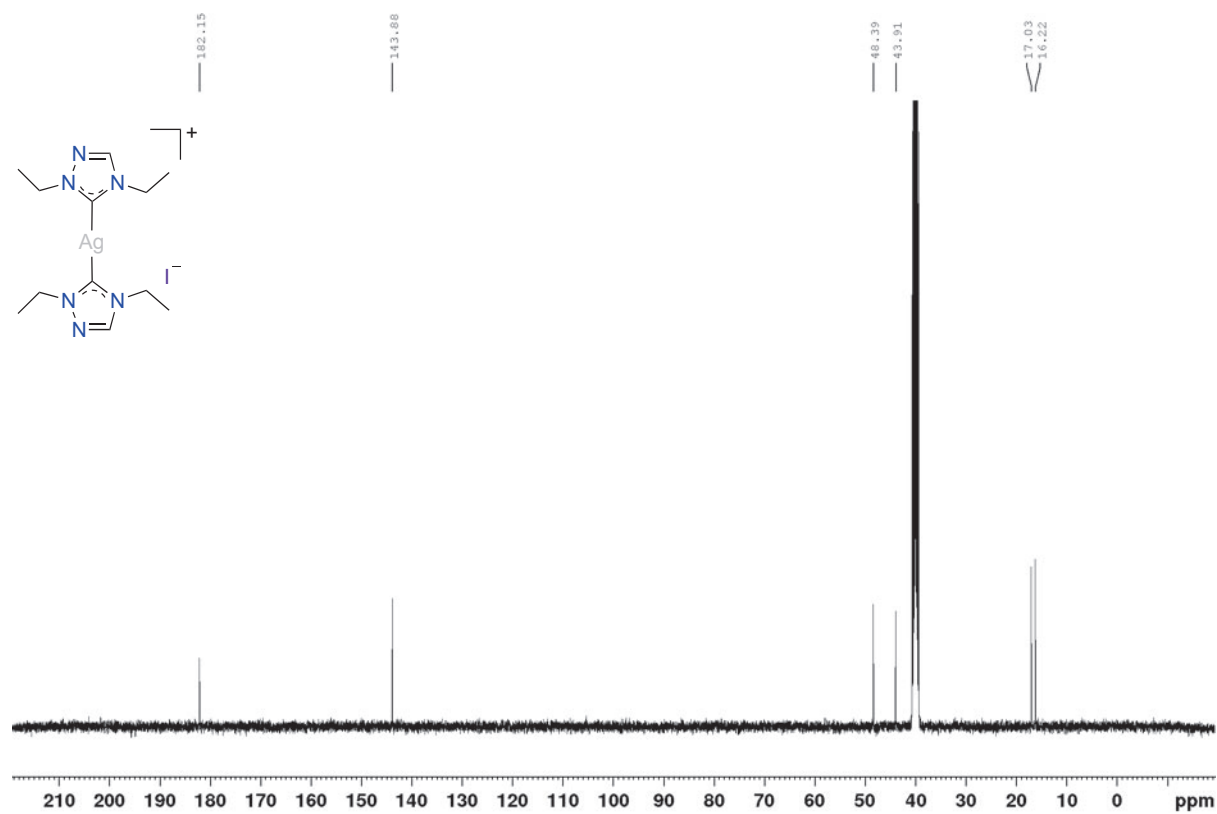


Figure S45. ^1H -NMR spectrum of compound **2.23**

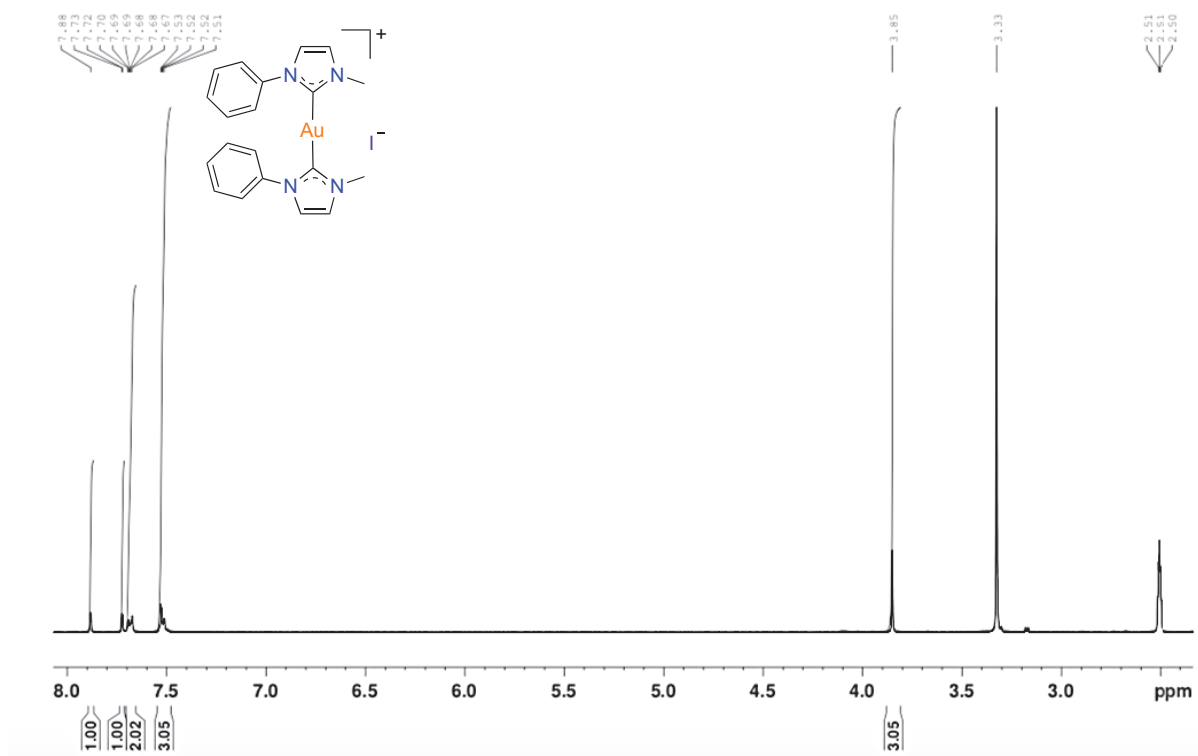


Figure S46. ^{13}C -NMR spectrum of compound **2.23**

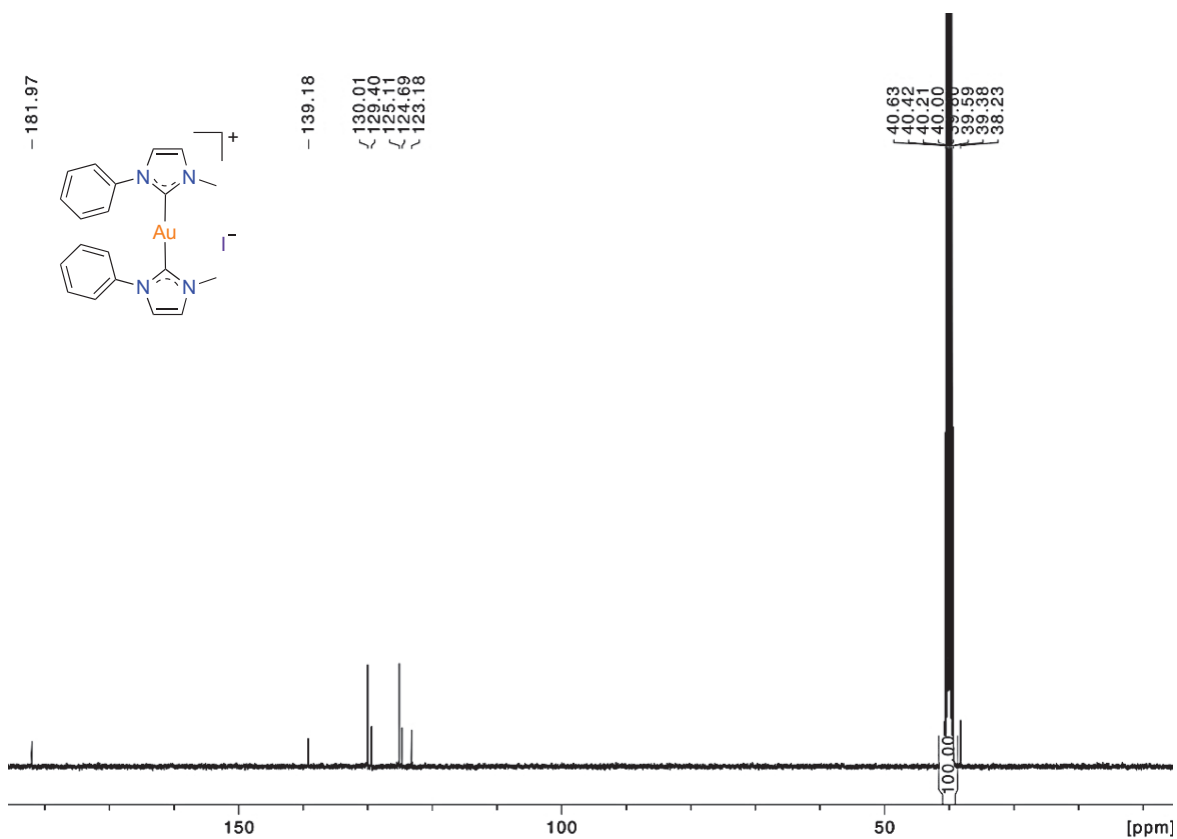


Figure S47. ^1H -NMR spectrum of compound **2.24**

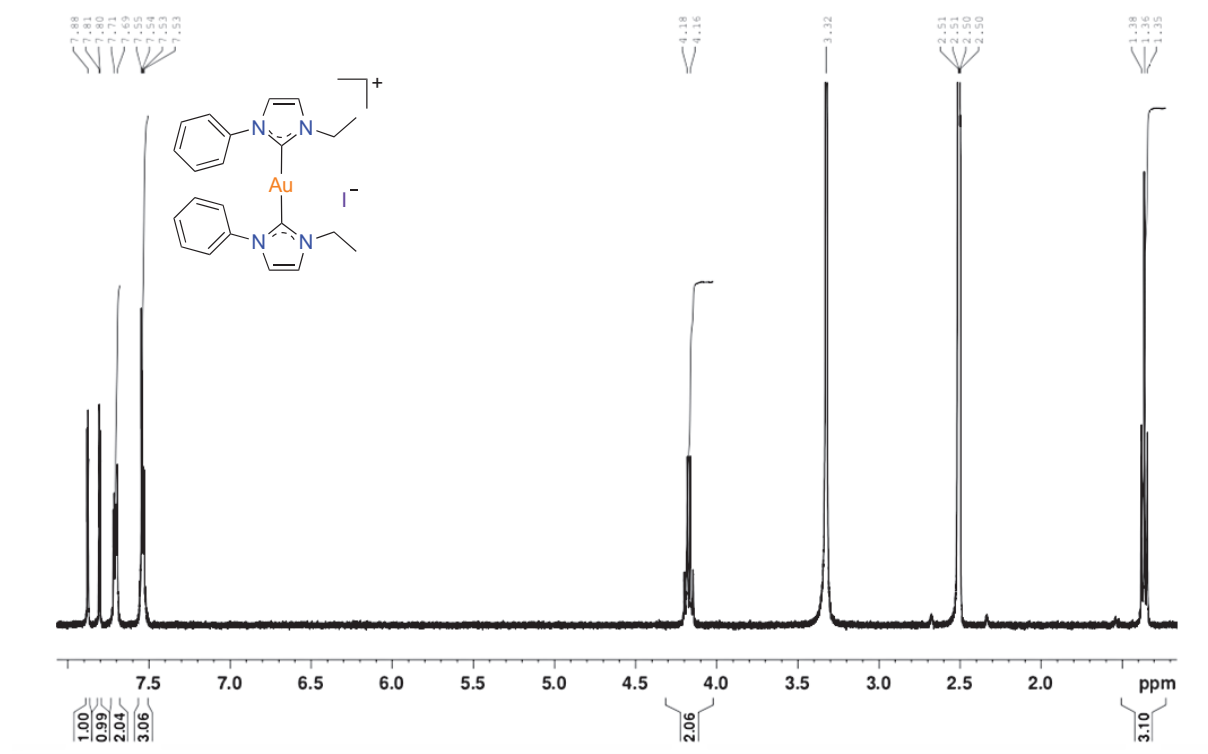


Figure S48. ^{13}C -NMR spectrum of compound **2.24**

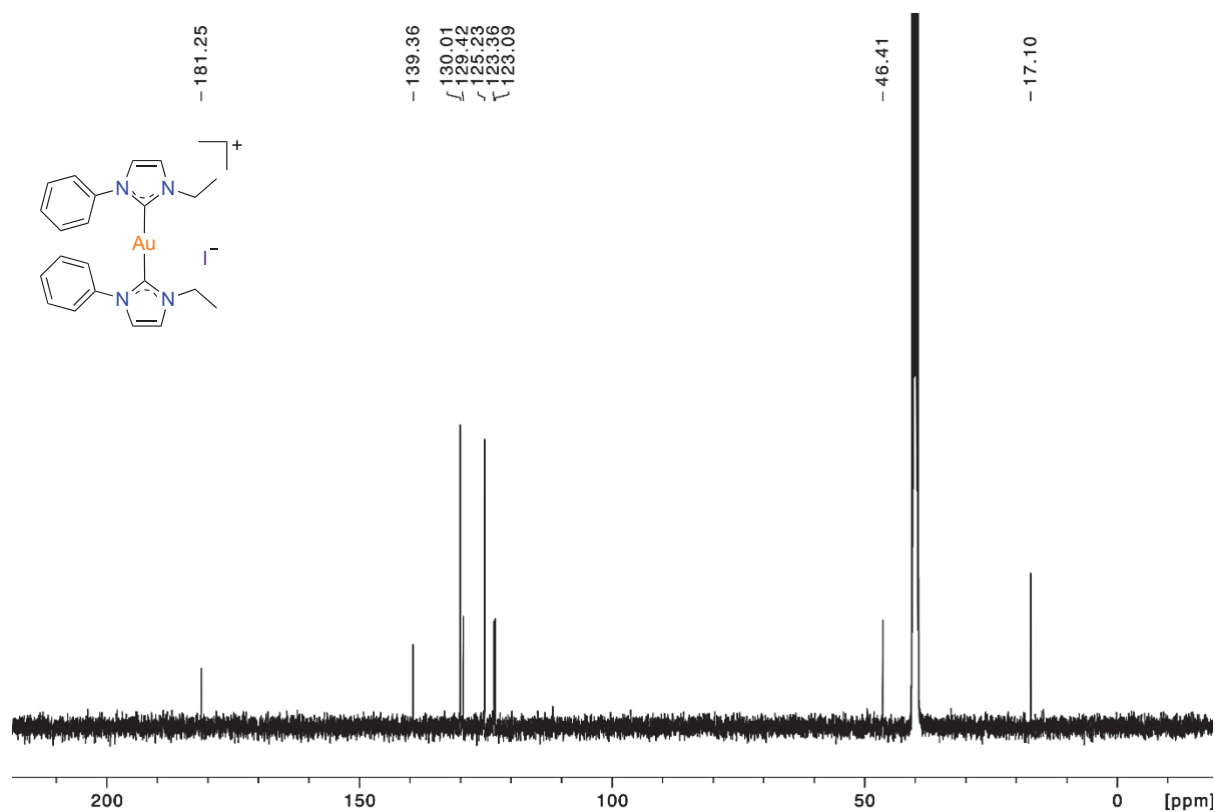


Figure S49. ^1H -NMR spectrum of compound **2.25**

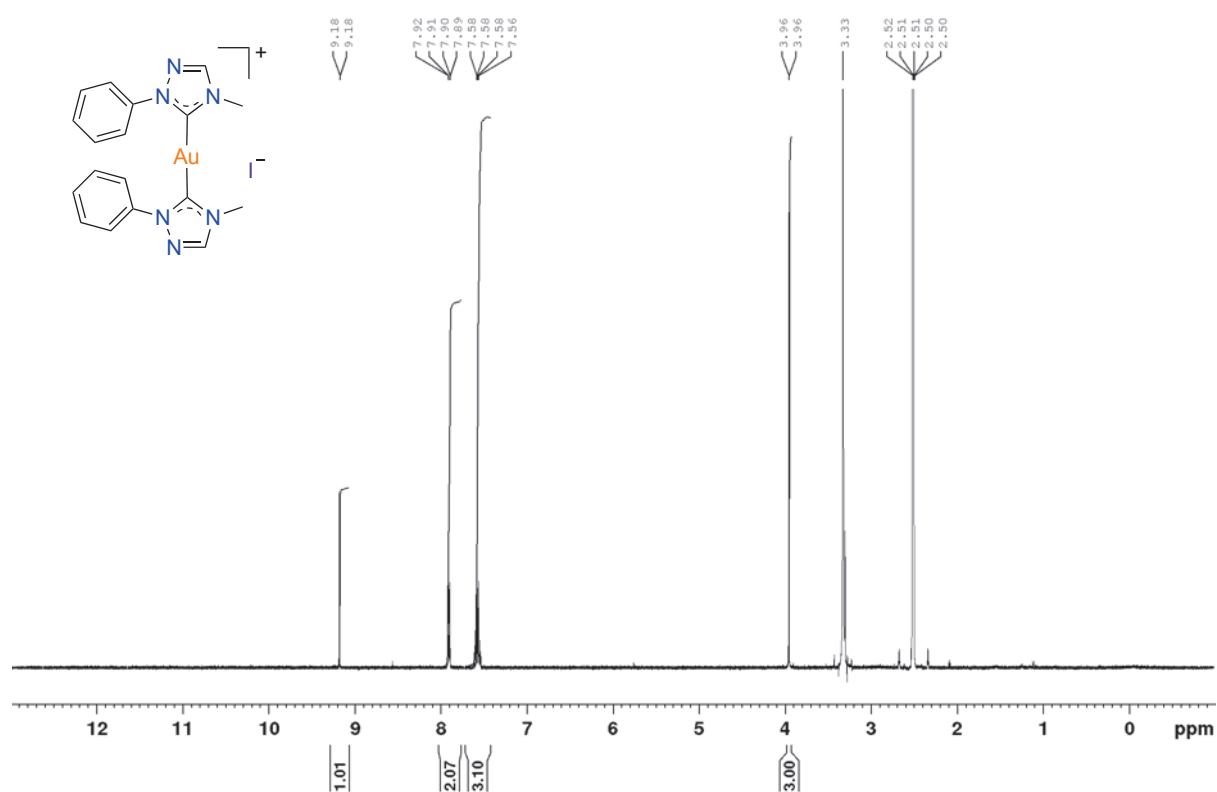


Figure S50. ^{13}C -NMR spectrum of compound **2.25**

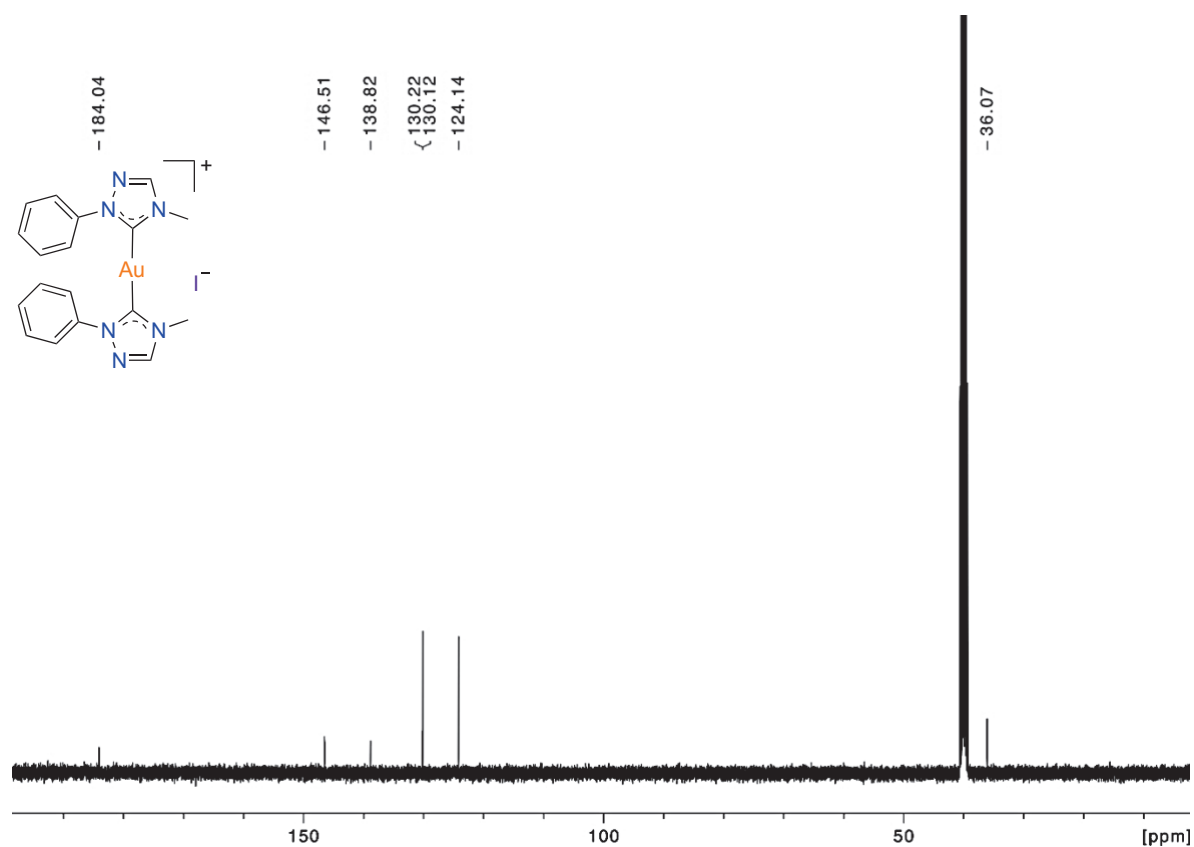


Figure S51. ^1H -NMR spectrum of compound **2.26**

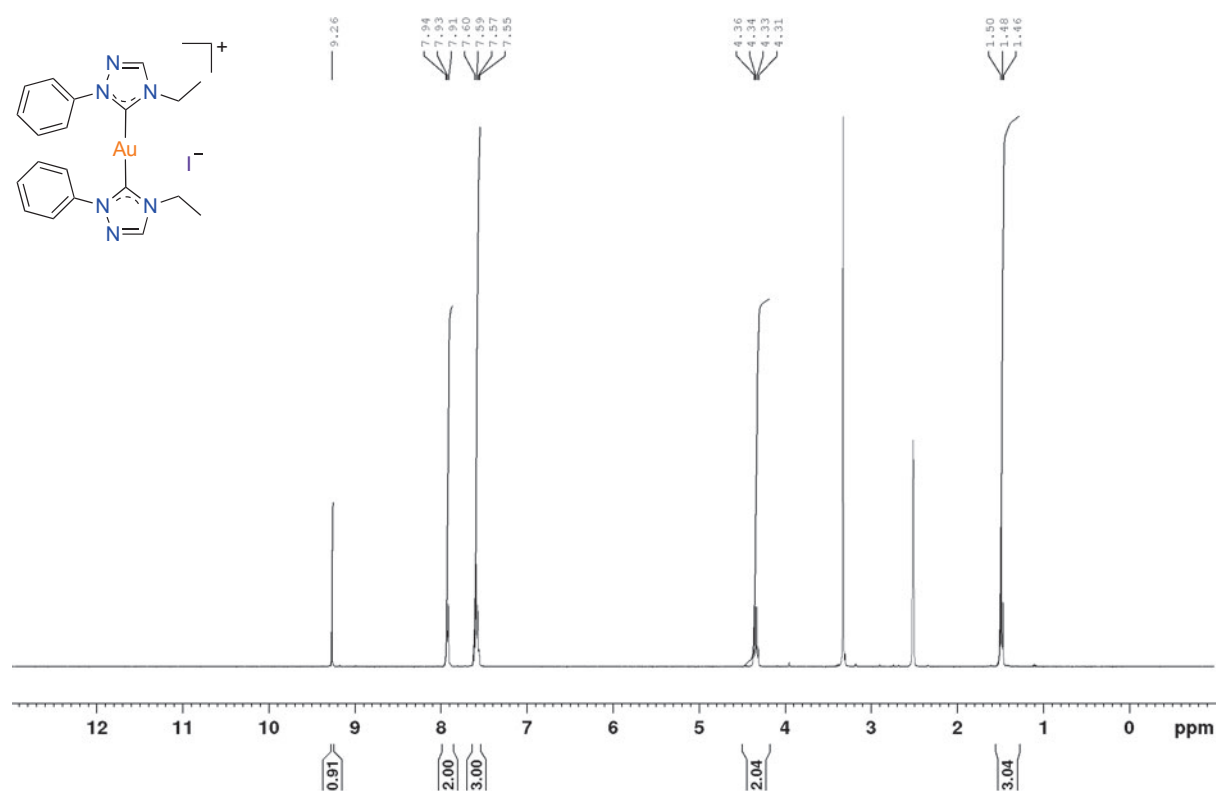


Figure S52. ^{13}C -NMR spectrum of compound **2.26**

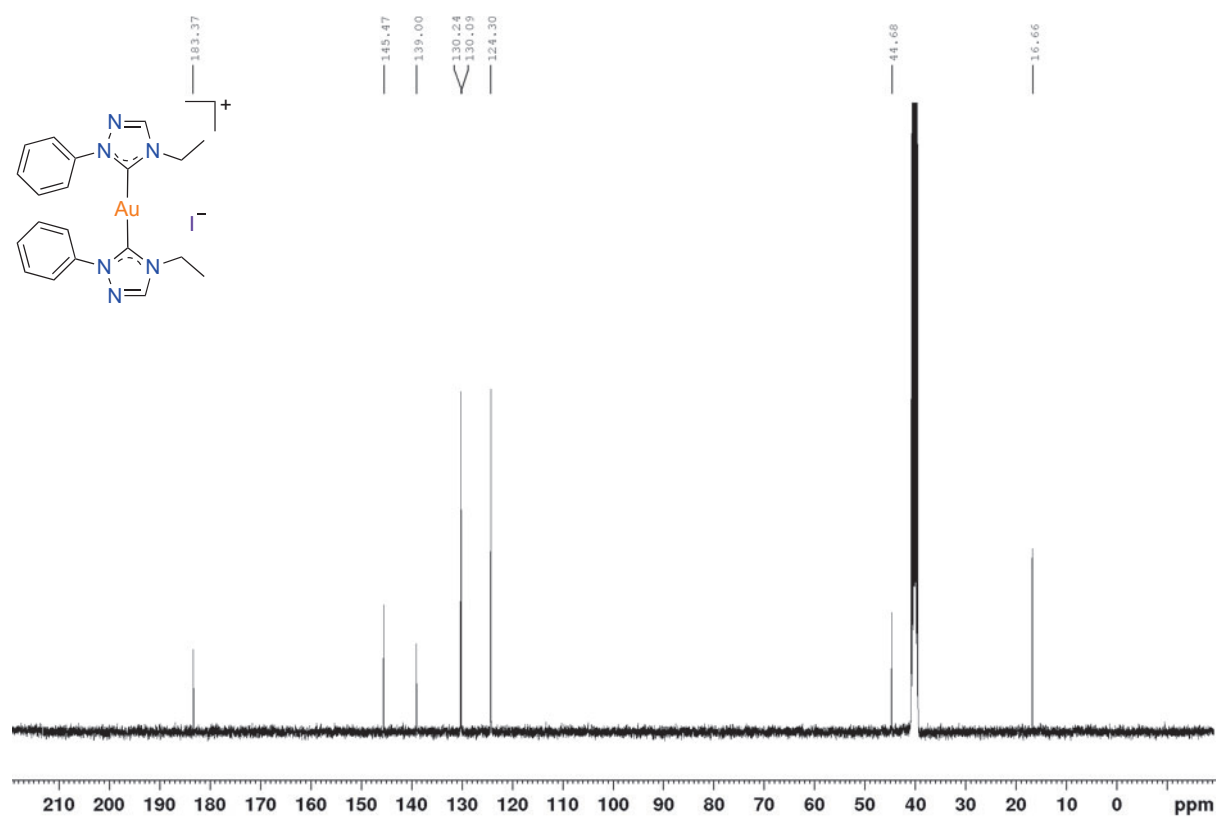


Figure S53. ^1H -NMR spectrum of compound **2.27**

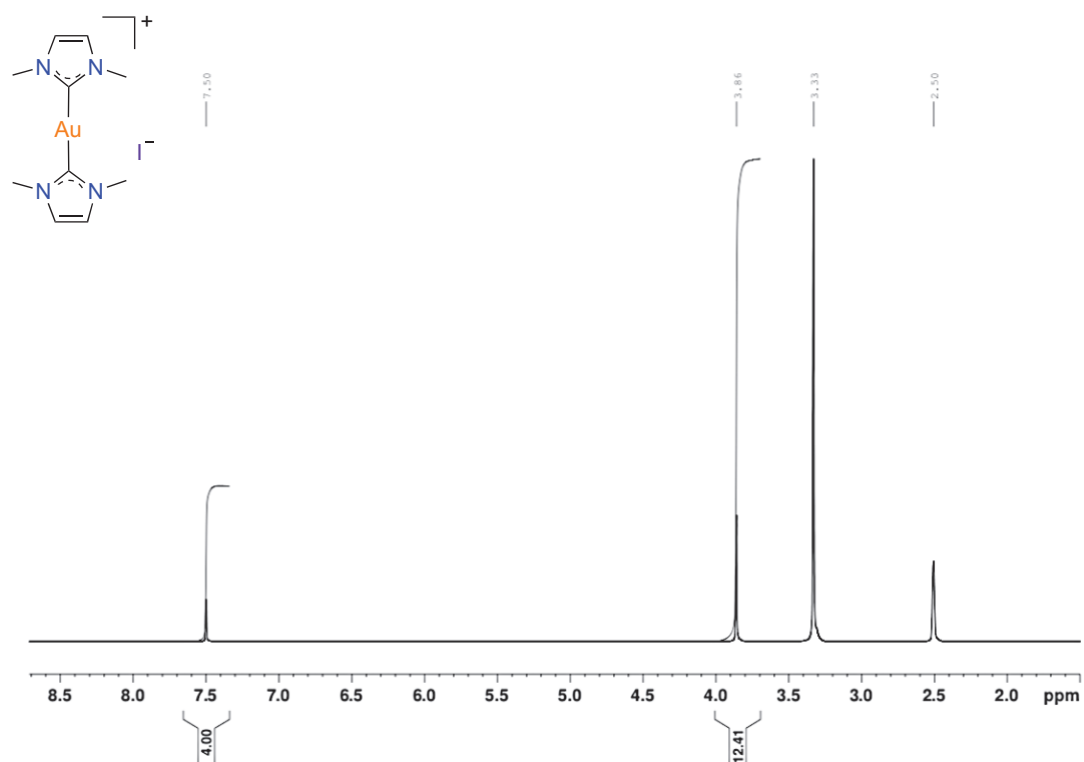


Figure S54. ^{13}C -NMR spectrum of compound **2.27**

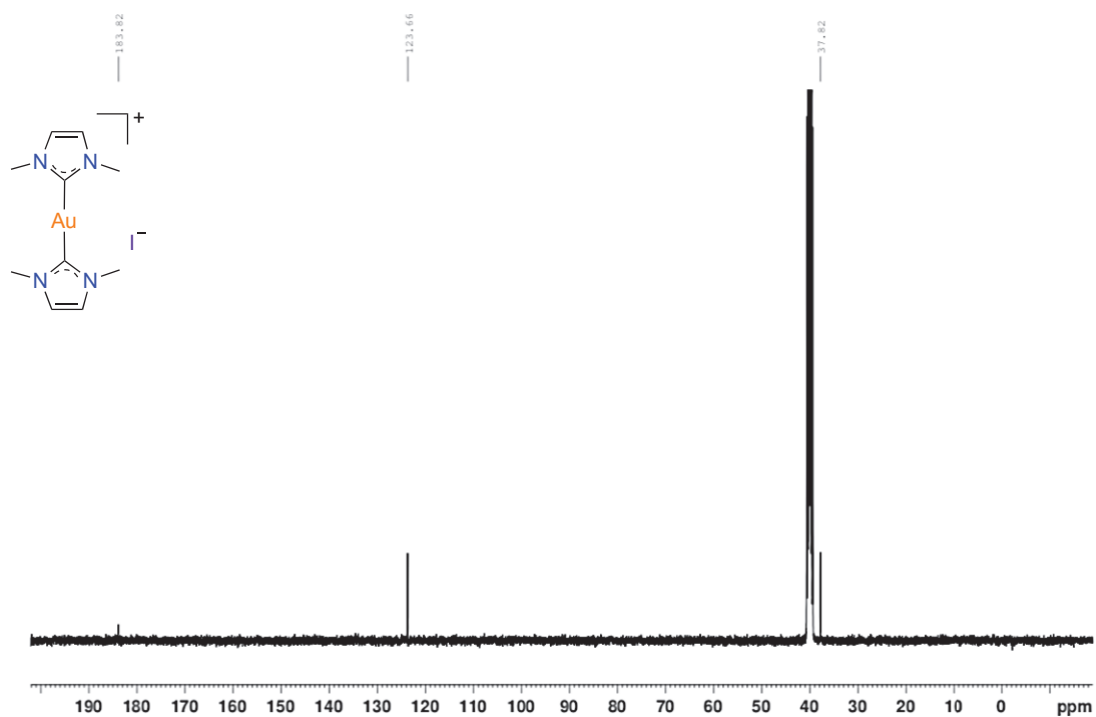


Figure S55. ^1H -NMR spectrum of compound **2.28**

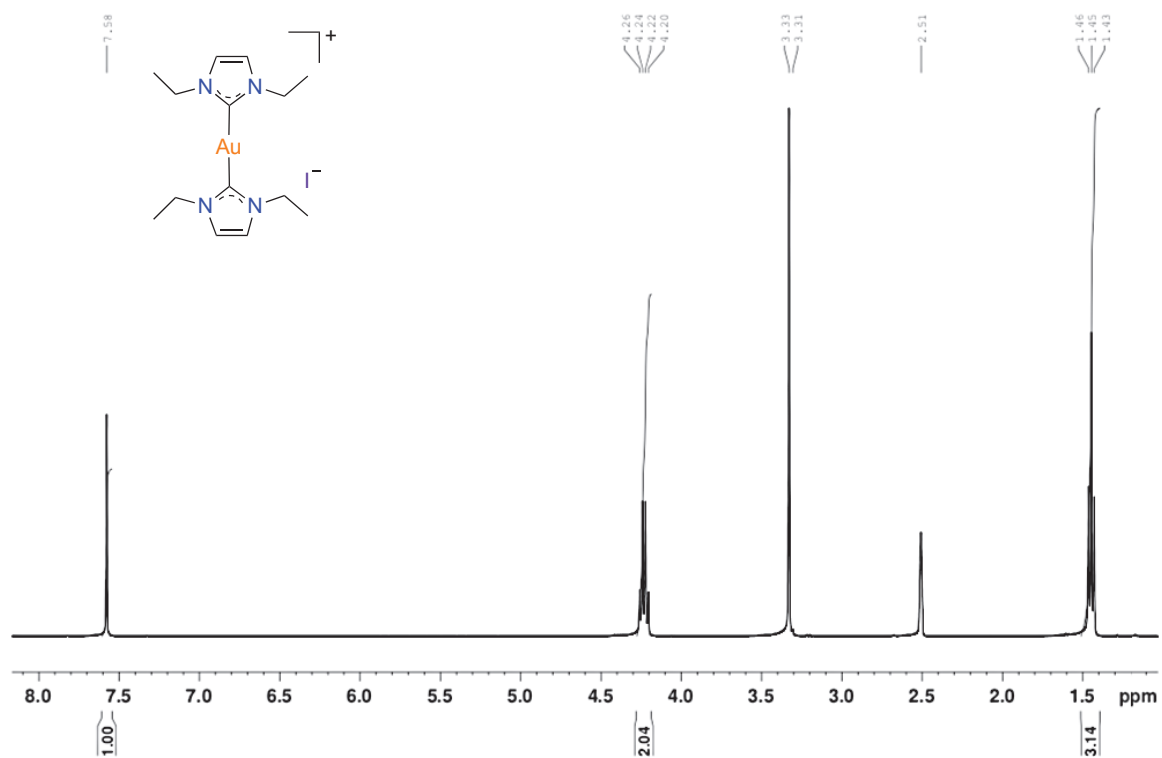


Figure S56. ^{13}C -NMR spectrum of compound **2.28**

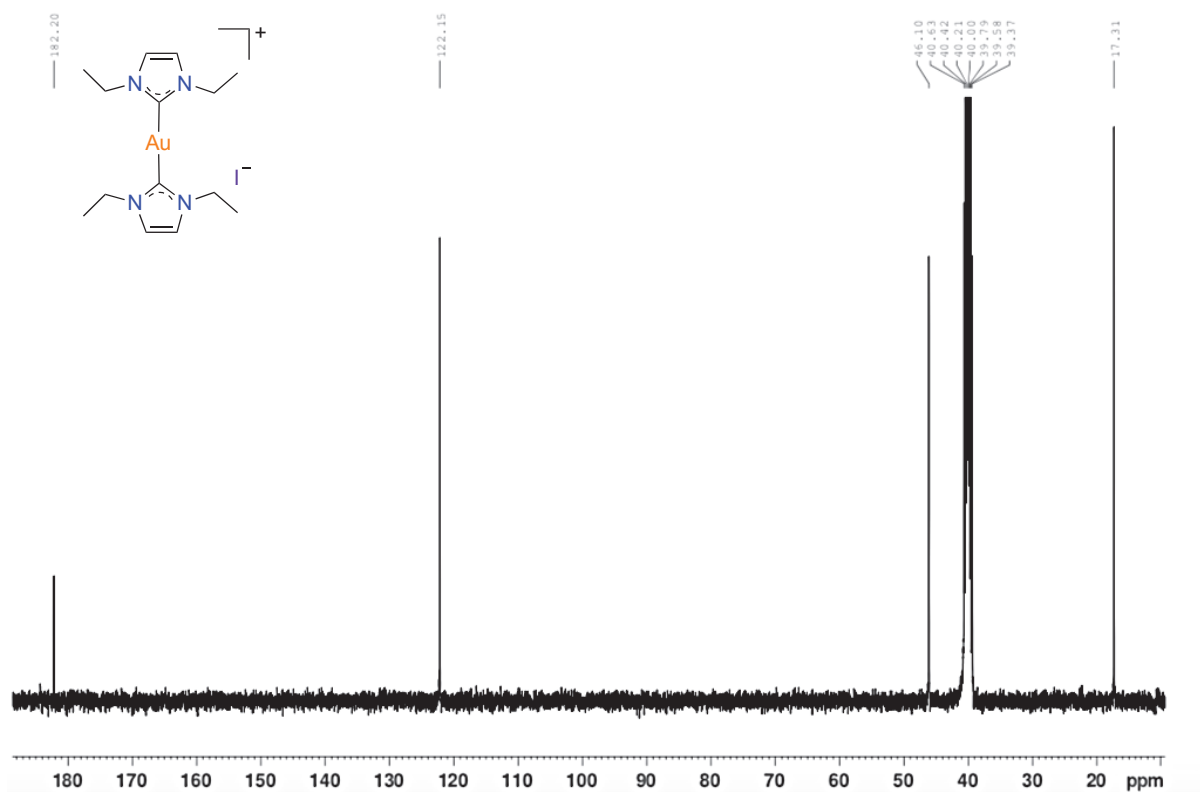


Figure S57. ^1H -NMR spectrum of compound **2.29**

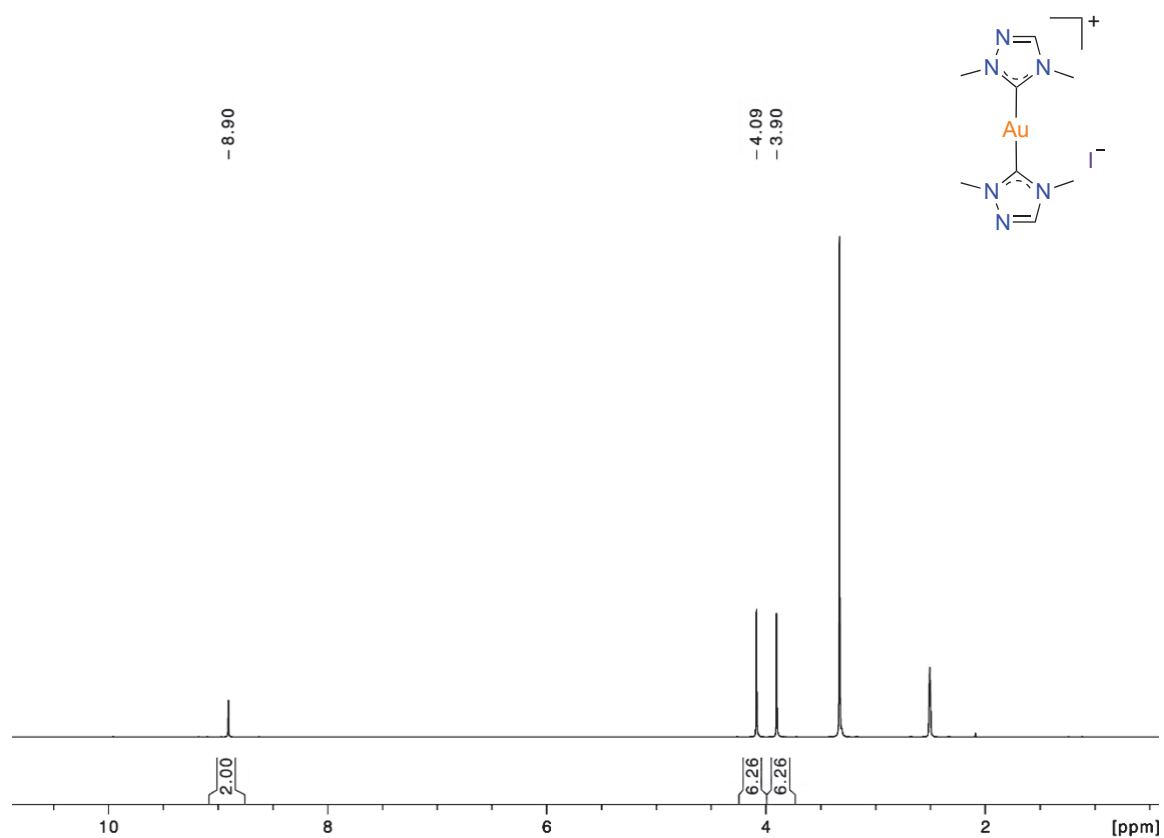


Figure S58. ^{13}C -NMR spectrum of compound **2.29**

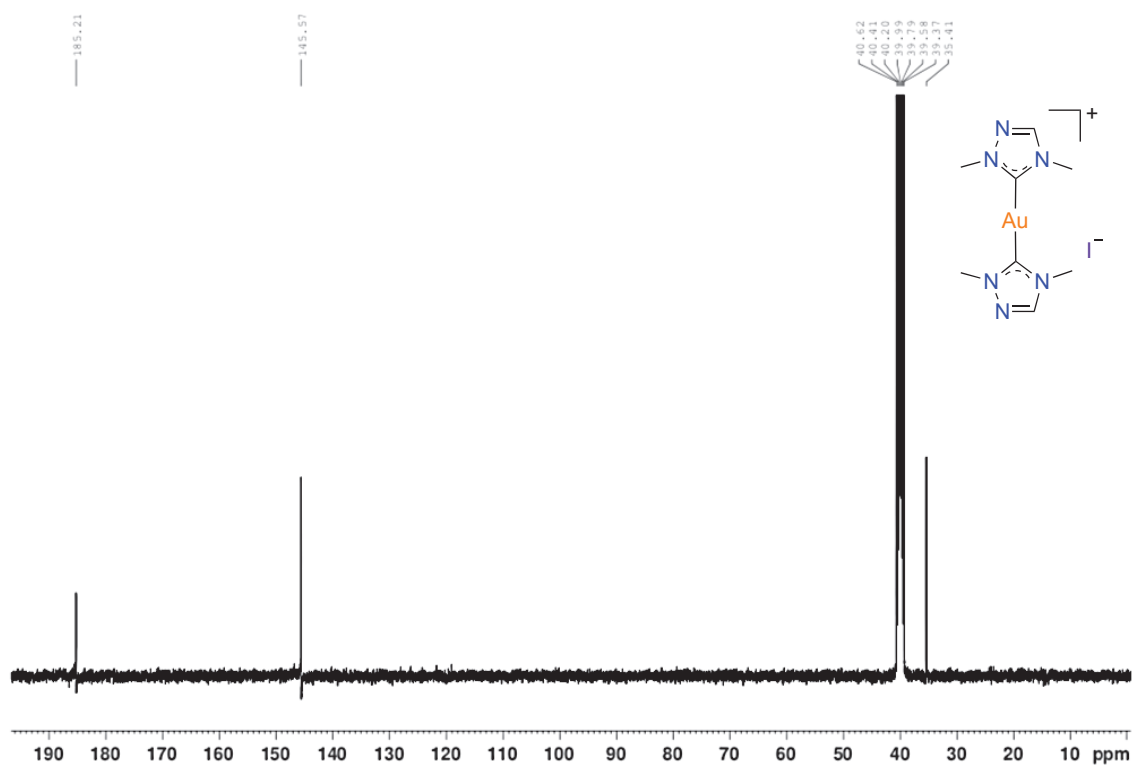


Figure S59. ^1H -NMR spectrum of compound **2.30**

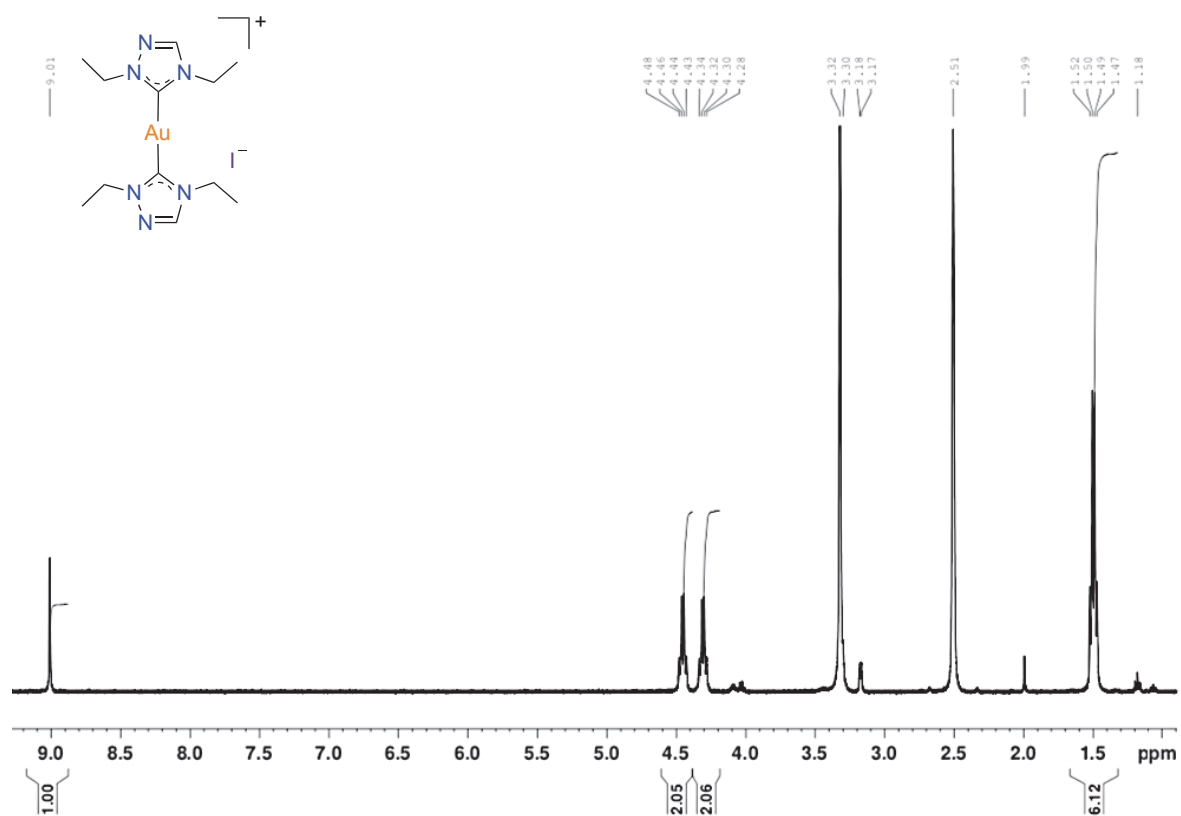


Figure S60. ^{13}C -NMR spectrum of compound **2.30**

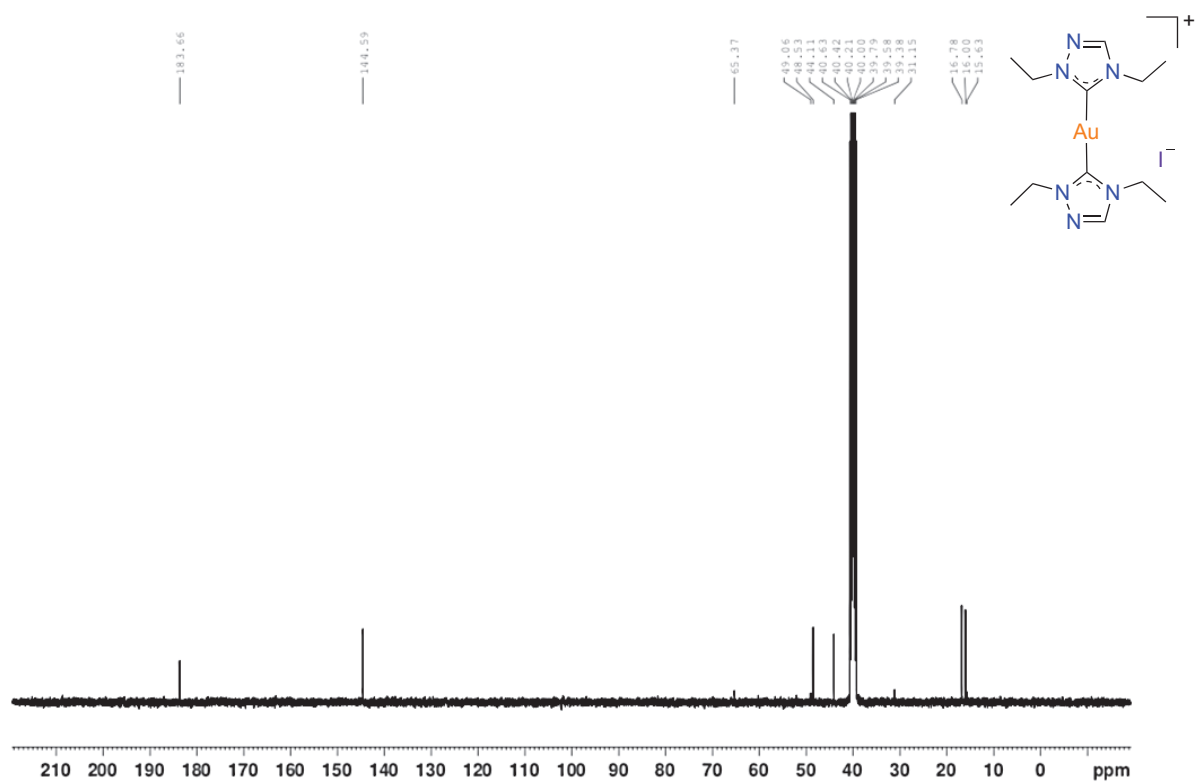


Figure S61. ^1H -NMR spectrum of compound **2.31**

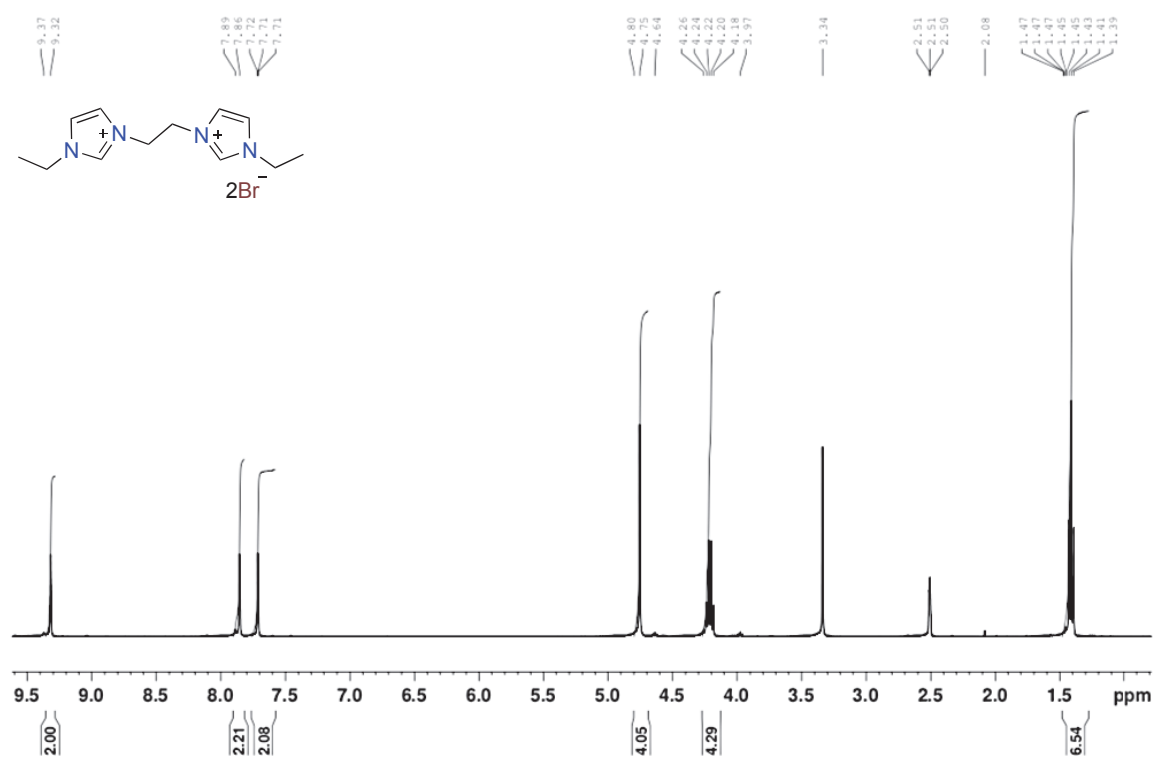


Figure S62. ^{13}C -NMR spectrum of compound **2.31**

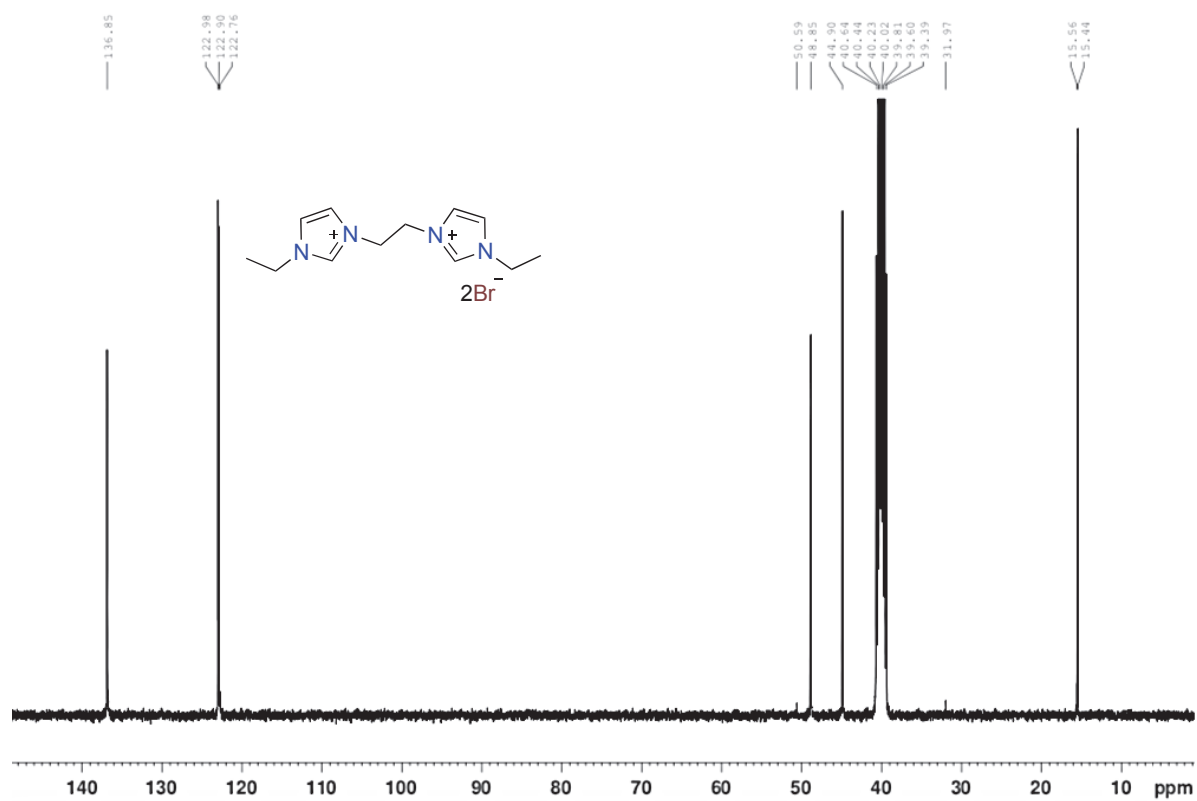


Figure S63. ^1H -NMR spectrum of compound **2.32**

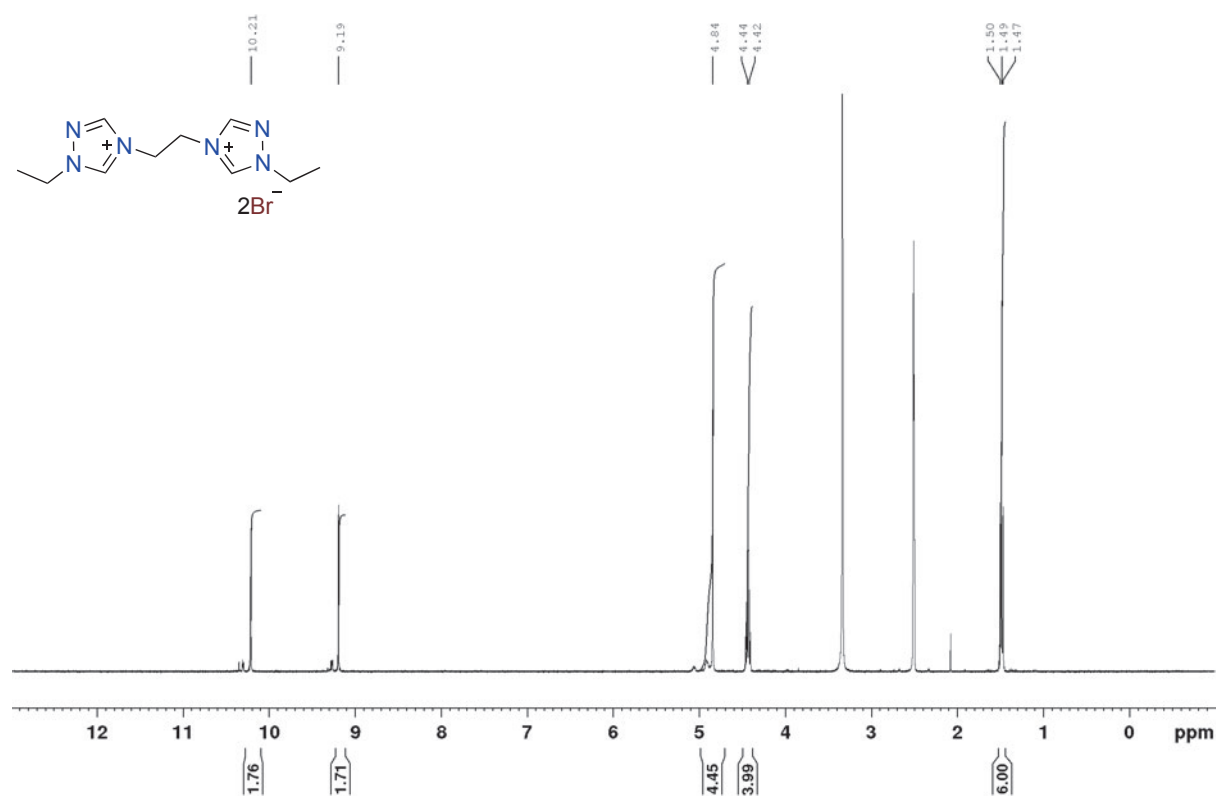


Figure S64. ^{13}C -NMR spectrum of compound **2.32**

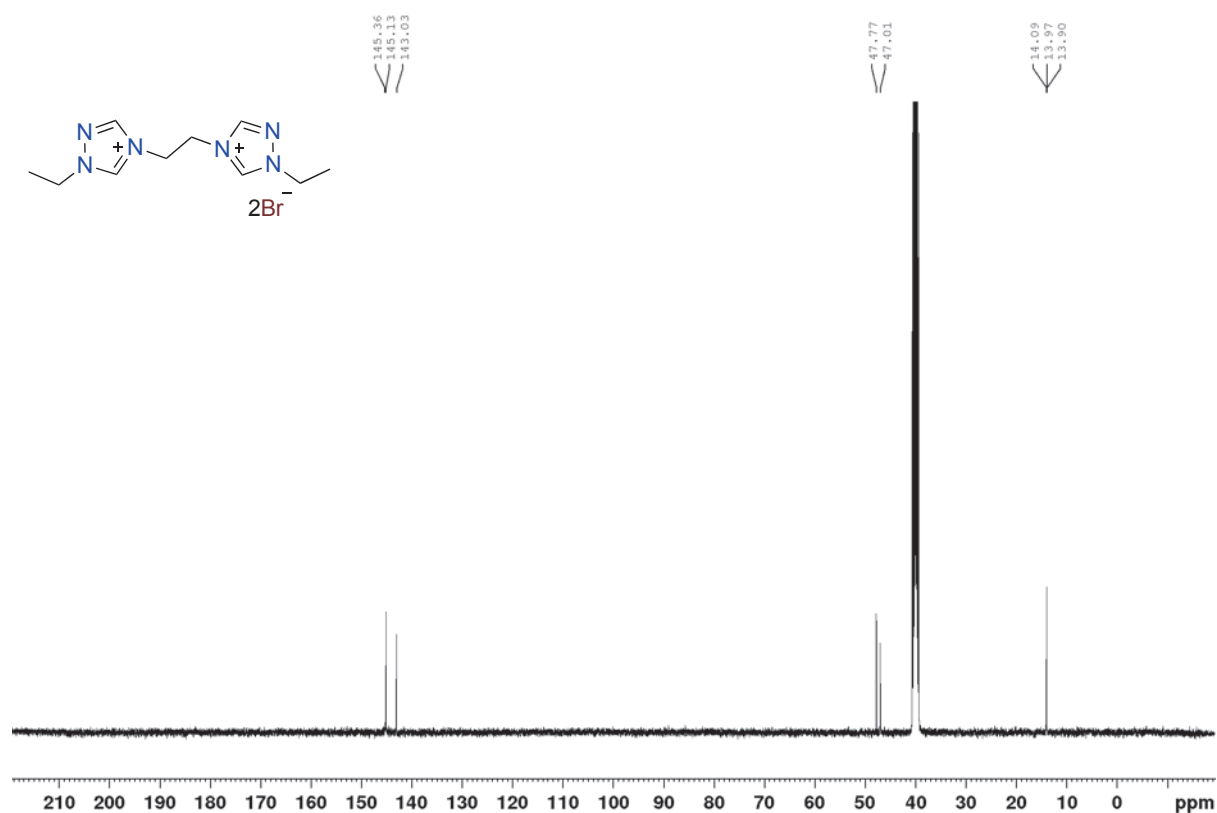


Figure S65. ^1H -NMR spectrum of compound **2.33**

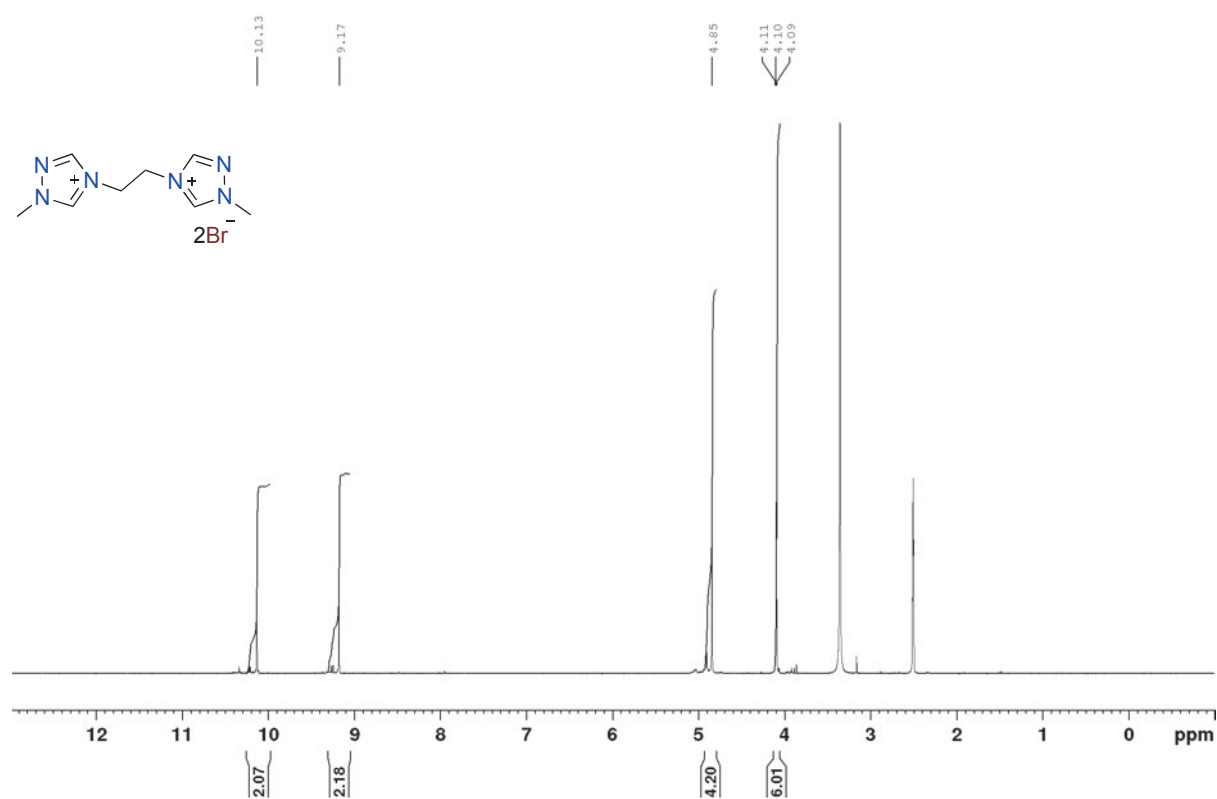


Figure S66. ^{13}C -NMR spectrum of compound **2.33**

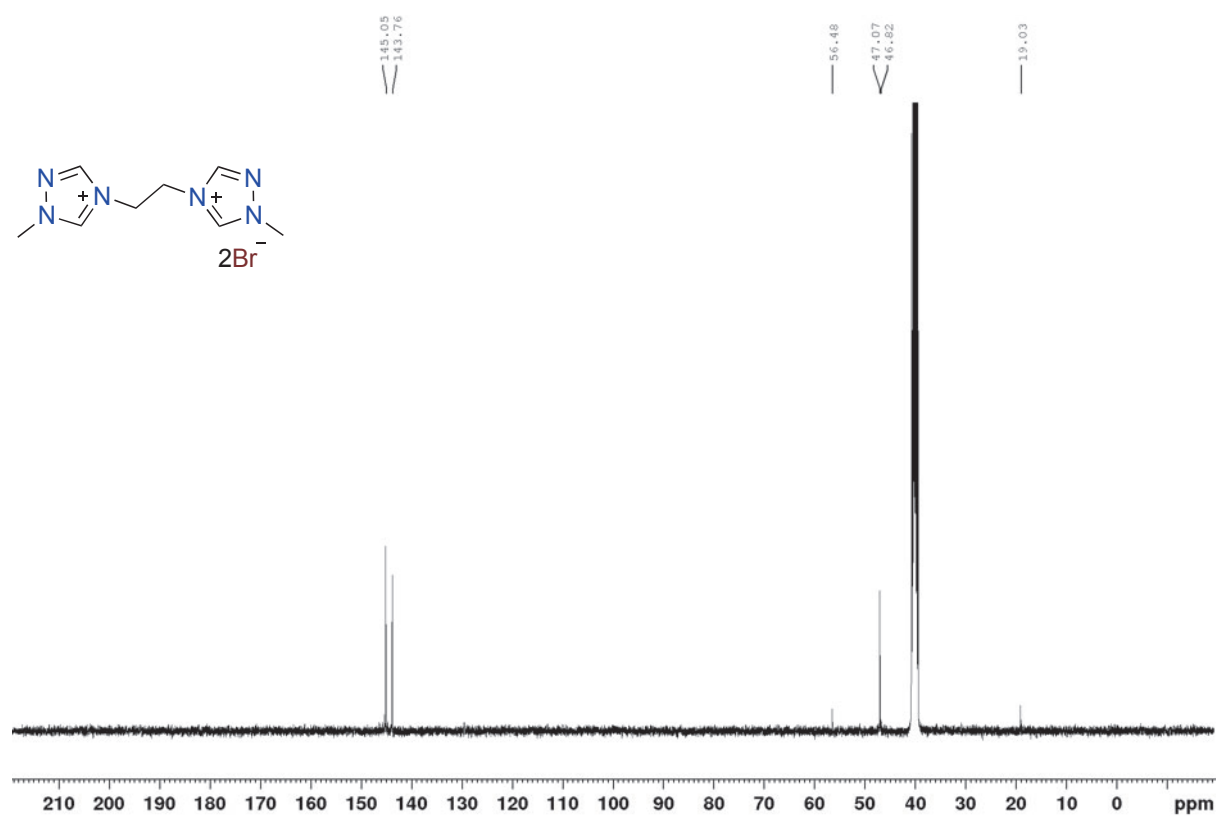


Figure S67. ^1H -NMR spectrum of compound **2.34**

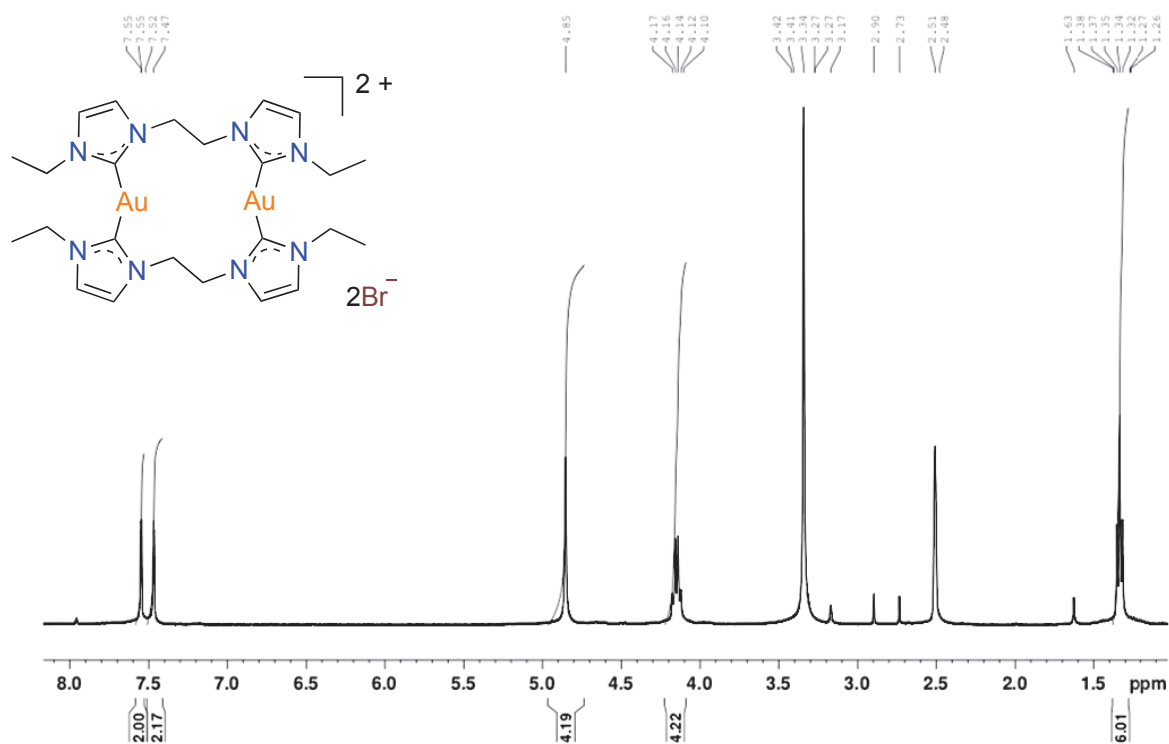


Figure S68. ^{13}C -NMR spectrum of compound **2.34**

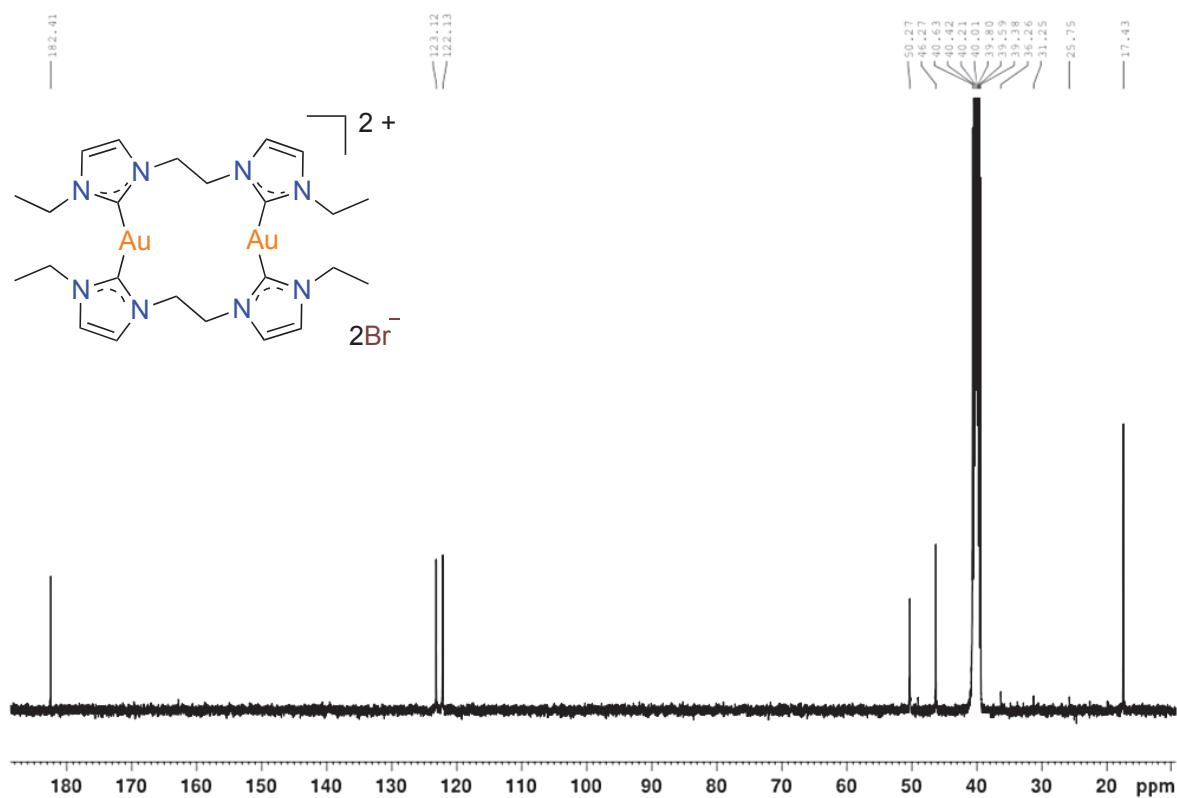


Figure S69. ^1H -NMR spectrum of compound **2.35**

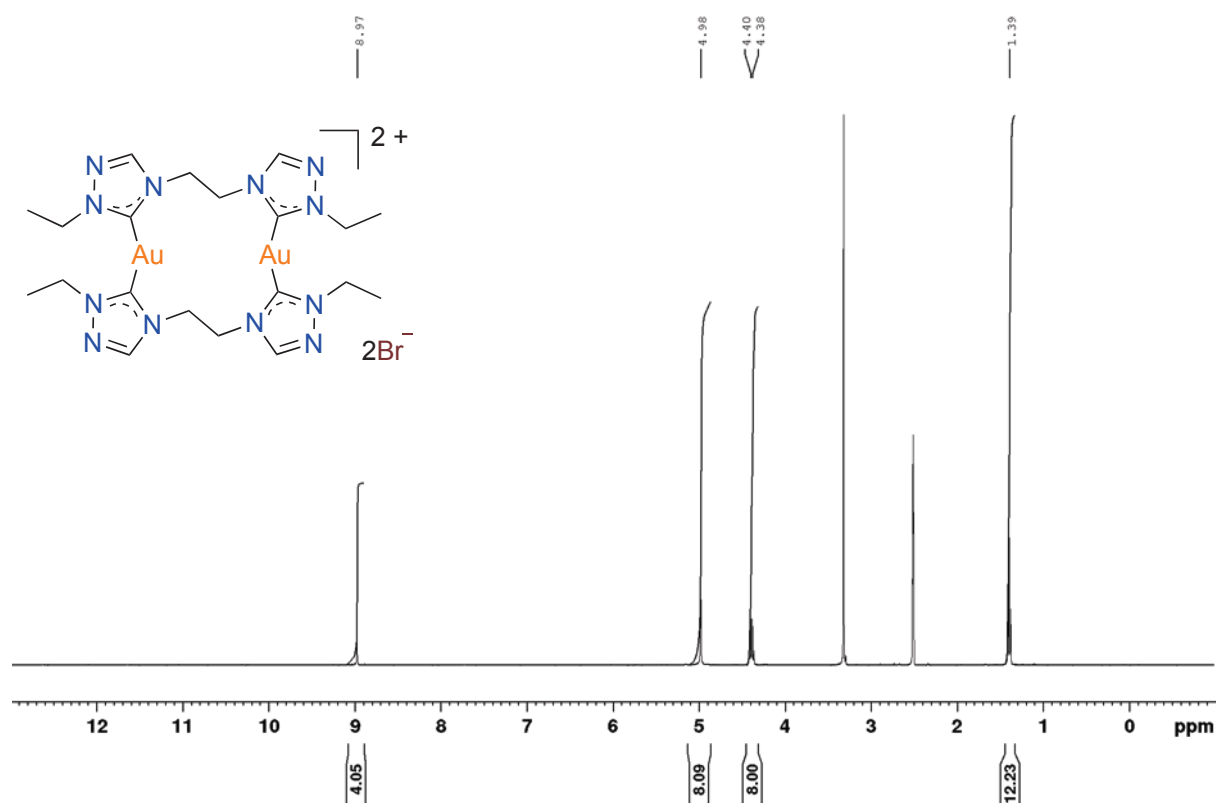


Figure S70. ^{13}C -NMR spectrum of compound **2.35**

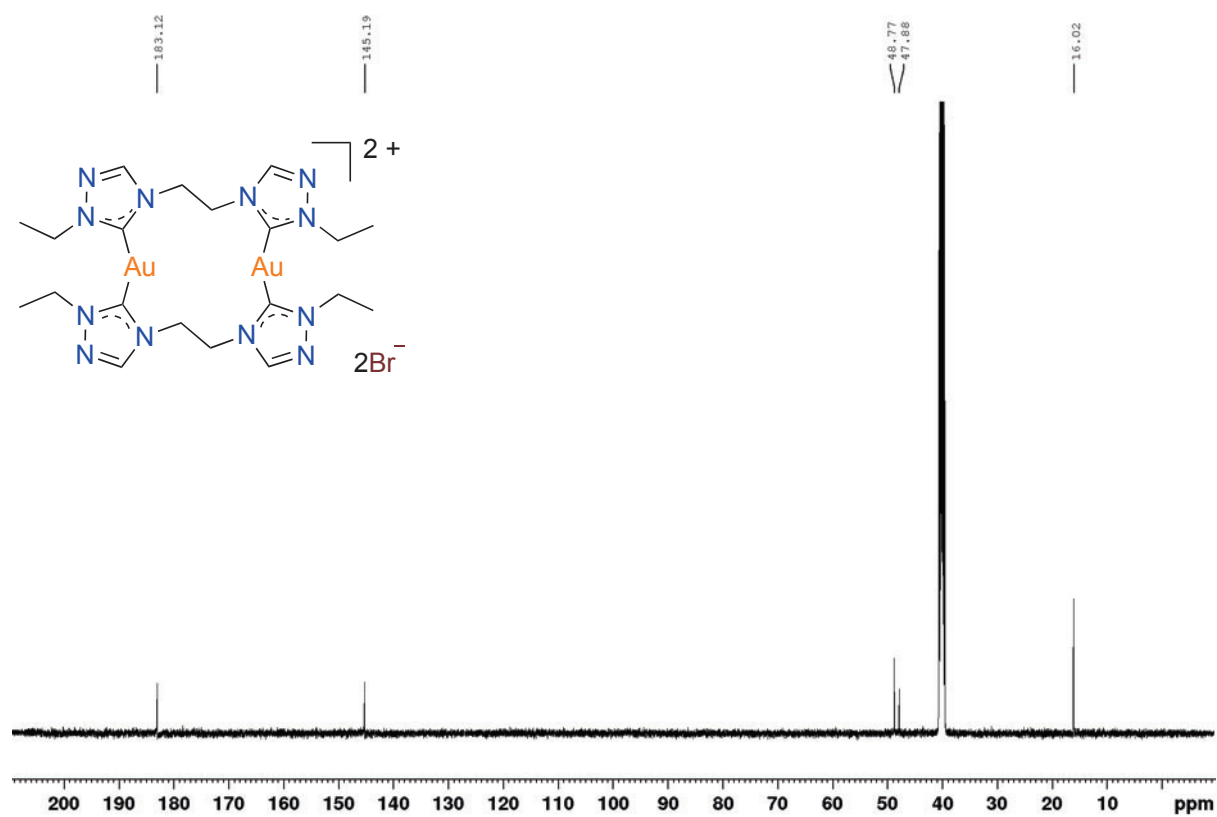


Figure S71. ^1H -NMR spectrum of compound **2.36**

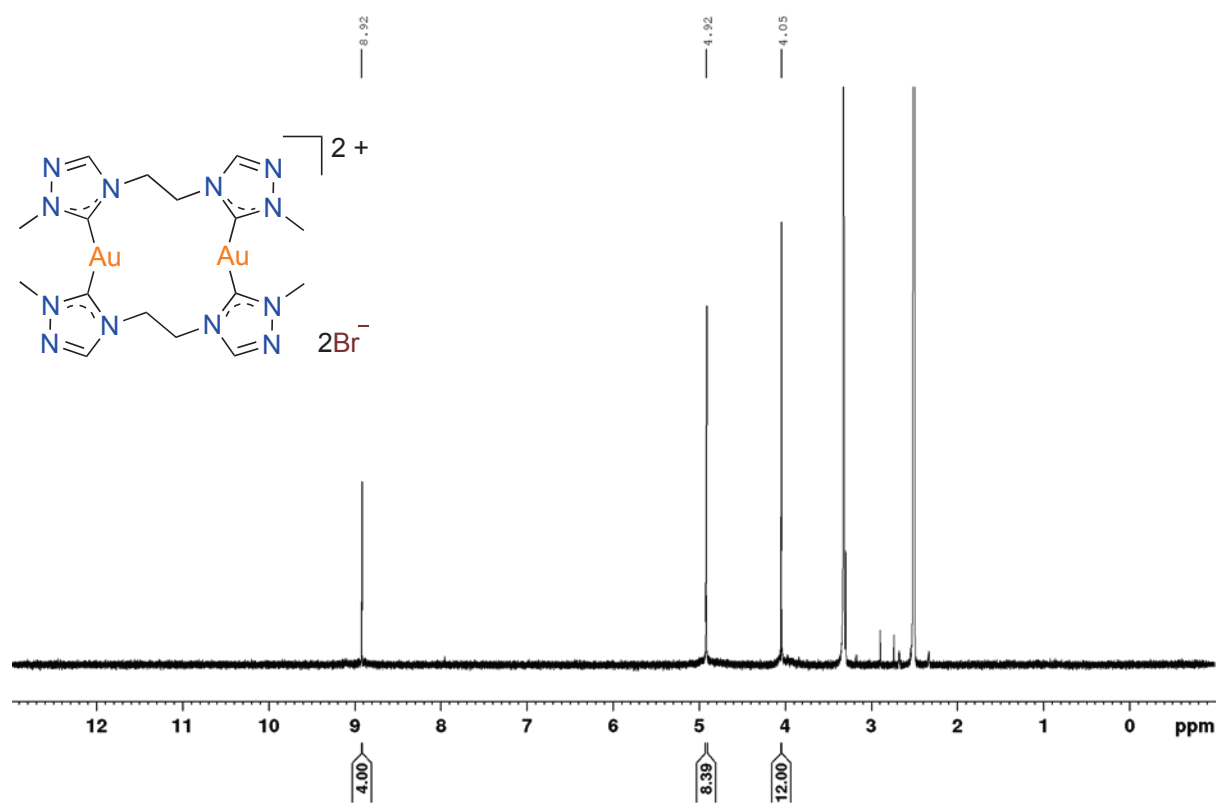


Figure S72. ^{13}C -NMR spectrum of compound **2.36**

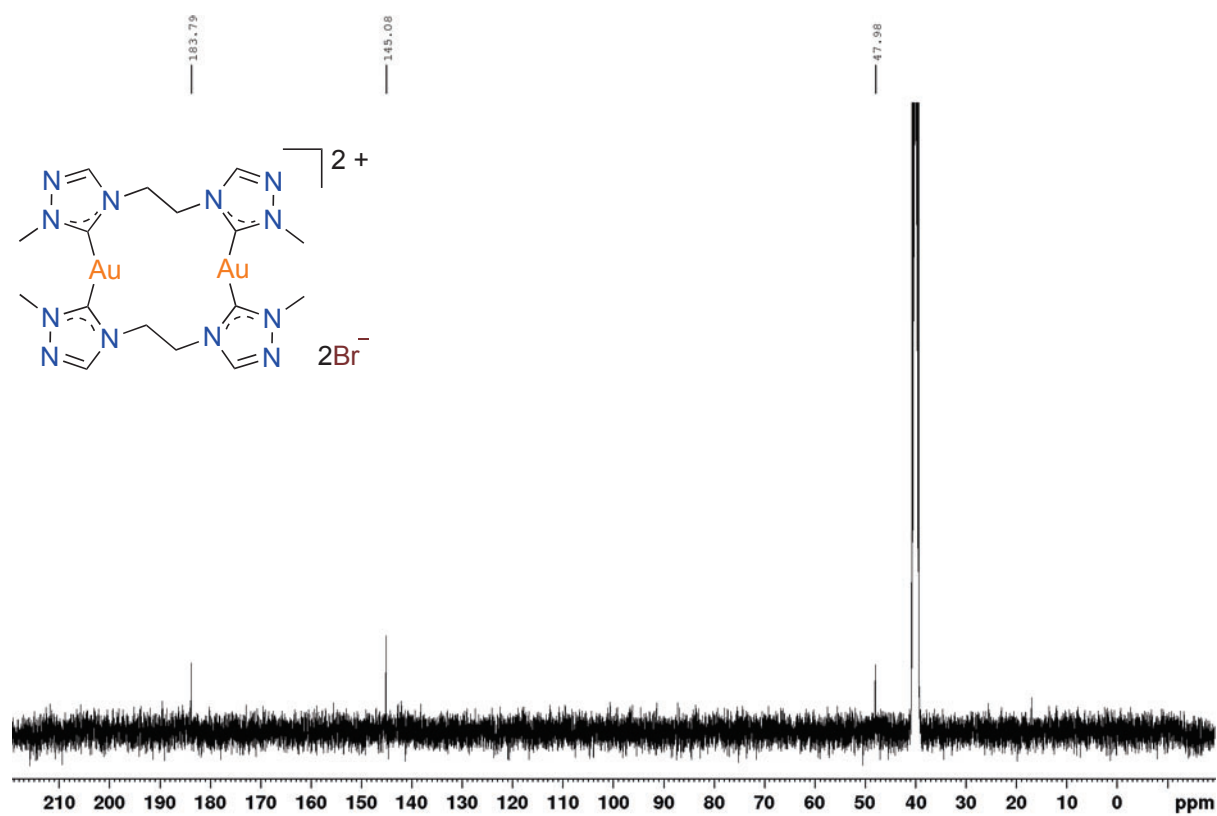


Figure S73. Stacked ^1H -NMR spectra of compound **2.20** in $\text{DMSO-}d_6$ over a period 1 week.

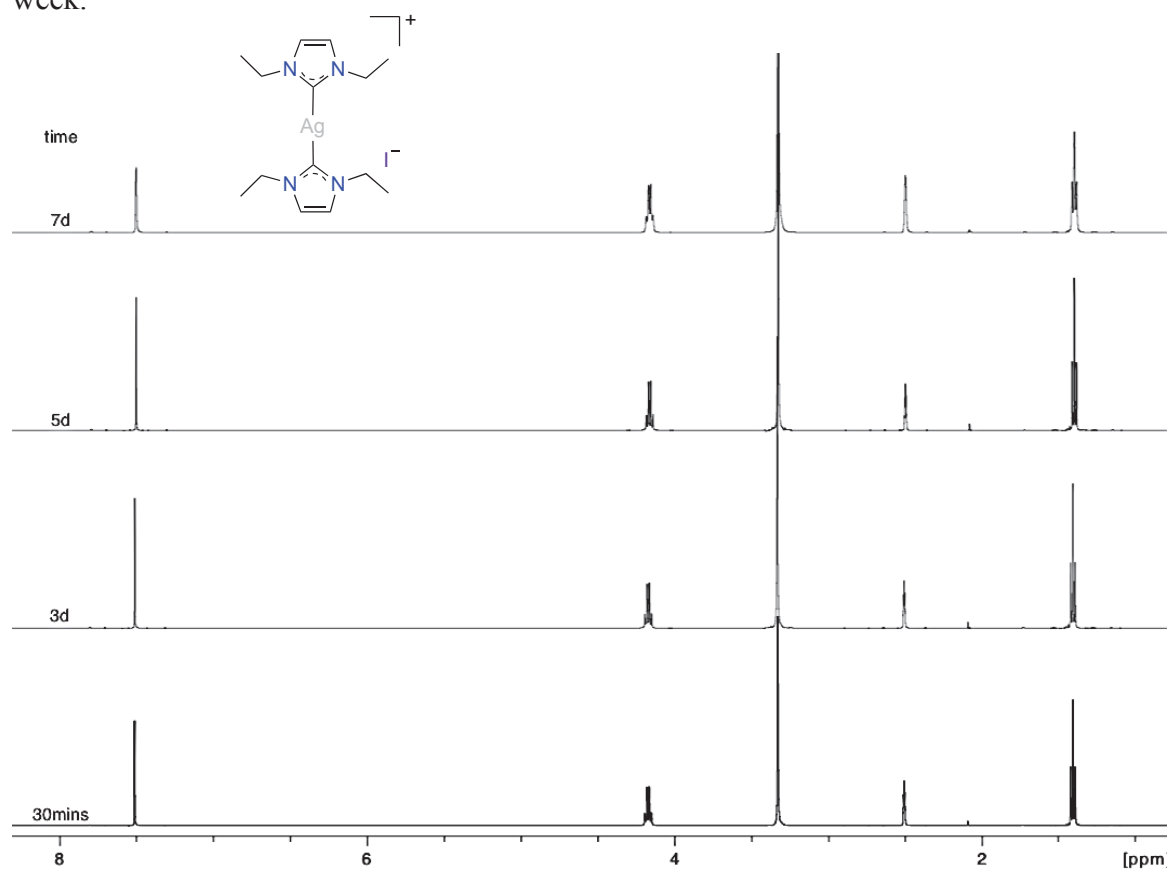


Figure S74. Normalised ESI-HRMS plots at 355 – 370 V CV for gold(I) complex of *bis*-1-phenyl-3-methyl-imidazole-2-ylidene ligands **2.23** (above) and 360 – 370 V CV gold(I) complex of *bis*-1-phenyl-4-methyl-1,2,4-triazol-5-ylidene ligands **2.25** (below). The ligand-Au peak of **2.23** (m/z 355.0768) has been omitted to allow visualisation of the low intensity gold peak m/z 196.974.

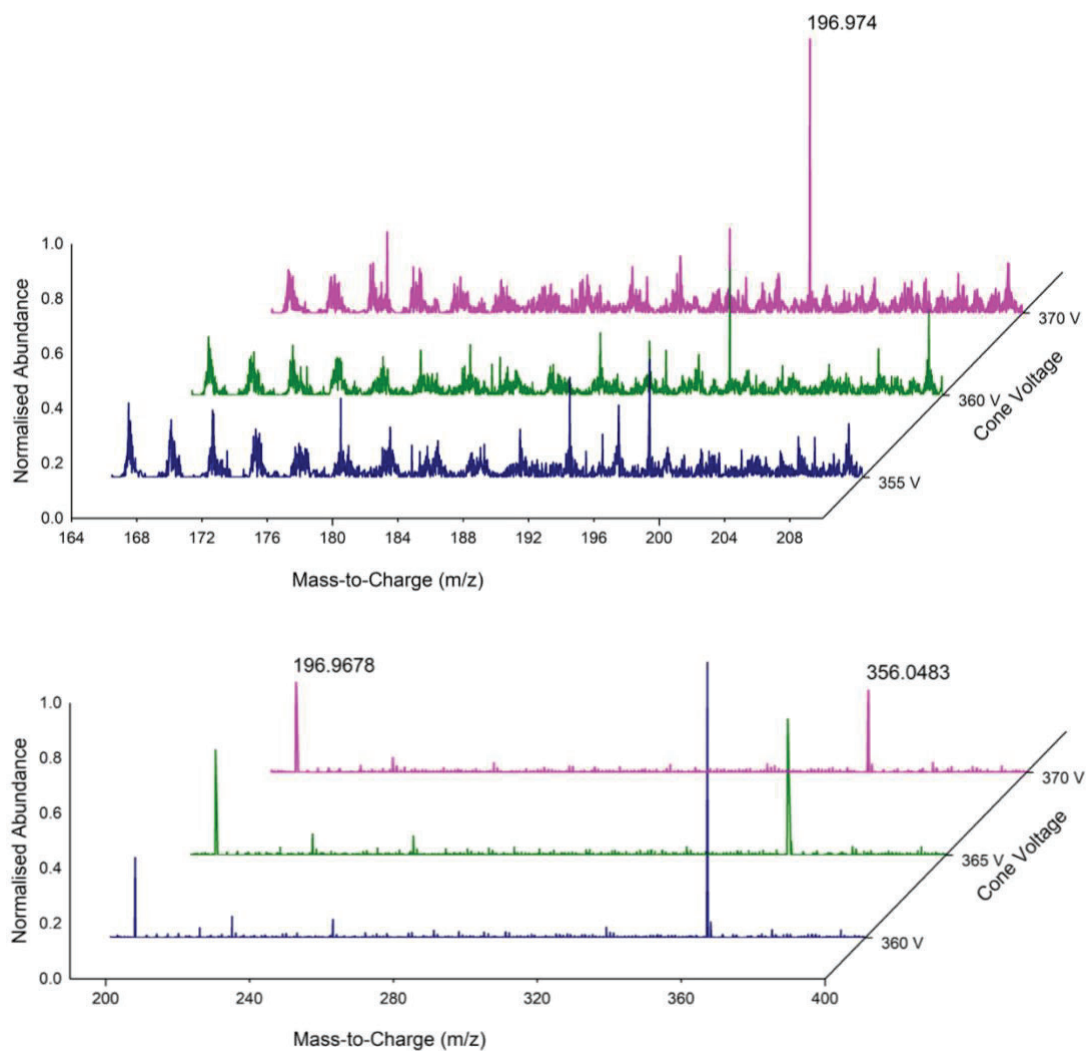


Table S1. Crystallographic data for **2.5**, **2.17**, **2.24**, **2.25**, **2.35**

Identification code	Compound 2.5	Complex 2.17	Complex 2.24	Complex 2.25	Complex 2.35
Empirical formula	C ₉ H ₁₀ IN ₃	C ₉ H ₉ Ag ₂ I ₂ N ₃	C ₂₂ H ₂₄ AuIN ₄	C ₈₄ H ₇₆ Au ₂ B ₂ N ₁₂	C ₂₀ H ₃₄ Au ₂ Br ₂ N ₁₂ O
Formula weight	287.10	628.73	668.32	1669.12	1012.34
Temperature/K	?	293(2)	293(2)	293(2)	293(2)
Crystal system	monoclinic	monoclinic	monoclinic	triclinic	triclinic
Space group	P2 ₁ /c	P2/n	P2 ₁ /n	$\bar{1}$ -P-1	P-1
a/Å	7.83570(10)	12.9749(2)	9.9001(3)	12.2740(2)	9.54745(7)
b/Å	12.72860(10)	7.37600(10)	17.1969(4)	17.4133(3)	9.97551(6)
c/Å	14.2408(2)	32.9550(5)	13.1878(3)	18.2302(5)	17.05412(8)
α /°	90	90	90	70.245(2)	99.8735(4)
β /°	131.433(2)	120.190(2)	90	82.615(2)	90.4278(5)
γ /°	90	90	90	86.3760(10)	112.6243(6)
Volume/Å ³	1064.87(3)	2726.10(8)	2245.24(10)	3635.81(14)	1472.226(16)
Z	4	8	4	8	2
$\rho_{\text{calc}}/\text{cm}^3$	1.791	3.064	1.977	1.525	2.284
μ/mm^{-1}	23.302	58.438	23.211	7.897	21.953
F(000)	552.0	2272.0	1264.0	1664.0	948.0
Crystal size/mm ³	0.04 × 0.03 × 0.02	0.03 × 0.02 × 0.02	0.04 × 0.02 × 0.03	0.05 × 0.07 × 0.04	0.06 × 0.02 × 0.02
Radiation	CuK α (λ = 1.54184)	CuK α (λ = 1.54184)	CuK α (λ = 1.54184)	CuK α (λ = 1.54184)	CuK α (λ = 1.54184)
2 θ range for data collection/°	10.816 to 142.474	6.866 to 142.48	8.45 to 129.664	7.264 to 79.894	9.782 to 130.164
Index ranges	-9 ≤ h ≤ 9, -15 ≤ k ≤ 15, -13 ≤ l ≤ 17	-15 ≤ h ≤ 11, -9 ≤ k ≤ 8, -38 ≤ l ≤ 40	-11 ≤ h ≤ 11, -19 ≤ k ≤ 20, -15 ≤ l ≤ 15	-10 ≤ h ≤ 10, -14 ≤ k ≤ 14, -15 ≤ l ≤ 15	-11 ≤ h ≤ 11, -11 ≤ k ≤ 11, -19 ≤ l ≤ 20
Reflections collected	21563	27986	16822	28148	26139
Independent reflections	2066 [R _{int} = 0.0585, R _{sigma} = 0.0182]	5280 [R _{int} = 0.0609, R _{sigma} = 0.0336]	3783 [R _{int} = 0.0277, R _{sigma} = 0.0196]	4379 [R _{int} = 0.0377, R _{sigma} = 0.0193]	5012 [R _{int} = 0.0522, R _{sigma} = 0.0227]
Data/restraints/parameters	2066/0/119	5280/0/296	3783/0/255	4379/0/905	5012/2/347
Goodness-of-fit on F ²	1.083	1.062	1.080	1.068	1.188
Final R indexes [I ≥ 2 σ (I)]	R ₁ = 0.0273, wR ₂ = 0.0754	R ₁ = 0.0364, wR ₂ = 0.1048	R ₁ = 0.0182, wR ₂ = 0.0461	R ₁ = 0.0179, wR ₂ = 0.0461	R ₁ = 0.0334, wR ₂ = 0.0876
Final R indexes [all data]	R ₁ = 0.0275, wR ₂ = 0.0757	R ₁ = 0.0404, wR ₂ = 0.1082	R ₁ = 0.0192, wR ₂ = 0.0467	R ₁ = 0.0183, wR ₂ = 0.0464	R ₁ = 0.0335, wR ₂ = 0.0876
Largest diff. peak/hole / e Å ⁻³	1.33/-1.01	2.25/-1.54	0.64/-0.93	0.27/-0.41	2.68/-2.26

